SYNTHESIS AND EVALUATION OF NAPHTHALIMIDES AND THEIR HYBRIDS WITH OTHER HETEROCYCLIC MOIETIES FOR ANTICANCER AND ANTIBACTERIAL ACTIVITIES

A dissertation as partial fulfillment for the
Degree of Doctor of Philosophy in
Chemistry by

Saurabh Gupta

(Roll No.901909017)

Under the
SupervisionOf

Dr. Kamaldeep Paul

Professor

DEPARTMENT OF CHEMISTRY AND BIOCHEMISTRY

THAPAR INSTITUTE OF ENGINEERING AND TECHNOLOGY

PATIALA, 147004

Thapar Institute of Engineering and Technology
Patiala
Department of Chemistry and Biochemistry

Statement

I hereby declare that matter embodied in this thesis is the result of the investigations carried out by me in the Department of Chemistry and Biochemistry, Thapar Institute of Engineering and Technology, Patiala, India under the supervision of Prof. Kamaldeep Paul. This thesis has been submitted by me to the Department of Chemistry and Biochemistry, Thapar Institute of Engineering and Technology, for the award of the degree of Doctorate of Philosophy.

In keeping with the general practice of reporting scientific observations, due acknowledgements have been made wherever the work described is based on the findings of other investigations. I further declare that this work has not been submitted anywhere else for any degree, diploma, or associateship. etc., of any institute or University to the best of my knowledge.

Saurabh Gupta.

Saurabh Gupta
Reg. No. 901909017
Department of Chemistry and Biochemistry,
Thapar Institute of Engineering and Technology
Patiala-147004, Punjab, India

Kamaldeep Paul.

Dr. Kamaldeep Paul
Professor
Department of Chemistry and Biochemistry,
Thapar Institute of Engineering and Technology
Patiala-147004, Punjab, India

Thapar Institute of Engineering and Technology
Patiala
Department of Chemistry and Biochemistry

Certificate

It is certified that the work contained in the thesis entitled **"SYNTHESIS AND EVALUATION OF NAPHTHALIMIDES AND THEIR HYBRIDS WITH OTHER HETEROCYCLIC MOIETIES FOR ANTICANCER AND ANTIBACTERIAL ACTIVITIES "** by Saurabh Gupta in fulfillment of the degree of Doctor of Philosophy is an authentic record of the candidate's own independent and original research work carried out under my supervision in the Department of Chemistry and Biochemistry, Thapar Institute of Engineering and Technology, Patiala, Punjab, India. The material embodied in this thesis has not been submitted in part or full to any other University or Institute for the award of any other degree.

Dr. Kamaldeep Paul
Professor
Department of Chemistry and Biochemistry,
Thapar Institute of Engineering and Technology
Patiala-147004, Punjab, India

Prof. Manmohan Chhibber
(Head, DCBC)
Department of Chemistry and Biochemistry,
Thapar Institute of Engineering and Technology
Patiala-147004, Punjab, India

DEDICATED TO MY BELOVED FAMILY

Acknowledgement

Doing a Ph.D. is simultaneously the most difficult and the most enriching experience I have undertaken. I may halt for a while to place on record my gratefulness to all those who have made a contribution towards the successful completion of this thesis. Above all, I express my gratitude to the family members for their blessings and support. I am deeply indebted to my adviser, **Prof. Kamaldeep Paul**, for accepting me into his group. During my tenure, he supported me in every step of this journey and provided just the right balance of independence and guidance, engaging me in new ideas and demanding a high quality of work in all my endeavors. I have learned a lot from you to take no assumption for granted, to distill every problem down to its essence, and many other valuable lessons that will hold me in good stead for my next adventure. I am glad to say that I have inherited from you a taste for real, practical problems and simple solutions that are grounded in theory.

I express my gratitude to the Director, Thapar Institute of Engineering and Technology, Patiala, Dr. N. Tejoprakash, Dean of Research and Sponsored Projects (DRSP), and Dr. Manmohan Chhibber (Head of DCBC) for all facilities that have been immensely helpful in completing my work. My sincere thanks must also go to the members of my thesis advisory committee: Prof. Manmohan Chhibber, Prof. Vijay Luxami, and Dr. Vasundhra Reddy. They generously gave their time to offer me valuable comments toward improving my work.

Sincere gratitude to **Dr. Iqubal Singh**, without whom this work would not have been accomplished. I greatly benefited from his keen scientific insight, his knack for solving seemingly intractable practical difficulties, and his ability to put complex ideas into simple terms. His teaching and support were very useful for carrying out my work.

I would also like to thank Dr. Gulshan Kumar, Dr. Sudesh Rani, and Dr. Ruhi Mehta for their guidance and support throughout my journey.

There is no way to express how much it meant to me to have been a member of the Organic and Medicinal Laboratory. I would like to acknowledge how grateful I am for having a group of people in my life who are always ready to listen to my rants about research with a smile on their faces. Dr. Dinesh Singla, Dr. Aastha Palta, Rekha Thakur, Rohini Gupta, Palak Sharma, Shifali, Sonia Mittal, Anmol Jain, Tanya, Priya Thakur, Vikash Kaushik, Sahil Rana.

I am thankful to master students Navneet Singh, Kuldeep Singh, Jaspreet Kaur, Navreet Sehgal, Sakshi, Abhishek Kaundal, Abhinav Prashar, Komal Verma, Rahul Rana, Pranav Sharma and

Gurpreet Kaur for creating a great work atmosphere. Mentoring them during their master's dissertation was helpful for me in learning new things, and their help at different stages made my journey work easily.

I extend my gratitude to other research scholars of the department: Parmadeep Kaur, Sunidhi Sharma, Anmol Singh, Arshdeep Kaur, Shreya Sharma, Gurmeet Kaur, Abinash and others who are not mentioned by name for their support and encouragement. I now have a forever collection of stories and a lot of everlasting memories to tell.

Besides the labmates and other colleagues of the department, friends play a crucial role in motivating you. Hence, I would like to thank Kanika Gupta, Shubham Rajput, Aashima Mahajan, Akshay Jain, and Ajay Singh for a laugh whenever possible.

I acknowledge the help of Mr. Mayank Sharma, office staff, and Chander Singh Thakur, Chandra Shekhar, Hemant Sharma, and Vishwanath Dass, technical staff of the Department of Chemistry and Biochemistry, for their support in various aspects.

I extend my thankful acknowledgment to SAI Labs, Thapar Institute of Engineering & Technology, Patiala; SAIF Lab, Panjab University, Chandigarh; CIL, IIT Ropar, for providing experimental instrumentation. I extend my gratitude to Mr. Mukesh Aggarwal and Mr. Pardeep Bhatia SAI Labs, Thapar Institute of Engineering & Technology, Patiala, for their cooperation during NMR data collection. Mr. Ajeeth Singh, Department of Physics and Material Sciences, TIET, for his support during FESEM data collection. I thankfully acknowledge Thapar Institute of Engineering & Technology, Patiala, for providing me with a teaching assistantship during my course. I am also thankful to CSIR (02(0310)/17/EMR-II) and SERB, New Delhi (CRG/2023/004080) for financial assistance and NIH, Bethesda for anticancer activity.

Finally, none of this would have been possible without the constant love, support, guidance, and patience of all my family members. I owe my gratitude to my respected father, **Mr. Ramakant Gupta**, and my mother, **Mrs. Sunita Gupta**, whose blessings, belief, and encouragement have shown methe path to pursue goals in my life. I thank my sister **Vishali Gupta**, for everything she has done for me. They all have been amazing and have always been there for me. I cannot thank them enough. Thank you for your everlasting love and support.

Besides this, I am thankful to all those people who have knowingly/ unknowingly helped me in successfully completing my work.

Saurabh Gupta

Contents

ABBREVIATIONS

µM	Micro molar
µmg/ml	Microgram per milliliter
5-FU	5-Fluorouracil
AR	Analytical reagents
ArH	Aromatic hydrogen
$B(OH)_2$	Boronic acid
$CDCl_3$	Deuterated chloroform
CDK	Cyclin-dependent kinase
CH_3COOH	Acetic acid
$CHCl_3$	Chloroform
Ct	Calf thymus
DHFR	Dihydrofolate reductase
DMF	Dimethylformamide
DMSO	Dimethylsulfoxide
DMSO-d_6	Hexadeuterodimethyl sulfoxide
DNA	Deoxyribonucleic acid
EtBr	Ethidium bromide
EGFR	Epidermal growth factor receptor
GI%	Percentage growth inhibition
GI_{50}	Median growth inhibition concentration
H_2SO_4	Sulphuric acid
H-bonding	Hydrogen bonding
HNO_3	Nitric acid
HSA	Human serum albumin
IC_{50}	Median inhibition concentration
IPA	Isopropanol
K_2CO_3	Potassium carbonate
KI	Potassium iodide
LC_{50}	Median lethal concentration
Mg	Milligram
MG-MID	Mean graph mid-point

min	Minutes
MTT	3-(4,5-Dimethylthiazol-2-yl)-2,5-diphenyl tetrazolium bromide
NCI	National cancer institute
NH_2NH_2	Hydrazine
NMR	Nuclear magnetic resonance
NT	Not treated
$Pd(PPh_3)_2Cl_2$	Bis(triphenylphosphine)palladium(II)chloride
$Pd(PPh_3)_4$	Tetrakis(triphenylphosphine)palladium(0)
$Pd(OAC)_2$	Palladium acetate
CuI	Copper Iodide
PDB	Protein data bank
Phe	Phenylalanine
SAR	Structure activity relationship
TFA	Trifluoroacetic acid
TGI	Total growth inhibition concentration
Trp	Tryptophan
Tyr	Tyrosine
USA	United States America
UV	Ultraviolet
HRMS	High-Resolution Mass spectrometry
ADME	Absorption, Distribution, metabolism and Excretion
MIC	Minimum inhibitory concentration
MBC	Minimum bactericidal concentration
SEM	Scanning electron microscopy

Introduction

During past several years, cancer has emerged out to be the most threatening disease in the world and it is one of the most serious health issues among people.[1] By 2040, there will be near about 27.5 million new cancer cases prevailing in the world, according to the cancer reports and about 9.6 million deaths have been reported due to cancer till 2018.[2] Cancer is caused due to unchecked cell growth and unusual divisions of normal cells.[3] When a damaged cell cannot repair itself, it often acquires a so-called program known as cell death or apoptosis.[4] The development of cytotoxicity and genotoxicity by available anticancer drugs towards healthy cells has caused a serious issue in the treatment of cancer.[5] The main purpose of chemotherapeutics is to target DNA as it plays a significant role in unchecked divisions of cells and cell growth.[6] After much advancement and years of research in medicinal chemistry, none of the marketed drugs could successfully eradicate and cure cancer as these develop resistance towards cancer cells.[7] So, there is a requirement of developing candidates that could exhibit potent anticancer properties and should have low cytotoxicity towards healthy cells.[8]

Moreover, people are also highly affected by diseases that are caused by bacterial pathogens, which have led to a higher death rate across the world.[9] Revolution in medicinal chemistry has taken place after the discovery of antibiotics and is thought to be a changing point in curing fungal and bacterial infections.[10] The discovery of most potent antibacterial agent, penicillin, in 1940s laid the foundation for building new synthetic candidates that can exhibit antibacterial properties.[11] The efficiency of the existing antibiotics to cure bacterial infection is decreasing as these developed resistances towards targeted bacteria and have caused serious health issues among the people.[12] There is also an urgent need for the development of drugs that could exhibit excellent antibacterial properties and overcome the resistance towards targeted bacteria.[13]

In search of new therapeutics with excellent anticancer and antibacterial properties, showing fewer side effects, and overcoming the resistance towards cancer cells and bacterial strains, heterocyclic moieties have received marked importance.[14] Heterocycles are class of organic compounds having heteroatom(s) such as nitrogen, oxygen, sulphur, etc., in their structures, and are the fundamental divisions of organic and medicinal chemistry.[15] Researchers nowadays are focusing on synthesizing new heterocycles due to their vast applications in medicinal, industrial, and drug-designing fields. Many naturally occurring biologically important molecules such as DNA, RNA, hemoglobin, vitamins, etc., which are building blocks of human growth, contain heterocyclic rings in their core structures.[16] The drugs

approved by FDA contain heterocyclic moieties such as naphthalimide, triazine, triazole, coumarin, benzimidazole, quinoline, and indole, etc., are used for the treatment of cancer disease and bacterial infections due to their enhanced lipophilicity, solubility, hydrogen bonding, and van der Waals interaction allowing them to bind with receptors in biological targets and inhibits various enzymatic processes for curing specific diseases.[17-19] Despite the various strategies and chemotherapy available for the treatment of cancer and bacterial infections, people are largely affected by these diseases due to the development of drug resistance to the present marketed drugs.[20] Even after years of extensive research and development in the field of medicinal chemistry, none of the drugs could successfully cure cancer and bacterial infections due to their serious side effects, low margin safety, non-specificity, and less efficacy towards target sites.[21] This present issue calls for urgent need for the development of new heterocyclic molecules with enhanced selectively, minimum severe side effects, high efficiency, low toxicity towards normal cells, and increased therapeutic effects than the present marketed drugs. Thus, overcoming these shortcomings and development of new drug molecules with broad spectrum activity, many new molecules by modifying, derivatization, and functionalization on naphthalimide, triazine, triazole, and coumarin have been reported in literature having good biological activity.[22-25] So, herein, we have designed new heterocycle-based drugs by adopting various synthetic routes.

Amongst these heterocyclic moieties, naphthalimide has received a great importance due to its broad spectrum of biological properties. Naphthalimides are the class of polycyclic imides that are π-deficient and have a flat aromatic ring structure. Naphthalimide, because of its planarity, can intercalate with DNA and prevent the alteration in DNA due to this property.

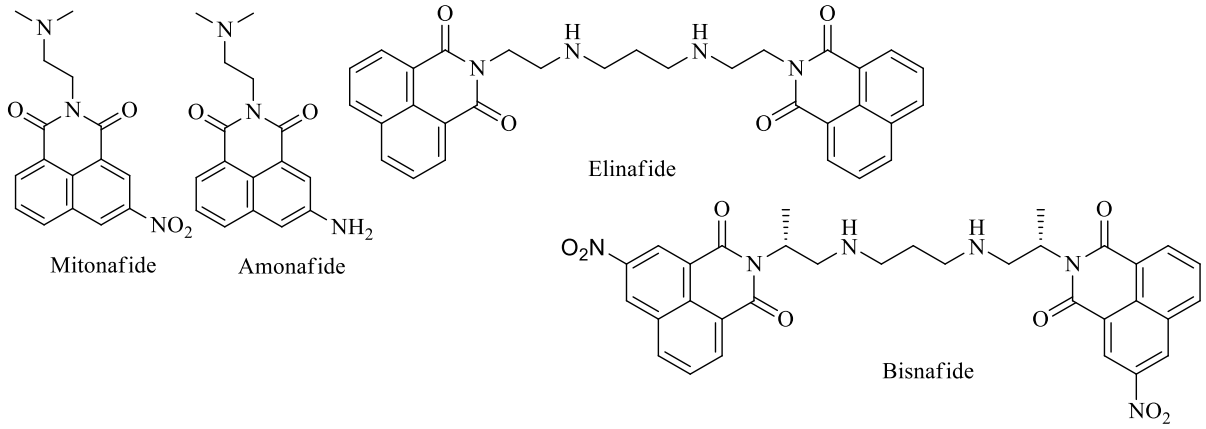

Figure 1: Anticancer active compounds of naphthalimide

Moreover, the hydrophobic nature of naphthalimide makes it easier to impede the cell membrane of bacteria pathogens, thus helping in building membrane targeting antibacterial agents. Many analogues were synthesized *viz*. amonafide, mitonafide, elinafide, and bisnafide (**Figure 1**) that have reached the clinical trials. Due to the dose-limiting toxicity of these naphthalimide drugs, none of the molecules have entered the market.[26]

In the present work, we have designed and synthesized bisnaphthalimides with and without spacer, hybrids of naphthalimide and coumarin, and hybrids of naphthalimide and triazine. The synthesized compounds were successfully characterized by NMR and HRMS techniques. Further, these compounds were evaluated for anticancer and antibacterial properties against a panel of 60 human cancer cell lines, and gram-positive and gram-negative bacterial strains, respectively. Spectroscopic techniques were employed to investigate the binding interactions of most potent compounds towards DNA and HSA to underline the mechanism for anticancer and antibacterial activities. The mode of action for antibacterial activity was also examined by membrane studies, biofilm inhibition, etc. Thus, in this dissertation, the work carried out during the research period is divided into the following parts:

Chapter 1: Review of literature

Chapter 2: Materials and Method

Chapter 3: Bis-naphthalimide conjugates and their biological evaluation

Chapter 4: Naphthalimide-coumarin hybrids and their biological evaluation

Chapter 5: Naphthalimide-triazine conjugates as an effective antibacterial agent

CHAPTER 1

Literature Survey

Several marketed drugs with excellent versatility and physicochemical properties contain various heterocyclic moieties in their core structure, which are the main pillars in medicinal chemistry. Ever since the development of new anticancer and antibacterial agents, heterocyclic moieties have attained great importance due to their diverse range of biological activities. Among various heterocyclic moieties available; naphthalimide, coumarin, triazole, and triazine etc. play crucial roles in cytotoxic drugs. Nowadays, researchers are focusing on the development of new analogues that must exhibit broad spectrum of biological properties and avoid resistance against targeted cancer or bacterial cells. For this purpose, changes or advancements are being made in the structures of biologically active moieties by derivatization or by combining two or more pharmacophores. The following literature has been studied for synthesizing new heterocycles with better biological properties.

1.1 Naphthalimide conjugates as anticancer and antibacterial agents

Ge *et al.* designed and synthesized a novel series of naphthalimides by modifying its third position with various substituents. The prepared derivatives were evaluated for their anticancer activity against human and murine cancer cell lines. Of all the tested derivatives, compounds **1a** and **1b** exhibited promising results against A549 cancer cell line with low IC_{50} value of 3 μM. Both compounds were able to cause DNA damage and induced autophagy in the cancer cells and inhibited the demethylase activity. The results showed that these compounds might play a crucial role in the study of cancer therapy.[27]

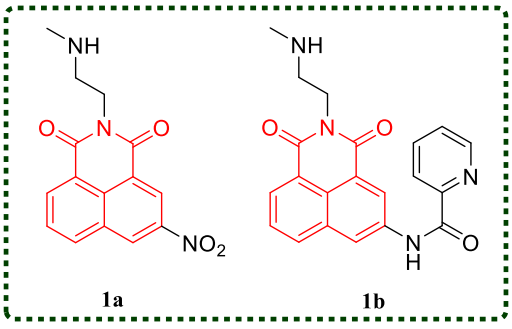

1a **1b**

Zhang and co-workers designed and formulated a series of piperazine-substituted naphthalimides. The synthesized compounds were tested against various tumor cell lines for their anticancer activity. The MTT assay results disclosed that compounds **2a**, **2b,** and **2c** displayed potent results in suppressing the growth of HepG-2, MGC-803, T24, SKOV-3, and

A549/DDP. Compound **2a** was least toxic against normal cell lines with low resistance towards cancer cell lines. The anticancer mechanism of compound **2a** was determined by various techniques such as western blot, flow cytometry, and confocal immunofluorescence, unfolding that **2a** exhibited multiple modes of action, including apoptosis, autophagy, cell cycle arrest, and ferroptosis.[28]

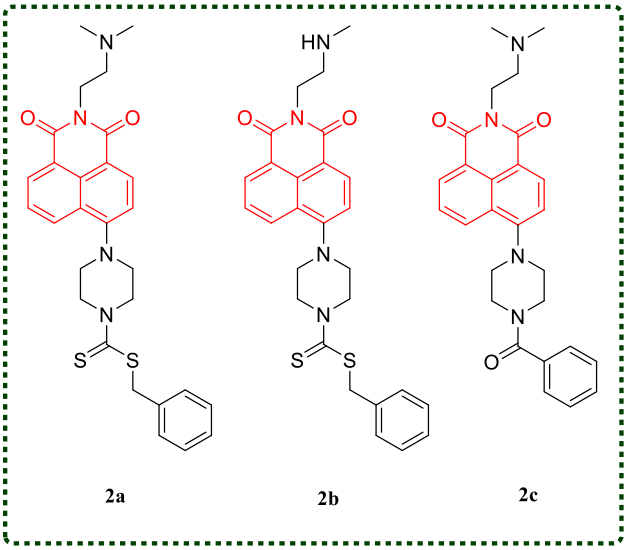

Chen *et al.* sketched and synthesized a series of mono and bis-naphthalimide conjugates having 4-morpholine and 3-nitro substituents and tested their anticancer potential towards four cancer cell lines. Few compounds relatively displayed better anticancer activity than mitonafide and amonafide. Of all the prepared compounds, **3a** and **3b** displayed the most promising results and later showed their best activity against MGC-803 cells with a low IC_{50} value of 0.09 μM. DNA and Topo I were found to be the main targets of both compounds for their anticancer activity. Moreover, both compounds induced apoptosis in the cell, which was confirmed by ROS generation, Hoechst staining, and flow cytometry assay. Further, *in vivo* studies disclosed that compound **3b** displayed more promising anticancer results than mitonafide in MGC-803 xenograft tumors.[29]

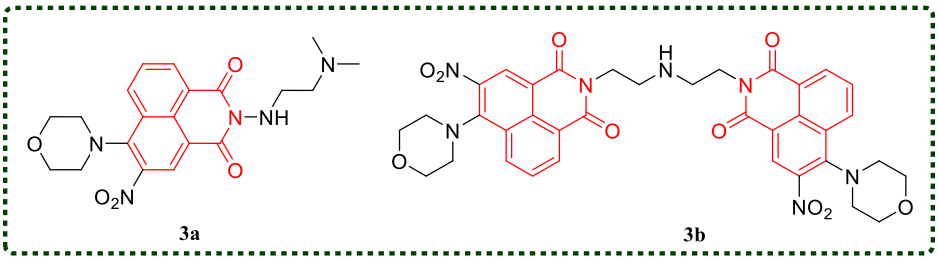

Paul and coworkers synthesized a novel hybrid of naphthalimide, benzothiazole, and indole moieties, and their analogs as potent antitumor agents. Anticancer evaluation inferred that compounds **4a** and **4b**, having substitution of respective ethanolamine and propargyl

amine, were better performers in inhibiting cancer growth than other analogs with low IC_{50} values of 140 and 310 nM, respectively. Both compounds effectively inhibited human-type IIa topoisomerase activity and interacted efficiently with HSA, having high binding constants of 1.75×10^5 M^{-1} and 1.88×10^5 M^{-1}, respectively. The interactions of **4a** and **4b** with topoisomerase were further confirmed by docking studies.[30]

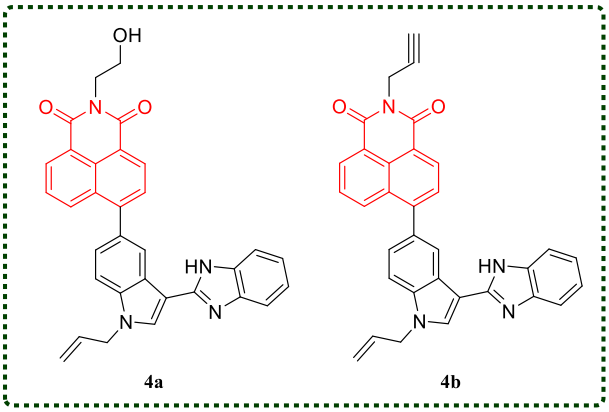

Patil *et al.* prepared and characterized sixteen new naphthalimide conjugates and examined their anticancer activity towards different cancer cell lines *viz.* B16F10, MCF7, PANC1, and CHO cell lines. Compounds **5a** and **5b** exhibited moderate activity against B16F10 cell lines. Compound **5c** displayed promising anticancer results towards B16F10, MCF7, and PANC1 cells. Toxicity and pharmacokinetic profiles of the synthesized compounds were evaluated by ADMET parameters. The molecular docking studies and *in vitro* anticancer evaluation manifested that these compounds could be used for structural manipulation for building new potent anticancer agents.[31]

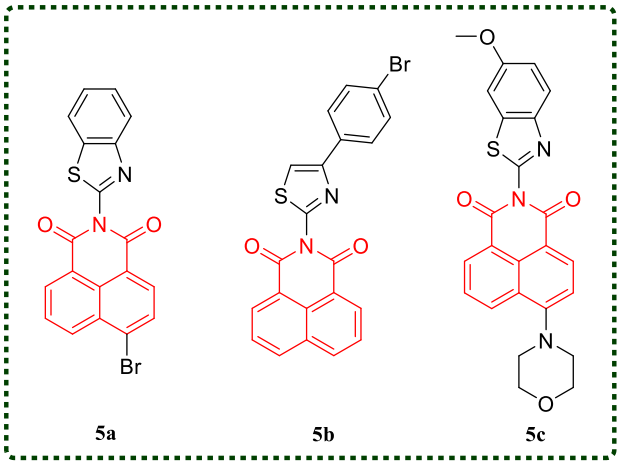

Zhou and co-workers formulated a series of naphthalimide and its conjugates, and further examined their antibacterial properties against various bacterial strains. Compounds **6a, 6b** and **6c** exhibited excellent antibacterial activities against *Staphylococcus aureus.* These compounds effectively suppressed bacterial growth and delayed the development of resistance.

Mechanistic studies disclosed their ability to damage the membrane of bacteria, causing the leakage of intercellular cytoplasmic contents. In addition, these compounds could induce oxidative stress in cells, leading to disruption of antioxidant defence system of *S. aureus*. Moreover, these compounds effectively inhibit the biofilm formation and metabolic dysfunction of *S. aureus*.[32]

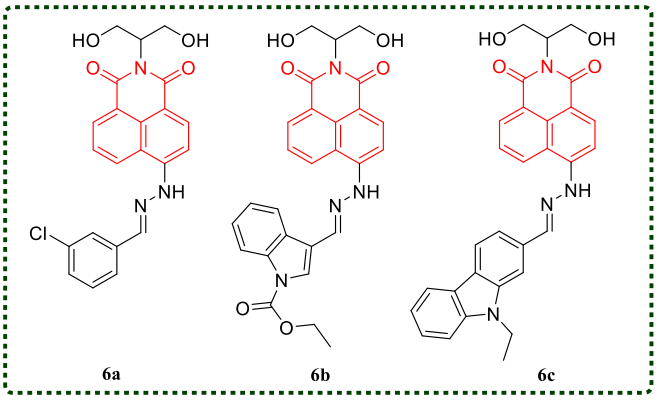

Zhang *et al.* put an effort into building a series of new antibacterial agents by incorporating aminothiazoximes with naphthalimide, having a unique mechanism of action to overcome resistance to present antibiotics by MRSA (Methicillin-resistant *Staphylococcus aureus*). Compound **7** displayed excellent results in suppressing the growth of MRSA with a MIC value of 0.5 μg/ml with significant membrane selectivity. Compound **7** effectively delayed the resistance development by MRSA. Mechanistic studies unfolded that compound **7** bound effectively with lipase, assisting the penetration of compound into the cell membrane, causing membrane disruption that led to leakage of proteins. The biological function of DNA was hampered by compound **7** as it intercalated with DNA, leading to disruption of antioxidant defence against MRSA *via* induction of oxidative stress in cells.[33]

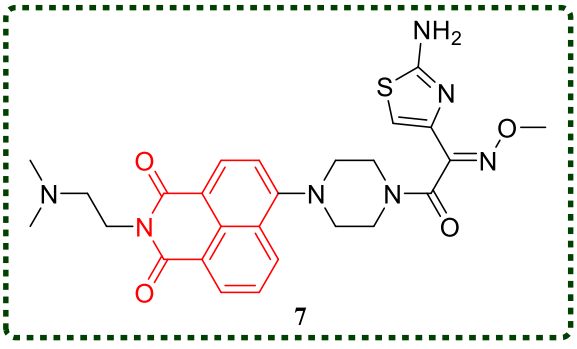

Chen and his colleagues designed and synthesized a novel series of naphthalimide-appended aminothiazoles to evaluate their antibacterial activity against different bacterial strains. Compound **8,** having piperazine in its structure, exhibited appreciable antibacterial activity towards *E. coli* and MRSA with MIC values of 8 and 4 μg/mL, respectively, and

outperformed reference drugs. Compound **8** exhibited bactericidal action and disrupted the membrane efficiently, causing leakage of intercellular proteins. Compound **8** intercalated into base pairs of MRSA-DNA and bound with gyrase-DNA *via* hydrogen bonding. Further studies inferred that compound **8** was effectively bound with human serum albumin and could be transported to target site easily.[34]

Zhou and co-workers successfully synthesized hybrids of naphthalimide-nitroimidazoles, which were confirmed by various characterization techniques. The prepared compounds were evaluated against various bacterial strains to check their antibacterial potential. Bioactivity assay disclosed that compound **9**, having substituted piperazine at C-4 position of naphthalimide, exhibited the most promising results in suppressing the growth of bacterial strains. It was found to be most active against resistant *A. baumannii* with MIC value of 0.013 μmol/ml and outperformed marketed drug clinafloxacin. It displayed a fast, rapid killing effect and inhibited the induction of drug resistance.[35]

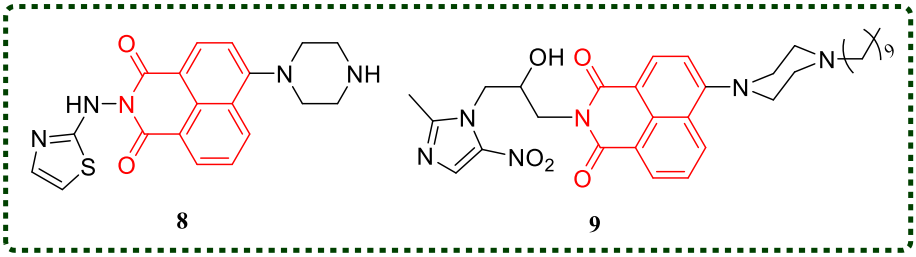

1.2 Coumarins as anticancer and antibacterial agents

Hu and co-workers prepared a novel series of coumarin and pyrimidinone moieties as potent anticancer agents. All the molecules were examined for their anticancer activities against cervical and HepG2 tumor cell lines. *In vitro* results manifested that compounds **10a** and **10b** displayed the most potent results in suppressing cancer growth. Both compounds exhibited potent concentration-dependent mode leading to apoptosis in HepG2 cells. The trans-well migration assay disclosed that compound **10b** potently suppressed the transportation and invasion of HepG2 cells. Moreover, compound **10b** inhibited the kinase activity with an inhibition rate of 40-20%. Structure-activity relationship revealed that the electropositive and bulkier groups on the pyrimidinone ring were superior in increasing bioactivity of compounds.[36]

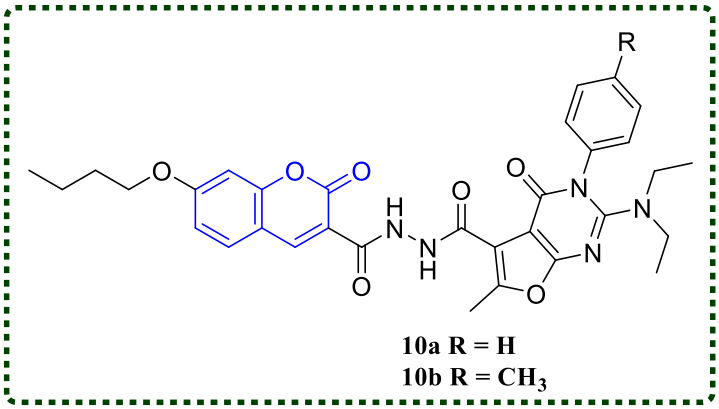

Supuran and his team successfully derived sixty compounds of coumarin incorporating monoterpene in two series having different triazole linker in one series and alkyl chain in others. Anticancer evaluation and inhibition properties on human carbonic anhydrase manifested that compounds **11a**, **11b** and **11c** potently inhibited CA IX and XII with Ki values of 1.9 nM, 4.9 nM, and 4.9 nM respectively. Cytotoxicity of these compounds on HT-29, MCF-7 and PC-3 disclosed that these compounds exhibited the most potent results in case of MCF-7 with IC_{50} values of 2.48 μM and 3.91 μM for **11a** and **11b,** respectively while **11c** showed its most potent activity towards PC-3 and HT-29. These compounds induced apoptosis in MCF-7 and HT-29 cells in concentration-dependent mode, while compound **11a** showed earlier apoptosis than other compounds, which was confirmed by the Hoechst staining assay. Thus, it is concluded that these prepared compounds precisely suppressed CA IX and XII and displayed cytotoxic effect in different cells.[37]

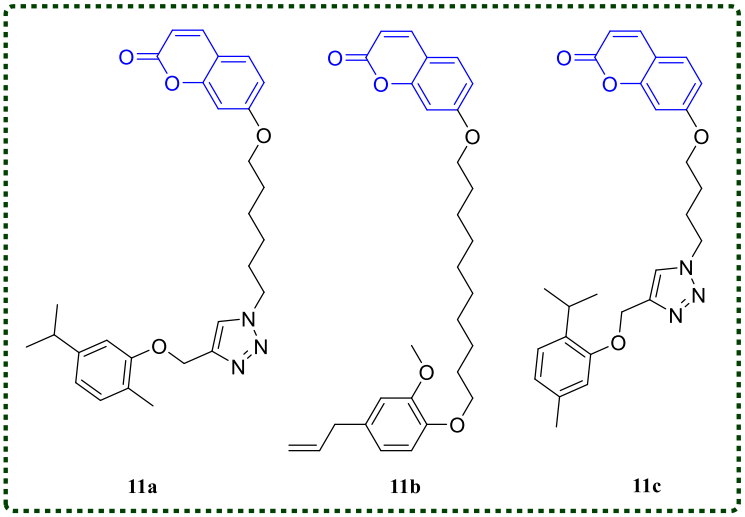

Sayed *et al.* have designed and formulated a coumarin based series incorporating triazole/tetrazole and glycosyl possessing glucose moieties. The cytotoxicity of prepared compounds was examined in a number of human tumor cell lines. The preliminary results disclosed that compounds **12a, 12b,** and **12c** displayed excellent cytotoxicity towards Mel-501,

Paca-2, A-375**,** and PC-3 tumor cell lines. The kinase inhibitory effects of the most potent compounds were evaluated against EGFR, CDK-2, and VEGFR-2. Of all three tested compounds, **12a** showed an excellent inhibitory effect on all tested enzymes compared to reference drugs sorafenib, roscovitine, and erlotinib. The mechanistic studies inferred that compound **12a** induced cell cycle arrest and apoptosis, which might be a possible reason for anticancer activity of the compound.[38]

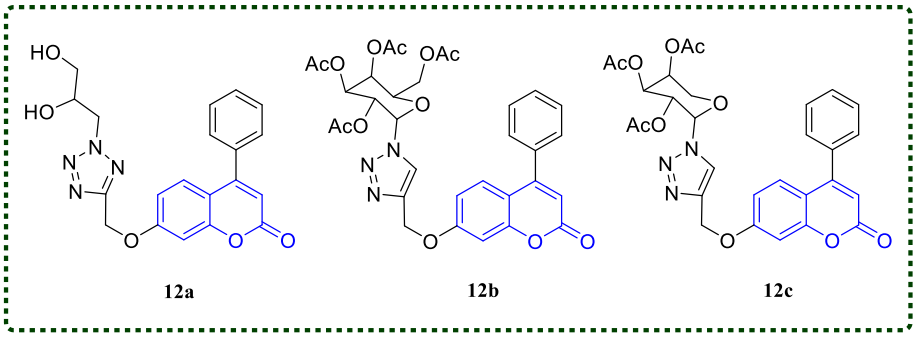

Kishk *et al.* prepared a series of coumarin conjugates which were further examined for their anticancer activity towards a panel of tumor cells by employing MTT assay. Compounds **13a** and **13b** exhibited the most promising results, and the mechanism for anticancer activity was defined by DNA fragmentation, RT-PCR, cell cycle analysis, and western blot methods. Compound **13a** was toxic to HL60 cells with an IC_{50} value of 8.09 μM whereas compound **13b** was toxic to HepG2 cells having an IC_{50} value of 13.14 μM. Both compounds inhibited the P13K/AKT pathway to exhibit their anticancer properties. The results obtained were further supported by molecular docking studies.[39]

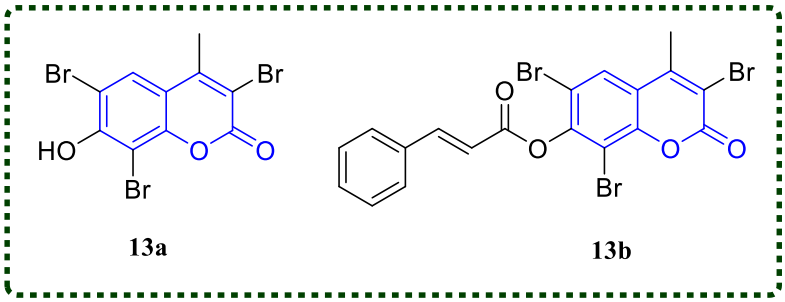

Aziem and co-workers put an effort to build new antibacterial agents by combining biologically active coumarin moiety with thiazoles, pyrazoles and pyridines, and further examined their antibacterial activities against two gram negative and two gram positive bacterial strains. Of all the tested derivatives, some compounds exhibited moderate to good activity compared to standard drugs. Compound **14a** significantly suppressed the growth of *Enterobacter cloacae* comparable to ciprofloxacin, whereas compound **14c** showed its best activity against *Bacillus pumilis* with a low MIC value of 7.69 μmol/ml. Compounds **14a, 14b,**

and **14c** significantly inhibited the bacterial growth of *Streptococcus faecalis* with MIC of 14.34, 3.67, and 15.36 μg/ml, respectively. This finding disclosed that these newly synthesized coumarin derivatives offered a class of potent antibacterial agents.[40]

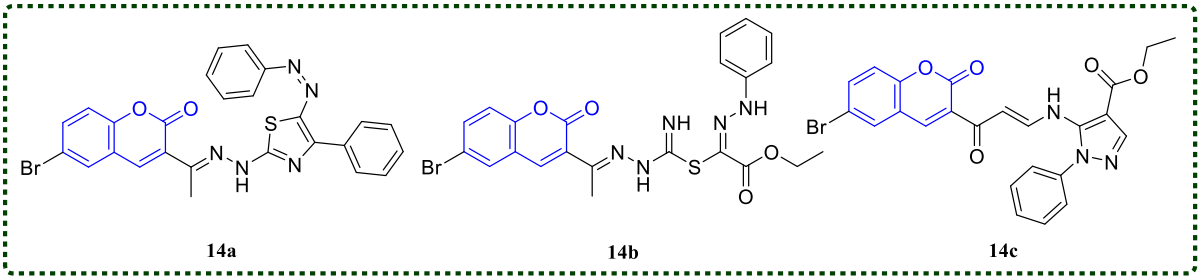

To treat the deadly bacterial infection, Yang *et al.* designed and synthesized a novel series of coumarin containing aminophosponates as an effective antibacterial agent. Bioactivity evaluation inferred that compound **15** having 3-hydroxylphenyl aminophosphonate in its structure displayed the most promising results in suppressing the bacterial growth of *Staphylococcus aureus* at low concentration of 0.5 μg/ml. Mechanistic evaluation manifested that compound **15** possessed low haemolytic activity with the potential to inhibit the biofilm formation of *S. aureus,* thus delaying the occurrence of bacterial resistance. Compound **15** has ability to penetrate the bacterial cell membrane, resulting in metabolic dysfunction and leakage of proteins. Induction of oxidative stress in cells by compound **15** led to lipid peroxidation and reduced glutathione activity, ultimately causing bacterial cell death. Compound **15** obstructed the normal functioning of the cells *via* intercalating into DNA base pairs.[41]

Zhou and co-workers synthesized a new series of coumarin as potent antibacterial agent to combat awful bacterial resistance by combining coumarin with thiazolidinone moiety to increase the bioactivity. Preliminary examination revealed that compound **16** having indole in its structure was beneficial for increasing the bioactivity of the compound and it excellently inhibited the growth of bacterial cells with a low value of MIC of 0.25 – 2.0 μg/ml. Compound **16** successfully eradicated the biofilm formation and delayed the development of drug resistance. Mechanistic studies disclosed the potential of **16** to disrupt the membrane causing the leakage of proteins and metabolic dysfunction. Compound **16** decreased the glutathione activity, causing lipid peroxidation due to the production of ROS inside the cell and further leading to cell death. The low energy gap between HOMO-LUMO of compound **16** was responsible for stable interaction with biological targets, thus, made the molecule biologically active.[42]

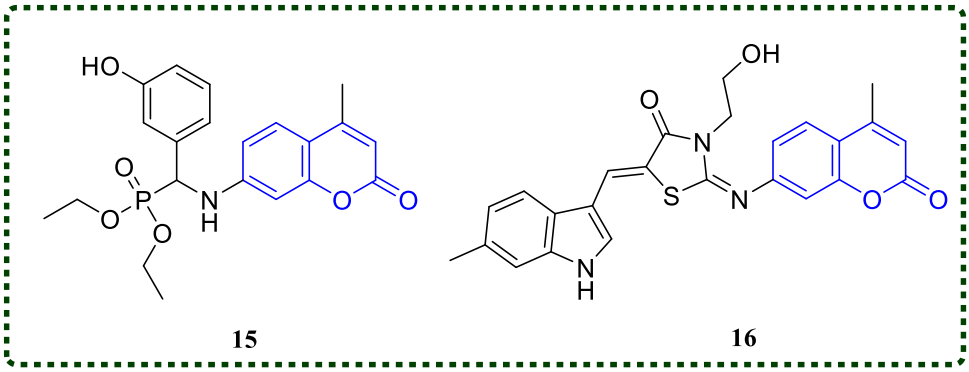

15 **16**

Salem and co-workers synthesized a number of derivatives by conjugating coumarin with sulphonamide and other amino-heterocycles at its 6th position and further examined their antibacterial activity against *E. coli*, *A. niger*, *C. albicans* and *S. aureus.* The initial results unfolded that compound **17b** displayed most promising results towards all the tested strains with low MIC values ranging from 4.88 to 39.06 μg/ml against *S. aureus, C. albicans* and *E. coli.* Compound **17b** exhibited 4-folds more promising results than standard drug neomycin whereas compound **17a** exhibited comparable antibacterial activity towards *S. aureus* and *C. albicans* with neomycin. Compounds **17a** and **17b** inhibited the DNA gyrase with an IC_{50} values of 2.46 and 1.76 μg/mL, respectively. Docking studies confirmed the binding of compounds **17a** and **17b** on the active site of DNA gyrase. ADMET studies disclosed that compound **17b** has high bioavailability score with pharmacological properties. Thus, results revealed that both compounds exhibited potent antibacterial activity and efficient DNA gyrase inhibitor.[43]

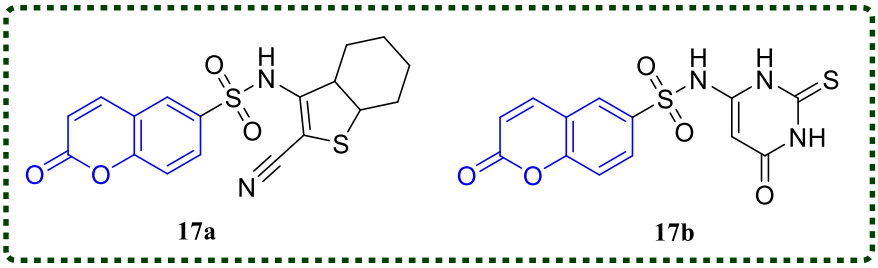

17a **17b**

1.3 Triazole as anticancer and antibacterial agents

Zhang and co-workers designed and prepared novel hybrids of 1,2,3-triazole-benzothiazole and screened for their anti-proliferative activities against Kyse30, HCT-116 and MGC-803. Their structure-activity relationships were studied to investigate the effect of various substituents on bioactivity of the compound. Among the tested compounds, **18** possessed the highest inhibition of the cancer cells while it was highly toxic to EC-109 cell lines with IC_{50} value of 38 nM. Compound **18** caused the denaturation of YAP protein through UPS pathway leading to cell

apoptosis and G2/M phase arrest in cells and also controlled the levels of proteins involved in cell cycle and apoptosis.[44]

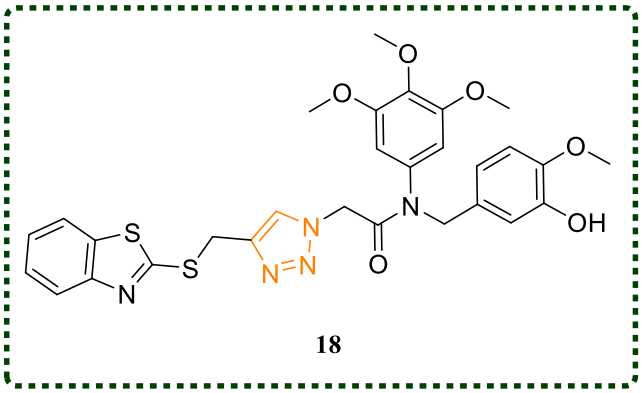

18

Tiwari and his colleagues put an effort to build novel anticancer agent by synthesizing the conjugates of triazole and pyrazolo[1,5-*a*] pyrimidinones having *N*-glycosides and further screened for their anticancer activity against different breast cancer cell lines MDA-MBA453, MCF-7 and MDA-MBA231. The preliminary results manifested that compounds **19a** and **19b** exhibited excellent results in suppressing the growth of cancer cells with IC_{50} values of 27.66 mM (MDA-MB231) and 4.93 mM (MCF-7), respectively. The experimental results were further supported by docking analysis. The results obtained open a new class of glycohybrid as potent anticancer agents.[45]

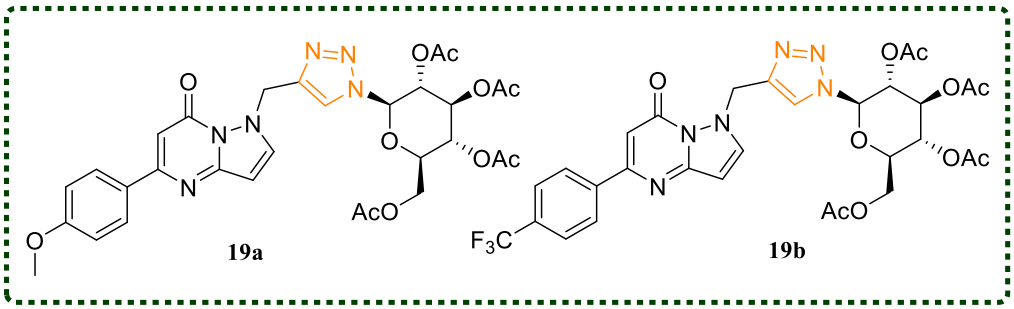

19a **19b**

Guo *et al.* synthesized a novel series of 28 compounds of cabotegravir appended with 1,2,3-triazole moiety and evaluated against HuH-7, MCF-7, SKOV3, and HCT-116 human cancer cell lines to check their anticancer potential. Preliminary results unfolded that few of the compounds exhibited good results in inhibiting the growth of cancer cells. Compound **20a** displayed best results with low IC_{50} values of 6.59, 27.24, 4.46, and 23.90 μM, whereas compound **20b** exhibited IC_{50} values of 7.83, 8.59, 6.30, and 17.00 μM towards HuH-7, MCF-7, SKOV3 and HCT-116 cancer cell lines, respectively. Mechanistic investigation inferred that both compounds **20a** and **20b** induced cell apoptosis and accumulation of oxidative stress leading to cancer cell death. Western blot assay disclosed that both compounds changed the

protein expression involved in DNA damage and autophagy. Both the molecules attained a planar conformation structure that were easier to intercalate into DNA base pair leading to DNA damage. The results showed that these triazole compounds have excellent anticancer properties.[46]

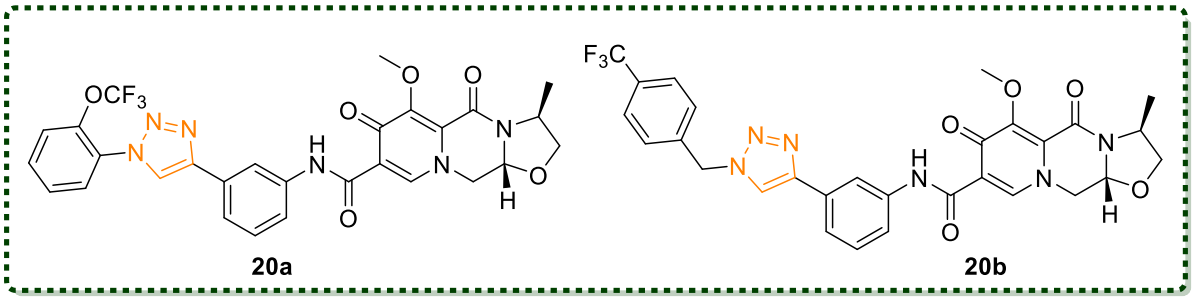

20a **20b**

Alves and co-workers synthesized two different series by hybridizing triazole and purine moieties using adenine and kinetin precursors. These prepared compounds were further examined for their anticancer activity against MCF-7 and MDA-MB-231 breast cancer cell lines. About 28 compounds were screened where compounds **21a** and **21b** displayed superior activity in inhibiting the growth of cancer cell lines than other compounds. Compounds **21a** and **21b** showed IC_{50} values of respective 9.3 and 16.7 μM towards MDA-MB-231 and 22.3 and 22.9 μM against MCF-7. The ADMET studies further put forward that these highly active molecules possessed drug-likeness properties and have the potential to emerge as potent anticancer agents.[47]

Chen and co-workers put an effort to build an effective antibacterial agent to fight the drug resistance by designing and synthesizing the hybrids of hydroxypyridinone and triazole moieties and screened their antibacterial activities against *P. aeruginosa*. Initial studies suggested that compound **22** exhibited excellent results in suppressing the growth of *P. aeruginosa* with IC_{50} value of 3.7 μM and its virulence factor pyocyanin with low value of IC_{50} (2.7 μM). Compound **22** significantly inhibited the biofilm formation and motility phenotypes of *P. aeruginosa* with low cytotoxicity towards normal cell lines. Compound **22** displayed synergistic effect when used in combination with marketed drugs such as tobramycin and

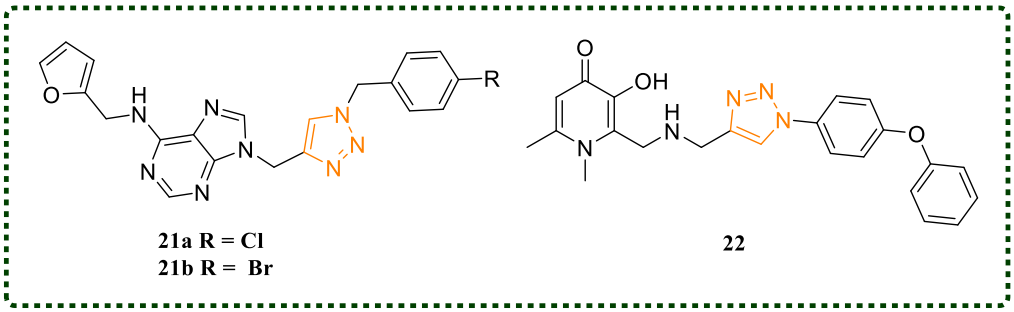

21a R = Cl
21b R = Br

22

ciprofloxacin. The excellent biofilm inhibition and anti-virulence properties of compound **22** can further be taken to clinical trials for its development as potent antibacterial agent.[48]

Bitla *et al.* designed and synthesized a novel series of bis-triazoles by employing methyl salicylate as precursor and characterized by NMR and mass spectrometry. The prepared compounds were subjected to bacterial strains *viz P. aeruginosa, E. coli, B. subtilus* and *S. aureus* to evaluate their antibacterial properties. Compounds **23a** and **23b** displayed broad spectrum antibacterial activities against all tested bacterial strains and these compounds significantly suppressed the growth of *S. aureus*. Molecular docking studies were performed to calculate binding affinities of the active molecules in the target region where compound **23b** displayed the best docking score indicating that it binds with MurB protein in the active site which might be responsible for growth inhibition of bacterial cells.[49]

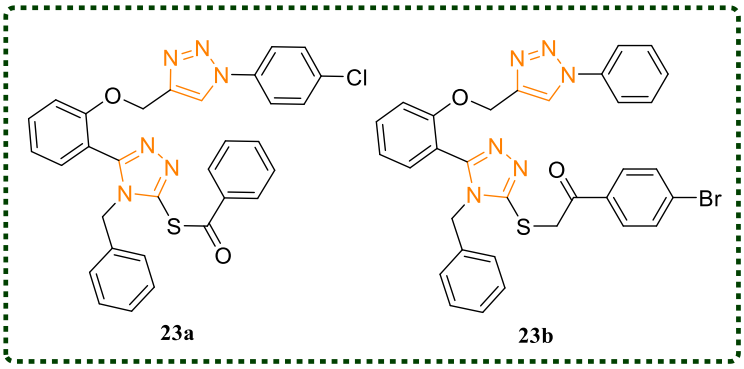

23a **23b**

Saeed and his colleagues in the present work have design and synthesized a unique series of triazole with benzofuran moiety and evaluated against two bacterial strains *E. coli* and *B. subtilis* to examine their antibacterial properties. Initial studies manifested that compounds **24a** and **24b** excellently inhibited the growth of bacterial cells. Compound **24a** exhibited its best activity against *E. coli* with MIC value of 1.80 μg/ml whereas **24b** showed its best activity against *B. subtilis* with MIC value of 1.25 μg/ml. Both the compounds exhibited antibacterial activities comparable to reference drug penicillin.[50]

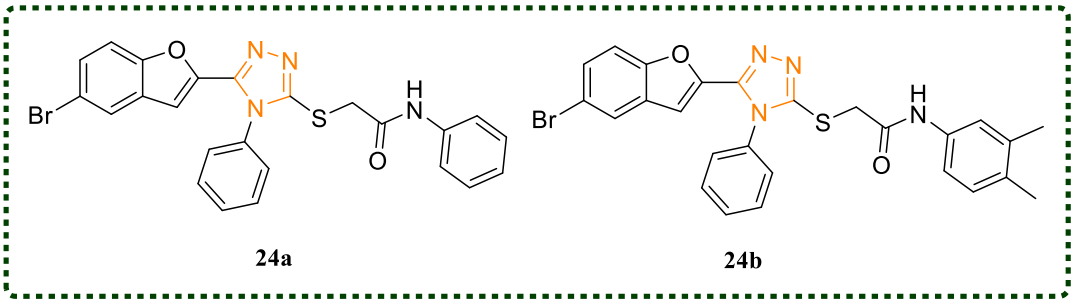

24a **24b**

Gadali *et al.* designed and formulated a series of triazole and pyrazolo-quinazoline hybrids as antibacterial agents. The synthesized compounds were screened for their potential to inhibit the bacterial growth for building new promising antibacterial agents. The bacterial

activity was examined by broth dilution method towards gram-positive and gram-negative bacteria. Of all the compounds screened for antibacterial activities, compounds **25a** and **25b** exhibited superior activity against *P. aeruginosa* (for **25a;** MIC = 18.54 μM) and *B. subtilis (*for **25b;** MIC = 89.76 μM). These compounds exhibited superior activity than marketed drugs.[51]

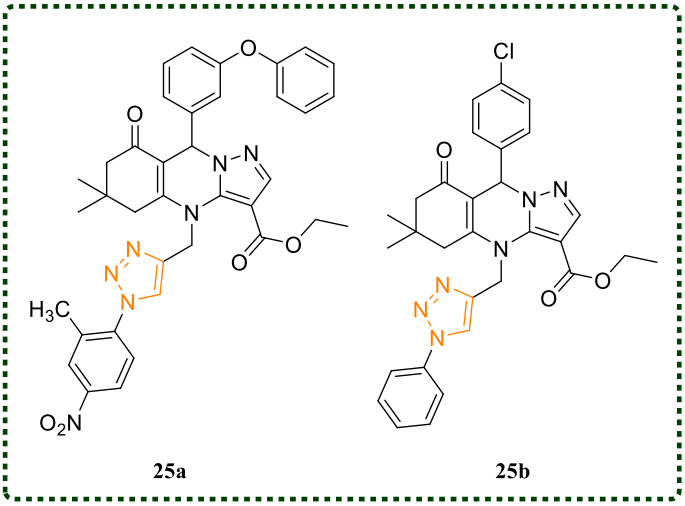

1.4 Triazine derivatives as anticancer and antibacterial agents

Shi and co-workers synthesized a series of 1,3,5-triazine based moieties by nucleophilic substitution incorporated with genistein and characterized by spectroscopic techniques. HPLC was employed to determine the purity of target compounds. MTT assay was used to examine the anticancer property of the prepared compounds towards HeLa, Huh-7, HCT-116 and MDA-MB-231 cancer cell lines. These genistein linked with 1,3,5-triazine displayed higher anticancer properties than genistein itself. Preliminary studies manifested that compound **26** exhibited the excellent growth inhibition of MDA-MB-231 breast cancer with low IC_{50} value of 23.13 mM which is better than reference drug 5-fluorouracil with IC_{50} value of 78.04 mM. Further evaluation of compound **26** inferred that it suppressed the adhesion, invasion and migration of breast cancer cell line MDA-MB-231. In addition, compound **26** showed excellent inhibition effect on the production of MDA-MB-231cancer xenografts *in vivo*.[52]

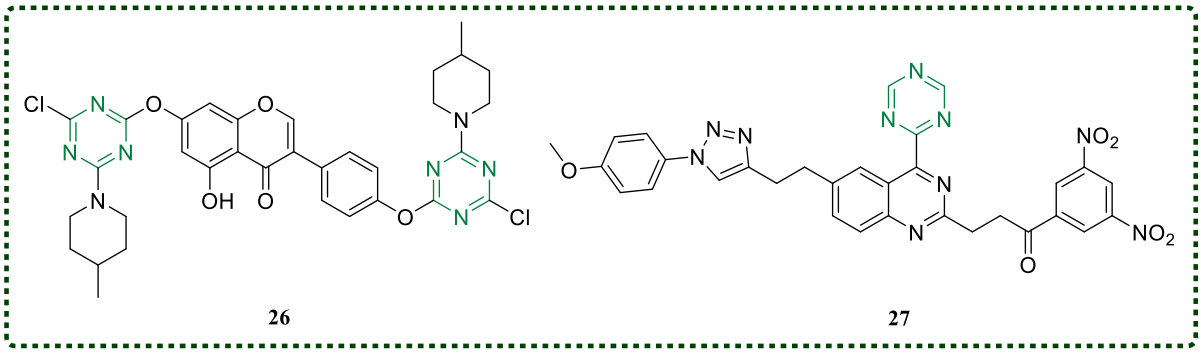

Haiba *et al.* in search of new anticancer agents, designed a new series of biological active pharmacophores *viz* triazole, triazine and quinazoline moieties in one structure to increase the bioactivity of compound. The prepared compounds were evaluated for their anticancer activities towards various cancer cell lines PC3, DU-145, MCF-7 and A549 by employing MTT assay. All the tested compounds displayed moderate to good activities. Surprisingly, compound **27** exhibited the excellent activity in suppressing the growth of cancer cells with low IC_{50} values. Further, docking studies between the tubulin complex and compound **27** were carried out to get the information about the binding interactions. Results revealed that the compound efficiently bound with active site of tubulin *via* π-π interactions, hydrophobic interactions, and H-bonding.[53]

Santra *et al.* designed and synthesized a novel hybrid by incorporating acridone, xanthone and triazine in one structure. These prepared derivatives were evaluated for their potential to exhibit anticancer properties towards various cancer cell lines such as A-172, HCT-116 and Hs578T. Among all screened compounds, **28a** and **28b** displayed the superior activity in suppressing the cancer growth with low toxicity to normal cell lines assisting the opportunity to further develop these compounds as potential anticancer agents. Mechanistic studies of compounds **28a** and **28b** were carried out by employing Annexin V assay. The results manifested that compound **28b** not only suppressed the production in glioblastoma cells but also triggered the apoptotic mechanism.[54]

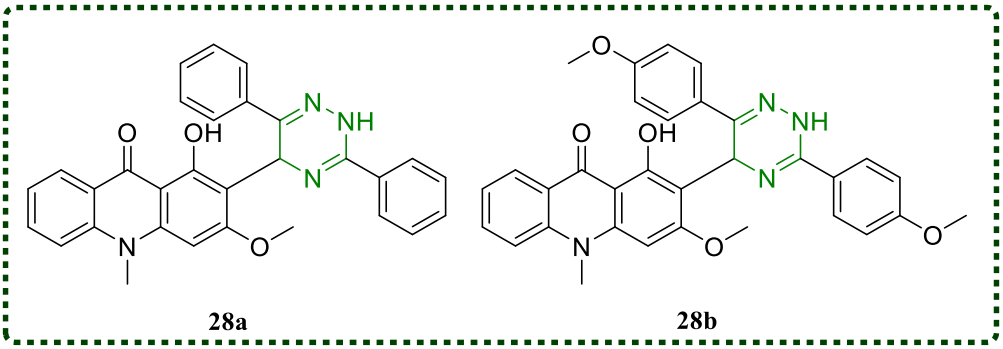

28a **28b**

Supuran and co-workers designed and synthesized a novel series of hCA IX inhibitors by appending benzene sulphonamide on triazine moiety to develop potent anticancer agents. These inhibitors were screened for their anticancer properties towards 60 human cancer lines. The results inferred that compounds **29a** and **29b** displayed the most promising activity against MDA-MB-468 breast cancer cell lines with growth inhibition rate 62%. The cytotoxicity of these active compounds against breast cancer cell line under hypoxic condition were examined and both the compounds exhibited low IC_{50} of 3.99 and 1.48 μM respectively. Further, studies

suggested that compound **29a** induced cell cycle arrest, apoptosis and S phases in MDA-MB-468 breast cancer leading to elevation in the level of cleaved caspases 3 and 9.[55]

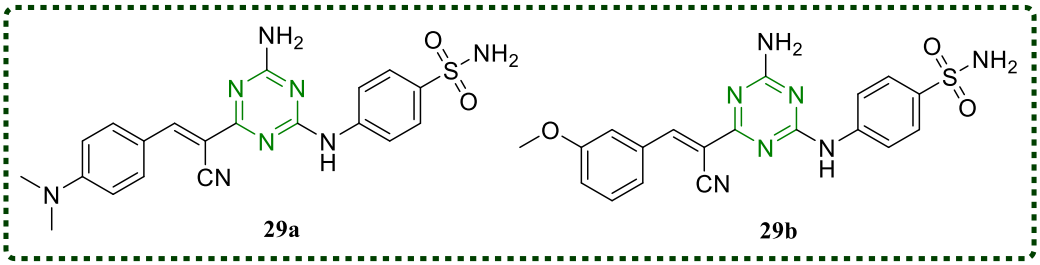

Mekheimer and his colleagues synthesized novel hybrids of tetrazole and triazine, and screened for their potential to inhibit bacterial growth against various bacterial strains. The initial results inferred that compounds **30a** and **30b** exhibited the most promising results against *P. aeruginosa* comparable to ciprofloxacin. Mechanistic investigation of the most potent compound **30a** revealed its ability to inhibit the topoisomerase IV and DNA gyrase of *E. coli.* and also suppressed the CYP51 protein. Further, ADMET studies predicted that these molecules possessed drug-likeness properties and could be developed further as the most potent antibacterial agents.[56]

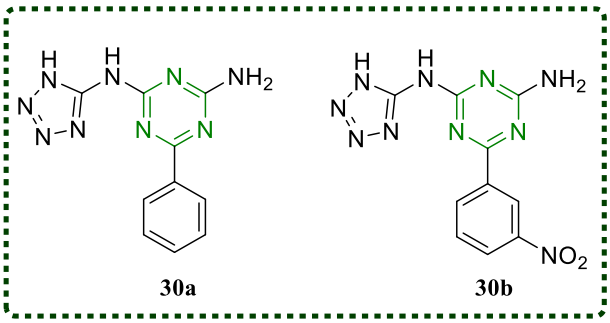

Tsodikova and co-workers in their present study designed and synthesized a series of pyrazole and triazine hybrids. The synthesized compounds were studied for their antibacterial properties against various bacterial strains. The preliminary results revealed that compounds **31a** and **31b** exhibited the most promising results in suppressing the growth of bacteria with low MIC values. Mechanistic evaluation inferred that these compounds exhibited bacteriostatic effect with low toxicity to normal cells. Moreover, these compounds inhibited the biofilm formation, thus assisting the delay in development of drug resistance.[57]

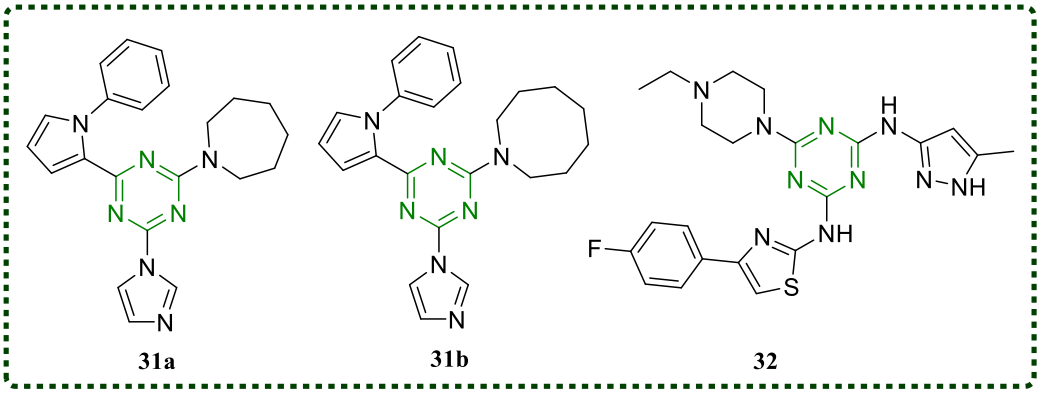

Xia and co-workers designed and synthesized new hybrids of triazine, thiazole and pyrazole and evaluated for their antibacterial activity against *E. coli.* These compounds were also examined for their potential to inhibit DNA gyrase. The results inferred that compound **32** showed the promising results in inhibiting the growth of *E. coli* and DNA gyrase. Antibiofilm property of compound **32** was also examined towards resistant *E. coli,* isolated clinically from urinary infected patients (CREC81, CREC106, CREC163). *In vivo* antibacterial properties were also examined in mice infected with CREC106 strains and the results revealed that the compound significantly decreased the bacterial load in infected mice comparable to standard drug novobiocin.[58]

Maliszewski *et al.* designed and prepared a novel series of 1,3,5 triazine conjugates and subjected to screen antibacterial properties against several bacterial strains. Initial assessment disclosed that compounds **33a** and **33b** displayed the broad-spectrum antibacterial activity towards the tested strains with bactericidal effect. Mechanistic studies inferred that these compounds efficiently inhibited the *S. aureus* and *E. coli* DNA gyrase, hindered the DNA relaxation process and inhibited the bacterial growth. Pharmacokinetic studies revealed that these active compounds exhibited drug-likeness properties and are safe to use. These experimental results were also supported by docking studies.[59]

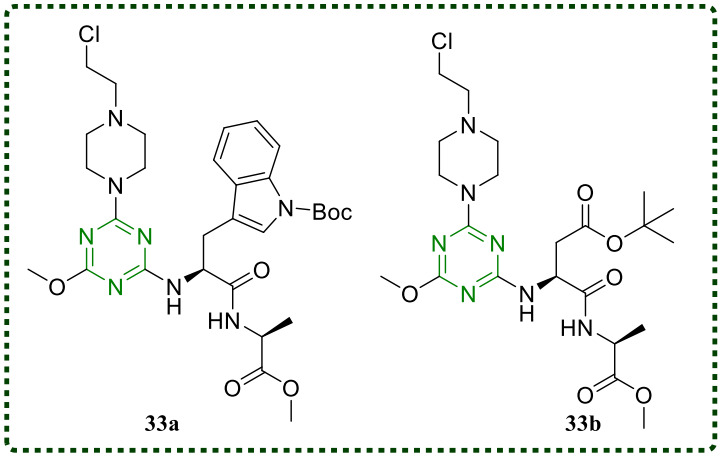

Chapter 2

Materials and Experimental Protocols

This chapter elaborates the protocols used for various assays carried out during present studies. The chemicals and solvents used in the present work are also incorporated briefly in this chapter.

2.1 Materials

The chemicals and solvents used are formulated as follows:

2.1.1 Chemicals

Chemicals	**Make**	**Chemicals**	**Make**
Acenaphthene	Loba Chemie	Triethyl orthoformate	Spectrochem
N-bromo succinimide	Loba Chemie	Ammonia	Loba Chemie
Potassium dichromate	Loba Chemie	Sodium bicarbonate	Spectrochem
Potassium carbonate	Loba Chemie	Tris HCl	Loba Chemie
Propargyl bromide	Spectrochem	Potassium chloride	Loba Chemie
Allyl amine	Spectrochem	Resazurin	High Media
Copper iodide	Loba Chemie	Crystal violet	Loba Chemie
Triethyl amine	Loba Chemie	Follin's reagent	High Media
Hydrazine hydrate	Loba Chemie	Ethidium bromide	High Media
Morpholine	Loba Chemie	D-Glucose	Spectrochem
Cyanuric chloride	Spectrochem	Hepes buffer	Loba Chemie
Palladium (II) acetate	Merck	Sodium sulphate	Loba Chemie
Bis(triphenyl)phosphine palladium (II) chloride	Spectrochem	*N*-Phenyl-1-naphthylamine	Avra
N,*N*-diisopropylethylamine	Spectrochem	Sulphuric acid	Loba Chemie

Sodium azide	Loba Chemie	Nitric acid	Loba Chemie
Tetrakis(triphenylphosphine) palladium (0)	Merck	Sodium hydrogen orthophosphate	Avra
7-Hydroxy-4-methylcoumarin	GLR Inovations	Sodium dihydrogen orthophosphate	Avra
Epichlorohydrin	Loba Chemie	Silica gel (60-120)	Loba chemie
o-Phenylene diamine	Loba Chemie	Silica gel GF 254	Spectrochem

2.1.2 Solvents

Solvents	**Make**	**Solvents**	**Make**
Isopropyl alcohol	Loba Chemie	Ethyl acetate	Rankem
Ethanol	China make	Dimethyl sulphoxide	Loba Chemie
Chloroform-d_3	Sigma Aldrich	*N*,*N*-Dimethyl formamide	Loba Chemie
Acetic acid	Loba Chemie	Glutaraldehyde	Spectrochem
Pyridine	Loba Chemie	Trifluoroacetic acid	Spectrochem
Chloroform	Rankem	Diethyl ether	Loba Chemie
Hexane	Rankem	Acetonitrile	Spectrochem
Methanol	Rankem	Dimethyl sulphoxide-d_6	Sigma Aldrich

2.2 Experimental Section

2.2.1 General procedure for synthesis

All the reactions were set in a clean and oven-dried round bottom flask. Silica plates coated with silica gel GF-254 were used for monitoring the reaction. The mobile phase was chosen depending on the polarity of the various synthesized compounds. In general, mixture of hexane-chloroform and chloroform-ethylacetate were used as mobile phases to run the TLC plates,

which were visualized under UV light (254 nm or 365 nm) or I_2 staining. On completion of the reaction, the required products were filtered out or extracted using an organic-aqueous layer. Further, the compounds were purified by column chromatography using silica (60-120 mesh).

2.2.2 Characterization of compounds

JEOL ECS-400MHz spectrophotometer was used to record the ^{1}H NMR and ^{13}C NMR of the synthesized compounds where ^{1}H NMR and ^{13}C NMR were recorded at 400 MHz and 100 MHz, respectively. TMS was used as an internal reference, and the chemical shifts were indicated in parts per million. The deuterated solvents $CDCl_3$ and DMSO-d_6 displayed residual peaks at 7.26 ppm and 3.33 or 2.50 ppm, respectively. In some cases, to dissolve compounds, TFA was used with $CDCl_3$ or DMSO-d_6. HRMS was recorded on XEVO G2-XS QTOF spectrometer of WATERS using an electron spray ionization technique. Thermo Scientific (Flash 2000) analyzer was used for CHN analysis. UV-Visible spectrophotometer (Shimadzu), Fluorescence spectrophotometer (Agilent Technologies), time-resolved spectrophotometer (Horiba), and Circular Dichroism (Jasco) were used to investigate the bindings of compounds with HSA and DNA.

2.3 *In vitro* anticancer activity

The human tumor cell lines of cancer screening panel were grown in RPMI 1640 medium containing 5% fetal bovine serum and 2 mM L-glutamine. Cells were inoculated into 96 well microtiter plates in 100 ml at plating densities ranging from 5,000 to 40,000 cells/well, depending on the doubling time of individual cell lines. The microtiter plates were then incubated at 37 ºC, 5% CO2, 95% air, and 100% relative humidity for 24h.

After 24h, two plates of each cell line were fixed *in situ* with TCA to represent a measurement of the cell population for each cell line. Experimental drugs were solubilized in DMSO at 400-fold the desired final maximum test concentration and stored frozen prior to use. At the time of drug addition, an aliquot of frozen concentrate was thawed and diluted to twice the desired final maximum test concentration with a complete medium containing 50 µg/ml gentamicin. Additional four, 10-fold or ½ log serial dilutions were made to provide a total of five drug concentrations plus control. Aliquots of 100 μl of these different drug dilutions were added to the appropriate microtiter wells, resulting in the required final drug concentrations. Following drug addition, the plates were incubated for an additional 48h at 37 ºC, 5% CO_2, 95% air and 100% relative humidity. For adherent cells, the assay was terminated by the addition of cold TCA. Cells were fixed *in situ* by the gentle addition of 50 μL of cold 50%

(w/v) TCA and incubated for 60 min at 4 ºC. The supernatant was discarded, and the plates were washed five times with tap water and air-dried. Sulforhodamine B (SRB) solution (100 μL) at 0.4% (w/v) in 1% acetic acid is added to each cell, and plates were incubated for 10 min at room temperature. After staining, unbound dye was removed by washing five times with 1% acetic acid, and the plates were dried and then subsequently solubilized with 10 mM trizma base, and the absorbance was read on the automated plate reader at a wavelength of 515 nm. Using the seven absorbance measurements [time zero (T_z), control growth (c), and test growth in the presence of drug at five concentration levels (Ti)], the percentage growth is calculated at each of the drug concentration levels. Percentage growth inhibition is calculated as: $[(T_i-T_z)/(C-T_z)] \times 100$ for concentration for which $T_i \geq T_z$; $[(T_i - T_z)/T_z] \times 100$ for concentration for which $T_i < T_z$. Three dose-response parameters were calculated for each experimental agent. Growth inhibition of 50 % (GI_{50}) was calculated from $[(T_i - T_z)/(C-T_z)] \times 100 = 50$. The drug concentration resulting in total growth inhibition (TGI) was calculated from $T_i = T_z$. The LC_{50} was calculated from $[(T_i - T_z)/ T_z] \times 100 = 50$.

Anticancer activities were evaluated against 60 human cancer cell lines at NCI, USA. These cancer cell lines are: panel (cell lines); Leukemia (CCRF-CEM, HL-60(TB), K-562, MOLT-4, RPMI-8226, SR), Non-small cell lung cancer (A549/ATCC, EXVX, HOP-62, HOP-92, NCI-H226, NCI-H23, NCI-H322M, NCI-460, NCI-522), Colon cancer (COLO 205, HCC-2998, HCT-116, HCT-15, HT29, KM12, SW-620), CNS cancer (SF-268, SF-295, SF-539, SNB-19, SNB-75, U251), Melanoma (LOX IMVI, MALME-3M, M14, MDA-MB-435, SK-MEL-2, SK-MEL-28, SK-MEL-5, UACC-257, UACC-62), Ovarian cancer (IGROVI, OVCAR-3, OVCAR-4, OVCAR-5, OVCAR-8, NCI/ADR-RES, SK-OV-3), Renal cancer (786-0, A498, ACHN, CAKI-1, RXF 393, SN12 C, TK-10, UO-31), Prostate cancer (PC-3, DU-145) and Breast cancer (MCF7, MDA-MB-231/ATCC, HS 578T, BT-549, T-47D, MDA-MB-468).

2.4 MTT assay

Human embryonic kidney (Hek293) cells were cultured in DMEM with 10% FBS, 50 mM glutamine, 100 mg/ml streptomycin, and 100 U/ml penicillin. Cells were seeded in two 96 well plates at the density of 1×10^{-5} cells/well in DMEM media supplemented with 10% FBS cells. Cells were incubated at 37 °C in a 5% CO_2 incubator. Cells were treated with active compounds at five concentrations (10^{-4}, 10^{-5}, 10^{-6}, 10^{-7}, 10^{-8} M) at 37 °C for 48 h. 10 μl of MTT (prepared in 1* PBS buffer) from 5 mg/ml stock was added in each well and incubated at 37 °C for 4h in dark. The formazan crystals were dissolved

using 100 μl of DMSO. Further, the amount of formazan crystal formation was measured as the difference in absorbance by Bio-Tek ELISA plate reader at 570 nm reference wavelength. All experiments were independently performed at least three times. The relative cell toxicity (%) related to control wells containing culture medium without test material was calculated using the following formula (Eq. (1))

$$\%\ \boldsymbol{Cell\ Toxicity} = \mathbf{100} - \frac{\boldsymbol{OD\ (compound\ treated\ wells)}}{\boldsymbol{OD\ (untreated\ wells)}} \times \mathbf{100} \qquad (1)$$

2.5 Antibacterial activity

Minimal inhibitory concentration (MIC, μg/mL) is defined as the lowest concentration of target compounds that ultimately inhibit the growth of bacteria, using a standard two-fold serial dilution method in 96-well micro test plates according to the National Committee for Clinical Laboratory Standards (NCCLS). The tested bacterial strains were purchased from the Institute of Microbial Technology (IMTech), Chandigarh. Chloromycin, tetracycline, and amoxicillin were used as control drugs. DMSO was inoculated with bacteria having no medicine as a positive control to check the effect of solvent bacterial growth. All the bacterial growths were monitored visually and spectrophotometrically, and the experiments were performed in triplicate.

2.5.1 Antibacterial assays

The synthesized compounds were examined for their antibacterial activities against four Gram-positive bacteria *viz* (*Staphylococcus aureus (*MTCC No-902), *Enterococcus faecalis* (MTCC No-6845), *Bacillus subtilis* (MTCC No- 441), *Listeria* (MTCC No- 4214) and four Gram-negative bacteria such as *Escherichia coli* (MTCC No-448), *Salmonella enterica* (MTCC No-1165), *Acinetobacter calcoaceticus* (MTCC No-1948), *Serratia marcescens* (MTCC No-2645). The bacterial suspension was adjusted with sterile saline to a concentration of 1×10^5 CFU/mL. The stock solutions were prepared by dissolving compounds in DMSO. The compounds and reference drugs were prepared in nutrient broth by two-fold serial dilution to obtain the required concentrations of 800, 400, 200, 100, 50, 25, 12.5, 6.25, 3.125, 1.56 μg/mL. These dilutions were inoculated and incubated at 37 ºC for 24h.

2.5.2 Minimal bactericidal concentration assay

The broth microdilution assay determined minimal bactericidal concentrations (MBC) of active compounds against *S. aureus*, *E. faecalis* and *E. coli*. These compounds were 2-fold serially

diluted and incubated with bacterial strains in a 96-well plate according to the procedure outlined for MIC determination. After 24 h incubation period, 50 μl of the suspension from microwell plate was plated onto tryptic soy agar (TSA). The lowest concentration with no visible growth on the scale was considered the MBC value.

2.5.3 Time-kill assay

S. aureus, E. faecalis and *E. coli* cells were incubated with active compounds at different concentrations (1/4 MIC, 1/2 MIC, MIC, 2 MIC, 4 MIC, 8 MIC) in a 96-well plate at 37 ˚C. The absorbance values of untreated and treated cells were recorded for 6h at an interval of 30 min, using an Elisa plate reader (Biotek, Power-Wave XS2). The decrease in value of absorbance was noted.

2.5.4 Multi-drug resistance passage assay

After determining the MIC values, multiple passaging was performed by transferring bacterial suspension grown at sub-MIC. After the growth of *S. aureus, E. faecalis* and *E. coli*, new MIC values were calculated towards each passage of the strain; tetracycline, chloromycin and amoxicillin were taken as controls. The experiment was continued for 20-25 days.

2.5.5 Antibiofilm assay

The respective bacterial suspension was incubated with active compounds at different concentrations in a 96-well plate for 72h at 37 ˚C. The culture supernatant was discarded, and the sediment was washed with phosphate buffer. Then the plate was incubated for 1h at 60 ˚C to fix the biofilm. After incubating for 1h, crystal violet dye (0.1%) was added for staining culture for 1h at room temperature. The excess dye was discarded and then rinsed with distilled water. Finally, 33% acetic acid was used to elute the stained biofilm. The absorbance was noted at 600 nm in a microplate reader.

2.5.6 Outer membrane assay

The grown bacterial cultures were harvested at 3500 rpm for 5 – 10 min, washed, and suspended in a mixture of 5 mM glucose and 5 mM Hepes buffer (1:1) at pH 7.2 to give a value of 10^6 CFU/ml. 150 μL of bacterial suspension was transferred to 96 well plates and 50 μL NPN (*N*-phenyl-1-naphthalene) dye (10 μM) was added to the well, and the plate was incubated for 1 h. Fluorescence intensity was measured using a fluorescence spectrophotometer at an excitation wavelength of 350 nm and emission wavelength of 420 nm for 30 min (control

group). Further, compounds were added, and the intensity of fluorescence was noted at various concentrations (1/4, 1/2, 1, 2, 4, 8 × MIC) under same conditions. Dimethyl sulfoxide was used as a negative control, and experiments were repeated in triplicates.

2.5.7 Inner membrane assay

The grown bacterial cultures were harvested at 3500 rpm for 5 – 10 min, washed, and suspended in a mixture of 5 mM glucose and 5 mM Hepes buffer (1:1) at pH 7.2 to give a value of 10^6 CFU/ml. 150 μL of this bacterial suspension was transferred to 96 well plates, and 50 μL ethidium bromide (EtBr) dye (10μM) was added to the well, and the plate was incubated for 30 min. Fluorescence intensity was measured using fluorescence spectrophotometer at an excitation wavelength of 520 nm and emission wavelength of 610 nm for 30 min (control group). Further, compounds were added, and the fluorescence intensity was noted at various concentrations (1/4, 1/2, 1, 2, 4, 8 × MIC) under the same conditions. Dimethyl sulfoxide was used as a negative control, and the experiment was repeated in triplicates.

2.5.8 Protein leakage assay

The grown culture of bacteria was incubated with increasing concentrations of various compounds (1/4, 1/2, 1, 2, 4, 8 ×MIC) for 24h. Then, the mixture was centrifuged at 3500 rpm for 10 min, and the supernatant was collected. The concentration of leaked protein in the supernatant was determined by standard follin assay.

2.5.9 Metabolic activity

The bacterial culture was treated with increasing concentrations of various compounds for 6h at 37 ºC. The untreated and treated cells were incubated with resazurin dye (50 μg/ml, 25 μl) for 1h at 37 ºC, and then the absorbance was measured at 570 nm on an Elisa plate reader. The average % reduction was used to determine the metabolic activity.

2.5.10 Reactive oxygen species (ROS) generation assay

Intracellular ROS was measured using a standard 2,7-dichlorofluorescein diacetate (DCFH-DA) assay. 10^6 CFU/mL of bacterial cells were treated with increasing concentrations of compounds for 6h at 37 ºC. Following treatment, both control and treated cells were harvested and washed with PBS, followed by incubation with 100 μM DCFH-DA probe for 30 min in dark at 37 ºC. The fluorescence originating from the oxidative cleavage of DCFH-DA to DCF

was measured with a fluorescence spectrophotometer with an excitation wavelength of 485 nm and an emission wavelength of 528 nm.

2.5.11 Glutathione assay (GSH)

The activity of intracellular GSH was determined using a standard Ellman's assay. The bacterial suspensions (~10^5 CFU/mL) were treated with increasing concentrations of compounds for 6h at 37 ºC. Both control and treated cells were centrifuged at 5000 rpm for 5 min, washed with PBS, and lysed. The clear supernatant was collected. Then, the Tris-HCl (50 mM) and 5,5-dithiobis (2-nitrobenzoic acid) (DTNB) (100 mM) were added and incubated for 30 min in dark at 37 °C. The resulting solution was measured at 412 nm by spectrophotometry (eq 2).

$$\left(1 - \frac{\text{OD@412 nm of treated}}{\text{OD@412 nm of control}}\right) \times 100 \qquad (2)$$

2.5.12 Lipid peroxidation assay

Malondialdehyde (MDA) is a natural product of lipid oxidation in organisms. Some aliphatic acids are gradually decomposed into complex compounds after oxidation, including MDA. Therefore, the level of lipid oxidation can be detected by detecting the level of MDA. The bacterial suspensions (~10^5 CFU/mL) were treated with increasing concentrations of compounds for 4h at 37 °C. Under the dark condition, trichloroacetic acid (TCA) was added to stop the reaction and then 0.5% thiobarbituric acid was added. The mixture was heated at 80 °C for 0.5 h. After cooling the mixture, both control and treated cells were centrifuged at 5000 rpm for 5 min, and then collected the supernatant and tested by a microplate reader at 535 nm.

2.5.13 Scanning electron microscopic (SEM) studies

The bacterial culture was centrifuged at 3500 rpm for 5 min, and the supernatant was discarded. The bacteria cells were washed with PBS and re-suspended with PBS. The bacterial suspension was incubated with compound (2 × MIC) for 6h at 37 ˚C, centrifuged at 3500 rpm for 5 min, then washed thrice with PBS. The cells were fixed with 2.5% glutaraldehyde overnight at 4 ˚C, washed with PBS buffer, and dehydrated with different concentrations of ethanol (45, 55, 65, 75, 95, and 100%). Then, the pellet was transferred to a silicon chip and dried. The samples were coated with gold and visualized under a scanning electron microscope.

2.6 Sample preparation for DNA and HSA

The stock solutions of compounds were prepared in DMSO, whereas the stock solution of HSA (10^{-3} M) was prepared in distilled water and was diluted to the required concentration using a phosphate buffer solution. To prepare the stock solution of ct-DNA, tris buffer (10 mM) of pH 7.4 containing 1mM EDTA was used at room temperature and stored at 4 °C for 24 h before use. The absorbance ratio at 260 nm and 280 nm was calculated to determine the purity of DNA solution. The concentration of DNA solution was calculated from the extinction coefficient of a single nucleotide (6600 M^{-1} cm^{-1}) at 260 nm.

2.6.1 Preparation of oligonucleotide (G4-DNA)

In our study, we have used Pu-27 (wild-type) 5- T GGGG A GGG T GGGG A GGG TGGGG AA GG-3 sequence. The oligos were incubated at 95 ℃ for 5 mins in 50 mM Tris-HCl and 100 mM KCl at pH 7.4; the samples were rapidly cooled for 30 mins on ice and preserved overnight at 37 ºC, aiming the formation of a stable G-quadruplex structure. The above-mentioned buffer was used for all the experiments with DNA quadruplex.

2.6.2 UV-visible studies protocols

A buffer solution having *p*H 7.4 was used to record the absorption spectra. For the DNA study, all the UV-visible spectra of various compounds at a concentration of 5 μM were noted with increasing concentrations of ct-DNA and G4-DNA. In the case of the HSA study, all the absorption spectra were recorded by taking HSA (7 μM) in phosphate buffer with incremental additions of various compounds. A 200-800 nm wavelength was used to record the absorption spectra using reference and cuvettes of 1 cm path length was used. The baseline was corrected using phosphate buffer in case of ct-DNA, HSA and Tris-HCl buffer in case of G4-DNA. The titrations were carried out until no further changes were observed in the spectrum, indicating that saturation had been attained in the binding process. Absorption data was used to determine the binding constant (K_b) by applying the Bensei-Hildebrand equation (Eq. 3)

$$\frac{A_0}{(A-A_0)} = \frac{\varepsilon_f}{(\varepsilon_b - \varepsilon_f)} + \frac{\varepsilon_f}{(\varepsilon_b - \varepsilon_f)\, K_b\, [Analyte]} \qquad (3)$$

A_o is the absorbance value of compounds / HSA in a free state, whereas A denotes the absorbance value of the fully bound form of HSA with compounds (HSA study) or bound form of compounds with ct-DNA and G4-DNA (DNA study). ε_f and ε_b are the molar extinction coefficients of compounds/HSA in the absence and presence of the

analyte, respectively. The binding constant (K_b) values were calculated from the ratio of intercept to the slope of plot [A_0/ (A-A_0) *vs.*1/Analyte].

2.6.3 Fluorescence studies

All the emission spectra were recorded in phosphate buffer and Tris-HCl buffer having *p*H 7.4 from 200-800 nm wavelength range. For G4-DNA and ct-DNA studies, all the fluorescence emission spectra of compounds at 5 μM were recorded with progressive addition of G4-DNA and ct-DNA. For HSA study, all the emission spectra were noted by taking HSA (10 μM) with increasing concentrations of compounds at 298 K. Stern-Volmer equation (eq. 4) and modified Stern-Volmer equation (eq. 5) were employed to calculate the binding constants K_{sv} and K_q. The emission data were corrected by the inner filter effect using equation 5.

$$\frac{Fo}{F} = 1 + K_{sv}[\text{Analyte}] = 1 + K_q\tau_o[\text{Analyte}] \qquad (4)$$

$$\log\frac{F_0-F}{F} = \log K_b + n\log[\text{Analyte}] \qquad (5)$$

F_o is the emission intensity of compounds/HSA in free form, F is the intensity of compounds/HSA in their bound state with ct-DNA and G4-DNA/compounds respectively. The quenching constant values (K_{sv}) were calculated from the ratio of slope-to-intercept of F_o/F and [analyte] plots. To calculate the value of the quenching rate constant (K_q), average value of fluorescence lifetime was used. The binding constant (K_b) and the number of binding sites (n) were calculated from the slope and intercept of the log [(F_o-F)/F] and log [Analyte] plot. The thermodynamic parameters were depicted from equations 6

$$\Delta G = -2.303RT\log K_c \qquad (6)$$

R is the gas constant, and T is the temperature (K).

2.6.4 Competitive displacement studies

Competitive displacement studies were carried out with incremental additions of compounds to complexes of EtBr-DNA and EtBr-G4-DNA. The titrations were performed in phosphate buffer having a pH of 7.4. The emission spectra were noted with a fixed amount of EtBr and ct-DNA (3 μM: 30 μM) with increasing concentrations of compounds. The emission spectra were noted in the 200-800 nm wavelength range using 520 nm as excitation wavelength.

2.6.5 Circular dichroism

An applied photophysical CD spectrophotometer was used to record the CD spectra of free ct-DNA and compound-ct-DNA; the temperature was maintained at 25 °C by the Peltier temperature controller. The spectra were recorded in wavelengths ranging from 220 nm to 400 nm. The spectrum was recorded in phosphate buffer *p*H = 7.4 at room temperature. Each spectrum has been recorded with an average of 3 scans. The spectrum obtained was then subtracted from the background spectrum of the buffer solution.

2.6.6 DNA melting studies

A UV-visible spectrophotometer fitted with a paltier was used for carrying out the DNA thermal denaturation experiment. The experiment was carried out by recording the absorbance of free ct-DNA at 260 nm in a 1 ml cuvette. The absorbance of free ct-DNA was recorded from 25 ºC to 100 ºC at an interval of 5 ºC. The experiment was repeated for a complex of DNA with compounds. Then, the graph between free ct-DNA versus temperature was plotted and the graph between DNA-compound complex versus temperature was plotted at 260 nm. The melting temperature (T_m) was calculated from the curve using the curve transition midpoint, and T_m was determined for both systems i.e. for free ct-DNA as well as DNA-compound complex. T_m is the temperature at which 50% of the DNA is denatured.

2.6.7 DNA damage assay

The standard procedure was followed for DNA damage. Lung cancer cells (A549) were incubated with compound at 37 ˚C for 6h followed by trypsinization. After incubation, the cells were washed with phosphate buffer, 40 μL of cells suspension and 140 μL of 0.1% low melting agarose were mixed and 150 μL pipetted on to comet slide and covered with a coverslip. The slide was kept in the refrigerator at 4 ºC for 10 min to allow the gel to settle. Upon removing the cover slip, the slide was immersed in lysis buffer for at least 1h. The slide was transferred to an electrophoresis buffer and immersed for at least 30 minutes at 4 ˚C. The slide was electrophoresed at a low voltage of 25 V for 25 min to allow the movement of damaged DNA. Finally, the slide was placed in a neutralization buffer for 10 min and then washed with distilled water. The staining of the slide was done with ethidium bromide solution and the results were depicted with the help of Raman images (make Horiba, France, model Labram HR Confocal Micro-Raman Spectrometer)

2.6.8 Time-resolved studies

Horiba Deltaflex Modular fluorescence lifetime spectrofluorimeter was used to examine the Time-resolved measurements of HSA, G4-DNA, and compound complexes. The spectra were recorded by fixing the concentration of HSA (7 μM) with varying concentrations of compounds. The spectra were recorded in phosphate buffer at *p*H = 7.4 at an emission wavelength of 330 nm. Whereas in the case of G4-DNA, the concentration of compounds was fixed at 5 μM, and G4-DNA was added to the system to record the spectra in Tris HCl buffer.

2.6.9 Dynamic light scattering experiment

The DLS analysis G4-DNA with/without compounds were performed on Zetasizer Nano ZEN3600 DLS (Malvern Instruments, Malvern, UK) with He–Ne laser (633 nm) and at 90º scattering angle. DLS measures the hydrodynamic diameter of G4-DNA, where the position and width of DLS peak provide the average hydrodynamic diameter (Z-average) and dispersion of the sample. The measurements were carried out in a quartz cuvette at 25 ◦C after providing 2 min sonication to the sample.

2.6.10 Zeta potential studies

The surface charge of free G4-DNA and in presence of compounds were determined through zeta potential measurements, which were also carried out on Zetasizer Nano ZEN3600 DLS (Malvern Instruments, Malvern, UK). The prepared solutions were directly used without any dilution for Zeta potential measurements. For analysis, the sample was injected into two capped folded capillary cells at room temperature with an applied voltage of 100V. The sample was analysed with triplicate measurements and the analysis time was 60s.

2.7 Quantum chemical studies

The 3D structure of synthesized compounds was built in by Gauss view. Gauss 09 was used to perform the quantum mechanics optimization for the molecules, and they were optimized with DFT calculation using the B3LYP and standard 6-31G(d) basis set. Finally, the cubegen module in the chemcraft was used to get HOMO and LUMO plots.

2.8 Molecular docking studies

Molecular dockings of all the compounds with DNA (PdB: 1BNA, 1XAV) were carried out using AutoDock package (vina). In the preparation of target (ct-DNA, G4-DNA), water

molecules were deleted, whereas all polar hydrogens were added to the target, then calculated gasteiger charges. The 3D structure of all the compounds were optimized using the Gaussian 09W program and the results from the file were saved as pdb format. The ADT package was used to modify the partial changes of the ligand and the resulted file was saved as pdbqt format. A grid having spacing 0.375 Å and pointing 44 Å, 78 Å, 106 Å in x, y, and z directions, respectively were used.

Chapter 3

Bis-naphthalimide conjugates and their biological evaluation

1 Introduction

Naphthalimide, a flat π-electron deficient heterocyclic pharmacophore, has been well exploited for decades because of its diverse biological activity, such as antifungal, anticancer, antibacterial, antiviral, and antiherpetic.[60] Few of the naphthalimide derivatives have reached clinical trial phase I, but failed due to serious side effects, and neurotoxicity.[61] Over the years, researchers have put efforts into designing and synthesizing new conjugates of naphthalimide by modifying its structure or by combining with another biologically active moiety to reduce the side effects and improve the bioactivity of compounds.[62] Combining two naphthalimides, i.e., synthesis of bis-naphthalimide, is an effective approach to improve the activity, efficiency, DNA binding properties, and selectively of the naphthalimides.[63] In general, bis-naphthalimide derivatives displayed better activity than monomeric conjugates. In addition, bis-naphthalimide also exhibited elevated DNA binding ability as it contains two intercalating units and is a fundamental area for research in DNA intercalators.[64] Elinafide and bisnafide, two bis-naphthalimides, showed promising bioactivity and have entered phase I clinical trials, thus revealing its significance in the research area in building more bis-naphthalimides. The bioactivity, photophysical, and DNA binding properties of bis-naphthalimide mainly depend upon the linker between the two naphthalimide units and substitution at naphthalimide skeleton.[61] The bis-naphthalimide derivatives are mainly constructed by polyamine spacers, as these have crucial role in cell growth expansion and biosynthetic pathways.[65] A number of bis-naphthalimides with different polyamine linkers have been synthesized and explored for their anticancer activity.

Till date, very few reports on the synthesis of bis-naphthalimide with an alkyl spacer and without any spacer have been reported. Moreover, the antibacterial properties of bis-naphthalimides have not been explored to date. This chapter describes the synthesis of two different types of bis-naphthalimide conjugates with and without spacers and their biological evaluation as anticancer and antibacterial agents. Therefore, the chapter is divided into two subsections that describe the effect of spacer on the bioactivity of bis-naphthalimide.

3.1 Alkyl chain bearing bis-naphthalimides as potent anticancer agents.

3.2 Bis-naphthalimides without spacer as potent antibacterial agents.

Sub Chapter 3.1

Alkyl chain bearing bis-naphthalimides as potent anticancer agents

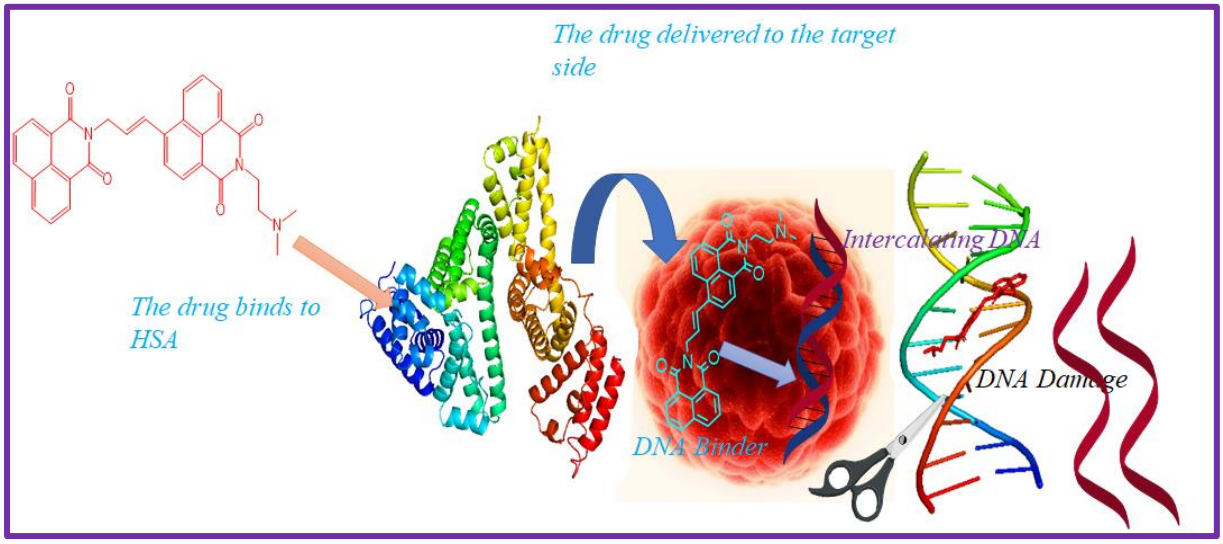

3.1.1 Introduction

Nowadays, cancer has emerged as a serious health issue among people, and it is the second highest cause of death around the globe.[66] Cancer is caused due to unchecked cell growth and cell division of healthy cells.[67] Cancer reports depicted that by 2040, there will be about 27.5 million new cancer cases worldwide.[2]The available anticancer drugs develop genotoxicity and cytotoxicity towards normal cells, leading to the main issue in treating cancer.[68-6]

[9] DNA is the main target of chemotherapeutics as it plays a crucial role in uncontrolled cell division and growth.[70] DNA synthesis is blocked or damaged by these anticancer agents, thus accountable for disrupting hormonal stimulation of average cell growth and inhibiting the biosynthesis of nucleic acid precursors.[71] Even after years of research in medicinal chemistry, none of the available drugs could successfully cure cancer due to the development of resistance by cells towards available narcotics, ill effects, and low-margin safety.[72] So, there is a need to develop anticancer drugs with low cytotoxicity towards normal cells and can cure cancer with fewer side effects.[73] The designing of an effective anticancer agent with better selectivity for cancer cells can be achieved by targeting DNA-associated mechanisms.[74] In the current research, bis-naphthalimide having polyamine as space linker is important as polyamine plays a crucial role in cell growth.[75] Few derivatives, such as elinafide and bisnafide, have reached clinical trials, but due to side effects and the development of resistance toward cancer cells, these have limited their use.[76]

3.1.2 Designing of bis-naphthalimide conjugates

Bis-naphthalimide derivatives such as elinafide and bisnafide, with promising anticancer activity, have reached clinical trial phase I, but due to serious side effects caused by these conjugates, these have failed in clinical trial phase II. Modification in the structure of elinafide can help in building new anticancer agents with fewer side effects and can be taken to clinical trials for further development as potent antitumor agents.

In this sub-chapter, we have developed a novel series of bis-naphthalimide with alkyl spacers between them. The target molecules were designed by modifying elinafide molecule in which the polyamine chain linking two naphthalimides was replaced with an unsaturated alkyl chain to provide rigidity to the molecule. We have also reversed the orientation of one of the naphthalimide units to improve their activity (**Figure 3.1**).

The synthesized compounds have been examined *in vitro* for their anticancer activity against 60 human tumour cell lines, and their antibacterial properties were also checked against eight bacterial strains. These compounds were further studied for their interactions with HSA and DNA using UV–visible, fluorescence, and other spectroscopic techniques.

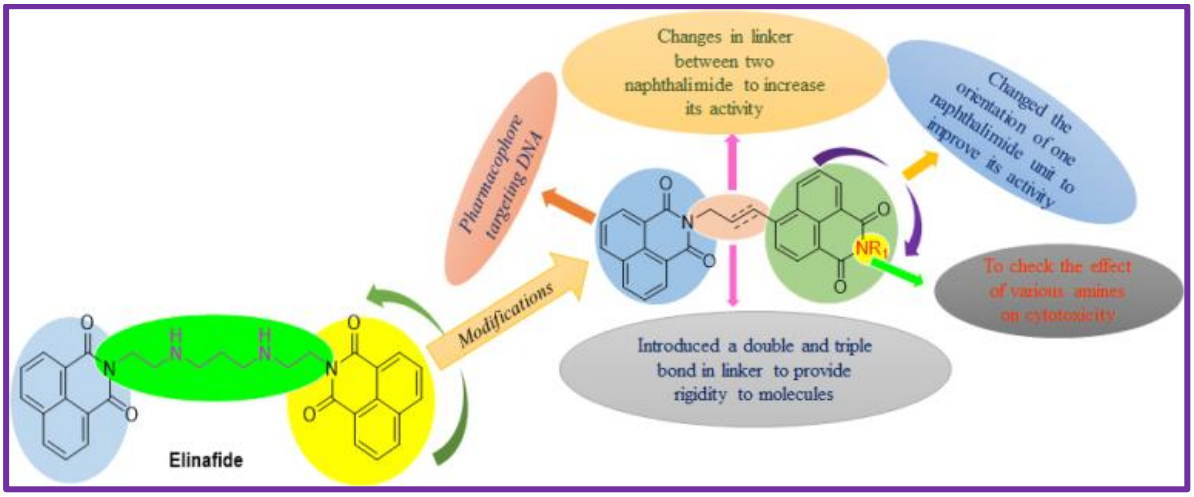

Figure 3.1 Designing of new bis-naphthalimides

3.1.3 Chemistry

The synthetic route adopted for the synthesis of desired bis-naphthalimides is represented in **Scheme 1**. Compound **2** was obtained by oxidation of commercially available acenaphthene (**1**) with sodium dichromate in acetic acid and was further reacted with allylamine in ethanol to obtain **3** in 84% yield. Heck coupling was performed by reacting **3** with 6-bromobenzo[*de*]isochromene-1,3-dione using acetonitrile and Pd(II) acetate to get the compound **4** in 80% yield. The appearance of 1H doublet at δ 7.59 ppm corresponds to CH allyl, 1H doublet of triplet at δ 6.65 ppm of CH allyl, 2H double doublet at δ 5.17 ppm of CH_2 allyl, and an increase of five protons in the aromatic region in ^{1}H NMR spectrum confirmed the formation of compound **4**. The appearance of signals at δ 165.3 ppm due to C=O, signals in the region from δ 135.6 to 110.1 ppm due to aromatic and allylic carbons, and signal at 42.8 ppm of CH_2 in ^{13}C NMR also supported the formation of compound **4.** The mass spectrum indicated the molecular weight of ESI-MS (m/z): $[M]^+$ = 433, further confirming the formation of this compound. Derivative **5a-i** was obtained by reacting compound **4** with different primary amines in ethanol under reflux conditions. ^{1}H NMR spectrum of compound **5a** showed increase in signals due to rings present at naphthalimide. Multiplet at δ 6.01-5.91 ppm of one proton of CH alkene, two doublets at δ 5.31 ppm

and δ 5.20 ppm due to two protons of CH_2 allyl and a 2H doublet at δ 4.79 ppm due to CH_2 allyl confirmed the formation of compound **5a**. The appearance of a new signal at δ 42.0 ppm in ^{13}C NMR spectrum and an increase of molecular weight to ESI-MS (m/z): $[M]^+$ = 472 also confirmed the formation of compound **5a**. Similarly, compound **5b-i** was also characterized by ^1H NMR, ^{13}C NMR, and mass spectrometry.

On the other hand, compound **2** was treated with ammonia solution in the presence of ethanol to obtain compound **6**, which was further reacted with propargyl bromide in potassium carbonate and DMF at 80-90 °C to get **7** in 80% yield. Sonogashira coupling of **7** was performed by the reaction of 6-bromobenzo[*de*]isochromene-1,3-dione in the presence of $Pd(PPh_3)_2Cl_2$, CuI, triethylamine in DMF to obtain compound **8** with 75% yield. The appearance of a 2H singlet at δ 5.42 ppm corresponding to CH_2 propargyl and increase of 5 protons in aromatic region of ^1H NMR spectrum confirmed the formation of compound **8**. The appearance of signal at δ 164.8 ppm due to C=O, signals in the region of δ 135.8 to 110.1 ppm, signals at δ 95.0 ppm of propargyl C and δ 31.1 ppm due to propargyl CH_2 in ^{13}C NMR spectrum confirmed the formation of compound **8**. The mass spectrum indicated that the molecular weight of ESI-MS (m/z): $[M]^+$ = 431, further confirmed the formation of desired compound. The final derivative **9a-i** was obtained by reacting compound **8** with primary amines in ethanol under reflux conditions. The compound **9a** was characterized by ^1H NMR spectroscopy where appearance of multiplet at δ 6.00-5.90 ppm of one proton of CH allyl, 1H multiplet at δ 5.32-5.26 ppm due to CH_2 allyl, 1H double doublet at δ 5.20 ppm due to CH_2 allyl and a 2H double doublet at δ 4.77 ppm due to CH_2 allyl confirmed the formation of compound **9a**. The appearance of a new signal at δ 42.6 ppm in ^{13}C NMR spectrum and an increase of molecular weight to ESI-MS (m/z): $[M]^+$ = 470 also confirmed the formation of compound **9a**. Similarly, compound **9b-i** was characterized by ^1H NMR, ^{13}C NMR, and mass spectrometry. All the products were synthesized in good to moderate yields ranging from 70-90%.

Scheme 1: Synthesis of bis-naphthalimides

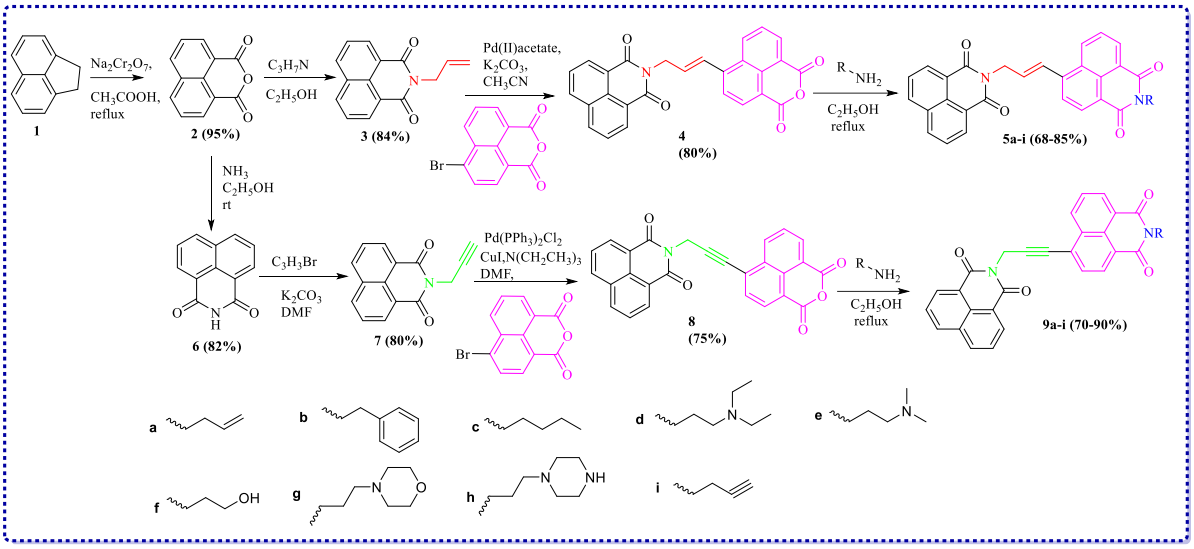

3.1.4. *In vitro* anticancer activity

All the 18 derived derivatives (**5a-i,** and **9a-i**) were selected by the National Cancer Institute (NCI), USA, to evaluate their anticancer properties.[77] The selected compounds were evaluated for their anticancer activity towards 9 different panels of human tumour cell lines (CNS, colon, non-small cell lung, leukemia, renal, breast, melanoma, ovarian, and prostate) comprising 60 different cell lines at a concentration of 10 μM where the percentage growth inhibitions were calculated (**Tables 3.1** and **3.2**).

Table 3.1: Cytotoxicity of derivatives **5a-i** at 10 μM concentration

Panel	5a	5b	5c	5d	5e	5f	5g	5h	5i
Leukemia									
CCRF-CEM	-	3.28	2.39	74.62	**-44.09**	16.66	1.49	3.91	-
HL-60(TB)	-	2.64	0.38	16.60	**87.15**	5.79	-	-	-
K-562	2.94	4.58	5.69	80.33	**-46.82**	20.05	0.39	-	-
MOLT-4	-	4.43	-	37.22	**65.70**	19.99	1.04	4.02	1.35
SR	-	9.49	11.59	61.36	**-16.37**	32.85	7.72	8.11	0.57
Lung Cancer									
A549	2.56	4.41	39.00	1.24	14.69	18.76	3.34	-	2.12
EKVX	4.41	1.16	5.59	-	-	8.51	9.71	1.16	8.09
HOP-62	19.56	2.95	6.64	10.54	11.09	29.49	1.55	9.55	4.52
HOP-92	10.6	11.77	17.09	11.93	5.82	97.91	5.13	9.12	6.56
NCI-H226	-	-	-	7.26	1.26	41.71	11.72	6.89	-
NCI-H23	2.16	2.57	-	1.92	6.22	30.42	4.16	4.72	3.07
NCI-H322M	2.04	5.11	7.38	2.58	15.69	37.11	11.24	11.01	4.23
NCI-H460	0.77	-	-	1.35	6.32	27.17	2.46	-	-
NCI-H522	1.97	3.87	2.08	2.06	-	10.78	3.17	2.74	4.83
Colon Cancer									
COLO 205	-	-	-	19.02	17.9	31.74	4.86	-	9.61
HCC-2998	-	-	-	-	**63.58**	14.34	-	-	-

HCT-116	1.68	-	-	4.46	**90.43**	24.01	11.22	-	8.06
HCT-15	-	-	-	4.23	**-75.33**	24.73	9.94	-	8.04
HT29	-	-	0.11	-	6.04	13.02	-	-	-
KM12	0.11	-	1.40	36.40	**-79.33**	23.81	-	-	-
SW-620	3.71	3.46	1.59	9.56	**88.11**	18.22	9.84	4.03	10.70
CNS Cancer									
SF-268	11.9	0.48	8.79	6.48	-	12.31	-	8.74	3.78
SF-295	-	-	-	-	-	23.46	1.19	-	-
SF-539	12.93	2.94	0.56	7.49	7.21	27.27	1.72	-	-
SNB-19	10.22	-	9.88	4.04	**81.26**	11.99	3.46	3.85	0.91
SNB-75	4.12	8.36	7.84	8.75	9.35	41.38	-	17.17	8.92
U251	-	4.41	1.77	-	9.16	28.92	-	0.26	-
Melanoma									
LOX IMVI	7.67	3.55	7.09	3.39	69.70	12.74	-	7.47	5.26
MALME-3M	-	-	4.23	8.08	**-62.38**	24.52	0.82	0.99	7.62
M14	-	-	1.93	-	22.05	12.19	5.11	-	17.48
MDA-MB-435	-	0.48	0.28	-	10.68	5.56	0.52	0.80	-
SK-MEL-2	-	-	-	-	-	9.33	-	-	-
SK-MEL-28	-	-	-	-	**-56.50**	15.11	-	-	-
SK-MEL-5	-	-	-	5.71	17.82	10.08	-	3.66	-
UAAC-257	-	-	-	-	8.00	20.21	6.36	-	6.95
UAAC-62	9.51	-	3.39	0.23	1.27	8.56	-	-	3.56
Ovarian Cancer									
IGROV1	8.65	-	3.21	9.95	10.65	21.27	7.25	13.37	1.14
OVCAR-3	-	-	-	-	-	12.05	-	-	-
OVCAR-4	-	3.11	-	-	**-5.61**	59.91	-	-	-
OVCAR-5	-	2.91	7.54	5.59	**-69.03**	20.78	-	-	-
OVCAR-8	11.72	0.79	2.07	7.90	**-43.49**	30.44	7.26	5.83	5.15
NCI-RES	4.94	2.94	5.85	0.22	24.03	19.77	-	-	0.13
SK-OV-3	5.63	0.57	1.08	-	18.77	27.71	4.01	3.72	2.08
Renal Cancer									
786-0	-	-	0.30	-9.45	**-84.53**	15.57	1.16	-	0.89
A498	-	15.55	-	22.31	18.62	25.30	21.54	13.31	22.38
ACHN	7.34	-	-	3.17	27.29	65.92	3.23	-	1.22
CAKI-1	41.2	-	19.11	10.95	8.96	36.90	6.59	13.25	6.31
RXF 393	2.09	-	-	25.82	43.04	72.13	2.93	-	-
SN12C	10.71	-	0.58	3.94	20.05	24.31	-	0.49	-
TK-10	-	-	-	-	-	1.31	-	-	-
UO-31	19.03	7.25	12.9	18.01	28.04	21.91	22.02	18.52	23.31
Prostate cancer									
PC-3	7.74	-	10.19	13.39	28.25	48.79	6.10	2.48	5.95
DU-145	-	-	-	-	-	29.61	-	-	-
Breast Cancer									
MCF7	-	3.55	8.65	95.25	**-71.57**	19.94	16.31	4.00	0.14
MDA-MB-231	23.65	-	7.88	4.47	**-57.41**	37.86	2.34	5.85	3.77
HS 578T	9.32	-	-	15.23	**82.62**	38.44	10.33	6.32	12.99
BT-549	1.89	-	-	10.24	3.03	59.68	15.68	-	11.54
T-47D	5.01	5.53	5.57	5.21	2.42	23.32	3.77	-	4.79
MDA-MB-468	1.56	4.85	8.14	0.84	11.05	20.17	6.18	-	-

Table 3.2: Cytotoxicity of derivative **9a-i** at 10 μM concentration

Panel	**9a**	**9b**	**9c**	**9d**	**9e**	**9f**	**9g**	**9h**	**9i**

Leukemia									
CCRF-CEM	2.73	3.76	5.85	79.26	26.73	19.43	4.31	**92.29**	4.81
HL-60(TB)	1.69	-	-	-	2.06	-	2.24	7.04	0.16
K-562	10.91	3.04	-	62.9	29.6	4.89	0.70	**-15.34**	6.87
MOLT-4	1.75	0.08	-	8.71	25.64	37.69	15.13	**93.26**	4.15
RPMI-8826				8.00	4.91	25.51		**91.34**	
SR	4.15	1.66	8.01	-	-	28.59	1.52	**97.77**	3.22
Lung Cancer									
A549	-	1.36	-	-	-	2.74	2.17	-	-
EKVX	3.15	0.46	-	4.57	4.10	23.65	5.86	-	2.55
HOP-62	10.36	4.11	3.55	6.42	13.84	15.55	10.07	-	-
HOP-92	9.38	12.74	11.93	13.05	7.13	13.56	25.03	12.35	10.34
NCI-H226	5.47	-	-	12.34	6.55	8.14	0.32	-	2.19
NCI-H23	4.75	3.31	5.69	4.11	1.93	18.99	11.71	26.32	3.59
NCI-H322M	6.23	4.95	6.00	-	-	5.08	5.68	1.41	3.31
NCI-H460	-	-	-	-	1.13	4.18	-	26.86	-
NCI-H522	0.09	2.19	3.07	1.98	2.97	8.05	1.31	0.16	5.21
Colon Cancer									
COLO 205	-	-	-	-	1.20	-	3.65	6.48	-
HCC-2998	-	-	-	-	-	-	8.28	-	-
HCT-116	2.62	0.97	-	8.61	12.41	21.57	-	**-64.14**	-
HCT-15	1.41	-	-	-	-	17.83	3.64	38.28	-
HT29	-	-	-	-	-	3.52	-	**76.47**	-
KM12	-	0.20	-	-	-	-	-	1.08	-
SW-620	5.53	6.81	4.21	-	12.46	7.81	11.31	**71.66**	2.91
CNS Cancer									
SF-268	6.44	4.98	3.68	8.80	11.81	21.09	16.31	6.17	9.67
SF-295	1.74	-	-	-	-	1.27	-	5.87	1.06
SF-539	4.46	6.51	4.15	2.83	-	9.18	16.66	**89.77**	3.29
SNB-19	7.79	3.61	8.17	-	0.31	3.73	6.24	13.79	4.25
SNB-75	6.99	26.64	36.86	3.37	36.23	30.08	69.8	0.36	6.92
U251	-	1.14	7.42		-	6.89	2.23	43.56	-
Melanoma									
LOX IMVI	8.93	10.03	11.22	9.47	13.59	-	15.66	-	7.13
MALME-3M	4.84	0.57	3.06	6.87	-	-	2.26	**-45.02**	2.79
M14	5.04	2.41	-	-	-	15.19	0.43	-	3.05
MDA-MB-435	-	0.48	-	-	-	7.71	3.98	-	-
SK-MEL-2	-	-	-	-	-	-	-	-	-
SK-MEL-28	-	-	-	-	-	-	-	**86.52**	0.75
SK-MEL-5	2.31	-	0.02	-	-	9.18	3.69	-	-
UAAC-257	-	2.46	-	-	-	5.75	-	-	-
UAAC-62	6.21	0.54	-	-	-	6.89	-	-	5.20
Ovarian Cancer									
IGROV1	7.67	5.22	5.13	-	1.57	51.48	29.01	8.63	-
OVCAR-3	-	-	-	-	-	12.98	5.16	-	-
OVCAR-4	-	-	-	3.16	4.62	7.29	2.64	14.68	-
OVCAR-5	-	8.38	0.58	-	-	-	12.85	7.85	-
OVCAR-8	3.49	4.09	10.24	-	11.05	13.57	2.17	6.13	3.46
NCI-RES	2.65	0.97	-	-	-	8.33	2.14	-	1.42

SK-OV-3	1.97	4.91	8.67	-	-	7.63	15.49	-	0.64
Renal Cancer									
786-0	-	-	-	18.24	3.88	1.95	2.38	**-2.58**	-
A498	-	-	0.38	27.65	6.05	-	42.97	-	5.58
ACHN	5.07	-	4.02	2.36	11.91	1.91	18.71	25.59	5.89
CAKI-1	21.26	10.89	9.48	9.28	21.58	43.23	13.26	17.57	18.96
RXF 393	-	-	-	5.41	13.86	14.88	16.11	17.12	-
SN12C	9.39	1.20	4.13	-	8.14	9.27	5.22	2.81	4.89
TK-10	-	-	-	-	-	-	10.34	-	-
UO-31	23.86	18.51	19.95	9.71	32.86	42.71	28.69	2.32	17.76
Prostate cancer									
PC-3	8.96	3.19	3.64	-	4.43	15.21	-	14.47	6.43
DU-145	-	-	-	-	-	11.44	-	0.54	-
Breast Cancer									
MCF7	3.89	6.23	7.17	13.54	7.80	-	-	**-43.91**	7.99
MDA-MB-231	24.48	-	2.57	-	3.63	33.92	4.94	**92.05**	11.31
HS 578T	0.39	11.61	16.76	-	-	16.72	13.84	-	2.67
BT-549	-	7.28	3.85	-	-	13.58	3.99	-	1.55
T-47D	0.71	5.75	5.78	4.27	3.11	1.78	0.59	**61.72**	-
MDA-MB-468	5.31	-	4.72	-	-	5.82	8.12	-	0.21

All the compounds showed moderate activity, but compounds **5e** and **9h** indicated promising cytotoxic and cytostatic activities compared to other compounds at 10 μM against most of the tested cell lines. Thus, both the compounds satisfied the condition of selection criteria by NCI for further evaluation; therefore, these compounds were studied against 60 human cancer cell lines at five dose concentrations (0.01–100 μM). Evaluation of these derivatives suggested that compounds **5e** and **9h** displayed a broad spectrum of anticancer activity against most tumor cell lines with values of MG-MID GI_{50} of 33.32 and 4.67 μM, respectively (**Table 3.3**). Both analogues exhibited greater efficacy towards melanoma cancer cells, having GI_{50} values of 8.90 and 1.44 μM, respectively. Compound **5e** was inactive against prostate cancer at 10 μM, whereas compound **9h** showed promising results with GI_{50} value of 2.64 μM. Derivative **5e** showed good selection against CCRF-CEM (GI_{50} = 0.33 μM), K-562 (GI_{50} = 0.28 μM) of leukemia cancer, and SK-MEL-28 (GI_{50} = 0.76 μM) of melanoma cancer. Hence, in the series of bis-naphthalimides, compound **9h** displayed more promising results than **5e**. Their results were also compared with two clinical trial drugs such as 5-fluorouracil (NSC: 19893) and amonafide (NSC: 308847). It was observed that derivatives **5e** and **9h** were more active than 5-fluorouracil, whereas **9h** appeared comparable to amonafide toward cancer cell lines.

Table 3.3 GI_{50} (μM), TGI (μM), and LC_{50} (μM) of derivatives **5e** and **9h** for *in vitro* tumor cell lines.

	Activity (μM)	**I**	**II**	**III**	**IV**	**V**	**VI**	**VII**	**VIII**	**IX**	**MG-MID**
5e	GI_{50}	13.2	15.8	56.9	23.9	8.9	19.3	22.7	-	25.6	33.3
	TGI	69.9	27.7	-	23.2	23.9	-	49.6	-	44.1	39.7
	LC_{50}	-	86.4	-	48.0	47.5	-	61.7	-	88.4	66.4
9h	GI_{50}	2.2	7.1	4.0	6.85	1.44	6.5	6.29	2.6	4.7	4.67
	TGI	4.4	21.3	5.7	16.7	15.7	17.8	19.9	7.8	14.3	13.7
	LC_{50}	19.0	34.7	12.3	38.4	36.4	42.2	38.0	24.3	15.3	29.0
A	GI_{50}	1.5	-	8.4	72.1	70.6	61.4	45.6	22.7	76.4	39.8
B	GI_{50}	2.0	3.3	2.9	4.1	3.4	4.2	2.7	2.5	3.9	3.3

Leukemia (I), non-small cell lung (II), colon (III), CNS (IV), melanoma (V), ovarian (VI), renal (VII), prostate (VIII), breast (IX) cancers; MG-MID: the average sensitivity of all cell lines towards the test compound (μM); GI_{50} = concentration for 50% of maximal inhibition of cell proliferation, TGI = concentration of the compound resulting in total growth inhibition, LC_{50} = lethal concentration required to kill 50% of the population; A = 5-Fluorouracil, B = Amonafide

3.1.5. Structure-Activity Relationship (SAR)

From the above-mentioned results, it is observed that compounds bearing allylamine (**5a** and **9a**), benzylamine (**5b** and **9b**), and butylamine (**5c** and **9c**) displayed less activity and were unable to suppress the cancer growth. The introduction of *N*,*N*-diethylethylenediamine in the compounds (**5d** and **9d**) improved activity to some extent; both compounds showed better inhibition effects against leukemia than other tested cell panels. Excellent anticancer activity was observed for **5e** having *N*,*N*-dimethylethylenediamine in its structure against all the tested cancer lines due to restricted rotation of the molecule around double bond and some electron-donating effect of amine, but the same result was not observed for **9e** having same amine substitution as that of **5e** due to free rotation of molecule. The introduction of another amine, such as ethanolamine (**5f** and **9f**) and *N*-(2-aminoethyl) morpholine (**5g** and **9g**), resulted in loss of bioactivity of compounds against tested cancer cell lines. The substitution of *N*-(2-aminoethyl)piperazine in the core structure improved the bioactivity of compound **9h**, which displayed potent anticancer properties against all the tested cancer cell lines. This can be attributed to the free rotation of molecule and also presence of interacting element NH which is capable of building hydrogen bonds with the base pairs of DNA, but the same is not observed for compound **5e** that might be due to restricted rotation of the molecule. Further substituting

compounds **4** and **8** with other amines resulted in loss of bioactivity of the molecules. Hence, the difference in the activity of compounds upon substitution of various amines is related to steric factor, electronic factor, and different interactions with the target sites.

3.1.6 Cytotoxicity toward human normal cell lines

To determine the cytotoxicity of most active compounds **5e** and **9h** against Hek293 non-cancerous human cell lines, the MTT assay was employed. Results depicted that compound **9h** showed only 17%, 14%, 14%, 13%, and 12% cytotoxicity, whereas compound **5e** represented 16%, 13%, 13%, 12%, and 10% cytotoxicity to normal cell lines at the concentrations of 10^{-4}, 10^{-5}, 10^{-6}, $10^{-7,}$ and 10^{-8} M, respectively (**Figure 3.2**). Both compounds having low cytotoxicity values against normal cell lines indicated that these compounds selectively kill the cancer cells.

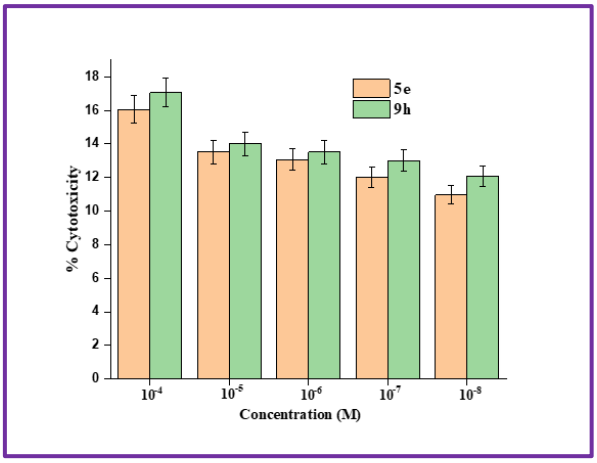

Figure 3.2 Cytotoxic effects of compounds **5e** and **9h** against normal cell line Hek293

3.1.7. DNA binding studies

The design of potent and novel anticancer agents is based on the efficiency of the drug-targeting DNA. Many heterocycles exhibit their properties by binding with DNA or obstructing DNA replication, thus inhibiting the growth of tumour cells. The ability of the target drug to bind with DNA depends mainly on its binding affinity and binding mode (*via* intercalation or groove binding).[78] Binding studies of small conjugates with DNA are the key to building novel anticancer agents.[79] Based on anticancer activity, the interaction of the most potent compounds with DNA was examined by various spectroscopic techniques such as UV-visible, fluorescence, and circular dichroism.

3.1.7a UV-visible studies

Compounds **5e** (5 μM) and **9h** (5 μM) in phosphate buffer (*p*H = 7.4) at room temperature exhibited absorption maxima at 360 nm and 344 nm, respectively. Upon titrating a solution of compounds **5e** and **9h** with an increasing concentration of ct-DNA (0–30 μM), a hypochromic

shift in the absorption band was observed at 360 nm for **5e** and 344 nm for **9h**, thus, revealing the bindings of these derivatives with ct-DNA. The decrease in absorption bands is characteristic of the interaction of both compounds with DNA base pairs (**Figures 3.3a** and **3.3b**). Further, to check the stability of the complex formed between compounds and DNA, and to calculate the binding constants (K_b) for both the compounds **5e** and **9h,** the Benesi-Hildebrand equation was used and were found to be 5.5×10^5 M^{-1} (for **5e**) and 2.4×10^5 M^{-1} (for **9h**).

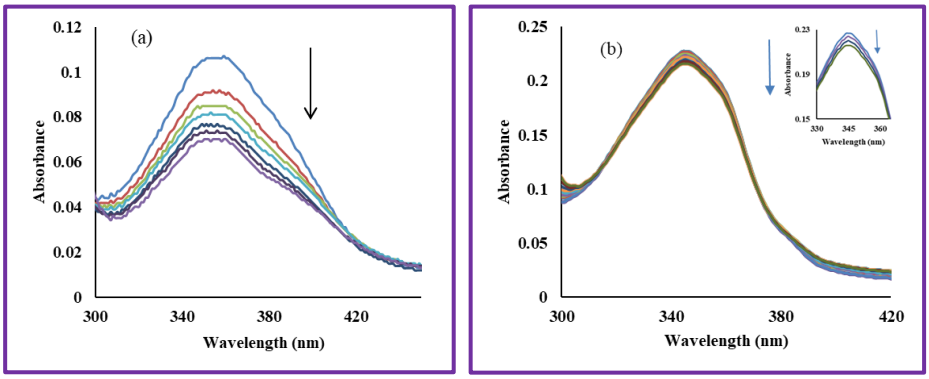

Figure 3.3 Absorption spectra of compounds (a) **5e** and (b) **9h** (5 μM) with increasing concentrations of ct-DNA (0–30 μM).

3.1.7b. Thermal denaturation

The change in conformation of DNA with increasing temperature upon addition of compounds **5e** and **9h** was carried out to get an idea about the interaction's type and strength of binding of compounds with DNA.[80] Thermal denaturation studies were performed for free ct-DNA, revealing the melting temperature of DNA (T_m) is 76 °C. Upon the addition of compound **5e,** the melting temperature of DNA was increased to 85.2 °C. The observed change in temperature value (ΔT_m) of 9.2 °C of DNA on addition of compound **5e** indicated the stabilization of DNA double helix after binding with compound **5e**, revealing the intercalative mode of binding. In comparison, a slight change in melting temperature of DNA (T_m = 78.3) was seen upon the addition of compound **9h**. The difference in temperature value of (ΔT_m) 2.3 °C of DNA on adding compound **9h** indicates the weak binding interaction with DNA.

3.1.7c. Fluorescence studies

To further investigate the interactions between bis-naphthalimide and ct-DNA, emission studies were performed with the help of fluorescence spectroscopy. The emission spectra showed an emission band at 470 nm upon excitation at 360 nm for **5e** (5 μM) and 390 nm upon excitation at 345 nm for **9h** (5 μM) in phosphate buffer (pH 7.4) at 298K. Significant quenching in fluorescence was observed upon increasing

concentration of ct-DNA (0-50 μM) in the case of **5e** (**Figure. 3.4a**)**,** but no change in fluorescence of compound **9h** was observed upon progressive addition of ct-DNA (**Figure 3.4b**). Interaction of compound **5e** with ct-DNA resulted in decrease in fluorescence intensity. Stern-Volmer equation was used to find out the value of the Stern-Volmer constant (K_{sv}) and was found to be 3.2×10^4 M^{-1} (for **5e)** (**Table 3.4).** Further investigating whether the quenching process is dynamic or static, K_q (bimolecular quenching rate constant) was calculated using the lifetime value of fluorophore ($\tau_o = 10^{-8}$s)[81] and was found to be 3.2×10^{12} $M^{-1}s^{-1}$ (for **5e)** (**Table 3.4**). The value of K_q was much higher than the dynamic quenching constant (1×10^{10} $M^{-1}s^{-1}$),[82] indicating that interaction between compounds and ct-DNA is mainly due to static quenching process. The number of binding sites (n) and binding constant (K_{bin}) were calculated from the Scatchard equation for the interaction between compound and ct-DNA. The high binding constant value (7×10^5 M^{-1}) suggested that compound **5e** has a strong binding affinity toward DNA.

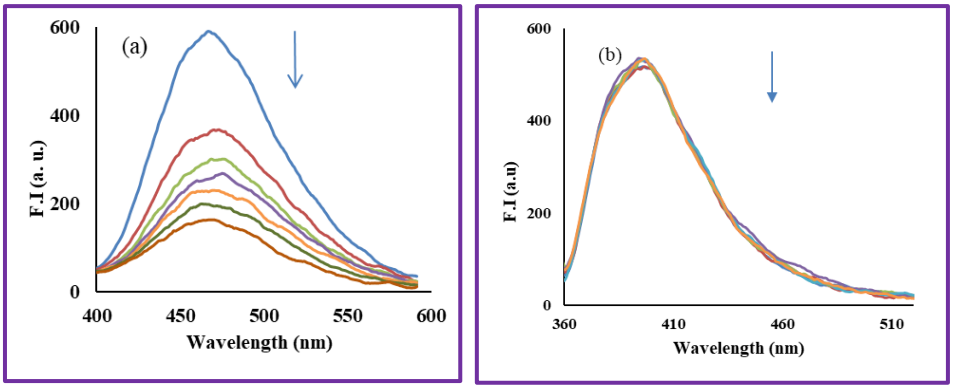

Figure 3.4 Emission spectra of (a) **5e** and (b) **9h** in phosphate buffer (*p*H 7.4) at 298 K upon increasing concentration of ct-DNA (0-50 μM).

Table 3.4 Quenching and binding parameters for interaction of compound **5e** with ct-DNA

Comp	$K_{sv}(\times 10^4)$ (M^{-1})	$K_q(\times 10^{12})$ $(M^{-1}s^{-1})$	R	$K_{bin}(\times 10^5)$ M^{-1}	n	R
5e	3.2	3.2	0.976	7.0	0.35	0.994

3.1.7d. Competitive displacement studies

Further, competitive displacement studies were conducted to check the binding mode of compounds **5e** and **9h** with ct-DNA. No emission band was shown by ethidium bromide (EtBr) in phosphate buffer (*p*H 7.4), but an intense emission band upon intercalating with DNA was observed at 600 nm when excited at 520 nm.[83] Decrease in intensity of emission band at 600 nm of ethidium bromide and ct-DNA complex (3 μM:30 μM) was

observed with increasing concentration of compounds **5e** (0-50 μM) and **9h** (0-80 μM). Displacement of EtBr from DNA resulted in quenching of fluorescence intensities, indicating the binding of compounds with DNA (**Figures 3.5a** and **3.5b**). The Stern-Volmer constant and apparent bimolecular quenching constant have been calculated using eq – 3[30] and were found to be 6.6 $\times 10^4$ M^{-1} and 6.6 $\times 10^{12}$ $M^{-1}s^{-1}$ (for compound **5e**) and 1.04 $\times$ 10^4 M^{-1} and 1.04 $\times 10^{12}$ $M^{-1}s^{-1}$ (for compound **9h**). The compounds' displacement of ethidium bromide from EtBr-DNA complexes confirmed the intercalation binding mode.

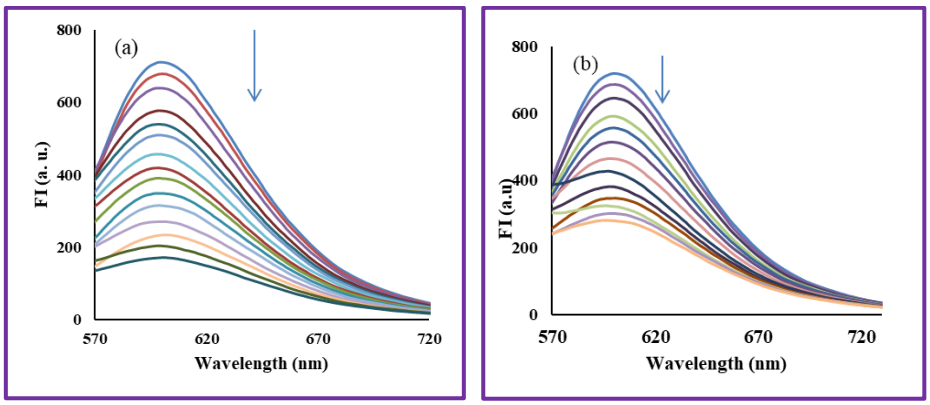

Figure 3.5 Emission spectra of ethidium bromide and ct-DNA complexes upon the increasing concentration of compounds (a) **5e** (0-50 μM) and (b) **9h** (0-80 μM).

3.1.7e. Circular Dichroism (CD) spectroscopy

Circular dichroism is the most reliable technique to determine any changes in the secondary structure of the DNA backbone. CD studies were conducted to confirm the interaction between ct-DNA and compounds **5e** and **9h**. The characteristics of the right-handed B form of DNA are established by the CD spectrum of free DNA that consisted of one negative band due to helicity at 246 nm and one positive band because of base stacking at 275 nm.[84] Upon the addition of compound **5e**, significant rise in intensities of ct-DNA band at 246 nm and 275 nm were observed (**Figure. 3.6**), and no negative induced CD bands in the region 350 nm and 400 nm were observed, thus indicating that compound **5e** binds to DNA *via* intercalative mode. On the other hand, upon the addition of **9h**, less CD spectrum intensity change was observed at 246 nm. Instead, a slight increase in intensity of the DNA band at 275 nm was observed, thus, revealing weak binding of compound **9h** to DNA.

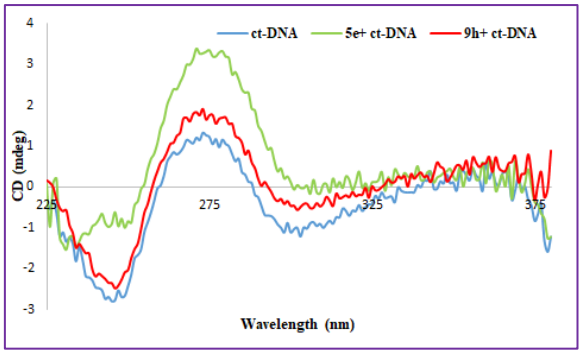

Figure 3.6 CD spectra of free ct-DNA (40 μM) (blue line), **5e**-DNA complex (green line), and **9h**-DNA complex (red line) at ratio $r_{[compound/ct\text{-}DNA]}$ = 0.025.

3.1.7f. DNA Damage Assay

In a day, in one cell, thousands of DNA are produced, and any damage caused to DNA leads to the formation of chromosomal aberration and mutations or may lead to cell death.[85] Comet assay was employed to measure the DNA damage in the cell by compound **5e**. **Figures 3.7a** and **3.7b** represent the photoluminescence (PL) microscopy images of untreated and treated cells, incubated with compound for 6 h at 37 ˚C under humidified conditions. In case of untreated cells, DNA was present inside the circular cell. On treatment of compound **5e** (10 μM) with cancer cells (A549), damaged DNA comes out of the cells and forms a comet-like shape when run under gel electrophoresis, and the undamaged DNA remains in the cells. Thus, unaffected DNA is observed in the head, and the damaged DNA is in the comet's tail.

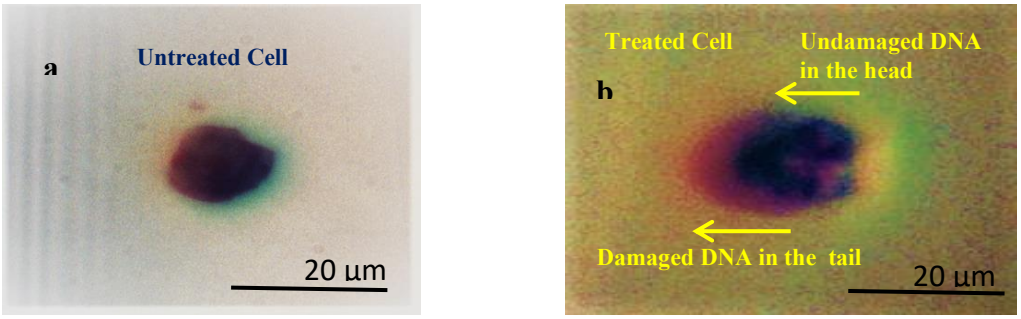

Figure 3.7 PL microscopy images for Comet assay of A549 (a) untreated and (b) treated cells with compound **5e** for 6 h at 37˚C under humidified conditions

3.1.7g. Molecular docking

Further, molecular docking studies of compounds **5e** and **9h** were carried out to evaluate the interaction between the target molecules and DNA (PDB: 1BNA) with the help of the Autodock program[86] and further visualization was done with the help of discovery studio. The molecular docked models of compounds **5e** and **9h** are shown in **Figures 3.8** and **3.9**. Energy levels were optimized for the obtained cluster in the most adequately suited DNA-ligand structure

conformation. The minimum binding energies of DNA with compounds **5e** and **9h** showed -13.19 kcal mol^{-1}, and -15.32 kcal mol^{-1}, respectively. The oxygen atom of the naphthalimide ring in compound **5e** forms hydrogen bonding with DG10 (*d* = 2.30 Å, chain A) and DG16 (*d* = 2.35 Å, chain B). Similarly, the two hydrogens attached to CH_2 in the ligand bind to DNA base pairs by H-bond; one H atom binds to DA18 of the B chain, and the other binds to DC9 of A chain with a distance of 2.09 Å and 2.03 Å, respectively. One H atom of CH_3 group of ligand binds to DC9 of A chain *via* hydrogen bond with a distance of 2.06 Å. In comparison to this, **9h** binds to DNA *via* H-bonding, and the oxygen atom of naphthalimide ring of compound **9h** form H-bond with DG10 (H21 and H3, chain A, *d* = 2.19 and 1.99 Å, respectively). Similarly, the hydrogen attached to nitrogen in piperazine binds to DT20 (*d* = 1.88 Å, chain B), and one hydrogen of piperazine binds to DT19 (*d* = 2.14 Å, chain B).

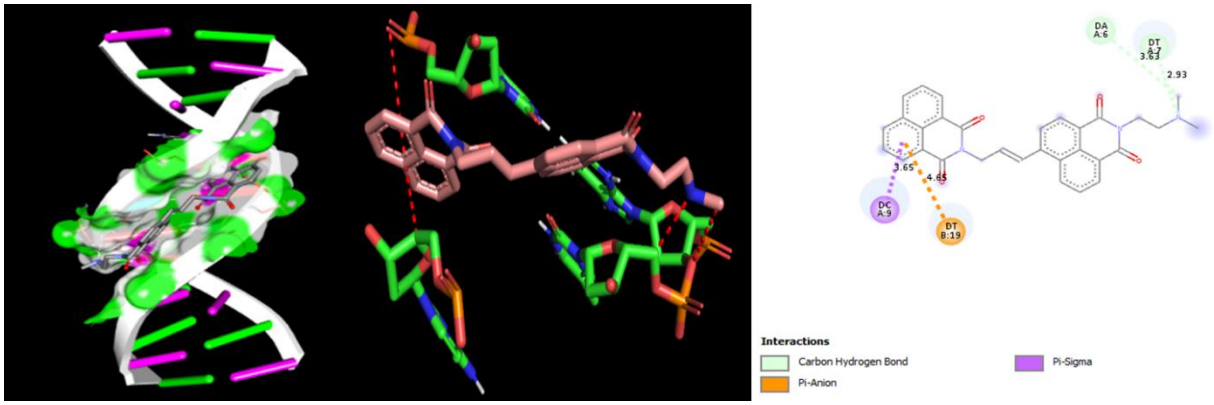

Figure. 3.8 Molecular docking of DNA (1BNA) with compound **5e**

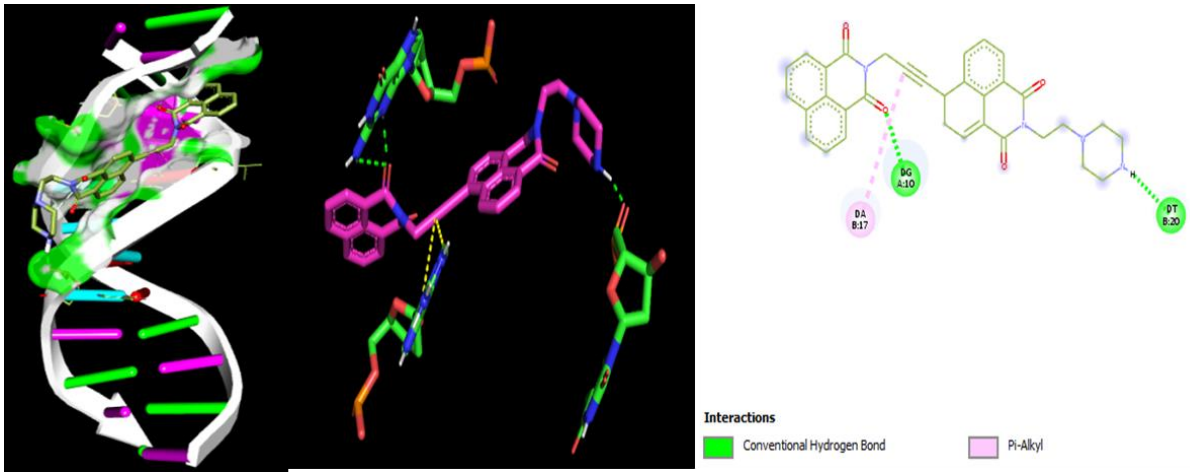

Figure. 3.9 Molecular docking of DNA (1BNA) with compound **9h**

3.1.8. Human Serum Albumin (HSA) studies

The main protein in human blood plasma is human serum albumin, which can bind with drugs that protect the oxidation in plasma, decrease toxicity, and improve the solubility of target drugs.[87] Because of these remarkable properties, HSA is the crucial target in

developing the most potent anticancer agent. Due to the dual properties of HSA, i.e., hydrophilic and hydrophobic, it acts as the leading carrier for several exogenous and endogenous substituents.[88] UV-visible and fluorescence spectroscopic techniques were investigated the binding affinities between most active compounds **5e** and **9h** with HSA.

3.1.8a. UV-visible studies

The absorption spectrum of HSA (7 μM) displayed an intense absorption band in phosphate buffer (*p*H 7.4, 298K) at 280 nm as a result of transitions in aromatic rings of tyrosine (Tyr), phenylalanine (Phe) and tryptophan (Trp) residues. A hyperchromic shift was observed at 280 nm upon progressive addition of compounds **5e** (0-20 μM) and **9h** (0-18 μM), along with the development and enhancement of a new band at 360 nm in case of compound **5e** and at 345 nm for compound **9h** (**Figures 3.10a** and **3.10b**). No change was observed in the wavelength maxima, indicating that compounds bind with HSA cavity through non-covalent interactions. Bensei-Hildebrand equation (eq. 3) was used to calculate the binding constants (K_b) and check the stability of complexes formed between HSA and target compounds and were found to be 7.0 $\times 10^4$ M^{-1} for **5e** and 7.5 $\times 10^4$ M^{-1} for **9h**. The binding constant value for compound **9h** was slightly higher than **5e,** indicating that the former binds more strongly to HSA.

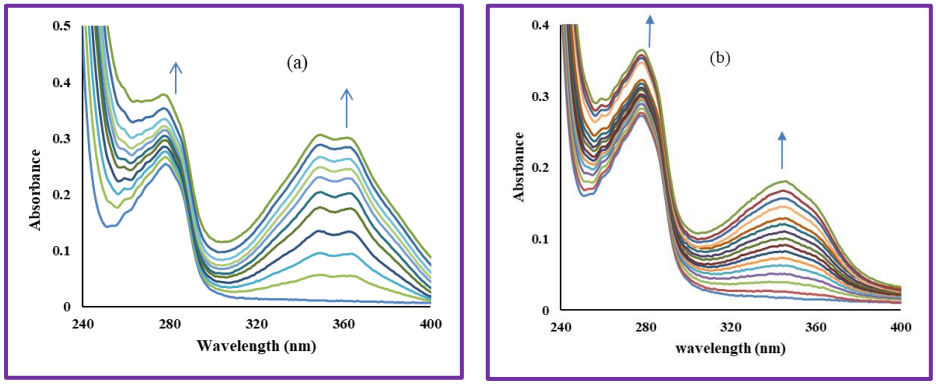

Figure 3.10 UV-visible spectra of HSA on increasing concentration of compounds (a) **5e** and (b) **9h** in phosphate buffer (pH 7.4) at 298K

3.1.8b. Fluorescence studies

The results showed that absorption spectra are insufficient to determine compounds' binding with HSA. Further, fluorescence spectroscopy was used to explore the interaction between compounds and HSA. Amino acid residues such as phenylalanine (Phe), tryptophan (Trp), and tyrosine (Tyr) are responsible for fluorescence of HSA. The fluorescence spectrum of HSA emitted an emission at 345 nm on excitation at 280 nm in phosphate buffer (*p*H 7.4). Quenching in fluorescence intensity of HSA was

observed for both compounds **5e** (0-60 μM) (**Figure 3.11)** and **9h** (0-50 μM) (**Figure 3.12)** on incremental additions at all said temperatures (298K, 308K, and 318K). A change in wavelength of 40 nm was observed in case of compound **5e**. The results indicated that both compounds interact with hydrophobic cavity of HSA. The inner filter effect has been corrected in emission data according to get the appropriate fluorescence intensity.

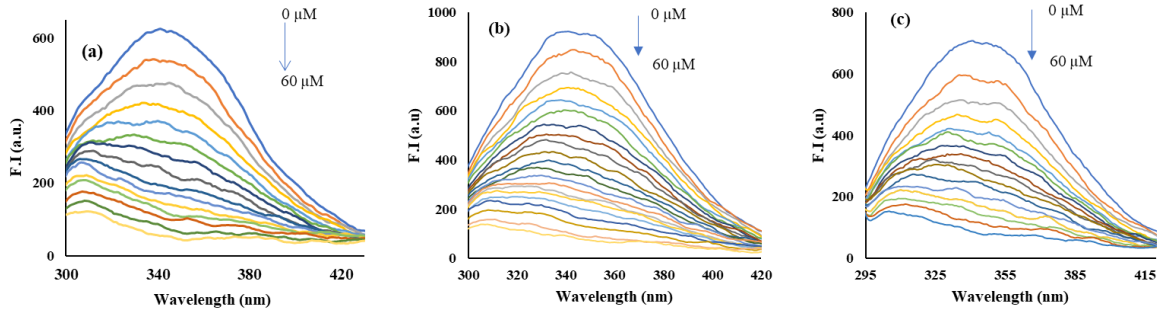

Figure 3.11. Emission spectra of HSA upon incremental addition of compound **5e** in phosphate buffer (pH 7.4) at (a) 298K, (b) 308K and (c) 318K.

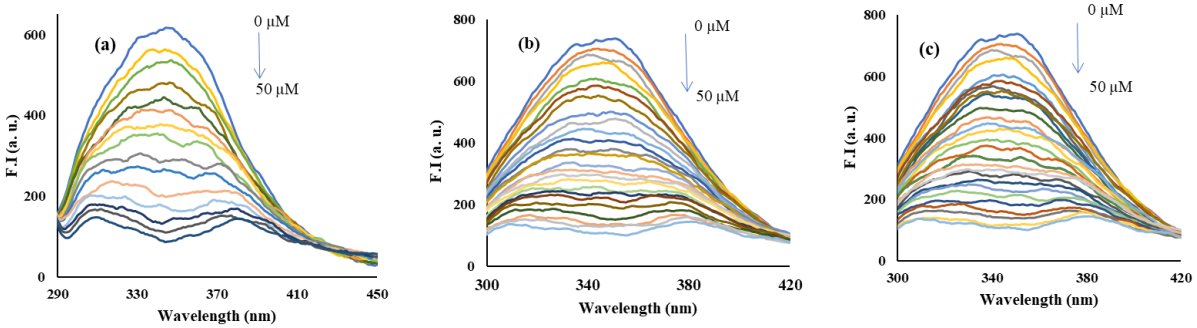

Figure 3.12 Emission spectra of HSA upon incremental addition of compound **9h** in phosphate buffer (pH 7.4) at (a) 298K, (b) 308K and (c) 318K.

The decrease in fluorescence intensity of HSA on progressive additions of compounds **5e** and **9h** is either due to static or dynamic quenching. Further, the Stern-Volmer equation was used to calculate the binding parameters, i.e., Stern-Volmer quenching constant (K_{sv}) and bimolecular quenching rate constant (K_q), which were found to be 1.30×10^5 M^{-1} and 1.30×10^{13} M^{-1} for compound **5e** and 1.70×10^5 M^{-1} and 1.70×10^{13} M^{-1} for compound **9h** at 298K, respectively. The values of K_{sv} for both compounds were very high, suggesting that both are efficient quenchers. The values of K_q for both compounds were much higher than the maximum limit of the dynamic quenching constant (1×10^{10} $M^{-1}s^{-1}$), revealing that quenching occurs through the static quenching process. The Stern-Volmer quenching constant was calculated with increasing temperature for both compounds; the decreasing trend in K_{sv} values

confirmed that quenching in fluorescence intensity occurs through static quenching (**Table 3.5**).

Table 3.5 Quenching and binding parameters for interaction of HSA with compounds **5e** and **9h** at various temperatures

Comp	T(K)	$K_{sv}(\times10^5)$ (M^{-1})	$K_q(\times10^{13})$ ($M^{-1}s^{-1}$)	R^2	$K_{bin}(\times10^4)$ M^{-1}	n	R^2
5e	298	1.30	1.30	0.9939	3.81	0.75	0.9837
	308	1.21	1.21	0.9754	2.50	0.81	0.9950
	318	1.10	1.10	0.9790	1.90	0.75	0.9778
9h	298	1.70	1.70	0.9753	11.80	1.09	0.9938
	308	1.44	1.44	0.9906	8.40	0.96	0.9922
	318	1.09	1.09	0.9904	3.97	0.92	0.9856

To calculate the binding constant (K_{bin}) and the number of binding sites (n) for compounds **5e** and **9h** at 298K, 308K, and 318K from fluorescence data, modified Stern-Volmer equation (eq. 5)was employed. The binding constant values suggested the strong binding of both compounds with HSA. For all the temperatures, the value of n was nearly one. With an increase in temperature, there was a gradual decrease in K_{bin} suggesting that the complex formed between HSA and compounds becomes unstable at higher temperatures; hence, it degrades. Van't Hoff equation was employed to calculate the binding forces, i.e., hydrophobic interactions, hydrogen bonds, electrostatic forces, and van der Waals forces involved between compounds **5e** and **9h** with HSA. To calculate the entropy change (ΔS) and enthalpy change (ΔH) for both compounds, Van't Hoff plot was used and binding free energy (ΔG) was calculated. The negative values of ΔH and ΔG for both compounds showed the spontaneous and exothermic nature of binding process (**Table 3.6**).

Table 3.6. Thermodynamic parameters of binding of HSA with compounds **5e** and **9h**

Comp	T(K)	ΔH (kcal mol^{-1})	ΔS ($calmol^{-1}K^{-1}$)	ΔG (kcal mol^{-1})	R
5e	298	-36.2	-32.7	-26.5	0.999
	308			-26.1	
	318			-25.8	
9h	298	-40.8	-39.3	-29.0	0.999
	308			-28.6	
	318			-28.2	

3.1.8c. Time-resolved fluorescence analysis

Furthermore, fluorescence lifetime analysis was performed to check the quenching mechanism between HSA and compounds **5e** and **9h** as steady-state fluorescence spectra indicated the static quenching. To further confirm the same, time decay spectra of HSA (7 μM) were recorded with increasing concentrations of **5e** (0-21 μM) and **9h** (0-21 μM), as shown in **Figure 3.13**. Dynamic quenching is generally observed with a decrease in decay time, while static quenching is depicted when there is no significant change in the decay time. Interaction results of HSA and compounds **5e** and **9h** showed a decreasing trend in the decay time of free HSA upon incremental addition of compounds, as depicted in **Table 3.7**, indicating the existence of dynamic quenching. At the same time, the steady-state fluorescence experiment demonstrates the possibility of static quenching. The above results inferred that both static and dynamic quenching might be responsible for the interaction of analogs to HSA.[89]

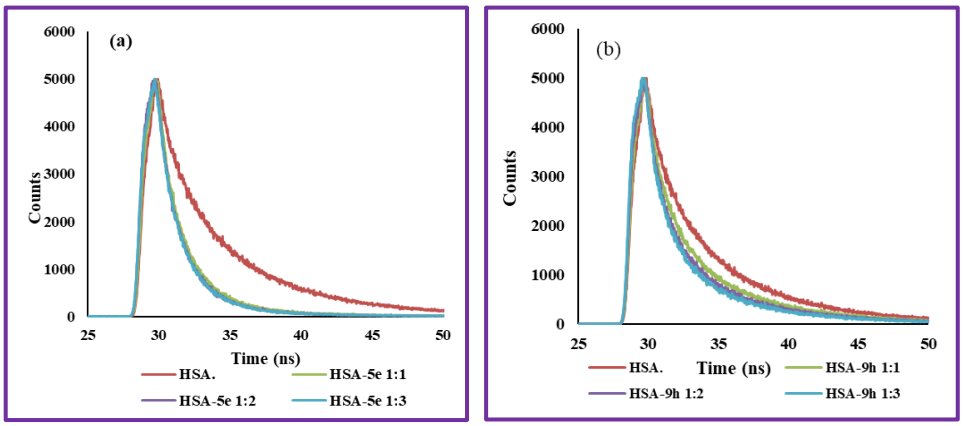

Figure 3.13. Fluorescence decay profile of HSA on addition of different concentrations of (a) compound **5e** and (b) compound **9h** in phosphate buffer (pH 7.4).

Table 3.7. Lifetime fluorescence decay of HSA on interaction with **5e** and **9h**

System	Conc.	τ_1 [ns]	τ_2 [ns]	τ_3 [ns]	α_1	α_2	α_3	τ_{av}	χ^2
HSA		2.40	6.43	0.42	0.51	0.09	0.10	2.86	1.16
HSA-5e	1:1	1.89	6.08	4.89	0.03	0.08	0.20	1.52	1.22
	1:2	1.01	2.32	4.45	0.06	0.06	0.22	1.46	1.20
	1:3	0.39	1.61	4.62	0.34	0.07	0.24	1.28	1.20
HSA-9h	1:1	1.77	6.18	0.03	0.09	0.07	0.03	2.01	1.09
	1:2	2.07	6.33	0.55	0.26	0.12	0.08	1.96	1.15
	1:3	1.86	6.08	0.47	0.25	0.13	0.07	1.67	1.20

3.1.9 *In vitro* antibacterial activity

Since naphthalimide exhibits antibacterial properties, we carried out preliminary antibacterial studies of the prepared compounds. Derivatives **5a-i** and **9a-i** were evaluated *in vitro* for their antibacterial activity towards eight bacterial strains; gram-positive strains *Staphylococcus aureus*, *Enterococcus faecalis*, *Bacillus subtilis*, *Listeria*, and gram-negative bacterial strain, *Salmonella enterica*, *Escherichia coli*, *Acinetobacter calcoaceticus*, *Serratia marcescens*.[90] A two-fold serial dilution method was adopted to evaluate the antibacterial properties in 96-well micro test plates as suggested by the National Committee for Clinical Laboratory Standards (NCCLS).[91] The prepared compounds could effectively inhibit the growth of tested bacterial strains with better antibacterial activity with a low MIC value than reference drugs amoxicillin and chloromycin, showing different amines' effects on bacterial growth.

Compounds **5a** and **5b** exhibited moderate activity against all the tested bacterial strains. In contrast, compound **5c** could effectively inhibit the growth of *Staphylococcus aureus* with the value of MIC 1.56 μg/ml, which was found to be 20 and 2 folds more potent than the reference drugs amoxicillin and chloromycin, respectively. Compound **5d** was active against two bacterial strains, i.e., *Staphylococcus aureus*, having MIC value of 25 μg/ml, and *Serratia marcescens* with MIC of 6.25 μg/ml. Compounds **5e** and **5f** displayed activity against *Serratia marcescens* bacterial strain with the value of MIC 1.56 μg/ml, comparable to reference drugs. Compound **5g** was inactive against most of the tested bacterial strains but could selectively inhibit the growth of *Salmonella enterica*, having MIC value of 1.56 μg/ml, which was 32-fold more active than chloromycin. Compound **5h** having *N*-(2-aminoethyl)piperazine displayed a wide range of antibacterial activities against all the tested bacterial strains and could inhibit the growth with low MIC values. Compound **5h** displayed MIC value of 1.56 μg/ml against *Staphylococcus aureus*, *Enterococcus faecalis*, *Salmonella enterica*, and *Serratia marcescens* and was found to two-fold more potent than chloromycin.

On the other hand, compounds **9b** and **9i** could effectively inhibit the growth of *Escherichia coli* with MIC values of 3.125 and 12.5 μg/ml, respectively. At the same time, **9c**, **9d**, and **9g** displayed low activity against all the tested bacterial strains. Compound **9e** showed a broad-spectrum activity towards the bacterial strains with low MIC values. Compound **9e** was two-fold more potent than chloromycin against *Staphylococcus aureus* and *Escherichia coli*. In contrast, it was 16- and 64-folds more active than

amoxicillin against *Staphylococcus aureus* and *Escherichia coli*, respectively. Compounds **9f** and **9h** were most active against *Bacillus subtilis* with a MIC value of 1.56 μg/ml. These derivatives were active against *Serratia marcescens* bacterial strain with respective MIC of 6.25 and 1.56 μg/ml. Thus, compounds **5h** and **9e** were most active against all the tested bacterial strains with low MIC values (**Table 3.8**). These were found more potent than reference drugs, amoxicillin and chloromycin, against some bacterial strains. Therefore, these candidates of naphthalimides could be considered for further evaluation.

Table 3.8. Antibacterial activity data as MIC (μg/ml) of the synthesized compounds

Comp	*E. faecalis*	*B. subtilis*	*Listeria sp.*	*S. aureus*	*E. coli*	*S. enterica*	*A. calcoacetius*	*S. marcescens*
5a	200	200	200	200	400	200	200	400
5b	200	100	200	200	200	200	200	200
5c	200	-	200	**1.56**	200	-	200	200
5d	200	200	200	**25**	-	400	200	**6.25**
5e	200	200	200	100	200	-	200	**1.56**
5f	200	100	200	100	200	-	400	**1.56**
5g	-	200	-	-	-	**1.56**	-	200
5h	**1.56**	**100**	**3.125**	**1.56**	**3.125**	**1.56**	**3.125**	**1.56**
5i	200	200	200	200	-	200	200	200
9a	-	-	-	-	-	-	-	200
9b	400	1.56	-	-	**3.125**	-	-	100
9c	-	-	-	-	-	-	-	200
9d	200	25	200	100	50	200	200	200
9e	**25**	**25**	**25**	**1.56**	**1.56**	**25**	**25**	**3.125**
9f	200	**1.56**	200	200	200	50	100	**6.25**
9g	-	200	400	-	50	-	-	-
9h	200	**1.56**	200	-	1.56	200	400	**1.56**
9i	400	**1.56**	-	200	**12.5**	-	-	**25**
A	**1.56**	**50**	**50**	**25**	100	200	**50**	**1.56**
B	**3.125**	**1.56**	**1.56**	**3.125**	**3.125**	**50**	**3.125**	**1.56**

A = Amoxicillin B = Chloromycin

3.1.10. Conclusions

In this sub chapter, we have reported 18 derivatives of bis-naphthalimide of two different series, **5a-i,** and **9a-i**. These compounds were examined for their antitumor activities against 9 cancer cell panels having 60 cell lines. Compounds **5e** and **9h**

displayed a wide range of activity against all the cancer cell lines with values of MG-MID GI_{50} 33.32 μM and 4.67 μM, respectively. Compounds **5e** and **9h** exhibited promising activity with a low value of GI_{50} against almost all the cancer cell lines. Further, interactions of compounds **5e** and **9h** with DNA and HSA were carried out with absorption and emission spectroscopy. The results revealed that compounds **5e** and **9h** interacted to DNA with a binding constant of 5.5×10^5 M^{-1} and 2.4×10^5 M^{-1}, respectively, indicating that compound **5e** binds more efficiently with DNA. Competitive displacement studies confirmed the intercalation binding mode of compound **5e**. Further, DNA damage studies confirmed the binding of compounds with DNA. The binding constant values for both compounds were 7.0×10^4 M^{-1} (for **5e**) and 7.5×10^4 M^{-1} (for **9h**); indicated that both compounds bind strongly with HSA.

These molecules were also evaluated for their antibacterial properties against eight bacterial strains, four gram-positive and four gram-negative bacterial strains. Compounds **5h** and **9e** displayed a broad antibacterial activity against all the tested bacterial strains with low MIC values. Compound **5h** showed more potent activity than compound **9e**, with MIC values ranging from 3.125 – 1.56 μg/ml against all the tested strains. Thus, we can conclude that compounds **5e** and **9h** were most active against most cancer cell lines and can be essential anticancer agents. In contrast, compound **5h** was most active against tested bacterial strains and, therefore, has potential as a potent antibacterial agent.

3.1.11. Experimental section

Benzo[*de*]isochromene-1,3-dione (2)[92]

To a stirred solution of acenaphthene (**1**) (2.0 g, 12.98 mmol) in acetic acid (50 ml), sodium dichromate (19.3 g, 65 mmol) was added in portions to an ice bath. The reaction was stirred at room temperature for 25 min, followed by refluxing for 3h. The monitoring of the reaction was done with the help of TLC. On completion of the reaction, water was added to it, and the precipitates formed were filtered; the product was oven-dried to obtain yellow solid in 2.2 g; 95%, R_f 0.4 (30% chloroform in hexane); m.pt 266–268 °C.

2-Allyl-*1H*-benzo[*de*]isoquinoline-1,3(*2H*)-dione (3)[93]

To a stirred solution of compound **2** (2.0 g, 8.34 mmol) in ethanol (30 ml), allylamine (2.40 g, 42.19 mmol) was added to the reaction mixture, and the reaction was stirred at room temperature for 3h. After completion of the reaction, the reaction mixture was filtered using ethanol, and the product obtained was thoroughly washed with hot ethanol to obtain light brown solid in 1.95 g; 84%, R_f 0.3 (40% chloroform in hexane); m.pt 103-105 ^oC

(*Z*)-2-(3-(1,3-Dioxo-1,3-dihydrobenzo[*de*]isochromen-6-yl)allyl)-*1H*-benzo[*de*]isoquinoline-1,3(*2H*)-dione (4)

Heck coupling of **3** (1.0 g, 4.29 mmol) was performed with 6-bromobenzo[*de*]isochromene-1,3-dione (1.16 g, 4.21 mmol) in acetonitrile and potassium carbonate (0.8 g, 6.32 mmol). Palladium(II) acetate was used as a catalyst for the reaction, and the reaction mixture was refluxed for 8h. On completion of the reaction, acetonitrile was evaporated. With the addition of 100 ml water, precipitates formed were collected by filtration, and the product was oven-dried. The crude was purified by column chromatography using chloroform as eluent.

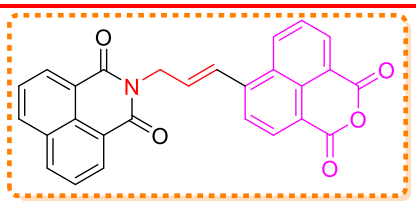

Light yellow solid; 80%, R_f 0.5 (chloroform); m.pt 210–212 ºC; ^{1}H NMR ($CDCl_3$, TFA (0.70 : 0.05 ml), 400 MHz); δ 8.70 (dd, ^2J = 7.30 Hz , ^3J = 0.90 Hz, 2H, ArH), 8.67–8.63 (m, 2H, ArH), 8.57 (d, J = 7.80 Hz, 1H, ArH), 8.34 (dd, ^2J = 8.20 Hz, ^3J = 0.80 Hz, 2H, ArH), 7.91 (d, J = 7.80 Hz, 1H, ArH), 7.87–7.83 (m, 3H, ArH), 7.59 (d, J = 15.7 Hz, 1H, CH allyl), 6.65 (dt, ^2J = 15.60 Hz, ^3J = 6.50 Hz, 1H, CH allyl), 5.17 (dd, ^2J = 6.50 Hz, ^3J = 1.20 Hz, 2H, CH_2 allyl); ^{13}C NMR ($CDCl_3$, 100 MHz): δ (ppm) 165.3, 135.6, 134.2, 133.9, 132.7, 132.6, 131.7, 130.8, 129.6, 129.3, 128.2, 127.6, 128.2, 127.6, 127.5, 125.2, 121.6, 118.6, 117.0, 115.7, 112.9, 110.1, 42.8; ESI-MS (m/z): $[M]^+$ = 433; Anal Calcd for $C_{27}H_{15}NO_5$: C, 74.82; H, 3.49; N, 3.23; found C, 74.80; H, 3.48; N, 3.20.

General procedure for synthesis of amino substituted (*Z*)-2-(3-(1,3-dioxo-1,3-dihydrobenzo[*de*]isochromen-6-yl)allyl)-*1H*-benzo[*de*]isoquinoline-1,3(*2H*)-dione (5a-i)

To a stirred solution of **4** (0.2 g, 0.46 mmol) in ethanol (20ml), different primary amine (0.92 mmol) was added, and the reaction was refluxed for 1h. The precipitates formed were filtered, and the product was collected after washing with ethanol.

(*Z*)-2-allyl-6-(3-(1,3-dioxo-*1H*-benzo[*de*]isoquinolin-2(*3H*)-yl)prop-1-en-1-yl)-*1H*-benzo[*de*]isoquinoline-1,3(*2H*)-dione (5a)

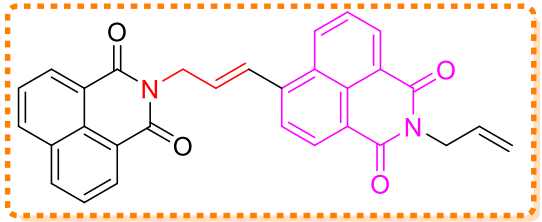

Light yellow solid; 81% Yield; R_f 0.6 (50% chloroform in hexane); m.pt 230-232 ºC; ^{1}H NMR ($CDCl_3$, 400 MHz): δ (ppm) 8.67 (d, J = 7.32 Hz, 2H, ArH), 8.61 (d, J = 7.24 Hz, 1H, ArH), 8.52 (q, J = 5.36 Hz, 2H, ArH),

1H, ArH), 8.52 (q, *J* = 5.36 Hz, 2H, ArH), 8.26 (d, *J* = 8.20 Hz, 2H, ArH), 7.85-7.75 (m, 4H, ArH), 7.57 (d, *J* = 15.68 Hz, 1H, CH allyl), 6.62-6.56 (m, 1H, CH allyl), 6.01-5.91 (m, 1H, CH allyl), 5.31 (d, *J* = 17.24 Hz, 1H, CH allyl), 5.20 (d, *J* = 10.24 Hz, 1H, CH allyl), 5.13 (d, *J* = 6.40 Hz, 2H, CH_2 allyl), 4.79 (d, *J* = 5.64 Hz, 2H, CH_2 allyl); ^{13}C NMR ($CDCl_3$, 100 MHz): δ (ppm) 164.1, 164.0, 141.0, 134.3, 132.2, 131.5, 131.3, 131.2, 130.5, 129.4, 128.2, 127.1, 126.8, 124.6, 122.8, 122.5, 121.6, 42.4, 42.2; ESI-MS (m/z): $[M]^+$ = 472; Anal Calcd for $C_{30}H_{20}N_2O_4$: C, 76.26; H, 4.27; N, 5.93; found C, 76.21; H, 4.17; N, 5.87.

(*Z*)-2-benzyl-6-(3-(1,3-dioxo-*1H*-benzo[*de*]isoquinolin-2(*3H*)-yl)prop-1-en-1-yl)-*1H*-benzo[*de*]isoquinoline-1,3(*2H*)-dione (5b)

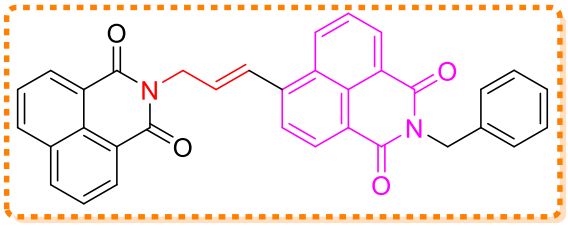

Off-white solid; 85% Yield; R_f 0.7 (50% chloroform in hexane); m.pt 230-233 ºC; ^{1}H NMR ($CDCl_3$, 400 MHz): δ (ppm) 8.62 (d, *J* = 7.24 Hz, 2H, ArH), 8.57 (d, *J* = 7.24 Hz, 1H, ArH), 8.46 (dd, ^2J = 11.40 Hz, ^3J = 8.10 Hz, 2H, ArH), 8.21 (d, *J* = 8.32 Hz, 2H, ArH), 7.74 (dd, ^2J = 16.40 Hz, ^3J = 8.10 Hz, 2H, ArH), 8.21 (d, *J* = 8.32 Hz, 2H, ArH), 7.74 (dd, ^2J = 16.40 Hz, ^3J = 8.40 Hz, 4H, ArH), 7.54-7.48 (m, 3H, ArH), 7.25 (t, *J* = 7.16 Hz, 2H, ArH), 7.19 (d, *J* = 7.20 Hz, 1H, CH allyl), 6.57 (dt, ^2J = 15.6 Hz, ^3J = 6.50 Hz, 1H, CH allyl), 5.32 (s, 2H, CH_2 benzyl), 5.08 (d, *J* = 6.36 Hz, 2H, CH_2 allyl); ^{13}C NMR ($CDCl_3$, 100 MHz): δ (ppm) 164.1, 141.1, 137.3, 134.4, 131.7, 131.6, 131.4, 131.3, 130.9, 130.5, 129.4, 129.0, 128.5, 127.5, 127.1, 126.8, 124.6, 122.9, 122.5, 121.7, 43.6, 42.2; ESI-MS (m/z): $[M]^+$ = 522; Anal Calcd for $C_{34}H_{22}N_2O_4$: C, 78.15; H, 4.24; N, 5.36; found C, 78.05; H, 4.21; N, 5.31.

(*Z*)-2-butyl-6-(3-(1,3-dioxo-1*H*-benzo[*de*]isoquinolin-2(*3H*)-yl)prop-1-en-1-yl)-*1H*-benzo[*de*]isoquinoline-1,3(*2H*)-dione (5c)

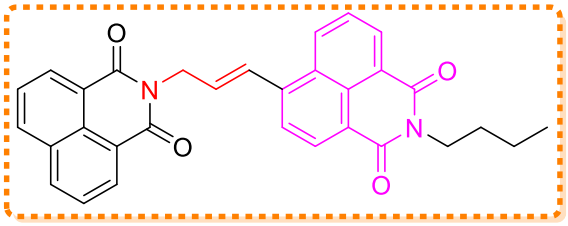

Creamish white solid; 83% Yield; R_f 0.6 (40% chloroform in hexane); m.pt 240-242 ºC; ^{1}H NMR ($CDCl_3$, 400 MHz): δ (ppm) 8.67 (d, *J* = 7.28 Hz, 2H, ArH), 8.60 (d, *J* = 7.24 Hz, 1H, ArH), 8.50 (t, *J* = 7.44 Hz, 2H, ArH), 8.26 (d, *J* = 8.20 Hz, 2H, ArH), 7.79 (dd, ^2J = 16.00 Hz, ^3J = 8.30 Hz, 4H, ArH), 7.57 (d, *J* = 15.68 Hz, 1H, CH allyl), 6.62 (dt, ^2J = 15.70 Hz, ^3J = 6.50 Hz, 1H, CH allyl), 5.12 (d, *J* = 6.50 Hz, 2H, CH_2 allyl), 4.19–4.13 (m, 2H, CH_2 butyl), 1.72-

1.64 (m, 2H, CH_2 butyl), 1.44 (dd, ^2J = 15.10 Hz, ^3J = 7.50 Hz, 2H, CH_2 butyl), 0.96 (t, J = 14.76 Hz, 3H, CH_3 butyl); ^{13}C NMR ($CDCl_3$, 100 MHz): δ (ppm) 164.3, 164.1, 140.9, 134.4, 131.7, 131.6, 131.2, 131.0, 130.8, 129.5, 129.4, 127.1, 126.8, 124.6, 122.5, 121.8, 42.2, 40.3, 30.2, 20.4, 13.9; ESI-MS (m/z): $[M]^+$ = 488; Anal Calcd for $C_{31}H_{24}N_2O_4$: C, 76.21; H, 4.95; N, 5.73; found C, 76.13; H, 4.92; N, 5.69.

(*Z*)-2-(2-(diethylamino)ethyl)-6-(3-(1,3-dioxo-*1H*-benzo[*de*]isoquinolin-2(3*H*)-yl)prop-1-en-1-yl)-*1H*-benzo[*de*]isoquinoline-1,3(*2H*)-dione (5d)

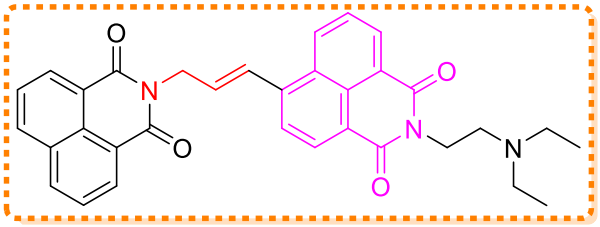

Light brown solid; 75% Yield; R_f 0.4 (50% chloroform in hexane); m.pt 232-235 ºC; ^{1}H NMR ($CDCl_3$, 400 MHz): δ (ppm) 8.66 (dd, ^2J = 0.80 Hz, ^3J = 0.76 Hz, 2H, ArH), 8.59 (d, J = 7.16 Hz, 1H, ArH), 8.50 (dd, ^2J = 7.80 Hz, ^3J = 4.20 Hz, 4H, ArH), 8.25 (dd, ^2J = 8.20 Hz, ^3J = 0.70 Hz, 2H, ArH), 7.81 - 7.71 (m, 4H, ArH), 7.56 (d, J = 15.68, 1H, CH allyl), 6.63-6.55 (m, 1H, ArH), 5.12 (dd, ^2J = 6.50 Hz, ^3J = 0.90 Hz, 2H, CH_2 allyl), 4.31-4.24 (m, 2H, CH_2 diethyl), 2.80-2.74 (m, 2H, CH_2 diethyl), 2.66 (q, J = 7.20 Hz, 4H, 2* CH_2 diethyl), 1.09 (t, J = 7.20 Hz, 6H, 2* CH_3 diethyl); ^{13}C NMR ($CDCl_3$, 100 MHz): δ (ppm) 164.3, 164.1, 140.9, 134.4, 131.6, 131.2, 131.0, 130.8, 130.4, 129.5, 127.1, 126.8, 124.6, 122.9, 122.5, 121.7, 49.8, 47.7, 42.2, 38.0, 12.3; ESI-MS (m/z): $[M]^+$ = 531; Anal Calcd for $C_{33}H_{29}N_3O_4$: C, 74.56; H, 5.50; N, 7.90: C, 74.50; H, 5.26; N, 7.89.

(*Z*)-2-(2-(dimethylamino)ethyl)-6-(3-(1,3-dioxo-*1H*-benzo[*de*]isoquinolin-2(*3H*)-yl)prop-1-en-1-yl)-1*H*-benzo[*de*]isoquinoline-1,3(*2H*)-dione (5e)

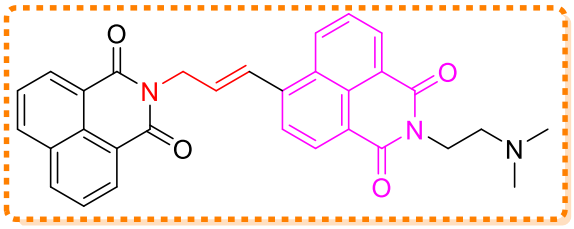

Creamish solid; 73% Yield; R_f 0.3 (50% chloroform in hexane); m.pt 250-254 ºC; ^{1}H NMR ($CDCl_3$, 400 MHz): δ (ppm) 8.65 (d, J = 7.32 Hz, 2H, ArH), 8.58 (d, J = 7.24 Hz, 1H, ArH), 8.49 (dd, ^2J = 8.00 Hz, ^3J = 5.60 Hz, 2H, ArH), 8.24 (d, J = 8.20 Hz, 2H, ArH), 7.81 (dt, ^2J = 16.20 Hz, ^3J = 8.30 Hz, 4H, ArH), 7.55 (d, J = 15.64, 1H, CH allyl), 6.63-6.55 (m, 1H, CH allyl), 5.10 (d, J = 6.32 Hz, 2H, CH allyl), 4.30 (t, J = 7.00 Hz, 2H, CH_2 dimethyl), 2.63 (d, J = 7.20 Hz, 2H, CH_2 dimethyl), 2.32 (s, 6H, 2* CH_3 dimethyl); ^{13}C NMR ($CDCl_3$, 100 MHz): δ (ppm) 164.4, 164.1, 140.9, 134.4, 131.6, 131.2, 131.1, 130.8, 130.4, 129.4,

127.1, 126.8, 124.6, 122.9, 122.5, 121.7, 57.0, 45.8, 42.2, 38.2; ESI-MS (m/z): $[M]^+$ = 503; Anal Calcd for $C_{31}H_{25}N_3O_4$: C, 73.94; H, 5.00; N, 8.34; found C, 73.84; H, 4.95; N, 8.32.

(*Z*)-6-(3-(1,3-dioxo-1*H*-benzo[*de*]isoquinolin-2(*3H*)-yl)prop-1-en-1-yl)-2-(2-hydroxy ethyl)-1*H*-benzo[*de*]isoquinoline-1,3(*2H*)-dione (5f)

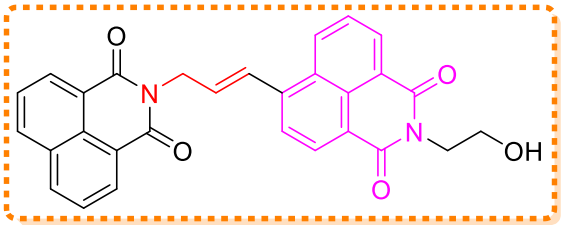

Light green solid; 70% Yield; R_f 0.5 (70% chloroform in hexane); m.pt 240-243 ºC; ^{1}H NMR (DMSO–d_6, 400 MHz): δ (ppm) 8.56 (d, *J* = 8.48 Hz, 1H, ArH), 8.48 (d, *J* = 7.24 Hz, 2H, ArH), 8.41 (d, *J* = 8.52 Hz, 3H, ArH), 8.31 (d, *J* = 7.80 Hz, 1H, ArH), 7.92 (d, *J* = 7.80 Hz, 1H, ArH), 7.84-7.75 (m, 3H, ArH), 7.54 (d, *J* = 15.58 Hz, 1H, CH allyl), 6.65-6.59 (m, 1H, CH allyl), 4.95 (d, *J* = 5.04 Hz, 2H, CH_2 allyl), 4.79 (br(t), OH), 4.08 (t, *J* = 6.48 Hz, 2H, CH_2 ethanol), 3.58 (q, *J* = 6.36 Hz, 2H, CH_2 ethanol); ^{13}C NMR ($CDCl_3$, 100 MHz): δ (ppm) 164.0, 163.9, 140.9, 134.8, 132.6, 131.8, 131.2, 131.1, 130.9, 129.1, 127.7, 127.5, 127.2, 124.5, 122.9, 121.4, 58.2, 42.3; ESI-MS (m/z): $[M]^+$ = 476; Anal Calcd for $C_{29}H_{20}N_2O_5$: C, 73.10; H, 4.23; N, 5.88; found C, 73.00; H, 4.11; N, 5.96.

(*Z*)-6-(3-(1,3-dioxo-1*H*-benzo[*de*]isoquinolin-2(*3H*)-yl)prop-1-en-1-yl)-2-(2-morph olinoethyl)-*1H*-benzo[*de*]isoquinoline-1,3(*2H*)-dione (5g)

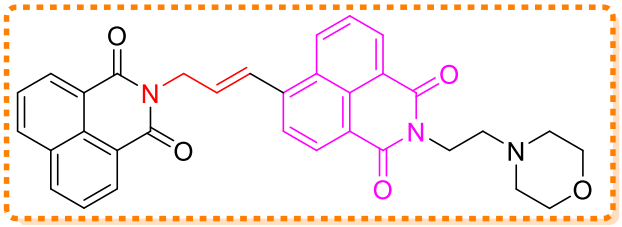

Light brown solid; 68% Yield; R_f 0.5 (chloroform); m.pt 220-224 ºC; ^{1}H NMR ($CDCl_3$, 400 MHz): δ (ppm) 8.65 (d, *J* = 7.28 Hz, 2H, ArH), 8.58 (d, *J* = 7.16 Hz, 1H, ArH), 8.49 (d, *J* = 7.92 Hz, 2H, ArH), 8.25 (d, *J* = 8.24 Hz, 2H, ArH), 7.82-7.74 (m, 4H, ArH), 7.56 (d, *J* = 15.64 Hz, 1H, CH allyl), 6.63-6.56 (m, 1H, CH allyl), 5.11 (d, *J* = 6.40 Hz, 2H, CH_2 allyl), 4.32 (t, *J* = 6.92 Hz, 2H, CH_2 ethyl morph), 3.67 (t, *J* = 4.48 Hz, 4H, CH_2 morph), 2.69 (t, *J* = 7.04 Hz, 2H, CH_2 ethyl), 2.57 (br(s), 4H, 2*CH_2 morph); ^{13}C NMR ($CDCl_3$, 100 MHz): δ (ppm) 164.3, 164.1, 141.0, 134.4, 131.6, 131.2, 131.1, 130.9, 130.5, 129.4, 127.1, 126.8, 124.6, 122.9, 122.5, 121.7, 67.1, 56.1, 53.8, 42.2, 37.2; ESI-MS (m/z): $[M]^+$ = 545; Anal Calcd for $C_{33}H_{27}N_3O_5$: C, 72.65; H, 4.99; N, 7.70; found C, 72.60; H, 4.91; N, 7.65.

(*Z*)-6-(3-(1,3-dioxo-1*H*-benzo[*de*]isoquinolin-2(3*H*)-yl)prop-1-en-1-yl)-2-(2-(piperazin-1-yl)ethyl)-1*H*-benzo[*de*]isoquinoline-1,3(2*H*)-dione (5h)

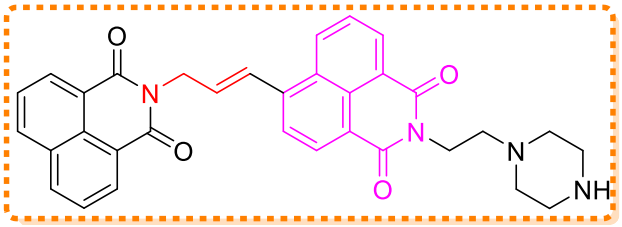

Yellow solid; 71% Yield; R_f 0.3 (chloroform); m.pt 245-248 ºC; ^{1}H NMR ($CDCl_3$, 400 MHz): δ (ppm) 8.67 (dd, ^2J = 1.88 Hz, ^3J = 0.88 Hz, 2H, ArH), 8.59-8.57 (m, 1H, ArH), 8.50 (d, J = 7.76 Hz, 2H, ArH), 8.26 (d, J = 7.44 Hz, 2H, ArH), 7.81–7.79 (m, 3H, ArH), 7.76 – 7.74 (m, 1H, ArH), 7.58 (d, J = 15.68 Hz, 1H, CH allyl), 6.65–6.58 (m, 1H, CH allyl), 5.13 (dd, ^2J = 0.92 Hz, ^3J = 1.92 Hz, 2H, CH_2 allyl), 4.33 (t, J = 7.04 Hz, 2H, CH_2 ethyl piperazine), 2.89 (t, J = 4.84 Hz, 4H, 2* CH_2 piperazine), 2.69 (t, J = 7.28 Hz, 2H, CH_2 ethyl piperazine), 2.57 (br(s), 4H, 2* CH_2 piperazine); ^{13}C NMR ($CDCl_3$, 100 MHz): δ (ppm) 164.1, 164.0, 140.9, 134.4, 131.7, 131.6, 131.2, 131.0, 130.8, 130.4, 129.4, 127.1, 126.8, 124.6, 122.8, 122.5, 121.6, 56.02, 54.5, 45.9, 42.2, 37.3; ESI-MS (m/z): $[M]^+$ = 544; Anal Calcd for $C_{33}H_{28}N_4O_4$: C, 72.78; H, 5.18; N, 10.25; found C, 72.72; H, 5.15; N, 10.23.

(*Z*)-6-(3-(1,3-dioxo-1*H*-benzo[*de*]isoquinolin-2(3*H*)-yl)prop-1-en-1-yl)-2-(2-(piperazin-1-yl)ethyl)-1*H*-benzo[*de*]isoquinoline-1,3(2*H*)-dione (5i)

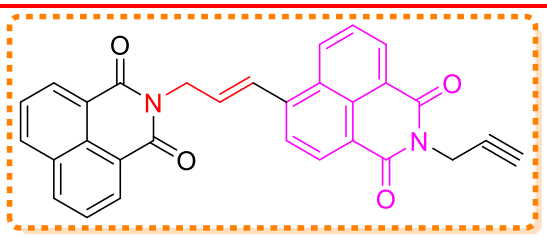

Off white solid; 84% Yield; R_f 0.5 (50% chloroform in hexane); m.pt 240-243 ºC; ^{1}H NMR ($CDCl_3$, TFA (0.70:0.05 ml), 400 MHz): δ (ppm) 8.72-8.67 (m, 3H, ArH), 8.60-8.57 (m, 2H, ArH), 8.34 (dd, ^2J = 1.88 Hz, ^3J = 0.80 Hz, 2H, ArH), 7.89-7.80 (m, 4H, ArH), 7.60 (d, J = 15.60 Hz, 1H, CH_2 allyl), 6.69–6.59 (m, 1H, CH_2 allyl), 5.17 (dd, ^2J = 6.50 Hz, ^3J = 1.04 Hz, 2H, CH_2 allyl), 4.97 (d, J = 2.47 Hz, 2H, CH_2 propargyl), 2.21 (dd, ^2J = 4.80 Hz, ^3J = 2.44 Hz, 1H, propargyl); ^{13}C NMR ($CDCl_3$, 100 MHz): δ (ppm) 164.9, 164.3, 142.0, 135.2, 132.3, 132.1, 131.7, 131.5, 130.9, 129.6, 129.4, 128.5, 128.2, 127.4, 127.2, 124.9, 121.9, 120.8, 78.0, 71.0, 42.6, 29.9; ESI-MS (m/z): $[M]^+$ = 470; Anal Calcd for $C_{30}H_{18}N_2O_4$: C,76.59; H, 3.86; N, 5.95; found C, 76.50; H, 3.75; N, 5.92

1*H*-Benzo[*de*]isoquinoline-1,3(2*H*)-dione (6)

To a stirred solution of benzo[*de*]isochromene-1,3-dione (2.0 g, 10.1 mmol) in ethanol, ammonia (10 ml) was added, and the reaction mixture was stirred at room temperature

for 3h. On completion of the reaction, the reaction mixture was filtered to get the desired product. The obtained product was thoroughly washed with ethanol, and oven-dried to obtain reddish-pink solid in 1.8 g; 82%; R_f 0.4 (50% chloroform in hexane); m.pt 110-114 ^oC

2-(Prop-2-yn-1-yl)-1*H*-benzo[*de*]isoquinoline-1,3(2*H*)-dione (7)[94]

To a stirred solution of 1*H*-benzo[*de*]isoquinoline-1,3(2*H*)-dione (1.0 g, 5.07 mmol) in *N*,*N*-dimethylformamide (20 ml), propargyl bromide (0.5 ml) and potassium carbonate (1.05 g, 7.61 mmol) were added, and the reaction was heated at 80–90 °C for 3h. On completion of the reaction, water (50 ml) was added, filtered the residues and the product was oven-dried to obtain a brown solid in 0.9g: 80%; R_f 0.4 (70% chloroform in hexane); m.pt 235-236 ^oC

2-(3-(1,3-Dioxo-1,3-dihydrobenzo[*de*]isochromen-6-yl)prop-2-yn-1-yl)-1*H*-benzo [*de*]isoquinoline-1,3(2*H*)-dione (8)

Sonagashira coupling of 2-(prop-2-yn-1-yl)-1*H*-benzo[*de*]isoquinoline-1,3(2*H*)-dione (1.0 g, 4.25 mmol) was performed with 6-bromobenzo[*de*]isochromene-1,3-dione (1.16 g, 4.21 mmol) in *N*,*N*-dimethylformamide (15 ml) and triethylamine (0.21g, 2.12 mmol), bis(triphenylphosphine)palladium(II)dichloride and copper iodide (0.04g, 0.212 mmol) were used as co-catalyst for the reaction and the reaction mixture was heated at 100–110 °C for 3h. On completion of the reaction, water was added, and the precipitates formed were filtered to get the cured product. The product was purified by column chromatography using chloroform: ethyl acetate (0.95:0.5) as eluents.

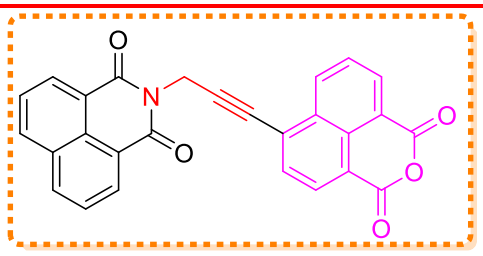

Light brown solid; 75%; R_f 0.5 (5% ethyl acetate in chloroform); m.pt 220-225 ^oC; ^1H NMR ($CDCl_3$ and TFA (0.70: 0.05 ml), 400 MHz) δ 8.77 (dd, ^2J = 8.40 Hz, ^3J = 1.10 Hz, 1H, ArH), 8.74(dd, ^2J = 7.30 Hz, ^3J = 0.90 Hz, 2H, ArH), 8.66 (dd, ^2J = 7.40 Hz, ^3J = 1.00 Hz, 1H, ArH), 8.54 (d, J = 7.60 Hz, 1H, ArH), 8.35 (dd, ^2J = 8.30 Hz, ^3J =0.90 Hz, 2H, ArH), 7.94–7.84 (m, 4H, ArH), 5.42 (s, 2H, CH_2 propargyl); ^{13}C NMR ($CDCl_3$, 100 MHz): δ (ppm) 164.8, 135.8, 134.8, 134.6, 134.0, 133.1, 132.9, 131.9, 130.1, 128.3, 127.5, 121.5, 118.5, 118.3, 115.7, 112.7, 110.0, 95.0, 31.1; ESI-MS (m/z): $[M]^+$ = 431; Anal Calcd for $C_{27}H_{13}NO_5$: C, 75.17; H, 3.04; N, 3.25; found C, 75.15; H, 3.02; N, 3.21.

General procedure for synthesis of amino substituted 2-(3-(1,3-dioxo-1,3-dihydrobenzo[*de*]isochromen-6-yl)prop-2-yn-1-yl)-1*H*-benzo[*de*]isoquinoline-1,3(2*H*)-dione (9a-i)

To a stirred solution of 2-(3-(1,3-dioxo-1,3-dihydrobenzo[*de*]isochromen-6-yl)prop-2-yn-1-yl)-1*H*-benzo[*de*]isoquinoline-1,3(2*H*)-dione (0.2 g, 0.46 mmol) in ethanol (20 ml), different primary amine (0.92 mmol) was added, and the reaction was refluxed for 1h. The reaction mixture was filtered, and the product was collected after washing it with ethanol.

2-allyl-6-(3-(1,3-dioxo-1*H*-benzo[*de*]isoquinolin-2(3*H*)-yl)prop-1-yn-1-yl)-1*H*-benzo[*de*]isoquinoline-1,3(2*H*)-dione (9a)

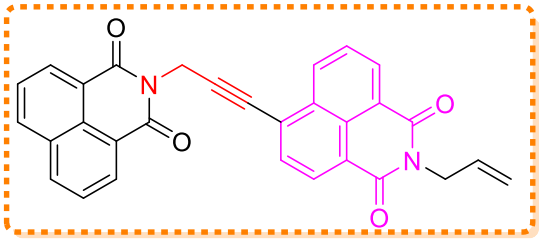

Light green solid; 80% Yield; R_f 0.5 (50% chloroform in hexane); m.pt 220-225 ºC; ^{1}H NMR ($CDCl_3$, TFA (0.70: 0.05 ml), 400 MHz): δ (ppm) 8.70 (td, ^2J = 7.2 Hz, ^3J = 1.0 Hz, 3H), 8.61 (dd, ^2J = 7.3 Hz, ^3J = 1.0 Hz, 1H, ArH), 8.48 (d, J = 7.7 Hz, 1H), 8.31 (dd, ^2J = 8.3 Hz, ^3J = 1.0 Hz, 2H, ArH), 7.88 – 7.81 (m, 4H, ArH), 6.00 – 5.90 (m, 1H, CH allyl), 5.39 (s, 2H, CH_2 propargyl), 5.32 – 5.26 (m, 1H, CH_2 allyl), 5.20 (dd, ^2J = 10.3 Hz, ^3J = 1.2 Hz, 1H, CH_2 allyl), 4.77 (dd, ^2J = 4.1 Hz, ^2J = 2.8 Hz, 2H, CH_2 allyl). ^{13}C NMR ($CDCl_3$, 100 MHz): δ (ppm) 163.9, 135.0, 132.0, 131.8, 131.3, 130.6, 127.7, 127.2, 122.0, 119.9, 119.7, 116.3, 113.4, 110.6, 94.3, 79.1, 42.6, 30.6; ESI-MS (m/z): $[M]^+$ = 470; Anal Calcd for $C_{30}H_{18}N_2O_4$: C, 76.59; H, 3.86; N, 5.95; found C, 76.55; H, 3.84; N, 5.91.

2-benzyl-6-(3-(1,3-dioxo-1*H*-benzo[*de*]isoquinolin-2(3*H*)-yl)prop-1-yn-1-yl)-1*H*-benzo[*de*]isoquinoline-1,3(2*H*)-dione (9b)

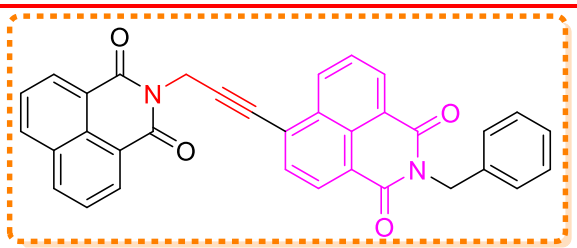

Creamish white; 90% Yield; R_f 0.6 (50% chloroform in hexane); m.pt 245-247 ºC; ^{1}H NMR ($CDCl_3$, DMSO–d_6 400 MHz): δ (ppm) 8.56 – 8.50 (m, 3H, ArH), 8.44 (dd, ^2J = 7.3 Hz, ^3J = 0.9 Hz, 1H, ArH), 8.32 (d, J = 7.7 Hz, 1H, ArH), 8.14 (d, J = 8.2 Hz, 2H, ArH), 7.68 (dd, ^2J = 16.2 Hz, ^3J = 7.9 Hz, 4H, ArH), 7.35 (d, J = 7.2 Hz, 2H, ArH), 7.16 – 7.11 (m, 2H, ArH), 7.07 (t, J = 7.2 Hz, 1H, ArH), 5.22 (s, 2H, CH_2 propargyl), 5.19 (s, 2H, CH_2 benzyl); ^{13}C NMR

(DMSO-d_6,100 MHz): δ (ppm) 163.5, 137.1, 134.6, 132.8, 131.7, 131.1, 130.3, 128.7, 128.4, 128.1, 127.5, 127.1, 122.1, 94.3, 78.9, 30.4; ESI-MS (m/z): $[M]^+$ = 520; Anal Calcd for $C_{34}H_{20}N_2O_4$: C, 78.45; H, 3.87; N, 5.38; found C, 78.41; H, 3.81; N, 5.35.

2-butyl-6-(3-(1,3-dioxo-1*H*-benzo[*de*]isoquinolin-2(3*H*)-yl)prop-1-yn-1-yl)-1*H*-benzo[*de*]isoquinoline-1,3(2*H*)-dione (9c)

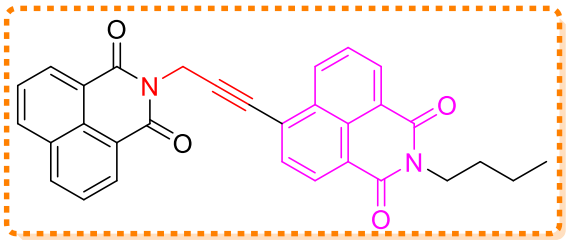

Off white solid; 75% Yield; R_f 0.7 (50% chloroform in hexane); m.pt 225-230 ºC; ^{1}H NMR ($CDCl_3$, 400 MHz): δ (ppm) 8.71 (d, *J* = 7.28 Hz, 2H, ArH), 8.67 (d, *J* = 8.26 Hz, 1H, ArH), 8.59 (d, *J* = 7.28 Hz, 1H, ArH), 8.47 (d, *J* = 7.64 Hz, 1H, ArH), 8.28 (d, *J* = 8.24 Hz, 2H, ArH), 7.86–7.79 (m, 4H, ArH), 5.38 (s, 2H, CH_2 propargyl), 4.17 (t, *J* = 7.52, Hz, 2H, CH_2 butyl), 1.73-1.64 (m, 2H, CH_2 butyl), 1.46-1.40 (m, 2H, CH_2 butyl), 0.98 (t, *J* = 7.28 Hz, 3H, CH_3 butyl); ^{13}C NMR ($CDCl_3$, 100 MHz): δ (ppm) 163.8, 163.6, 134.6, 132.6, 132.0, 131.8, 131.6, 131.3, 130.2, 128.3, 127.9, 127.6, 127.1, 122.8, 122.3, 94.0, 79.1, 40.3, 30.5, 30.2, 20.4, 13.9; ESI-MS (m/z): $[M]^+$ = 486; Anal Calcd for $C_{31}H_{22}N_2O_4$: C, 76.53; H, 4.56; N, 5.76; found C, 76.23; H, 4.21; N, 5.60.

2-(2-(diethylamino)ethyl)-6-(3-(1,3-dioxo-1*H*-benzo[*de*]isoquinolin-2(3*H*)-yl)prop-1-yn-1-yl)-1*H*-benzo[*de*]isoquinoline-1,3(2*H*)-dione (9d)

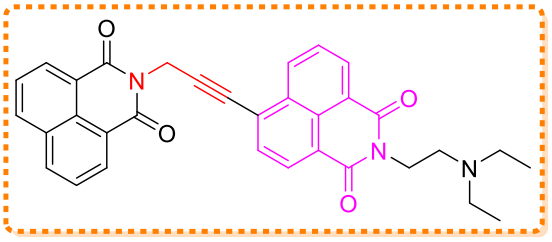

Off white solid; 72% Yield; R_f 0.4 (60% chloroform in hexane); m.pt 233-237 ºC; ^{1}H NMR ($CDCl_3$, TFA (0.70: 0.05 ml) 400 MHz): δ (ppm) 8.61 (t, *J* = 4.88 Hz, 3H, ArH), 8.57 (d, *J* = 7.48 Hz, 1H, ArH), 8.39 (d, *J* = 8.48 Hz, 1H, ArH), 8.30 (d, *J* = 8.28 Hz, 2H, ArH), 7.87 (t, *J* = 8.16 Hz, 1H, ArH), 7.79 (d, *J* = 8.12 Hz, 3H, ArH), 5.22 (s, 2H, CH_2 propargyl), 4.58-4.54 (m, 4H, 2*CH_2 diethyl), 3.56 (q, *J* = 5.84 Hz, 2H, CH_2 diethyl), 3.44 (q, *J* = 6.84 Hz, 2H, ArH), 1.40 (t, *J* = 7.12 Hz, 6H, 2*CH_3 diethyl) ^{13}C NMR ($CDCl_3$, 100 MHz): δ (ppm) 165.2, 164.7, 135.6, 132.6, 132.3, 132.2, 131.7, 131.0, 129.7, 128.3, 127.8, 127.3, 121.6, 121.3, 121.0, 116.0, 113.0, 50.2, 49.0, 47.8, 34.9, 8.5; ESI-MS (m/z): $[M]^+$ = 529; Anal Calcd for $C_{33}H_{27}N_3O_4$: C, 74.84; H, 5.14; N, 7.93; found C, 74.81; H, 5.11; N, 7.91.

2-(2-(dimethylamino)ethyl)-6-(3-(1,3-dioxo-1*H*-benzo[*de*]isoquinolin-2(3*H*)-yl)prop-1-yn-1-yl)-1*H*-benzo[*de*]isoquinoline-1,3(2*H*)-dione (9e)

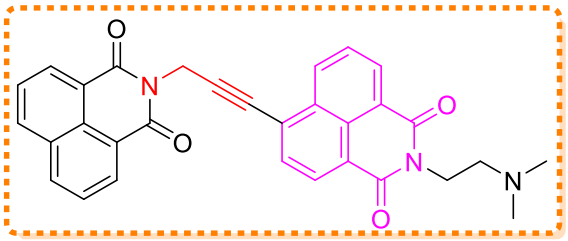

Light yellow solid; 84% Yield; R_f 0.3 (60% chloroform in hexane); m.pt 240-243 ºC; ^{1}H NMR ($CDCl_3$, 400 MHz): δ 8.60 (dd,^2J = 7.3 Hz, ^3J = 0.7 Hz, 1H), 8.57 – 8.54 (m, 3H, ArH), 8.31 – 8.28 (m, 1H, ArH), 8.23 (dd, ^2J = 8.2 Hz, ^3J = 0.7 Hz, 2H, ArH), 7.82 – 7.67 (m, 4H, ArH), 5.10 (s, 1H, CH_2 propargyl), 4.47 (s, 1H, CH_2 propargyl), 4.34 (t, J = 8 Hz, 2H, CH_2 dimethyl), 2.67 (d, J = 8.0 Hz, 2H, CH_2 dimethyl), 2.34 (s, 6H, 2* CH_3 dimethyl); ^{13}C NMR ($CDCl_3$, 100 MHz): δ (ppm) 163.8, 137.3, 134.6, 131.7, 131.3, 131.0, 130.7, 130.5, 129.1, 128.6, 128.2, 127.3, 123.1, 122.0, 121.9, 56.9, 48.6, 45.7, 38.1; ESI-MS (m/z): $[M]^+$ = 501; Anal Calcd for $C_{31}H_{23}N_3O_4$: C, 74.24; H, 4.62; N, 8.38; found C, 74.00; H, 4.50; N, 8.21.

6-(3-(1,3-dioxo-1*H*-benzo[*de*]isoquinolin-2(3*H*)-yl)prop-1-yn-1-yl)-2-(2-hydroxyethyl)-1*H*-benzo[*de*]isoquinoline-1,3(2*H*)-dione (9f)

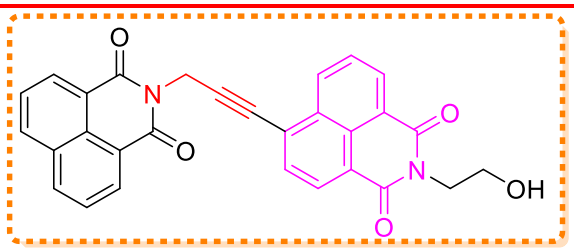

Light green solid; 87% Yield; R_f 0.4 (70% chloroform in hexane); m.pt 225-230 ºC; ^{1}H NMR ($CDCl_3$, TFA (0.70 : 0.05 ml) 400 MHz): 8.74-8.71 (m, 3H, ArH), 8.63 (dd, ^2J = 7.40 Hz, ^3J = 1.00 Hz, 1H, ArH), 8.51 (d, J = 7.68 Hz, 1H, ArH), 8.34 (d, J = 8.24 Hz, 2H, ArH), 7.88–7.84 (m, 4H, ArH), 5.41 (s, 2H, CH_2 propargyl), 4.70 (t, J = 5.12 Hz, 2H, CH_2 ethanolamine), 4.61 (t, J = 5.20 Hz, 2H, CH_2 ethanolamine); ^{13}C NMR ($CDCl_3$, 100 MHz): δ (ppm) 165.0, 164.6, 135.6, 132.8, 132.7, 132.0, 131.7, 131.6, 131.3, 128.7, 128.0, 127.4, 121.6, 121.1, 94.2, 79.3, 65.1, 38.7, 31.0; ESI-MS (m/z): $[M]^+$ = 474; Anal Calcd for $C_{29}H_{18}N_2O_5$: C, 73.41; H, 3.82; N, 5.90; found C, 73.11; H, 3.62; N, 5.76.

6-(3-(1,3-dioxo-1*H*-benzo[*de*]isoquinolin-2(3*H*)-yl)prop-1-yn-1-yl)-2-(2-morpholino ethyl)-1*H*-benzo[*de*]isoquinoline-1,3(2*H*)-dione (9g)

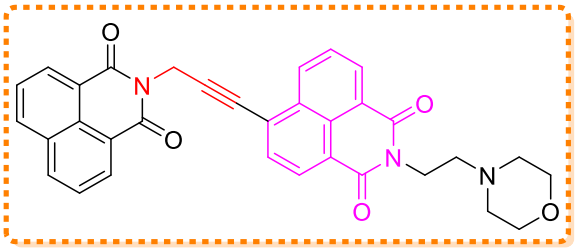

Light brown solid; 75% Yield; R_f 0.5 (chloroform); m.pt 240-242 ºC; ^{1}H NMR (DMSO-d_6, TFA (0.70 : 0.05 ml), 400 MHz): δ (ppm) 8.63 (d, *J* = 8.36 Hz, 1H, ArH), 8.56 (d, *J* = 7.28 Hz, 2H, ArH), 8.51 (d, *J* = 7.32 Hz, 1H, ArH), 8.49 (d, *J* = 8.04 Hz, 2H, ArH), 8.40 (d, *J* = 7.68 Hz, 1H, ArH), 7.96-7.86 (m, 4H, ArH), 5.24 (s, 2H, CH_2 propargyl), 4.37 (t, *J* = 5.76 Hz, 2H, CH_2 morpholinoethyl), 3.98 (d, *J* = 12.36 Hz, 2H, CH_2 morpholinoethyl), 3.63-3.46 (m, 6H, 3*CH_2 morpholinoethyl), 3.12 (br(s), 2H, CH_2 morpholinoethyl), ^{13}C NMR ($CDCl_3$, 100 MHz): δ (ppm) 163.9, 163.5, 135.4, 132.5, 131.9, 131.8, 131.7, 130.6, 128.8, 127.9, 126.6, 123.1, 122.5, 122.3, 122.1, 96.2, 78.4, 63.6, 54.4, 52.0, 34.8, 30.5; ESI-MS (m/z): $[M]^+$ = 543; Anal Calcd for $C_{33}H_{25}N_3O_5$: C, 72.92; H, 4.64; N, 7.73; found C, 72.89; H, 4.61; N, 7.71.

6-(3-(1,3-dioxo-1*H*-benzo[*de*]isoquinolin-2(3*H*)-yl)prop-1-yn-1-yl)-2-(2-(piperazin-1-yl)ethyl)-1*H*-benzo[*de*]isoquinoline-1,3(2*H*)-dione (9h)

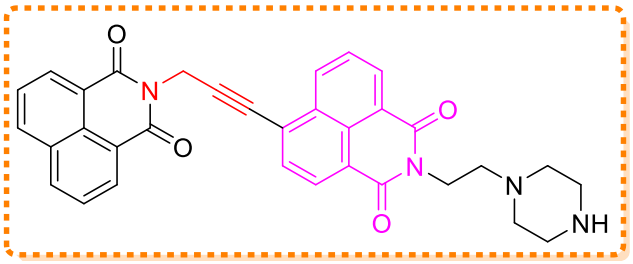

Red solid; 70% Yield; R_f 0.4 (chloroform); m.pt 250-254 ºC; ^{1}H NMR ($CDCl_3$, 400 MHz): δ (ppm) 8.60-8.54 (m, 4H, ArH), 8.31 (d, *J* = 8.40 Hz, 1H, ArH), 8.24 (d, *J* = 7.68 Hz, 2H, ArH), 7.82-7.69 (m, 4H, ArH), 4.48 (s, 2H, CH_2 propargyl), 4.34 (t, *J* = 5.20 Hz, 2H, CH_2 ethyl piperazine), 2.88 (t, *J* = 4.76 Hz, 4H, 2*CH_2 ethyl piperazine), 2.69 (t, *J* = 7.20 Hz, 2H, CH_2 ethyl piperazine), 2.58 (br(s), 4H, 2*CH_2 ethyl piperazine); ^{13}C NMR ($CDCl_3$, 100 MHz): δ (ppm) 164.2, 164.0, 137.4, 134.7, 131.8, 131.7, 131.3, 131.0, 130.8, 130.6, 129.3, 128.6, 128.3, 127.4, 127.1, 123.1, 122.4, 122.0, 78.8, 56.2, 54.4, 48.7, 45.9, 45.6, 37.3; ESI-MS (m/z): $[M]^+$ = 543; Anal Calcd for $C_{33}H_{26}N_4O_4$: C, 73.05; H, 4.83; N, 10.33; found C, 72.92; H, 4.61; N, 10.30.

6-(3-(1,3-dioxo-1*H*-benzo[*de*]isoquinolin-2(3*H*)-yl)prop-1-yn-1-yl)-2 -(prop-2-yn-1-yl)-1*H*-benzo[*de*]isoquinoline-1,3(2*H*)-dione (9i)

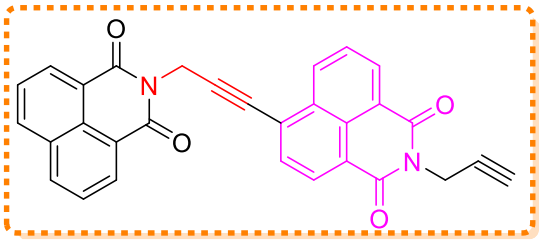

Whitish cream solid; 84% Yield; R_f 0.5 (60% chloroform in hexane); m.pt 230-233 ºC; ^{1}H NMR (DMSO-d_6, 400 MHz): δ (ppm) 8.62 (d, *J* = 8.12 Hz, 1H, ArH), 8.57 (d, *J* = 7.16 Hz, 2H, ArH), 8.53-8.45 (m, 4H, ArH), 8.41 (d, *J* = 7.64 Hz, 1H, ArH), 7.90 (t, *J* = 7.96 Hz, 3H, ArH), 5.24 (s, 2H, CH_2 propargyl), 4.71 (s, 2H, CH_2 propargyl), 3.11 (s, 1H, CH propargyl); ^{13}C NMR ($CDCl_3$, 100 MHz): δ (ppm) 163.5, 163.2, 134.5, 133.1, 131.9, 131.7, 131.3, 130.6, 128.3, 127.9, 127.6, 127.1, 122.4, 122.3, 94.4, 78.4, 70.5, 30.4, 29.4; ESI-MS (m/z): $[M]^+$ = 468; Anal Calcd for $C_{30}H_{16}N_2O_4$: C, 76.92; H, 3.44; N, 5.98; found C, 76.90; H, 3.40; N, 5.96.

Sub Chapter 3.2

Bis-naphthalimides without spacer as potent antibacterial agents

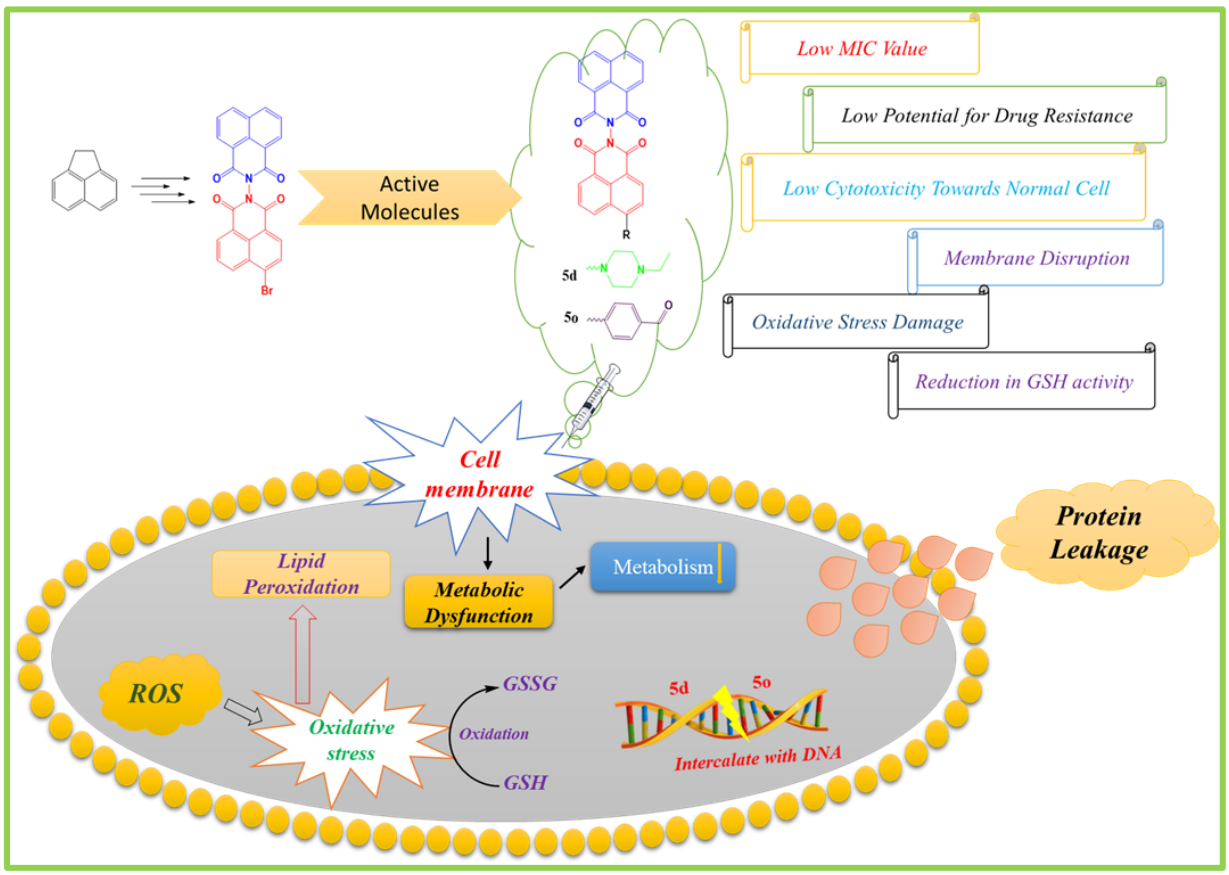

3.2.1 Introduction

The deadly infectious diseases caused by bacterial pathogens are spreading around the globe and pose serious health safety issues to people.[95] The primary treatment for controlling these pathogenic infections is exhibited with the use of antibiotics.[96] However, antibiotics are incapable of treating these deadly pathogens due to their abuse and overuse, thus serving large socio-economic effects and threats to human health. If these drug-resistant pathogens responsible for infections are left untreated, then these will kill more people than cancer. According to reports in 2016, about 1 million people were killed due to bacterial infections, and the number of deaths will rise to 10 million per year by 2050 if no crucial steps are taken to prevent bacterial resistance.[97] Moreover, bacterial pathogens have become resistant to present antibiotics due to modification in their genome by random mutations, thus making the treatment of infectious diseases an extensive challenge and an obvious issue to science community.[98] Various multidrug-resistant (MDR) bacterial pathogens such as vancomycin-resistant *Enterococcus faecalis* (VRE), methicillin-resistant *Staphylococcus aureus* (MRSA) and carbapenem-resistant *Acinetobacter baumannii* are responsible for the infections prevailing around the world.[99] Of all the bacterial pathogens responsible for infectious diseases, treatment of *E. faecalis* pathogens causing infections remains a serious challenge as it is found as a symbiotic organism on the intestinal tract, mucosal surface, skin of human hosts and oral cavities.[100] Some *E. faecalis* cause extensive infection due to changes in genes in long-term evolution, such as pelvic, urinary tract and abdominal infections.[101] Most of the clinically isolated *E. faecalis* have the ability to form a biofilm, leading to multi-drug resistance as it safeguards the bacteria by forming extracellular polymer substances, restricting penetration and diffusion of antibiotics into the cells.[102] *E. faecalis* is susceptible to inducing resistance to various clinically antibacterial agents such as linezolid, daptomycin and vancomycin due to the thick cell wall associated with them.[103] Nowadays, number of drugs having a single target is increasing day by day, but these are inefficient in inhibiting the MDR bacterial pathogens due to target failure because of bacterial genetic mutation. Hence, there is an urgent need to develop new antibacterial agents having dual targets towards biofilm formation and planktonic growth against *E. faecalis*, thus opening new aspects for treating threatful infections.[104]

3.2.2 Designing of the antibacterial agents

Naphthalimide, a well-known DNA intercalator, has been well-explored for its anticancer properties. Nowadays, researchers are focusing on developing naphthalimide-based

antibacterial agents by modifications in their structure, as its hydrophobic nature makes it easier to impede into phospholipid layer of the bacterial membrane. To the best of our knowledge, bis-naphthalimides have not been explored for antibacterial properties.

So, in view of the prevailing problems and considering the above analysis, we have designed and synthesized novel bis-naphthalimide scaffolds by substituting secondary amines and aryl groups to explore the effect on bioactivity of compounds. All the prepared bis-naphthalimides were examined for their antibacterial potential against eight bacterial strains. The most potent compounds, **11d** and **11o,** were further examined for their mode of action *via* membrane disruption, protein leakage, biofilm inhibition, metabolic dysfunction, oxidative stress damage, and lipid peroxidation of *E. faecalis*. Moreover, interactions of **11d** and **11o** with DNA were studied with spectroscopic techniques to build DNA-targeted antibacterial agents. Furthermore, the binding behaviour of active compounds with HSA was explored for the transportation of potent drug candidates to the target site.

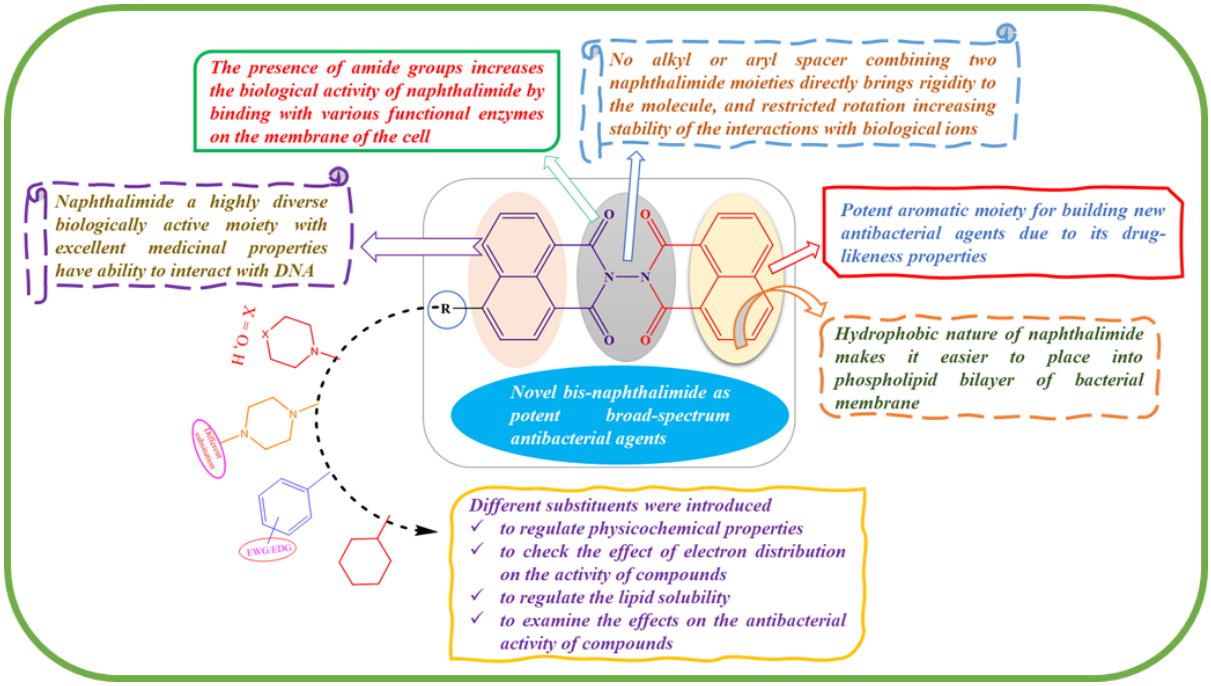

Figure 3.14. Designing of bis-naphthalimides as potent antibacterial agents

3.2.3. Chemistry

The anticipated intermediates and substituted bis-naphthalimides were furnished in line with the route shown in **Scheme 1.** The commercially available acenaphthene (**1**) was oxidised using sodium dichromate in refluxing acetic acid to afford **2**. Compound **2** underwent nucleophilic addition followed by elimination of water with hydrazine hydrate in ethanol at room temperature to get intermediate **10**, that was further reacted with 6-bromo-1*H*,3*H*-

benzo[*de*]isochromene-1,3-dione in the presence of zinc acetate in refluxing ethanol to afford intermediate **11**. The bis-naphthalimides **11a-h** were prepared by reacting compound **11** with corresponding amines in the presence of potassium carbonate in heated *N*,*N*-dimethylformamide for 3-4 h, whereas derivatives **11i-p** were obtained by Suzuki-Miyaura coupling reaction with different boronic acids in the presence of potassium carbonate and tetrakis(triphenylphosphine)palladium (0) in refluxing acetonitrile and water (9:1) for 5-7 h. ^{1}H NMR, ^{13}C NMR, and HRMS were used for the characterization of synthesized compounds. All the compounds were synthesized in moderate to good yields ranging from 65% to 85%.

Scheme 1: Synthesis of 6-bromo-1*H*,1'*H*,3*H*,3'*H*-[2,2'-bibenzo[*de*]isoquinoline]-1,1',3,3'-tetraone

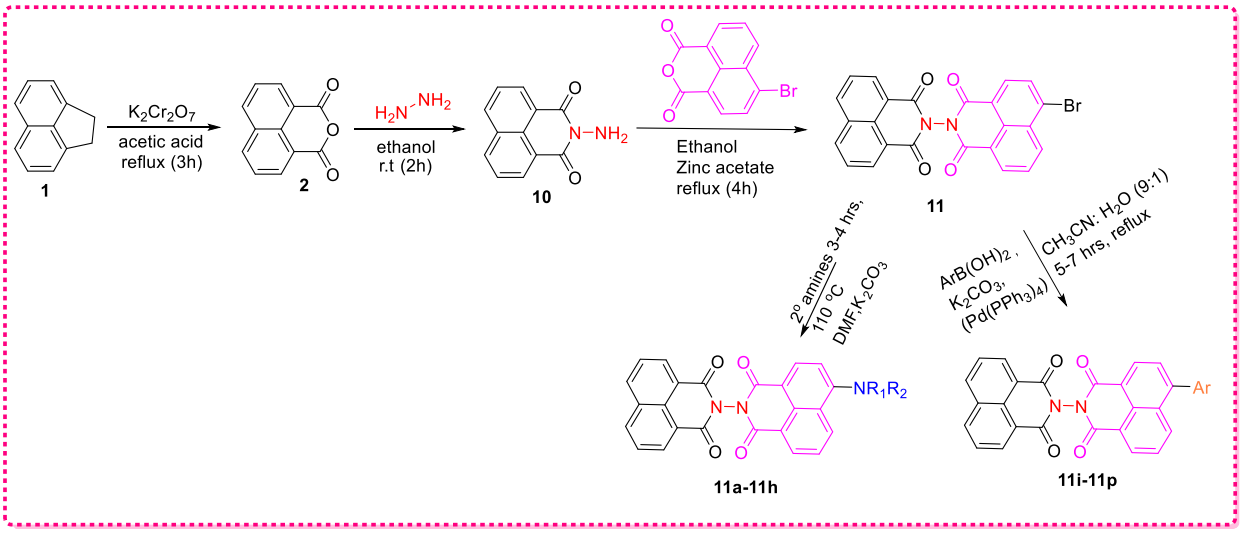

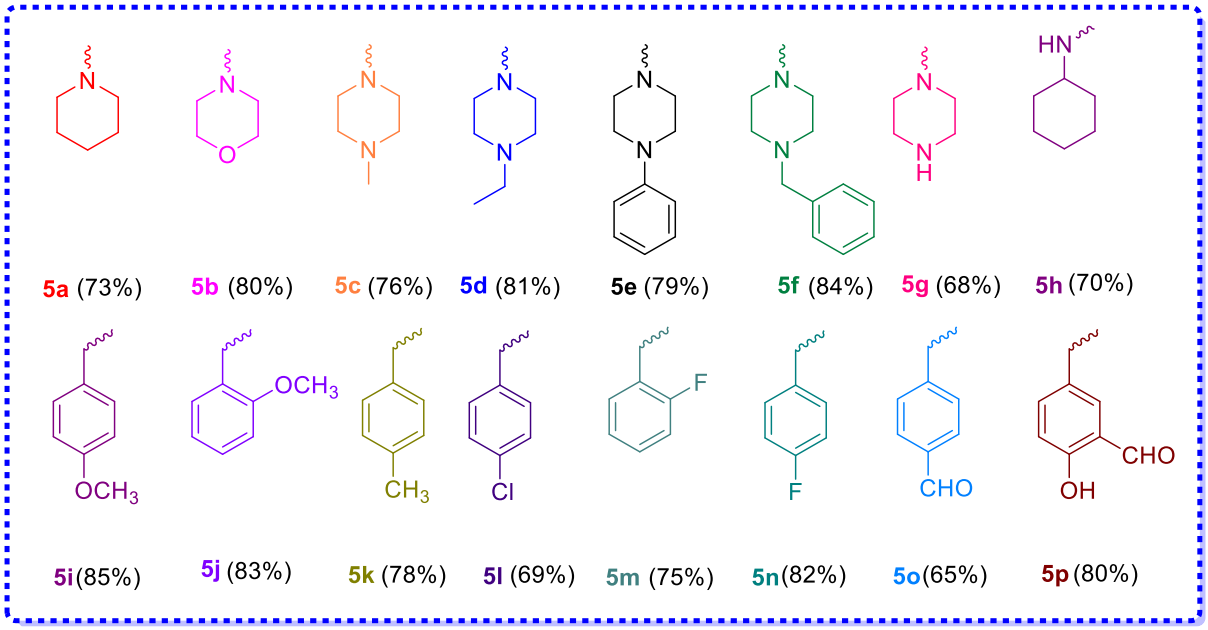

3.2.4. *In vitro* antibacterial activity

The newly synthesized bis-naphthalimides were evaluated for their potential to exhibit antibacterial properties, as recommended by CLSI, using a two-fold serial dilution method.[90,91] These derivatives were examined against four gram-positive *viz. Staphylococcus aureus*, *Enterococcus faecalis*, *Bacillus subtilis*, *Listeria,* and four gram-negative such as *Escherichia coli, Salmonella enterica*, *Acinetobacter calcoaceticus, Serratia marcescens* bacteria strains. As depicted in **Table 3.9**, piperidine substituted bis-naphthalimide (**11a**) showed better bioactivity towards gram-positive than gram-negative bacteria, particularly against *E. faecalis* and *S. aureus* (MICs = 6.25 μg/ml). The introduction of morpholine group (**11b**) led to decrease in bioactivity against all the tested bacteria, but it could selectively suppress the growth of *E. coli* bacteria with MIC value of 1.56 μg/ml. The methyl piperazine substituted **11c** was able to inhibit the growth of *E. faecalis* and *A. calcoaceticus* at a low concentration (MIC = 12.5 and 6.25 μg/ml). Further structural optimization showed that the substitution of ethyl piperazine increased the bioactivity of compound **11d,** which exhibited broad-spectrum antibacterial activities against all the tested bacteria with a low value of MIC ranging from 1.56 – 25 μg/ml. The antibacterial activity of **11d** outperformed the marketed amoxicillin, and the results were comparable to tetracycline and chloromycin. Further, the substitution of **11** with phenyl piperazine (**11e**), benzyl piperazine (**11f**) and cyclohexylamine (**11h**) resulted in loss of bioactivity due to increase in electron density on the ring, and these were poor performers in inhibiting the bacterial growth whether gram-positive or gram-negative. In contrast, compound **11g** showed moderate activity against the gram-positive bacteria, with a MIC value of 25 μg/ml, whereas it remarkably inhibited the growth of *E. coli* with a MIC of 3.125 μg/ml. In the present study, by replacing the amine substitution with substituted aryl groups, **11i**–**11j** was purposely synthesized to explore their effects on bioactivity. Compound **11,** when substituted with the aryl group having different electron-donating groups (**11i-l**)**,** showed no activity against all the tested bacteria and was unable to restrict the growth of the bacterial strains. In contrast, the introduction of electron-withdrawing groups on the ring proved beneficial in suppressing bacterial growth. Compound **11m,** having fluoro at *ortho* position, exhibited better activity than **11i-l**. The compound was active against *E. faecalis* and *E. coli,* having MIC values of 6.25 and 3.125 μg/ml, respectively. It could also effectively suppress the growth of *S. enterica* with low MIC value of 1.56 μg/ml. Swapping fluorine from *ortho* to *para* position did not affect bacterial growth and was unable to suppress the bacterial growth. To strengthen the bioactivity of compounds, electron-withdrawing groups (**11o** and **11p**), were introduced to compound **11**; as expected, these compounds exhibited excellent activity in suppressing

bacterial growth. Compared with the results of former compounds, **11o** having carbaldehyde group exhibited promising results against all the tested bacterial strains. The compound **11o** (MIC = 6.25-1.56 μg/ml) was able to suppress the growth of all the tested bacterial strains except *E. coli*. It outperformed the marketed drug amoxicillin, and results were comparable to tetracycline and chloromycin, indicating a potent antibacterial agent and would be taken further for clinical trials. The addition of hydroxy group, as in **11p**, resulted in slight decrease in bioactivity but was still better than amoxicillin and comparable to the other two marketed drugs.

In view of the above-discussed antibacterial activities of the synthesized compounds **11a-p**, the introduction of electron-withdrawing groups was favourable for improving the bioactivity. Therefore, compounds **11d** and **11o** were selected as highly active molecules for further evaluation for their antibacterial studies and the preliminary mechanism depiction based on their potency against *E. faecalis*.

Table 3.9. Antibacterial activity data as MIC (μg/ml) for compounds **11a-p**

Comp	Gram Positive Bacterial Strains				Gram Negative Bacterial Strains			
	E. faecalis	*B. subtilis*	*L. species*	*S. aureus*	*E. coli*	*S. enterica*	*A. calcoaceticus*	*S. marcescens*
11a	6.25	-	-	6.25	12.5	-	-	-
11b	-	-	-	-	1.56	-	-	-
11c	12.5	-	-	-	-	-	6.25	-
11d	3.12	-	25	1.56	1.56	3.125	-	3.125
11e	-	-	-	-	-	-	-	-
11f	-	-	-	-	-	-	-	-
11g	25	-	25	25	3.125	-	-	-
11h	-	-	-	-	-	-	-	-
11i	-	-	-	-	-	-	-	-
11j	-	-	-	-	-	-	-	-
11k	-	-	-	-	-	-	-	-
11l	-	-	-	-	-	-	-	-
11m	6.25	-	-	-	3.125	1.56	-	25
11n	-	-	-	-	-	-	-	-
11o	1.56	1.56	1.56	3.125	-	6.25	3.125	1.56
11p	-	3.125	-	3.125	3.125	1.56	1.56	1.56
A	6.25	50	50	25	100	200	50	1.56
B	3.125	1.56	6.25	1.56	1.56	100	1.56	1.56
C	3.125	1.56	1.56	3.125	3.125	50	3.25	1.56

A - amoxicillin; B - tetracycline; C – chloromycin, - > 200

3.2.5. Bactericidal or bacteriostatic action

In view of the results depicted in the antibacterial evaluation, the Minimal Bactericidal Concentration (MBC) was calculated to get insight into the mode of action of most active compounds **11d** and **11o** against *E. faecalis* (**Table 3.10**), whether bactericidal or bacteriostatic

nature. The results revealed that both compounds **11d** and **11o** have MBC/MIC values of 4 and 2, respectively, indicating the bactericidal nature of both derivatives.

Table 3.10. Evaluation of MBC and MIC values of active compounds against *E. faecalis*

Compound	MBC (μg/ml)	MIC (μg/ml)	MBC/MIC
11d	12.5	3.12	4
11o	3.12	1.56	2

3.2.6 Bacterial susceptibility evaluation

The purpose of developing new antibacterial agents is to overcome the emergence of resistance by bacterial strains and to present antibiotics in treating infectious diseases.[105] Thus, bacterial susceptibility studies of **11d** and **11o** were performed against *E. faecalis* as the tested strain. As represented in **Figure 3.15**, **11d** and **11o** displayed better and prolonged inhibitory abilities against the tested strains compared to control drugs amoxicillin and tetracycline. MIC remains consistent in both the compounds and stable even after 20 passages. In contrast, MIC values of positive controls increase dramatically after 6th day in case of tetracycline and 9th day for amoxicillin. While comparing the results of both the compounds **11d** and **11o**, the latter exhibited better results than the former in resistance studies. The MIC of **11d** increased 2-fold after 15 passages, whereas MIC value of **11o** did not change till 18 passages. These results revealed that both compounds could effectively hinder the development of resistance by bacteria.

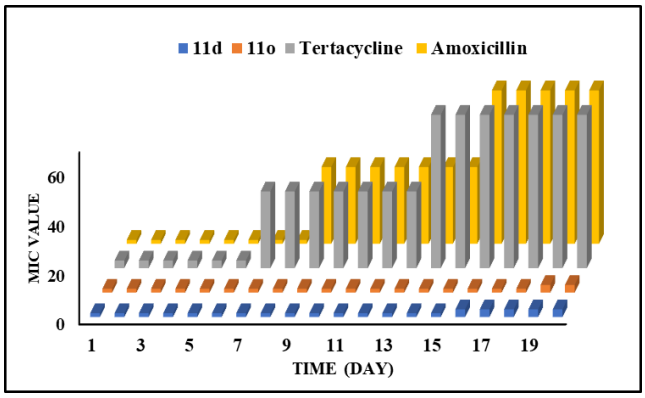

Figure 3.15. Bacterial suppressibility evaluation of **11d, 11o,** tetracycline, and amoxicillin towards *E. faecalis*

3.2.7. Kinetics of bactericidal activity

Rapid bactericidal action is crucial for a drug to exist as a promising antibacterial agent, helping to delay the progress of drug resistance and shortening treatment time.[106] Thus, a time-kill assay of most active compounds, **11d** and **11o**, was examined against *E. faecalis* as a function of time and different concentrations (**Figures 3.16a** and **3.16b**). *E. faecalis* in the control group entered the exponential phase within 3h, whereas the growth of bacteria was suppressed and killed in the presence of both compounds. Compound **11o** was able to kill the bacteria within 4h, whereas **11d** killed the same within 5h at MIC value. At concentrations of 2×MIC, 4×MIC, and 8×MIC, the killing time of bacteria by both compounds **11d** and **11o** was decreased from 5h to 3.5h and 4h to 2.5h, respectively, indicating the rapid bactericidal action by both compounds at higher concentrations.

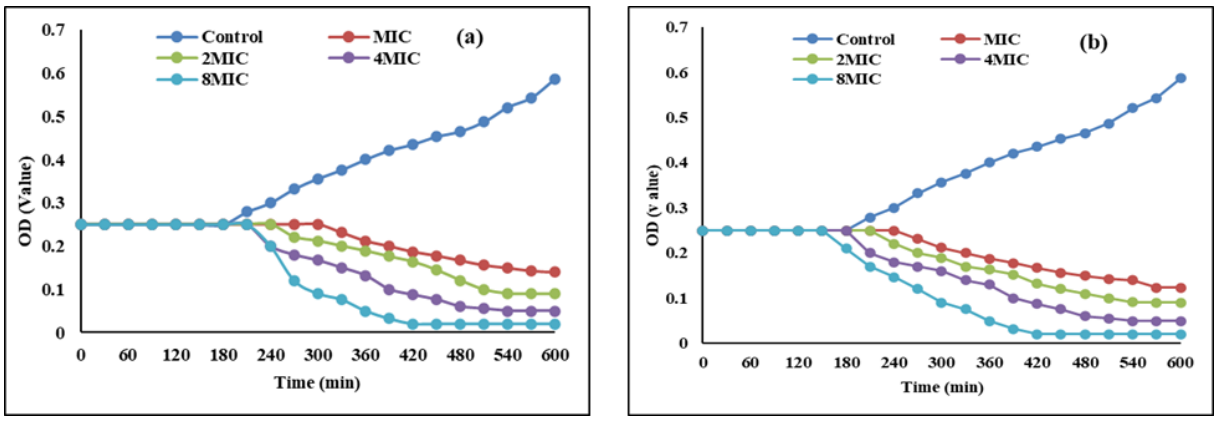

Figure 3.16: Time-killing kinetics of *E. faecalis*; (a) **11d** and (b) **11o** at various concentrations

3.2.8 Cytotoxicity assay

Abnormal toxicity risks and death of organisms may be triggered due to cytotoxicity of new drugs toward normal cell lines.[107] The ability of potent candidates to selectively kill bacterial cells over normal cells is an important element for their further growth as antibacterial agents. Hence, cytotoxicity effects of compounds, **11d** and **11o,** were evaluated against normal cell line (Hek293) using MTT assay. The results revealed that compound **11d** showed 8.2%, 12.0%, 14.9%, 15.4%, and 16.3%, whereas **11o** displayed only 4.9%, 10.6%, 12.0%, 13.5%, and 14.0% cytotoxicity against normal cell lines at various concentrations (**Figure 3.17a**). Compound **11o** was less toxic to normal cells than **11d,** thus more selective towards bacteria cells.

Furthermore, the cytotoxicity effect of these compounds towards cancer cells was also evaluated to confirm whether these compounds are selectively toxic to bacterial cells only or

can have the potential to kill cancer cells. The National Cancer Institute, USA selected all the synthesized bis-naphthalimides (**11a-11p**), on the fact that these have different substitutions for evaluating their cytotoxicity towards 60 human tumour cell lines at a dose of 10 μM concentration, where growth inhibitions in percentage were calculated. All the molecules exhibited low toxicity against all the tested cancer cells. Compounds **11d** and **11o** were mostly inactive against all the tested human carcinoma cell lines (**Figure 3.17b**). Thus, these results displayed that both compounds selectively kill bacterial cells only.

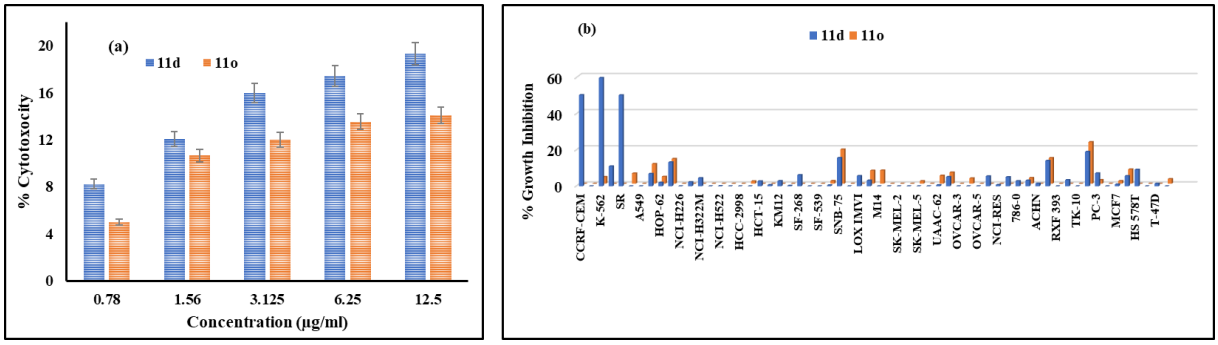

Figure 3.17: Cytotoxicity of compounds **11d** and **11o** towards (a) normal cell line Hek293 and (b) 60 human cancer cell lines.

3.2.9 ADME studies of active compounds

Further, to explore the medicinal properties of active compounds, ADME studies were conducted with the help of Swiss ADME software, where pharmacokinetic properties and drug-likeness were explored.[108] **Table 3.9** suggests that both compounds have better intestinal absorption than reference drugs. The bioavailability scores of both compounds were similar to those of tetracycline and amoxicillin. Furthermore, these compounds were unable to penetrate the blood-brain barrier, indicating the biosafety and non-toxic nature of compounds. Remarkably, compound **11o** satisfied the Lipinski's rule of five, but in **11d,** molecular weight exceeds 500 g/mol, violating one rule of Lipinski. Thus, **11o** displayed better bioactivity than **11d**. These results depicted that **11d** and **11o** displayed a high degree of drug-likeness and can be taken for further studies to explore the mechanism of bioactive compounds.

Table 3.9: The ADME evaluation data of compounds **11d, 11o,** tetracycline and amoxicillin

	11d	**11o**	**Tetra**	**Amox**
M.W	505.5	496.4	444.5	365.4
M logP	4.0	3.19	2.17	0.95
H-Bond acceptor	5	5	7	6
H-Bond donor	0	0	5	4
Rotatable bond	3	3	2	5

Bioavailability score	0.55	0.55	0.55	0.55
TPSA	84.62	95.21	144.3	158.2
Lipinski rule	1	0	0	0
BBB	No	No	No	No
GI absorption	High	High	Low	Low

3.2.10 Biofilm inhibition assay

Biofilm-growing bacteria on their surface are more resistant to attack by the host immune system than in their planktonic state, thus facilitating drug resistance and reducing the drug's therapeutic values.[109] Compounds **11d** and **11o** were further evaluated for their potential to inhibit the growth of *E. faecalis* biofilm by employing crystal violet assay. As shown in **Figure 3.18**, the formation of biofilm by *E. faecalis* was significantly inhibited and decreased with increasing concentrations (MIC, 2×MIC, 4×MIC, 8×MIC) of compounds. Both compounds inhibited biofilm formation up to 27% and 30% at MIC values, respectively. These compounds displayed better inhibitory effects compared to reference drugs tetracycline (20% inhibition) and amoxicillin (21% inhibition). The inhibition of the biofilm of *E. faecalis* by **11d** and **11o** were increased with increasing concentration of compounds, and up to 80% and 86% inhibitions of the biofilm were observed at 8×MIC value. These results suggested that both compounds could resist the formation of biofilm effectively, thus delaying the development of bacterial resistance.

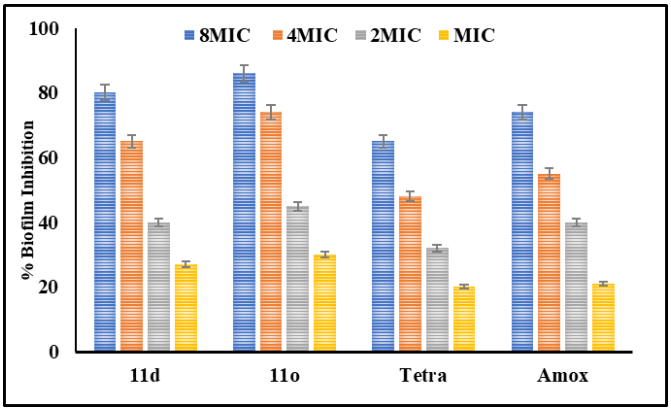

Figure 3.18. Inhibition of biofilm of *E. faecalis* in the presence of compounds **11d** and **11o** at different concentrations.

3.2.11 Membrane permeability

The bacterial cell membrane plays a crucial role in maintaining bacteria's morphological behaviour and energy metabolism.[110] Cell membrane is an obstacle for extracellular substances from entering the cell freely, thus securing the relative stability of intracellular environment and allowing the proper functioning of various biochemical reactions.[111] Many available

antibiotics have poor membrane permeability, thus accelerating the development of drug resistance. Disrupting the cell membrane of bacteria leads to morphological breakage or physiological dysfunction. Therefore, we have explored the effect of active compounds on membrane permeability and checked whether these can effectively penetrate the cell membrane.

3.2.11a Outer membrane permeability

E. faecalis does not have any outer membrane; rather, it contains a thick cell wall of peptidoglycan, which is difficult to break, thus assisting the growth of drug resistance. The ability of compounds **11d** and **11o** to disrupt this thick bacterial cell wall was explored by using 1-*N*-phenylethylamine (NPN). The fluorescence increased gradually upon incubating with **11d** and **11o** in both concentrations and time-dependent modes (**Figures 3.19**), and this increase in fluorescence intensity was more in **11o** than **11d**. These compounds also displayed better results than reference drugs, suggesting that **11d** and **11o** have a greater ability to pierce the thick cell wall.

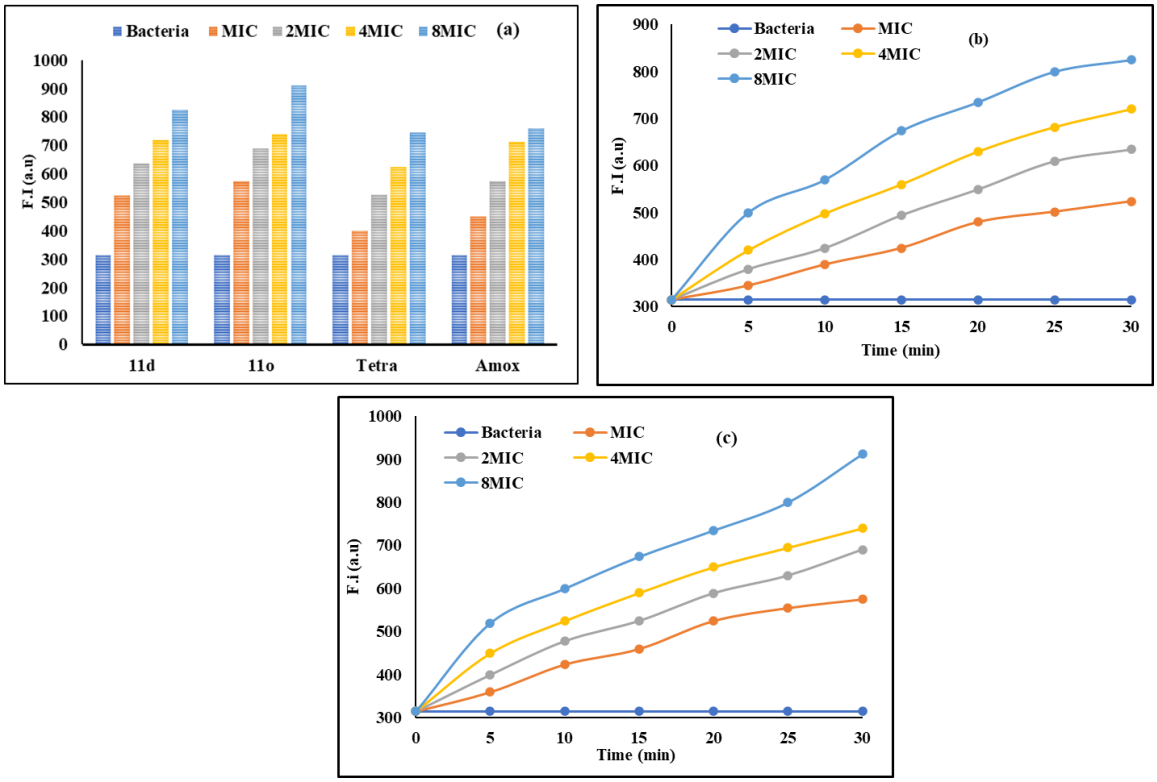

Figure 3.19: Outer membrane permeability of *E. faecalis* with compounds **11d, 11o,** tetracycline, and amoxicillin (a) at different concentrations, and in a time-dependent mode; (b) compound **11d** and (c) compound **11o**

3.2.11b Inner membrane permeability

The selective permeability of cell membrane vanishes by destroying the structural integrity of cell membrane, disrupting the intracellular environment and persuading cell death.[112] The penetration of inner cell membrane by active compounds **11d** and **11o** was further explored using ethidium bromide (EtBr) assay.[113] *E. faecalis* was treated with increasing concentrations of compounds **11d** and **11o** and a known amount of EtBr dye. Significant enhancement was observed on treating bacterial cells with compounds, and the fluorescence intensity increased in a time and concentration-dependent mode, revealing the increase in number of cells with damaged membranes (**Figures 3.20)**. The increase in fluorescence intensity was higher in compound **11o** as compared to **11d,** suggesting that **11o** has a greater potential to penetrate the cell's inner membrane. Furthermore, these displayed greater inner membrane permeability compared to reference drugs tetracycline and amoxicillin.

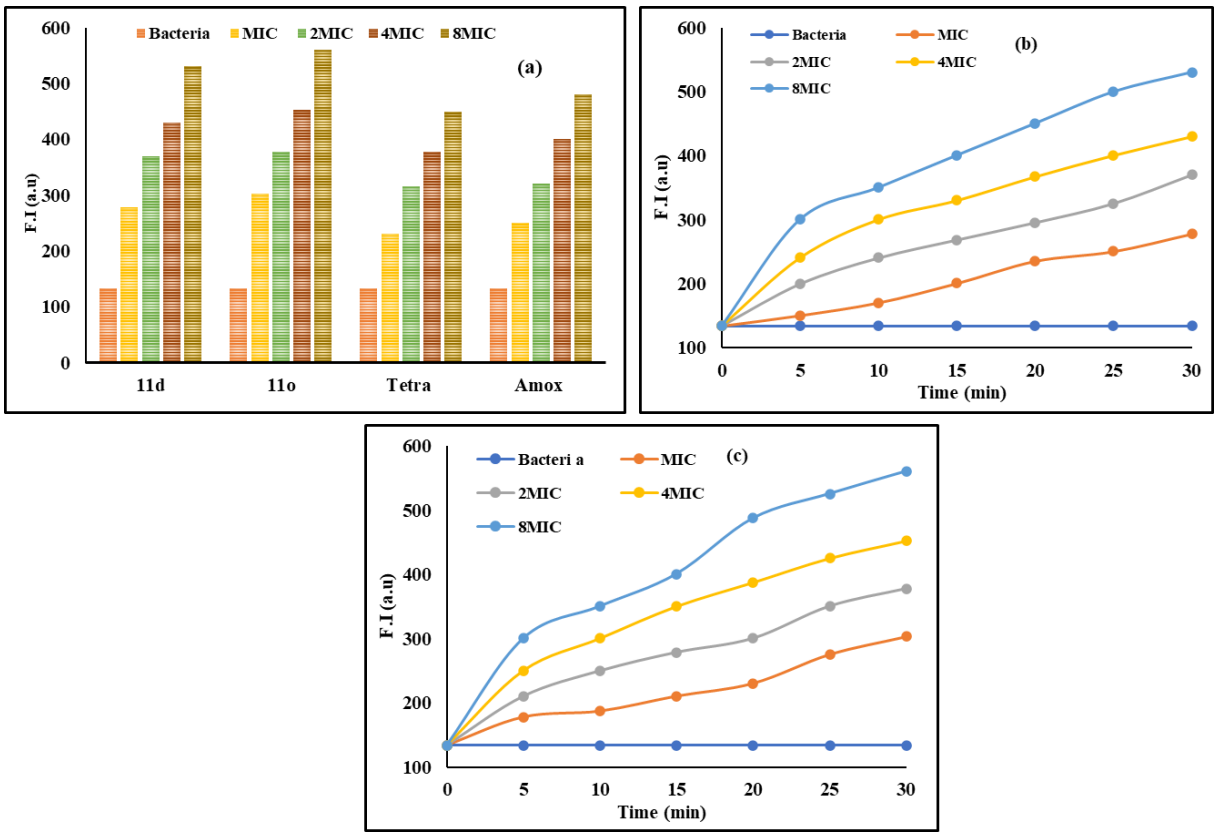

Figure 3.20: Inner membrane permeability of *E. faecalis* with **11d, 11o,** tetracycline and amoxicillin (a) at different concentrations, and in a time-dependent mode (b) compound **11d** and (c) compound **11o**

3.2.12 Protein leakage assay

The stability and biological activity of bacterial strains are maintained due to the integrity of the bacterial membrane. Any disruption caused to cell membrane leads to cell lysis, resulting

in leakage of intercellular proteins from the cells, which causes apoptosis.[114] Folin's assay was employed to estimate the content of proteins leaked from *E. faecalis* treated with different concentrations of compounds. **Figure 3.21a** shows that the concentration of protein leakage in *E. faecalis* rises in a concentration-dependent mode, promising proof of membrane damage.

3.2.13 Metabolic dysfunction assay

The normal metabolic process of bacteria is regulated by the protein on its cell membrane, thus activating bacterial growth such as fats, nucleic acids, polysaccharides and different coenzymes; hence, the metabolic activity depicts the viability of bacteria cells.[115] Denaturation of protein causes metabolic dysfunction due to cell membrane disruption which was examined by Almar blue dye assay.[116] The metabolic activity of *E. faecalis* was decreased remarkably in the presence of **11d** and **11o** in a concentration-dependent mode, reflecting the membrane damage of *E. faecalis* (**Figure 3.21b**). Compared to reference drugs amoxicillin and tetracycline, these drug candidates have greater ability to inhibit bacterial metabolism.

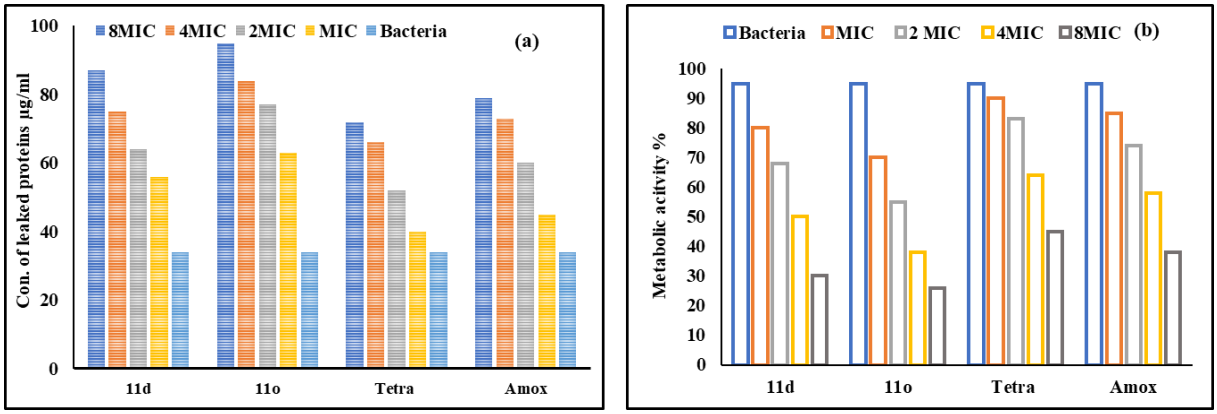

Figure 3.21. (a) Protein leakage from *E. faecalis* and (b) metabolic activity of *E. faecalis* in the presence of compounds **11d** and **11o**, tetracycline, and amoxicillin at different concentrations.

3.2.14 Change in morphology of *E. faecalis* cells

Scanning Electron Microscope (SEM) studies were conducted to confirm the membrane damage caused by active drug candidates and to observe morphological changes of *E. faecalis* upon incubating with **11d** and **11o**. Figure **3.22a.** displayed the SEM images of untreated *E. faecalis* manifesting the regular, smooth and circular surfaces. The cell wall of the *E. faecalis* incubated with active drugs **11d** (**Figures 3.22b** and **3.22c**) and **11o** (**Figures 3.22d** and **3.22e**) at 2 × MIC concentration was found to be disrupted and broken, causing the leakage of cytoplasmic contents and causing corrugation, thus confirming the cell wall cleavage and membrane disruption with both the compounds.

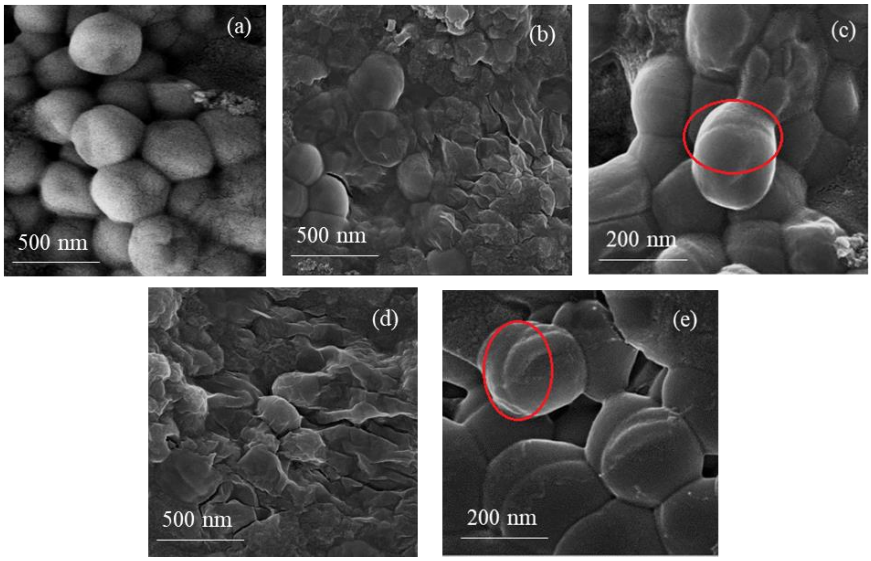

Figure 3.22 SEM images of (a) untreated *E. faecalis* and treated *E. faecalis* with compounds **11d** (b,c) and **11o** (d,e) at 2 × MIC

3.2.15 Intracellular oxidative stress

3.2.15a Reactive oxygen species

The disruption of cell membranes and cell dysfunction proliferated due to an increase in the level of reactive oxygen species (ROS), leading to cell death.[117] On receiving any external stress, the ROS level inside the bacterial cell increases drastically, leading to cellular structure damage and causing oxidative stress.[118] 2',7'-Dichlorofluorescein dye (DCFH-DA) was used to examine the level of ROS in treated and untreated cells by fluorometric assay, and the fluorescence intensity is proportional to ROS level in cells. Fluorescence intensities of *E. faecalis*, incubated with increasing concentrations of **11d** and **11o** were increased (**Figure 3.23a**), demonstrating that the level of intercellular ROS rises significantly in a concentration-dependent mode following the membrane damage. Compounds **11d** and **11o** were able to produce better oxidative stress in *E. faecalis* compared to reference drugs; tetracycline and amoxicillin, thus activating ROS accumulation in *E. faecalis*, leading to oxidative damage and cell death.

3.2.15b Glutathione activity

Any damage caused to bacteria cells due to the production of oxidative stress in a cell is protected by glutathione (GSH), a tripeptide thiol-containing antioxidant that helps in regulating the healthy functioning of immune system of organisms.[119] Elman's method was employed to examine the loss in GSH activity of *E. faecalis* on incubating with different concentrations of **11d** and **11o**. GSH levels in cells were decreased progressively upon incubating *E. faecalis* with rising concentrations of **11d** and **11o**, and the loss in GSH activity

of the cells treated with **11d** and **11o** reached upto 35% and 40%, respectively at 8×MIC (**Figure 3.23b**). Compared to reference drugs tetracycline and amoxicillin, these drug candidates resulted in greater loss of GSH activity.

3.2.15c Lipid peroxidation

The main threat to the production of ROS is that it facilitates the lipid peroxidation of the cell, leading to cell death. The degree of cell peroxidation damage and antioxidant potential is reflected by the level of malondialdehyde (MDA) in cells.[120] The enhancement in production of MDA in *E. faecalis* was observed with increasing concentrations of compounds **11d** and **11o** as represented in **Figure 3.23c**. The MDA production was greater when the cells were incubated with **11d** and **11o** compared to reference drugs amoxicillin and tetracycline. Thus, the above results demonstrated that the production of MDA was in accordance with the accumulation of ROS. Hence, the produced ROS effectively triggers lipid peroxidation, leading to bacterial damage.

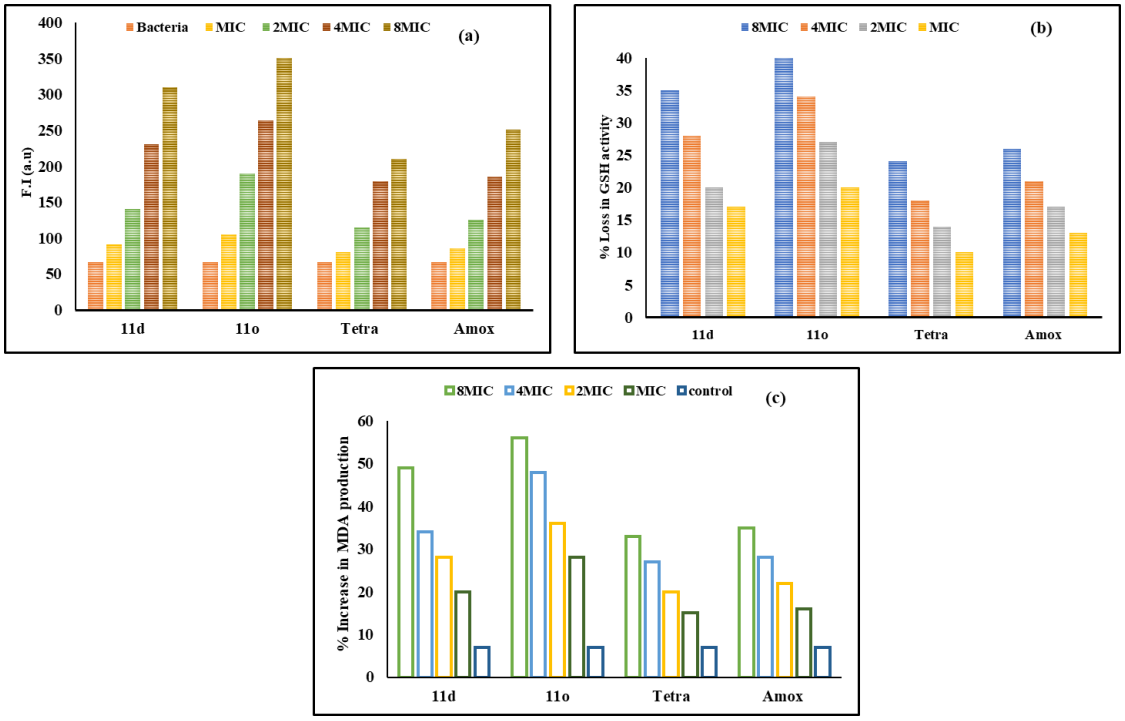

Figure 3.23. (a) Intracellular ROS production, (b) loss in GSH activity, and (c) malondialdehyde (MDA) production of *E. faecalis* upon treatment with **11d, 11o,** tetracycline, and amoxicillin at different concentrations.

3.2.16 Interaction with DNA

DNA, a biomacromolecule is the main target in designing DNA-targeted antibacterial agents, as it helps in controlling metabolic processes and production of protein.[121] DNA damage occurs

due to increased oxidative stress in cells since compounds **11d** and **11o** can disrupt the cell membrane, leading to the induction of ROS in cells; hence, the binding abilities of **11d** and **11o** with DNA were evaluated by absorption and emission spectroscopic techniques.

Initially, absorption spectroscopy was employed to study the interaction between compounds **11d** and **11o** with ct-DNA. Compound **11d** (5 μM) displayed two absorption maxima at 347 nm and 423 nm, while **11o** (5 μM) showed an absorption band at 348 nm in phosphate buffer (pH = 7.4) at room temperature. Hypochromic shifts in their respective absorption bands were observed upon gradual addition of ct-DNA (0-30 μM) to solutions of compounds **11d** and **11o**, indicating the effective binding of compounds with ct-DNA (**Figure 3.24**).

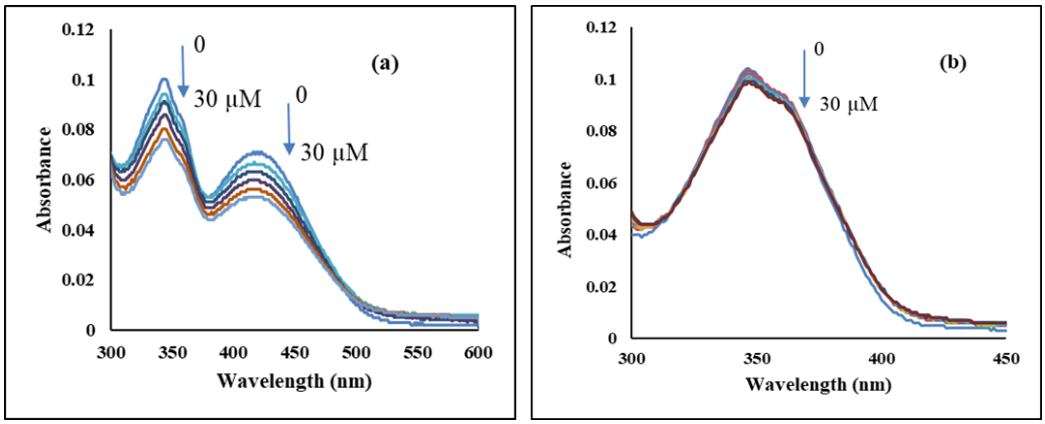

Figure 3.24: Absorption spectra of (a) **11d** (5 μM) and (b) **11o** (5 μM) with increasing concentration of ct-DNA (0–30 μM).

Furthermore, the binding of molecules with DNA was explored by emission studies. Compounds **11d** and **11o** (5 μM) exhibited an intense emission band at 475 nm upon excitation at 348 nm in phosphate buffer (pH = 7.4). Incremental addition of ct-DNA (0-30 μM) resulted in enhancement of fluorescence intensity of **11d**, whereas quenching in case of **11o** was observed, further confirming the binding of compounds with ct-DNA (**Figures 3.25**). The values of binding constant for both systems were calculated using equation-7.

$$\frac{E-E_o}{E\,max-E} = K[M] \ldots\ldots (7)$$

Where E_o, E and E_{max} are the emissions of compounds **11d** and **11o** in the absence of ct-DNA, at an intermediate and at saturation, respectively, K is the binding constant, and [M] is the concentration of ct-DNA at an intermediate.

The binding constants for the interaction of **11d** and **11o** with ct-DNA were found to be 2×10^5 M^{-1} and 4.5×10^5 M^{-1}, respectively. The values of binding constant revealed the effective binding of both compounds with ct-DNA, and **11o** binds more efficiently than **11d**. The results obtained from DNA studies followed the inner membrane damage of the cells by both compounds.

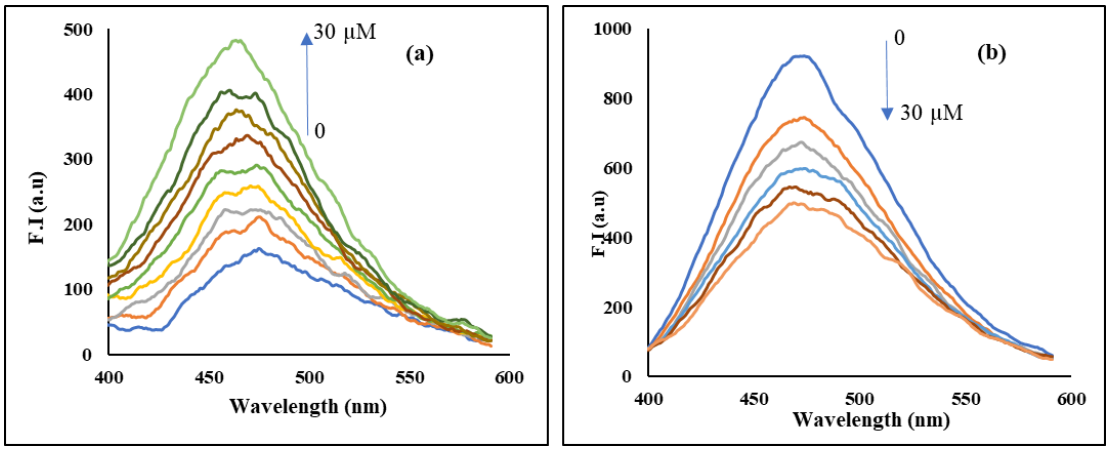

Figure 3.25: Emission spectra of (a) **11d** and (b) **11o** in phosphate buffer (*p*H 7.4) at 298 K upon progressive addition of ct-DNA (0–30 μM).

Further, to get insight into the binding mode of compounds with ct-DNA, whether intercalation or groove binding, displacement studies using ethidium bromide were performed. Upon incremental addition of compounds **11d** (0-30 μM) and **11o** (0-40 μM) to EtBr-ct-DNA (3 μM-30 μM), a decrease in fluorescence intensity was observed at 601 nm due to displacement of EtBr from the complex (**Figure 3.26**). EtBr is a well-known DNA intercalator, and its displacement from the EtBr-DNA complex by the compounds **11d** and **11o** confirmed the intercalation binding mode.

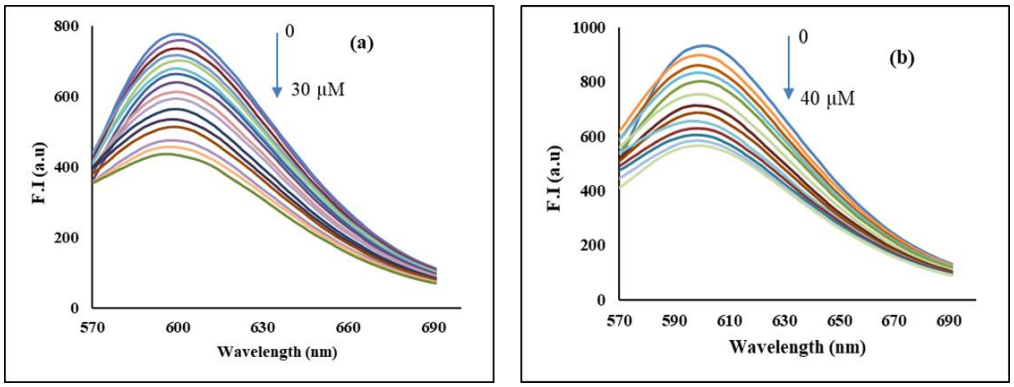

Figure 3.26: Fluorescence spectra of ethidium bromide and ct-DNA complexes upon gradual addition of compounds (a) **11d** (0–30 μM) and (b) **11o** (0–40 μM)

Further, the interactions of drug candidates **11d** and **11o** with DNA (PDB: 1BNA) have been explored with molecular docking studies using an Autodock program, and the visualisations were done by Discovery Studio[86] **Figures 3.27** and **3.28** represent the molecular docked model of compounds **11d** and **11o** in 2-D and 3-D posess with DNA. Compounds **11d** and **11o** exhibited the minimum binding energies of -10.56 kcal/mol and -10.98 kcal/mol, respectively. Oxygen atom of one naphthalimide ring in **11d** binds to DA18 (*d* = 2.72 Å, chain B), DG10 (*d* = 2.03 Å, chain A) and DG16 (*d* = 1.85 Å, chain B), whereas oxygen atom of second naphthalimide interacts DG16 (*d* = 1.92 Å, chain B) and DA17 (*d* = 2.43 Å, chain B) *via* conventional hydrogen bonds. The carbon atom of the piperazine ring binds to DT19 (*d* = 3.01 Å, chain B) *via* carbon-hydrogen bond. In case of compound **11o,** the oxygen atom of formyl group binds to DA18 (*d* = 2.46 Å, chain B) through hydrogen bonds, whereas the oxygen atom of naphthalimide ring binds to DA18 (*d* = 3.14 Å, chain B) *via* carbon-hydrogen bond. Comparing the docking results of both compounds, **11o** binds more firmly to DNA than **11d**, thus supporting the experimental results.

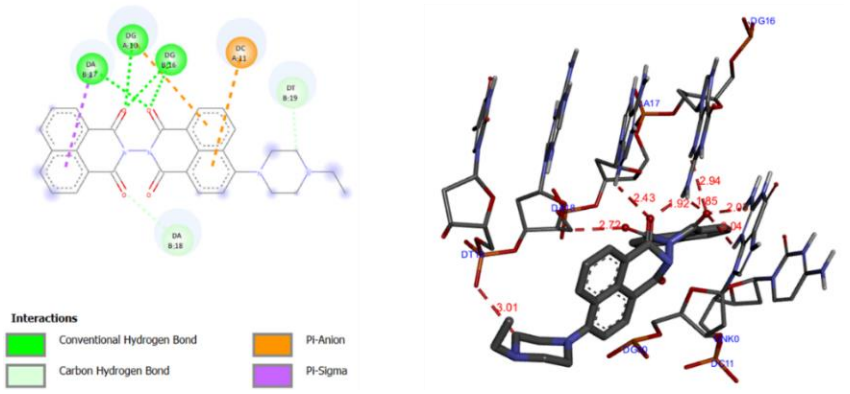

Figure 3.27: Molecular docking of DNA (1BNA) with compound **11d**.

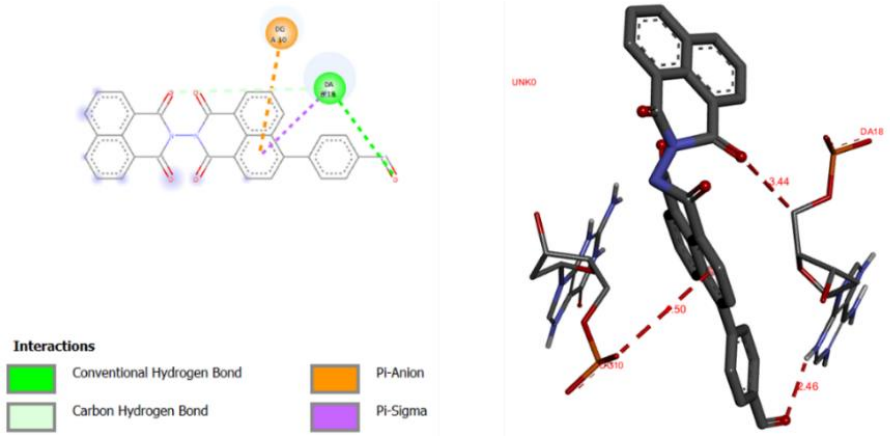

Figure 3.28: Molecular docking of DNA (1BNA) with compound **11o**.

3.2.17 HSA binding studies

After carrying out the studies for possible mechanism of antibacterial activities for **11d** and **11o**, its necessary to explore whether these drug candidates can bind to HSA as it is a crucial transport protein found in blood that bind with drugs readily to deliver to target sites, thus boosting the solubility of drug substance, protecting the oxidation in plasma and decreasing the toxicity.[122] Due to these excellent properties, HSA is considered as an important target in building potent antibacterial agents. Therefore, spectroscopic techniques were explored for binding affinities of **11d** and **11o** with HSA.

The absorption spectrum of HSA (10 μM) in phosphate buffer at 298K exhibited an intense band at 280 nm due to transitions in aromatic rings of tryptophan (Trp), tyrosine (Tyr), and phenylalanine (Phe) residues.[56] Incremental additions of compounds **11d** (0-10 μM) and **11o** (0-8 μM) to a solution of HSA resulted in hyperchromic shift at 280 nm and development of a new band at 347 nm, followed by enhancement for both compounds **(Figure 3.29**). No change in absorption maxima of HSA with the addition of compounds was observed, manifesting the existence of non-covalent interactions. The binding constants were calculated by employing the Bensei-Hildebrand equation and came out to be $8.5 \times 10^4\ M^{-1}$ for **11d** and $18 \times 10^4\ M^{-1}$ for **11o**. These binding constants reflected the efficient interactions of compounds with HSA, where **11o** binds more strongly than **11d.**

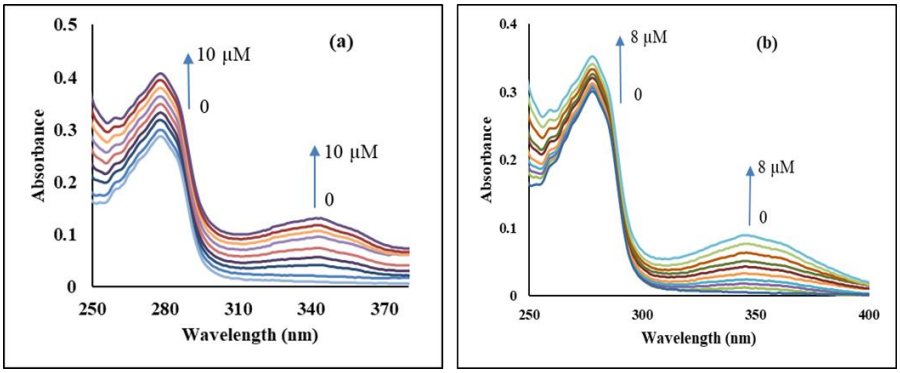

Figure 3.29: Absorption spectra of HSA on increasing concentrations of (a) **11d** and (b) **11o** in phosphate buffer (*p*H 7.4) at 298 K.

Further, fluorescence studies were performed to explore the interactions of compounds **11d** and **11o** with HSA. Upon excitation of HSA at 280 nm, it exhibited an intense fluorescence band at 340 nm due to transitions in aromatic rings of amino acid residues in phosphate buffer (*p*H = 7.4). Incremental additions of compounds **11d** (0 – 60 μM) and **11o** (0 – 20 μM) to a solution of HSA (10 μM) resulted in fluorescence quenching (**Figure 3.30**). Upon progressive

addition of **11o**, a new band at 490 nm was observed with development of an isosbestic point at 400 nm. Static or dynamic quenching is responsible for decrease in fluorescence intensity of HSA with gradual additions of **11d** and **11o**.

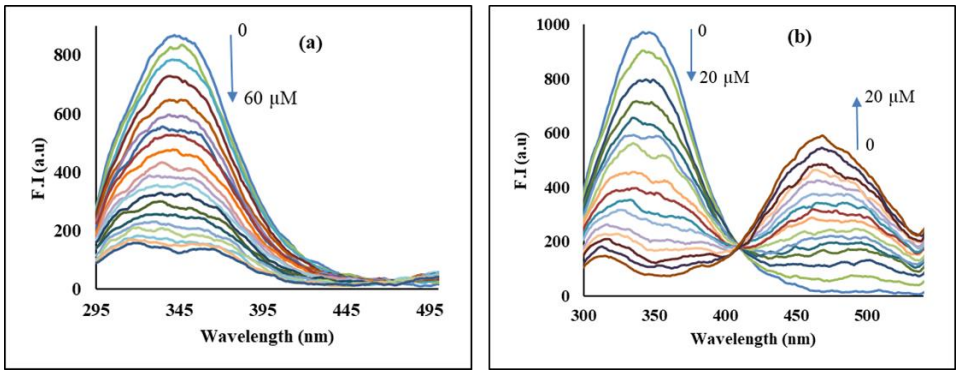

Figure 3.30: Fluorescence spectra of HSA upon progressive additions of (a) **11d** and (b) **11o** in phosphate buffer (*p*H 7.4) at 298 K.

The Stern-Volmer equation was employed to compute the binding parameters and were found to be $0.6 \times 10^5\ M^{-1}$ (K_{sv}) and $0.6 \times 10^{13}\ M^{-1}$ (K_q) for **11d**, and $1.6 \times 10^5\ M^{-1}$ (K_{sv}) and $1.6 \times 10^{13}\ M^{-1}$ (K_q) for **11o** (**Table 3.10)**, indicating the existence of static quenching. Further, a modified Stern-Volmer equation was used to analyse binding constants and binding stoichiometry (n) and found to be $2.4 \times 10^4\ M^{-1}$ for **11d** and $18.5 \times 10^4\ M^{-1}$ for **11o** (**Table 3.10**). The number of binding sites for both compounds was found to be 1, manifested that both compounds bound to HSA specifically at one site.

Table 3.10. Binding parameters for compounds **11d** and **11o** at three different temperatures

Compound	K_{sv} ($10^5\ M^{-1}$)	K_q ($10^{13}\ M^{-1}\ S^{-1}$)	[a]R	K_b ($10^4\ M^{-1}$)	n	[a]R
11d	0.6	0.6	0.9954	2.4	0.95	0.9928
11o	1.6	1.6	0.9934	18.5	1.0	0.9949

[a]R is the correlation coefficient

Gibb's free energies (ΔG) were calculated as -5.96 kcal M^{-1} for **11d** and -7.183 kcal M^{-1} for **11o** (**Table 3.11**) using eq-6. The negative values of ΔG indicated the spontaneous nature of binding process. The negative value of binding for **11o** with HSA was greater than **11d,** indicating the effective binding of **11o** than **11d**.

Table 3.11: Thermodynamic parameters of HSA binding with compounds **11d** and **11o**

T (K)	ΔG, kcal M^{-1} (11d)	ΔG, kcal M^{-1} (11o)
298	-5.96	-7.18

Further, time-resolved fluorescence studies were performed to confirm the quenching mechanism for binding between compounds and HSA. Steady-state fluorescence revealed static quenching for the interaction of both compounds with HSA. To confirm the same, time decay spectra of HSA in absence and presence of compounds **11d** (0-30 μM) and **11o** (0-30 μM) were recorded (**Figure 3.31)**.

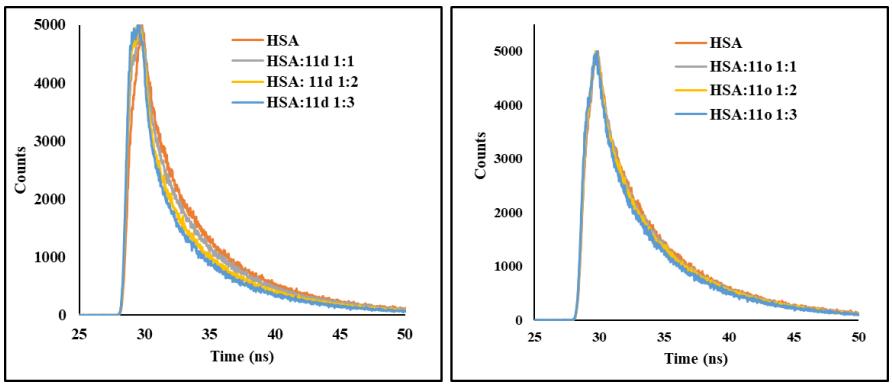

Figure 3.31: Time decay profile of HSA on progressive addition of compounds (a) **11d** and (b) **11o** in phosphate buffer (*p*H 7.4).

Static quenching occurs when there is no change in time decay of free analyte, whereas significant change refers to dynamic quenching, as predicted by the average lifetime values. A declining trend in lifetime decay of free HSA upon gradual addition of compound **11d** was observed, indicating dynamic quenching, whereas no change in time decay of HSA was observed upon progressive addition of compound **11o**, manifesting the static quenching (**Table 3.12**). The results obtained from steady-state fluorescence and time-resolved inferred that in case of **11d**, both static and dynamic quenchings are accountable for its binding with HSA, whereas only static quenching is responsible for the interaction of **11o** with HSA.

Table 3.12. Lifetime fluorescence decay of HSA on interaction with **11d** and **11o**

System	Conc.	τ_1 [ns]	τ_2 [ns]	τ_3 [ns]	α_1	α_2	α_3	τ_{av}	χ^2
HSA		2.8	6.64	0.57	0.56	0.1	0.09	3.12	1.16
HSA-11d	01:01	2.44	6.35	0.45	0.34	0.09	0.04	2.23	1.17
	01:02	2.05	6.1	0.35	0.29	0.08	0.47	1.63	1.18
	01:03	2.01	6.06	0.32	1.36	0.27	0.09	1.36	1.20

HSA-11o	01:01	2.94	6.63	0.64	0.67	0.12	0.09	3.1	1.15
	01:02	3.11	6.7	0.66	0.71	0.13	0.4	3.06	1.18
	01:03	2.93	6.48	0.64	0.68	0.14	0.08	2.85	1.2

3.2.18 Quantum chemical studies

The crucial pharmacokinetic properties of drug candidates and their interaction with biomolecules were examined with the help of computational studies. The intermolecular interactions are managed by the frontline molecular orbitals, where HOMO, LUMO, and the energy difference between them help to differentiate the molecular activity of compounds.[123] **Table 3.13** represents the atomic orbitals of HOMO-LUMO compositions of compounds **11d** and **11o**. The HOMO of **11d** is located on naphthalimide ring having ethyl piperazine substitution, whereas LUMO is located on other naphthalimide ring, indicating that the substituted naphthalimide ring interacts with positively charged biological ions *via* electrostatic interactions whereas other naphthalimide ring interacts with negatively charged ions or residues. In comparison to **11d**, HOMO-LUMO of compound **11o** is located on the same naphthalimide ring having 4-formyl phenyl substitution, revealing only one ring interacts with both positive and negatively charged biological ions. Of all the synthesized compounds, **11d** and **11o** exhibited the lowest energy gap of 3.420 eV and 3.148 eV between HOMO and LUMO orbitals, i.e., these exhibited better bioactivity towards bacterial strains than the rest of the compounds. Comparing the energy gaps of compounds **11d** and **11o,** the later exhibited less energy gap than the former, indicating higher reactivity of **11o** towards the microbes to enhance the inhibition potency. Hence, these computational studies further supported the experimental results.

Table 3.13: Atomic orbitals HOMO-LUMO compositions of compounds **11d** and **11o**

Comp	**HOMO (eV)**	**LUMO (eV)**	**ΔE (eV)**
11a	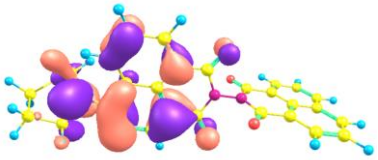	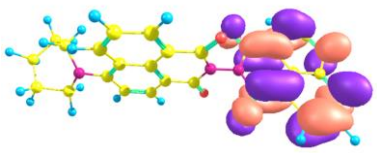	3.642

11b	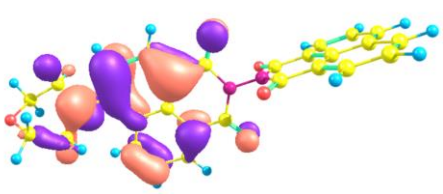	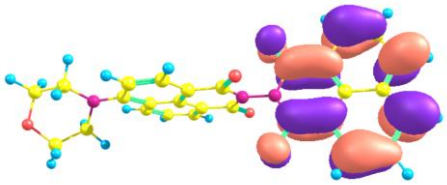	3.462
11c	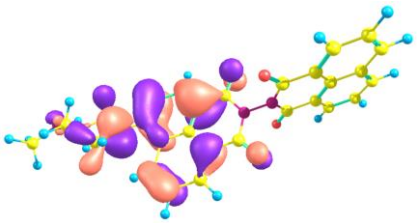	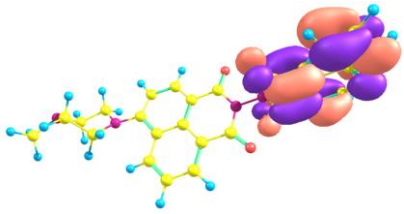	3.820
11d		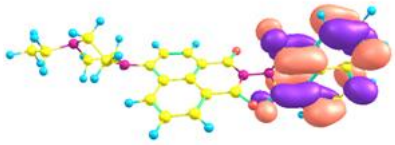	3.420
11e	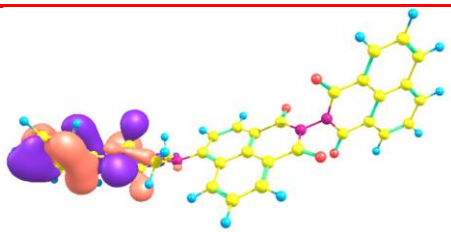	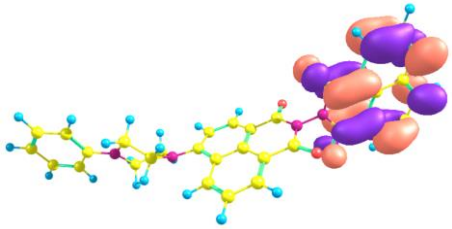	3.576
11f	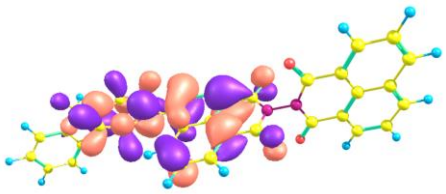	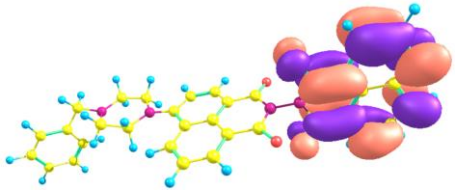	3.737
11g	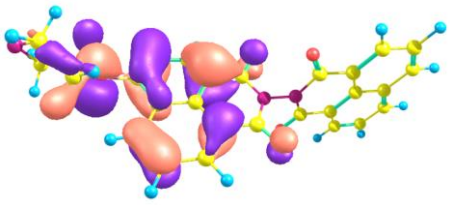	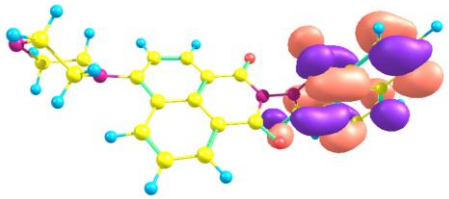	3.862
11h	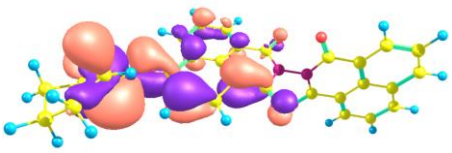		3.573

11i	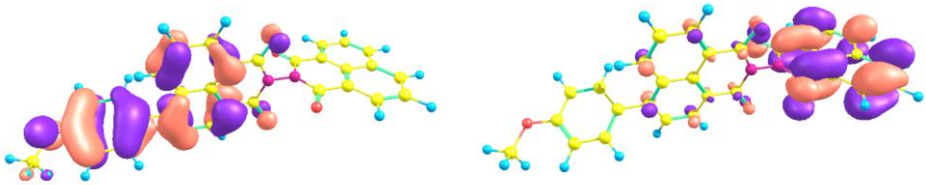		3.531
11j	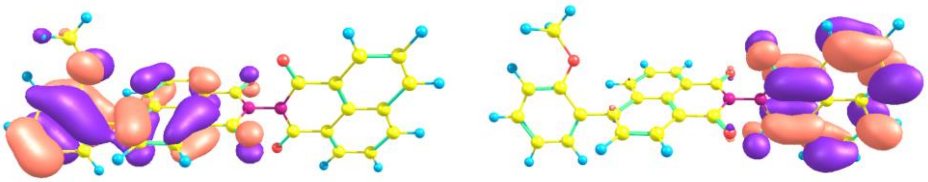		3.712
11k	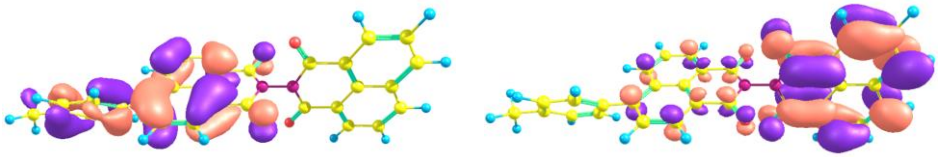		3.770
11l	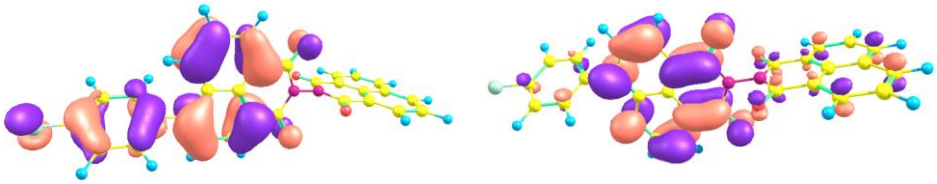		3.792
11m	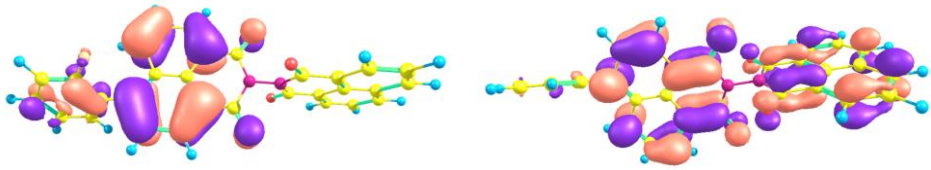		3.871
11n	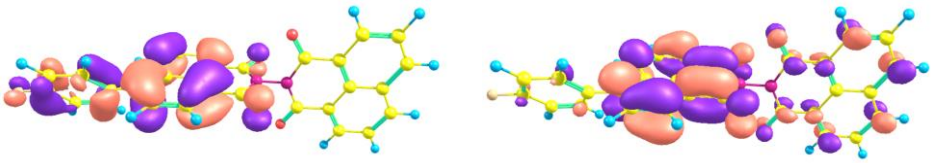		3.803
11o	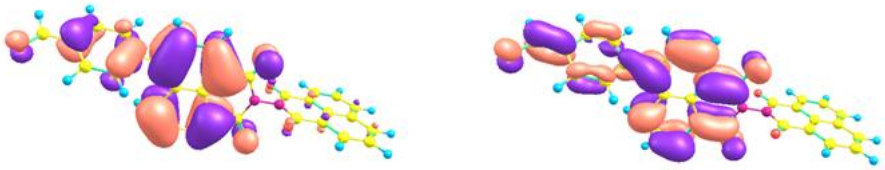		3.148

11p	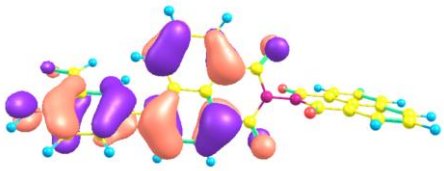	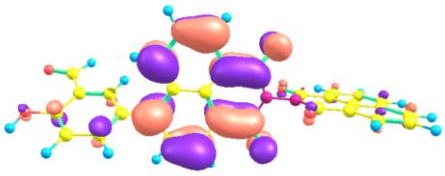	3.599

3.2.19 Conclusion

In the present work, we have synthesized a series of bis-naphthalimides as efficient antibacterial agents to combat freighting bacterial resistance. Structure-activity relationship and bioactivity examination inferred that some synthesized molecules exhibited potent activity in inhibiting the growth of tested bacterial strains. Impressively, compounds **11d** and **11o** displayed the most promising results against all the tested bacterial strains with MIC values ranging from 6.25 μg/ml to 1.56 μg/ml and outperformed the marketed drugs. Both the compounds significantly inhibit the biofilm formation, thus, delaying the development of resistance upto 30 passages. The bio-functional studies manifested that compounds **11d** and **11o** not only disrupted the cell membrane but also reduced metabolic activity, leading to leakage of intercellular contents. Further, mechanistic exploration inferred that these compounds induced oxidative stress damage leading to loss in GSH activity and intercalated with DNA to form supramolecular complexes, thus exhibiting potent bioactivity. Furthermore, the binding behaviour of both compounds towards HSA was also explored for easy delivery to target sites. Computational and molecular docking studies further supported the experimental results. Comparing the bioactivity of these compounds, **11o** displayed better activity towards bacterial strains in light of antibacterial activity, drug-likeness, membrane disruption ability, oxidative stress damage and possible multitargeting membrane. Thus, these compounds were found to be superior in overcoming dreadful drug resistance and could be considered further for clinical evaluation for their development as an effective antibacterial agent.

3.2.20. Experimental section

2-Amino-1*H*-benzo[*de*]isoquinoline-1,3(*2H*)-dione (10)

Hydrazine hydrate (320 mg, 5.05 mmol) was added to a stirred solution of compound **2** (2 g, 5.05 mmol) in ethanol (30 mL), and the reaction was stirred at room temperature for 2h. The resulting residue was filtered to get a yellow solid product in 0.9 g; 84%, R_f 0.4 (50% chloroform in hexane); m.pt. 269-272 °C (Lit. m.pt – 270-272 °C).

6-Bromo-1*H*,1'*H*,3*H*,3'*H*-[2,2'-bibenzo[*de*]isoquinoline]-1,1',3,3'-tetraone (11)

To a stirred solution of 2-amino-*1H*-benzo[*de*]isoquinoline-1,3(*2H*)-dione (**3**) (500 mg, 2.3 mmol) in ethanol (50 ml), 6-bromo-1*H*,3*H*-benzo[*de*]isochromene-1,3-dione (780 mg, 2.8 mmol) and a catalytic amount of zinc acetate was added to reaction mixture followed by refluxing for 4h, and the monitoring of reaction was done with TLC. On completion of reaction, the reaction mixture was filtered and purified by column chromatography using hexane and chloroform (8:2) as eluents to obtain white solid product 80%, R_f 0.6 (chloroform); m.pt. 289–292 °C; ^{1}H NMR ($CDCl_3$, 400 MHz): δ 8.80 – 8.76 (m, 2H, ArH), 8.73 (d, *J* = 7.3 Hz, 2H, ArH), 8.54 (d, *J* = 7.9 Hz, 1H, ArH), 8.41 (d, *J* = 8.3 Hz, 2H, ArH), 8.17 (d, *J* = 7.9 Hz, 1H, ArH), 7.99 – 7.94 (m, 1H, ArH), 7.87 (t, *J* = 7.8 Hz, 2H, ArH);

6-(Amino substituted)-1*H*,1'*H*,3*H*,3'*H*-[2,2'-bibenzo[*de*]isoquinoline]-1,1',3,3'-tetraone (11a-h): To a stirred solution of compound **11** (200 mg, 0.42 mmol) in DMF (10 ml) and K_2CO_3 (80 mg, 0.6 mmol), substituted secondary amine (2.1 mmol) was added, and the reaction was allowed to heat at 110 ºC for 3-4 h. On completion, 20 ml cold water was added to the reaction mixture, and the formed precipitate was filtered.

6-(piperidin-1-yl)-1*H*,1'*H*,3*H*,3'*H*-[2,2' bi benzo [*de*] iso qui noline]-1,1',3,3'-tetraone (11a)

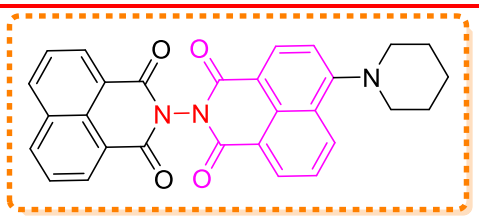

Yield: 73%; colour: yellow; m.pt: 231-233 ºC; ^{1}H NMR ($CDCl_3$, 400 MHz): δ (ppm) 8.68 (d, *J* = 7.28 Hz, 2H, ArH), 8.64 (d, *J* = 7.24 Hz, 1H, ArH), 8.57 (d, *J* = 8.12 Hz, 1H, ArH), 8.48 (d, *J* = 8.36 Hz, 1H, ArH), 8.31 (d, *J* = 8.28 Hz, 2H, ArH), 7.81 (t, *J* = 7.80 Hz, 2H, ArH), 7.73 (t, *J* = 7.80 Hz, 1H, ArH), 7.21 (d, *J* = 8.16 Hz, 1H, ArH), 3.28 (t, *J* = 4.64 Hz, 4H, 2*CH_2 piper), 1.91 (t, *J* = 5.40 Hz, 4H, 2* CH_2 piper), 1.76-1.73 (m, 2H, CH_2 piper); ^{13}C NMR ($CDCl_3$ + TFA, 100 MHz): δ (ppm) 161.9, 143.6, 136.6, 134.1, 133.4, 132.3, 129.5, 127.8, 127.5, 124.1, 121.0, 119.0, 113.3, 58.9, 23.6, 21.5; HRMS (ESI) Calcd. for $C_{29}H_{21}N_3O_4$ $[M+H]^+$ 476.1610 Found 476.1613.

6-morpholino-1*H*,1'*H*,3*H*,3'*H*-[2,2'-bibenzo[*de*]iso quino line]-1,1',3,3'-tetraone (11b)

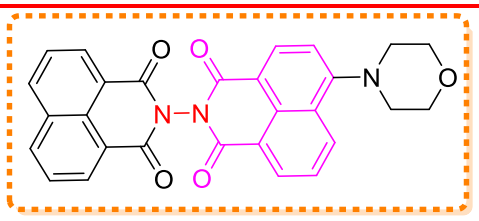

Yield: 80%; colour: bright yellow; m.pt: 235-238 ºC; ^{1}H NMR ($CDCl_3$, 400 MHz): δ (ppm) 8.68 (d, *J* = 6.96 Hz, 3H, ArH), 8.61 (d, *J* = 8.08 Hz, 1H, ArH), 8.52 (d, *J* = 8.52 Hz, 1H, ArH), 8.32 (d, *J*

= 8.20 Hz, 2H, ArH), 7.82 – 7.73 (m, 3H, ArH), 7.28 (d, *J* = 8.24 Hz, 1H, ArH), 4.05 (t, *J* = 4.24 Hz, 4H, 2*CH_2 morph), 3.30 (t, *J* = 4.40 Hz, 4H, 2*CH_2 morph); ^{13}C NMR ($CDCl_3$ + TFA, 100 MHz): δ (ppm) 152.4, 137.2, 134.7, 134.4, 134.1, 132.0, 131.0, 130.3, 128.5, 127.4, 126.9, 125.9, 122.1, 121.4, 116.9, 116.1, 113.2, 54.2, 50.0, ; HRMS (ESI) Calcd. for $C_{28}H_{19}N_3O_5$ $[M+H]^+$ 478.1403 Found 478.1406. 43.9; HRMS (ESI) Calcd. for $C_{28}H_{19}N_3O_5$ $[M+H]^+$ 478.1403 Found 478.1406.

6-(4-methylpiperazin-1-yl)-1*H*,1'*H*,3*H*,3'*H*-[2,2'-bibenzo[*de*]isoquinoline]-1,1',3,3'-tetraone (11c)

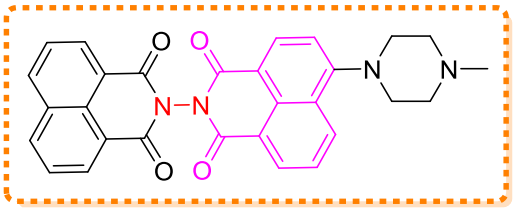

Yield: 76%; colour: pale yellow; m.pt: 230-232 ºC; ^{1}H NMR ($CDCl_3$ + TFA (0.70: 0.05ml), 400 MHz): δ (ppm) 8.68 (d, *J* = 7.28 Hz, 2H, ArH), 8.50 – 8.46 (m, 2H, ArH), 8.39 – 8.35 (m, 3H, ArH), 7.85 (t, *J* = 7.56 Hz, 2H, ArH), 7.64 (t, *J* = 7.52 Hz, 1H, ArH), 7.19 (d, *J* = 8.08 Hz, 1H, ArH), 3.90 (d, *J* = 11.20 Hz, 2H, CH_2 pip), 3.64 (d, *J* = 13.00 Hz, 2H, CH_2 pip), 3.57 (q, *J* = 11.80 Hz, 2H, CH_2 pip), 3.41 (t, *J* = 12.12 Hz, 2H, CH_2 pip), 3.02 (d, *J* = 4.56 Hz, 3H, -N-CH_3); ^{13}C NMR ($CDCl_3$ + TFA, 100 MHz): δ (ppm) 161.9, 154.5, 136.2, 133.8, 133.2, 132.0, 130.8, 129.7, 128.5, 127.4, 126.9, 125.9, 122.1, 121.4, 116.9, 116.1, 113.2, 54.2, 50.0, 43.9; HRMS (ESI) Calcd. for $C_{29}H_{22}N_4O_4$ $[M+H]^+$ 491.1719 Found 491.1756.

6-(4-ethylpiperazin-1-yl)-1*H*,1'*H*,3*H*,3'*H*-[2,2'-bibenzo[*de*]isoquinoline]-1,1',3,3'-tetraone (11d)

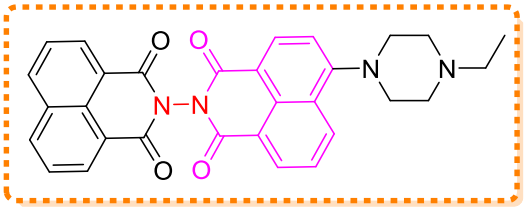

Yield: 81%; colour: yellow; m.pt: 236-239 ºC; 1H NMR ($CDCl_3$ + TFA (0.70: 0.05ml), 400 MHz): δ (ppm) 8.69 (d, *J* = 7.28 Hz, 2H, ArH), 8.47 (d, *J* = 8.04 Hz, 1H, ArH), 8.43 (d, *J* = 7.28 Hz, 1H, ArH), 8.39 (d, *J* = 8.28 Hz, 2H, ArH), 8.35 (d, *J* = 7.64 Hz, 1H, ArH), 7.86 (t, *J* = 7.92 Hz, 2H, ArH), 7.60 (t, *J* = 7.64 Hz, 1H, ArH), 7.16 (d, *J* = 8.08 Hz, 1H, ArH), 3.93 (d, *J* = 10.8 Hz, 2H, CH_2 pip), 3.64 (d, *J* = 11.88 Hz, 2H, CH_2 pip), 3.51 – 3.36 (m, 4H, 2*CH_2 pip), 3.31 – 3.25 (m, 2H, N-CH_2), 1.41 (t, *J* = 7.32 Hz, 3H, CH_3); ^{13}C NMR ($CDCl_3$ + TFA, 100 MHz): δ (ppm) 161.6, 154.3, 135.8, 133.4, 132.6, 132.0, 130.5, 129.6,

128.5, 127.3, 126.7, 125.8, 122.4, 121.8, 117.1, 116.4, 113.5, 52.9, 51.7, 50.0, 9.1; HRMS (ESI) Calcd. for $C_{30}H_{24}N_4O_4$ $[M+H]^+$ 505.1876 Found 505.1885.

6-(4-phenylpiperazin-1-yl)-1*H*,1'*H*,3*H*,3'*H*-[2,2'-bibenzo[*de*]isoquinoline]-1,1',3,3'-tetraone (11e)

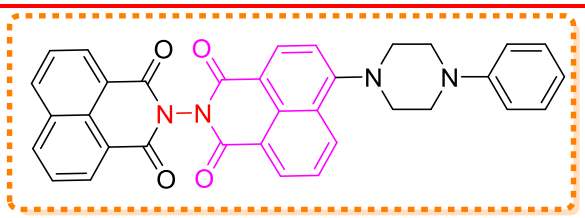

Yield: 79%; colour: reddish yellow; m.pt: 240-243 ºC; ^{1}H NMR ($CDCl_3$, 400 MHz): δ (ppm) 8.68 (d, *J* = 7.32 Hz, 2H, ArH), 8.52 (d, *J* = 8.48 Hz, 1H, ArH), 8.46 (d, *J* = 8.04 Hz, 1H, ArH), 8.44 – 8.42 (m, 3H, ArH), 7.87 (t, *J* = 8.08 Hz, 2H, ArH), 7.67 (t, *J* = 8.40 Hz, 1H, ArH), 7.59 (d, *J* = 7.84 Hz, 2H, ArH), 7.46 (t, *J* = 7.56 Hz, 1H, ArH), 7.32 (t, *J* = 8.24 Hz, 2H, ArH), 7.17 (d, *J* = 8.08 Hz, 1H, ArH), 4.13 (br(s), 4H, 2*CH_2 pip), 3.99 (br(s), 4H, 2*CH_2 pip); ^{13}C NMR ($CDCl_3$ + TFA, 100 MHz): δ (ppm) 162.2, 161.4, 154.6, 140.7, 136.2, 133.5, 133.0, 132.0, 131.0, 130.8, 129.4, 128.5, 127.4, 126.9, 122.1, 121.5, 120.7, 120.3, 116.4, 115.8, 55.9, 50.4; HRMS (ESI) Calcd. for $C_{34}H_{24}N_4O_4$ $[M+H]^+$ 553.1876 Found 553.1877.

6-(4-benzylpiperazin-1-yl)-1*H*,1'*H*,3*H*,3'*H*-[2,2'-bibenzo[*de*]isoquinoline]-1,1',3,3'-tetraone (11f)

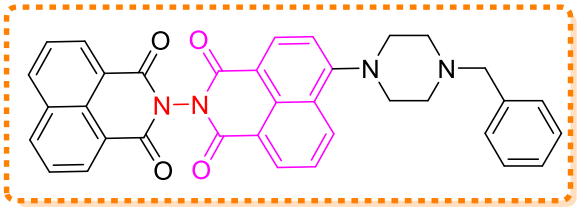

Yield: 84%; colour: brown yellow; m.pt: 238-241 ºC; ^{1}H NMR ($CDCl_3$, 400 MHz): δ (ppm) 8.68 (d, *J* = 7.08 Hz, 2H, ArH), 8.65 (d, *J* = 7.16 Hz, 1H, ArH), 8.58 (d, *J* = 8.08 Hz, 1H, ArH), 8.50 (d, *J* = 8.56 Hz, 1H, ArH), 8.31 (d, J= 8.12 Hz, 2H, ArH), 7.81 (t, *J* = 7.76 Hz, 2H, ArH), 7.73 (t, *J* = 8.12 Hz, 1H, ArH), 7.38 - 7.29 (m, 6H, ArH), 3.66 (s, 2H, CH_2 benzyl pip), 3.33 (br(s), 4H, 2* CH_2 pip), 2.79 (br(s), 4H, 2* CH_2 pip); ^{13}C NMR ($CDCl_3$ + TFA, 100 MHz): δ (ppm)161.8, 161.5, 161.3, 136.1, 133.8, 132.9, 132.0, 131.0, 130.8, 129.8, 129.7, 127.4, 127.0, 126.8, 125.8, 122.3, 121.5, 116.8, 116.2, 113.3, 61.7, 52.0, 49.9; HRMS (ESI) Calcd. for $C_{35}H_{26}N_4O_4$ $[M+H]^+$ 567.2036 Found 567.2032.

6-(piperazin-1-yl)-1*H*,1'*H*,3*H*,3'*H*-[2,2'-bibenzo[*de*]isoquinoline]-1,1',3,3'-tetraone (11g)

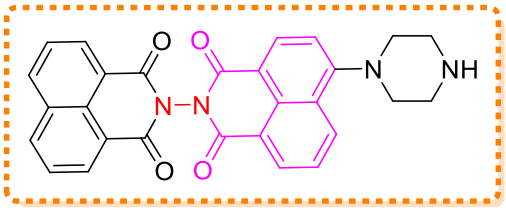

Yield: 68%; colour: brick red; m.pt: 245-247 ºC; ^{1}H NMR ($CDCl_3$ + TFA (0.70 : 0.05ml), 400 MHz): δ (ppm) 8.72 (d, *J* = 7.52 Hz, 3H, ArH), 8.65 (d, *J* = 8.00 Hz, 1H, ArH), 8.50 (d, *J* = 7.68 Hz, 1H, ArH), 8.42 (d, *J* = 8.48 Hz, 3H, ArH), 7.88 – 7.84 (m, 3H, ArH), 7.35 (d, *J* = 8.12 Hz, 1H, ArH), 3.73 (br(s), 4H, 2*CH_2 pip), 3.57 (br(s), 4H, 2* CH_2 pip); ^{13}C NMR ($CDCl_3$ + TFA, 100 MHz): δ (ppm)162.1, 155.1, 136.4, 134.4, 133.5, 133.4, 131.0, 130.2, 127.5, 127.3, 126.4, 121.2, 118.7, 117.4, 116.3, 115.8, 113.0, 110.2, 49.8, 44.8; HRMS (ESI) Calcd. for $C_{28}H_{20}N_4O_4$ $[M+H]^+$ 477.1563 Found 477.1569.

6-(cyclohexylamino)-1H,1'H,3H,3'H-[2,2'-bibenzo[de]isoquinoline]-1,1',3,3'-tetraone (11h)

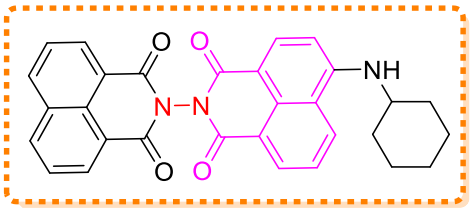

Yield: 70%; colour: yellowish brown; m.pt: 242-244 ºC; ^{1}H NMR ($CDCl_3$ + TFA (0.70: 0.05ml), 400 MHz): δ (ppm) 8.67 (d, *J* = 7.28 Hz, 3H, ArH), 8.38 – 8.30 (m, 5H, ArH), 7.85 – 7.78 (m, 3H, ArH), 3.55 (br(s), 1H, -N-CH cyclohexyl), 2.15 (br(s), 2H, - CH_2 cyclohexyl), 1.81–1.66 (m, 4H, 2 * CH_2 cyclohexyl), 1.41 – 1.35 (m, 4H, 2* CH_2 cyclohexyl); ^{13}C NMR ($CDCl_3$ + TFA, 100 MHz): δ (ppm) 162.5, 162.1, 161.9, 150.0, 136.5, 136.0, 133.0, 132.0, 130.3, 128.6, 127.3, 125.1, 121.5, 121.1, 120.5, 107.3, 106.5, 53.2, 32.1, 25.4, 24.8; HRMS (ESI) Calcd. for $C_{30}H_{23}N_3O_4$ $[M+H]^+$ 490.1767 Found 490.1773.

6-(Substituted aryls)-1*H*,1'*H*,3*H*,3'*H*-[2,2'-bibenzo[*de*]isoquinoline]-1,1',3,3'-tetraone (11i-p): To a stirred solution of compound **4** (200 mg, 0.42 mmol) in a mixture of CH_3CN : H_2O (9:1) in the presence of K_2CO_3 (0.08 mg, 0.6 mmol) and [($Pd(PPh_3)_4$)], various substituted boronic acid (0.5 mmol) was added and the reaction was refluxed for 5-7h. Upon completion of reaction, the solvent was distilled off under vacuum and then water (20 ml) was added to the reaction mixture to obtain a solid product, which was further purified by column chromatography using chloroform and ethyl acetate as eluents.

6-(4-methoxyphenyl)-1*H*,1'*H*,3*H*,3'*H*-[2,2'-bibenzo[*de*]isoquinoline]-1,1',3,3'-tetraone (11i)

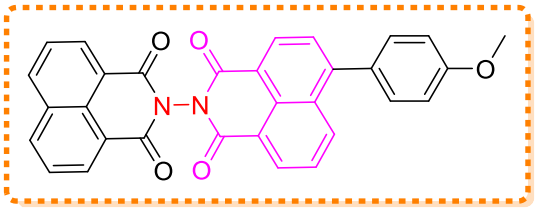

Yield: 85%; colour: white; m.pt: 250-253 ºC; ^{1}H NMR ($CDCl_3$, 400 MHz): δ (ppm) 8.72 – 8.67 (m, 4H, ArH), 8.42 (d, *J* = 8.56 Hz, 1H, ArH), 8.33 (d, *J* = 8.32 Hz, 2H, ArH), 7.83 (t, *J* = 7.64 Hz, 2H, ArH), 7.77 (t, *J* = 9.08 Hz, 2H, ArH), 7.49 (d, *J* = 8.36 Hz, 2H, ArH), 7.11 (d, *J* = 8.40 Hz, 2H, ArH), 3.92 (s, 3H, -OCH_3); ^{13}C NMR ($CDCl_3$, 100 MHz): δ (ppm) 161.3, 161.1, 160.5, 160.1, 148.0, 135.1, 132.3, 132.1, 132.0, 131.3, 130.7, 127.1, 126.9, 122.5, 122.3, 114.3, 55.5; HRMS (ESI) Calcd. for $C_{31}H_{18}N_2O_5$ $[M+H]^+$ 499.1294 Found 499.1293.

6-(2-methoxyphenyl)-1*H*,1'*H*,3*H*,3'*H*-[2,2'-bibenzo[*de*]isoquinoline]-1,1',3,3'-tetraone (11j)

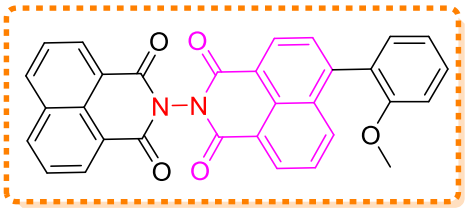

Yield: 83%; colour: creamish white; m.pt: 255-257 ºC; ^{1}H NMR ($CDCl_3$, 400 MHz): δ (ppm) 8.74 (d, *J* = 7.52 Hz, 1H, ArH), 8.69 (d, *J* = 7.32 Hz, 3H, ArH), 8.32 (d, *J* = 8.24 Hz, 2H, ArH), 8.06 (d, *J* = 8.52 Hz, 1H, ArH), 7.82 (t, *J* = 7.60 Hz, 2H, ArH), 7.73 – 7.67 (m, 2H, ArH), 7.53 (t, *J* = 8.52 Hz, 1H, ArH), 7.33 (d, *J* = 7.28 Hz, 1H, ArH), 7.16 – 7.08 (m, 2H, ArH), 3.72 (s, 3H, -OCH_3); ^{13}C NMR ($CDCl_3$, 100 MHz): δ (ppm) 161.4, 161.2, 161.1, 156.8, 145.4, 135.1, 132.4, 132.3, 132.0, 131.5, 128.7, 127.1, 122.3, 120.9, 111.1, 55.9; HRMS (ESI) Calcd. for $C_{31}H_{18}N_2O_5$ $[M+H]^+$ 499.1294 Found 499.1293.

6-(*p*-tolyl)-1*H*,1'*H*,3*H*,3'*H*-[2,2'-bibenzo[*de*]isoquinoline]-1,1',3,3'-tetraone (11k)

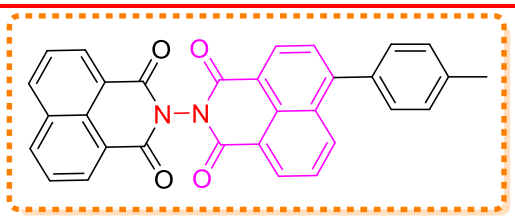

Yield: 78%; colour: white; m.pt: 253-256 ºC; ^{1}H NMR ($CDCl_3$, 400 MHz): δ (ppm) 8.74 (d, *J* = 7.48 Hz, 1H, ArH), 8.70 (d, *J* = 7.24 Hz, 3H, ArH), 8.33 (d, *J* = 8.32 Hz, 2H, ArH), 7.95 (d, *J* = 8.48 Hz, 1H, ArH), 7.83 (d, *J* = 8.12 Hz, 2H, ArH), 7.72 – 7.66 (m, 2H, ArH), 7.44 – 7.36 (m, 3H, ArH), 7.28 – 7.25 (m, 1H, ArH), 2.05 (s, 3H, -CH_3); ^{13}C NMR ($CDCl_3$, 100 MHz): δ (ppm) 161.3, 161.2, 161.1, 148.0, 138.1, 136.3, 135.2, 133.8, 132.4, 132.0, 131.0,

130,4, 129.9, 129.0, 128.7, 128.0, 127.1, 126.0, 122.5, 122.3, 121.4, 20.2; HRMS (ESI) Calcd. for $C_{31}H_{18}N_2O_4$ $[M+H]^+$ 483.1345 Found 493.1345.

6-(4-chlorophenyl)-1*H*,1'*H*,3*H*,3'*H*-[2,2'-bibenzo[*de*]isoquinoline]-1,1',3,3'-tetraone (11l)

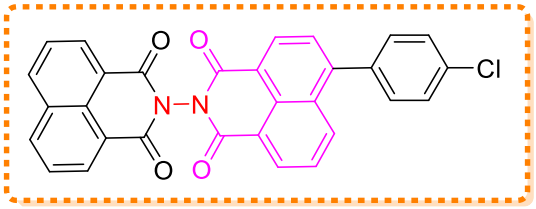

Yield: 69%; colour: white; m.pt: 257-259 ºC; ^{1}H NMR ($CDCl_3$, 400 MHz): δ (ppm) 8.75 – 8.70 (m, 2H, ArH), 8.68 (d, *J* = 8.12 Hz, 4H, ArH), 8.51 (d, *J* = 8.72 Hz, 1H, ArH), 8.33 (d, *J* = 8.52 Hz, 4H, ArH), 8.12 (d, *J* = 7.96 Hz, 1H, ArH), 7.83 – 7.79 (m, 3H, ArH); ^{13}C NMR ($CDCl_3$, 100 MHz): δ (ppm) 161.2, 161.1, 160.6, 135.2, 135.0, 133.4, 133.2, 132.5, 132.4, 132.3, 132.0, 131.9, 131.7, 131.4, 131.1, 130.4, 129.5, 129.1, 128.7, 128.3, 128.0, 127.2, 122.7, 122.6, 122.3, 122.2, 121.9, 121.7; HRMS (ESI) Calcd. for $C_{30}H_{15}N_2O_4Cl$ $[M+H]^+$ 503.0794 Found 503.0794.

6-(2-fluorophenyl)-1*H*,1'*H*,3*H*,3'*H*-[2,2'-bibenzo[*de*]isoquinoline]-1,1',3,3'-tetraone (11m)

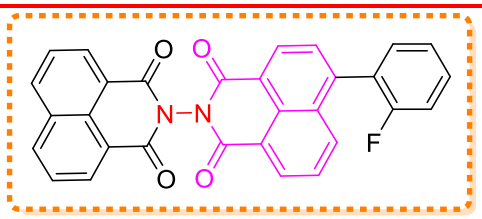

Yield: 75%; colour: cream; m.pt 252-255 ºC; ^{1}H NMR ($CDCl_3$, 400 MHz): 8.77 – 8.73 (m, 3H, ArH), 8.72 (d, *J* = 7.32 Hz, 2H, ArH), 8.53 (d, *J* = 7.88 Hz, 1H, ArH), 8.39 (d, *J* = 8.16 Hz, 3H, ArH), 8.16 (d, *J* = 7.88 Hz, 1H, ArH), 7.97 (t, *J* = 7.36 Hz, 1H, ArH), 7.88–7.84 (m, 3H, ArH), 7.25 (s, 1H, ArH); ^{13}C NMR ($CDCl_3$ + TFA, 100 MHz): δ (ppm)161.8, 161.2, 136.0, 135.2, 133.8, 133.1, 132.8, 132.6, 132.0, 131.6, 131.1, 129.4, 128.6, 128.5, 127.4, 122.1, 121.5, 121.2, 115.9, 115.3; HRMS (ESI) Calcd. for $C_{30}H_{15}N_2O_4F$ $[M+H]^+$ 487.1094 Found 487.1097.

6-(4-fluorophenyl)-1*H*,1'*H*,3*H*,3'*H*-[2,2'-bibenzo[*de*]isoquinoline]-1,1',3,3'-tetraone (11n)

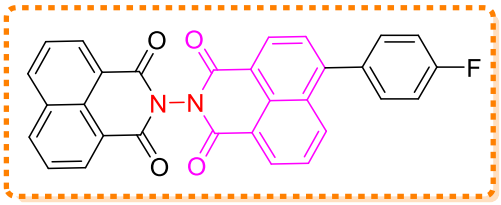

Yield: 82%; colour: off white; m.pt: 259-262 ºC; ^{1}H NMR ($CDCl_3$, 400 MHz): δ (ppm) 8.73 – 8.66 (m, 4H, ArH), 8.33 (d, *J* = 8.20 Hz, 3H, ArH), 7.82 (t, *J* = 8.04 Hz, 2H, ArH), 7.76 (d, *J* = 7.80 Hz, 2H, ArH), 7.53 – 7.50 (m, 2H, ArH),7.29 – 7.25 (m, 2H, ArH); ^{13}C NMR ($CDCl_3$, 100 MHz): δ (ppm) 161.2, 161.1, 161.0, 147.0, 135.3, 135.2, 134.7, 134.6, 133.6, 132.4, 132.0, 131.9, 131.7, 131.4, 130.6, 129.2, 128.7, 128.3, 128.1, 127.2, 122.6, 122.3, 121.5, 116.0, 115.8; HRMS (ESI) Calcd. for $C_{31}H_{15}N_2O_4F$ $[M+H]^+$ 487.1094 Found 487.1097.

4-(1,1',3,3'-tetraoxo-1*H*,1'*H*,3*H*,3'*H*-[2,2'-bibenzo[*de*]isoquinolin]-6-yl)benzaldehyde (11o)

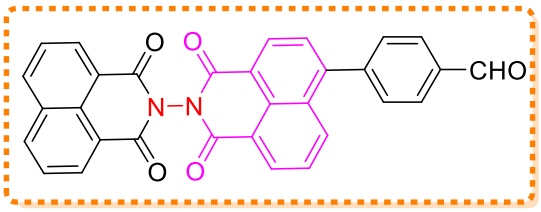

Yield: 65%; colour: white; m.pt: 265-267 ºC; ^{1}H NMR ($CDCl_3$ + DMSO d_6, (0.70 : 0.05 ml), 400 MHz): δ (ppm) 9.74 (s, 1H, CHO), 8.32 – 8.23 (m, 4H, ArH), 8.03 (d, *J* = 8.48 Hz, 2H, ArH), 7.70 (d, *J* = 9.60 Hz, 2H, ArH), 7.49 – 7.41 (m, 5H, ArH), 7.34 – 7.32 (m, 2H, ArH); ^{13}C NMR ($CDCl_3$ + TFA, 100 MHz): δ (ppm)193.7, 170.7 161.7, 161.5, 161.4, 146.8, 145.3, 135.9, 135.8, 133.7, 133.1, 133.0, 132.3, 132.0, 130.8, 130.6, 130.2, 129.1, 128.6, 128.2, 127.7, 127.3, 122.1, 121.6, 118.8, 116.0, 113.1, 110.3; HRMS (ESI) Calcd. for $C_{31}H_{16}N_2O_5$ $[M+H]^+$ 497.1137 Found 497.1139.

2-hydroxy-5-(1,1',3,3'-tetraoxo-1*H*,1'*H*,3*H*,3'*H*-[2,2' bibenzo [*de*]iso qui nolin]-6-yl)benzaldehyde (11p)

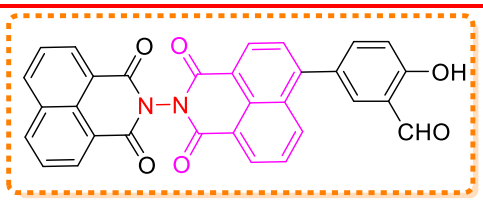

Yield: 80%; colour: yellow; m.pt: 269-272 ºC; ^{1}H NMR ($CDCl_3$ and TFA (0.70 : 0.05 ml), 400 MHz): δ (ppm) 10.02 (s, 1H, CHO), 8.76 – 8.71 (m, 5H, ArH), 8.38 – 8.31 (m, 3H, ArH), 7.87 – 7.82 (m, 3H, ArH), 7.80 – 7.77 (m, 2H, ArH), 7.74 – 7.72 (m, 1H, ArH); ^{13}C NMR ($CDCl_3$ and TFA, 100 MHz): δ (ppm) 162.0, 161.5, 161.4, 161.3, 159.1, 158.6, 146.4, 138.4, 135.6, 134.9, 133.6, 132.9, 132.8, 132.3, 132.0, 130.5, 130.4, 129.3, 128.7, 128.2, 127.5, 127.3, 122.4, 121.9, 121.3, 120.6, 118.5; HRMS (ESI) Calcd. for $C_{31}H_{16}N_2O_6$ $[M+H]^+$ 513.1087 Found 513.1084.

Summary of Chapter 3

The deaths caused by cancer and bacterial infections are increasing day by day, and the present drugs are incapable of treating these diseases due to serious side effects and the development of drug resistance by cancer and bacterial cells. So, in light of the above-prevailing problems, we have successfully designed and synthesized two different series of bis-naphthalimide with spacers (**5a-i, 9a-i)** and without spacer (**11a-11p**) and were evaluated for their biological properties against 60 human cancer cell lines and eight bacterial strains.

Bis-naphthalimide having alkyl spacer displayed more potent results in inhibiting the growth of cancer cells. Mainly, compounds **5e** and **9h** displayed excellent results at one-dose concentration of 10 μM and were examined further at five dose concentrations (0.01 to 100 μM). Both compounds effectively suppress the growth of cancer cells with low values of GI_{50} **5e** (33.3 μM) and **9h** (4.67 μM), comparable to the marketed drug amonafide (GI_{50} = 3.3 μM). Mechanistic studies disclosed that **5e** and **9h** have the ability to bind with DNA, thus hindering the cell replication process and also causing DNA damage in the cells, ultimately leading to cancer cell death.

In contrast, bis-naphthalimide without spacer selectively inhibited the growth of bacterial strains. Mainly, compounds **11d** and **11o** showed excellent broad-spectrum antibacterial activity against most of the tested bacterial strains, which outperformed the marketed drugs. Both compounds exhibited rapid bactericidal properties, inhibited the biofilm formation in *E. faecalis*, and delayed the development of drug resistance upto 20 passages. Further mechanistic exploration revealed that these compounds disrupt the bacterial cell membrane, cause metabolic dysfunction, interact with DNA, induce accumulation of ROS species, and inhibit the GSH activity, leading to oxidative damage and cell death of *E. faecalis*. Moreover, compounds **5e, 9h, 11d** and **11o** were explored for their ability to bind with HSA and the results inferred that these compounds could effectively bind with HSA and can be transported to target site easily.

Hence, to sum up our finding manifested that these newly synthesized bis-naphthalimide derivatives have the potential to be taken to clinical trials for their further development as anticancer and antibacterial agents.

Chapter 4

Naphthalimide-coumarin hybrids and their biological evaluation

1. Introduction

Naphthalimide and coumarin are highly diverse functionalized heterocyclic moieties that have been explored over past decades due to their versatile biological properties such as antifungal, anticancer, antibacterial, antidiabetic, antiviral, antiherpetic, etc.[124-125] Some of the naphthalimide and coumarin derivatives have successfully entered clinical trials but failed due to side effects caused by them. In search of new therapeutics with increased biological properties and lesser effect, natural products are the main source. One such naturally occurring heterocyclic moiety is coumarin which contains lactones and binds with many active sites in organisms. Coumarin exerts its biological activities by inhibiting the key enzyme of biosynthetic pathway; moreover, it binds DNA *via* non-covalent interactions, thus making it a crucial pharmacophore for building new compounds with enhanced therapeutic values.[126] On the other hand, naphthalimide is a known DNA intercalator, and its hydrophobic nature makes it easier to penetrate the membrane of the cell. The heteroatoms in naphthalimide bind to various biological targets *via* hydrogen bonding and bring stable interactions.[32] Combining naphthalimide with naturally occurring coumarin can prove to be of great importance that helps in increasing the bioactivity, efficiency, selectively and reduced the side effects of the molecule. Over the past years, various naphthalimide and coumarin derivatives with other heterocyclic moieties have been reported as efficient anticancer and antibacterial agents.[33, 127] To the best of our knowledge, a hybrid of naphthalimide-coumarin having triazole or alkyl chain linker is rarely reported, and their biological properties have not been explored. This chapter outlines in details the synthesis of two different series of naphthalimide-coumarin derivatives, one having a triazole linker and the other with an alkyl chain linker, and their biological evaluation as antibacterial and anticancer agents. Thus, the chapter is divided into two sub-chapters that underline the effect of different linkers on the bioactivity of compounds.

4.1 Naphthalimide-coumarin hybrids having triazole linker as potent anticancer agents

4.2 Naphthalimide-coumarin hybrids with alkyl chain linker as potent antibacterial agents

Sub Chapter 4.1

Naphthalimide-Coumarin hybrids having triazole linker as potent anticancer agents

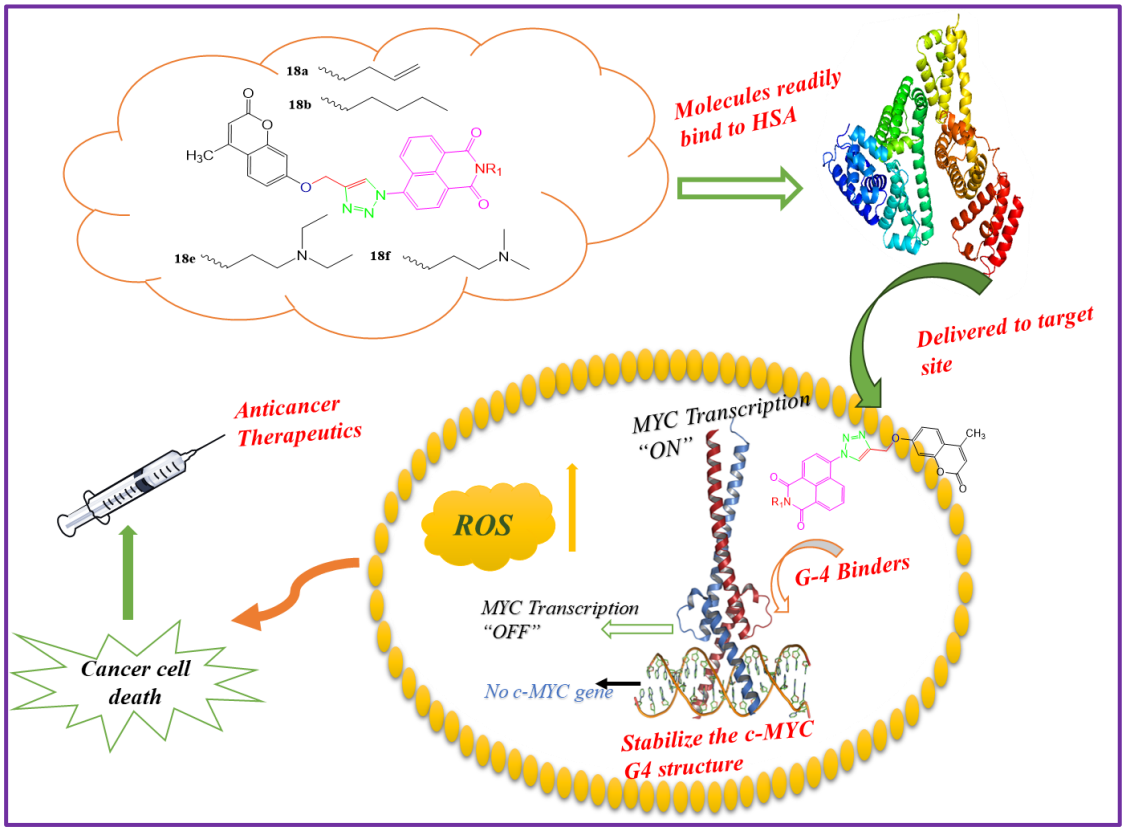

4.1.1 Introduction

Cancer is one of the deadliest diseases prevailing around the globe and is the major cause of human death. According to reports issued by WHO, there will be 21.9 million new cases and about 11.4 million deaths by 2025.[128] The death rate due to cancer has reached an alarming level, regardless of the availability of various methods for cure. Radiation therapy, immunotherapy, surgery, targeted therapy and chemotherapy are present methods to cure cancer, but in most of cases, these treatments are unable to recover due to development of resistance, toxic side effects, cancer heterogeneity, efficiency and presence of metastasis.[129] These limitations have called for finding of new therapies having alternative approach with lesser side effects. Cancer pathways are regulated by various proteins, and targeting these proteins can be an effective technique to overcome the above-mentioned problems.[132] Although there are many drugs available that bind to proteins, but due to the development of resistance, these have lost their effectiveness.[131] The resistance arises due to activation of adaptive loops, mutation in the target or involvement of different oncogenic pathways. Inhibiting the transcription of protein by small molecules can help to resolve these resistance issues, especially due to secondary mutations.

Targeting the canonical structures of DNA, a direct strategy to control DNA replication, is an insignificant method due to non-selectivity, thus making these structures vulnerable to side effects. The non-selectivity concern in cancer therapies can be resolved by targeting the non-canonical DNA structure termed ‘G-quadruplex’ (G4).[132] The stabilization of G-quadruplex DNA has gained significant importance in recent years due to the fact that these guanine-rich DNA are present in biologically important regions of human genome, such as telomerase and oncogene promoters.[133] These G4’s are formed in promoter regions of oncogenes such as c-MYC,[134] BLCP,[135] KRAS,[136] and VEGF[137] whose upregulation is associated with human cancer such as colon, osteosarcoma, breast, and leukaemia.[138] c-MYC, is overexpressed in a wide range of solid tumors, including breast, lung and ovarian carcinomas.[139] c-MYC comprises of transcription factor that regulates the synthesis of various genes participating in cell growth, metabolism, cell cycle progression, differentiation, DNA replication, apoptosis and mRNA maturation.[140] The flat structure and multiple binding sites of c-MYC make it difficult to inhibit the c-MYC directly. c-MYC gene expression can be inhibited by stabilization of G4 structure in the promoter region due to the fact that G-quadruplex is responsible for c-MYC transcriptional silencing.[141] The drug that readily binds and stabilizes the G4 structure can downregulate the gene production, leading to inhibition of

cancer, which is of great importance for building new anticancer agents.[142] Hence, a potent approach is generated from this concept that targeting G4 structures, which are necessary for c-MYC transcription and can affect their expression in tumor cells, but designing a molecule possessing anticancer potential that has greater affinity towards G4-DNA is a major concern.[143] Over the past years, a number of reports has been available on molecules that have the ability to bind with c-MYC quadruplex. These include derivatives of porphyrin, carbazole, benzothiazole, perylene, naphthalimide, coumarin, triazine, phenanthroimidazole, indole etc,[144-147] containing flat π-surface and planar aromatic ring(s) that can bind with G4-DNA through π-π interactions, and can be used to build potent G4 binding agents with potent anticancer properties. Some of these moieties have also entered various phases of clinical trials (**Figure 1**).

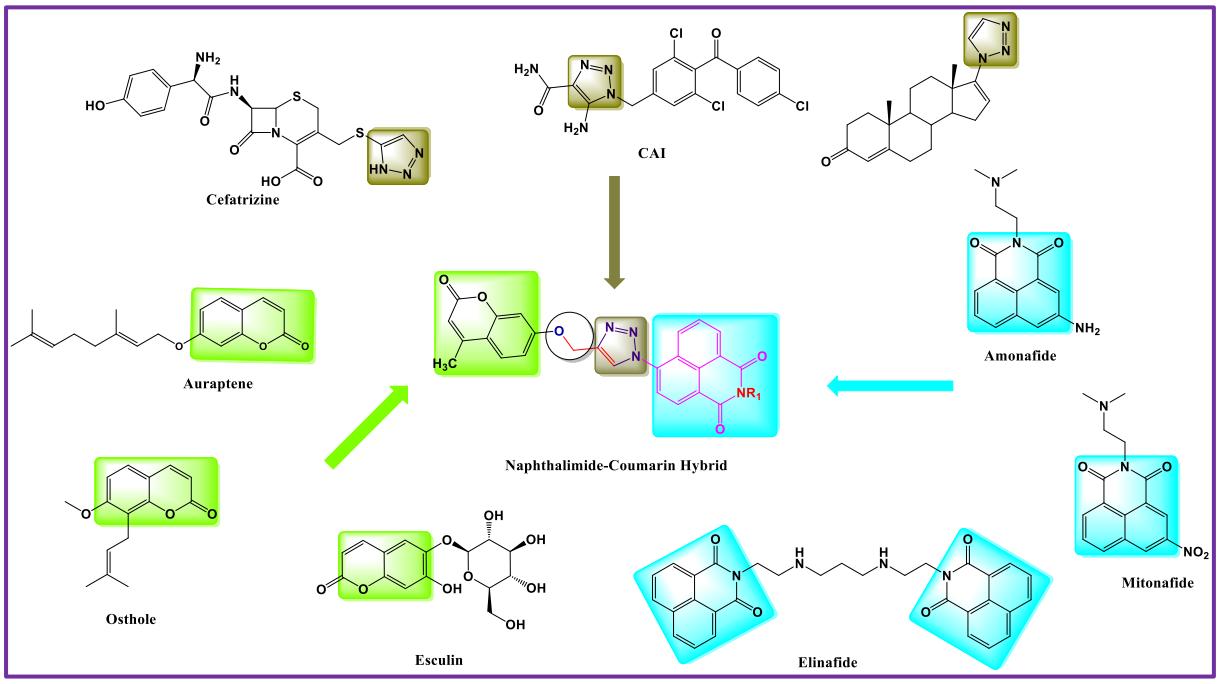

Figure 4.1. Clinical trial drugs containing various pharmacophores.

4.1.2 Designing of the targeted compounds

Naphthalimide is a flat π-aromatic planar moiety that binds well with nucleic acids and exhibits potent anticancer activity. The heteroatoms present in naphthalimide rings bring about stable interactions with biological ions *via* hydrogen bonding. Coumarin, a planar aromatic ring, binds with various active sites in target to exert its biological activity and binds with nucleic acids through non-covalent interactions. Triazole, another biologically active moiety with three consecutive nitrogens, has a conjugated system, and the intramolecular hydrogen

bonding of triazole binds more readily with guanine-rich region of G-quadruplex. The triazole derivatives exhibit fewer side effects, low toxicity, high bioavailability, drug delivery diversity, and good water solubility.

Individually, naphthalimide and coumarin derivatives have been reported as G4-DNA binding ligands to exert their anticancer activity, but very few reports are available in which napthalimide and coumarin are conjugated and their binding behavior towards G4-DNA is explored for their anticancer activity. Over the past few years, naphthalimide derivatives reported as anticancer with poor water solubility, thus decreasing the efficacy of the molecule. Naphthalimide having benzotriazole is reported as an anticancer agent against A549 cells *via* targeting *BCL2* G-quadruplex with IC_{50} value greater than 10 μM against the tested cell lines.[144] Considering the above-reported naphthalimide-benzotriazoles, we have modified the structure by replacing benzotriazole with triazole and introduced coumarin in the structure to increase the anticancer activity of the molecule. Triazole was used to increase the water solubility of the compound and providing selectivity towards G4-DNA over ds-DNA, whereas coumarin was helpful in increasing the anticancer potential of the molecule. Here, we report the design and synthesis of new naphthalimide-coumarin conjugates having triazole as linker *via* click chemistry and further derivatized with nucleophilic addition using various primary amines on the anhydric position of naphthalimide (**Figure 4.2**). The prepared compounds were evaluated for their potential to exhibit anticancer properties. The mode of action of most potent compounds was defined by targeting G4-quadruplex in the promoter region of c-MYC. The bindings of these molecules with G4-DNA were explored by various spectroscopic techniques. The bindings of active molecules with serum albumin were also examined for their transportation to the target site to cure cancer. This manuscript presents an effort to improve the anticancer potential of naphthalimide-benzotriazole system. As expected, our synthesized naphthalimide-triazole-coumarin conjugates exhibit broad-spectrum anticancer activity towards the tested 60 human cancer cell lines with lower GI_{50} values than reported derivatives. Moreover, these molecules selectively target c-MYC G4-DNA over other sequences of quadruplex and ds-DNA to exert their anticancer activity.

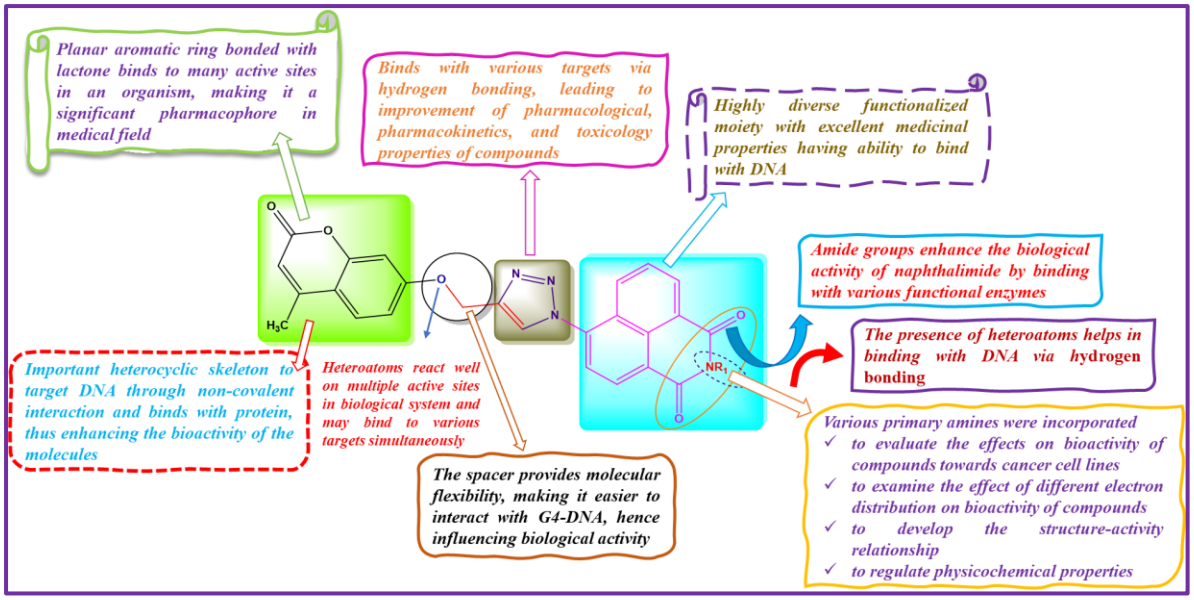

Figure 4.2: Designing of the target compounds

4.1.3. Chemistry

The synthetic route for preparation of intermediates and conjugates of naphthalimide-coumarin is depicted in **Scheme 1**. Bromination of commercially available acenaphthene (**1**) was done with the help *N*-bromosuccinimide in DMF at room temperature to afford 5-bromo-1,2-dihydroacenaphthylene (**12**) in 95% yield. Compound **12** was oxidized with sodium dichromate in refluxing acetic acid to afford compound **13** in 90% yield, which was further nucleophilic substituted with sodium azide in the presence of heated DMF: water (9.5:0.5) at 80 ºC to afford compound **14** in 83% yield**.** On the other hand, compound **16** was prepared by reacting commercially available 7-hydroxy-4-methyl-2*H*-chromen-2-one (**15**) with propargyl bromide in the presence of DMF using potassium carbonate at room temperature. The precursor compound **17** was prepared *via* click reaction of 6-azido-1*H*,3*H*-benzo[*de*]isochromene-1,3-dione (**14**) and 4-methyl-7-(prop-2-yn-1-yloxy)-2*H*-chromen-2-one (**16**) in the presence of CuI and DIPEA in acetonitrile at refluxing temperature. Further, compound **17** was substituted with various primary amines in the presence of zinc acetate and ethanol to synthesize different conjugates **18a-n**. All the conjugates were synthesized in good yields ranging from 65% to 86% and were characterized with the help of ^{1}H NMR, ^{13}C NMR, and HRMS.

Scheme 4.1: Synthesis of 2-substituted-6-(4-(((4-methyl-2-oxo-2*H*-chromen-7-yl)oxy)methyl)-1*H*-1,2,3-triazol-1-yl)-1*H*-benzo[*de*]isoquinoline-1,3(2*H*)-dione

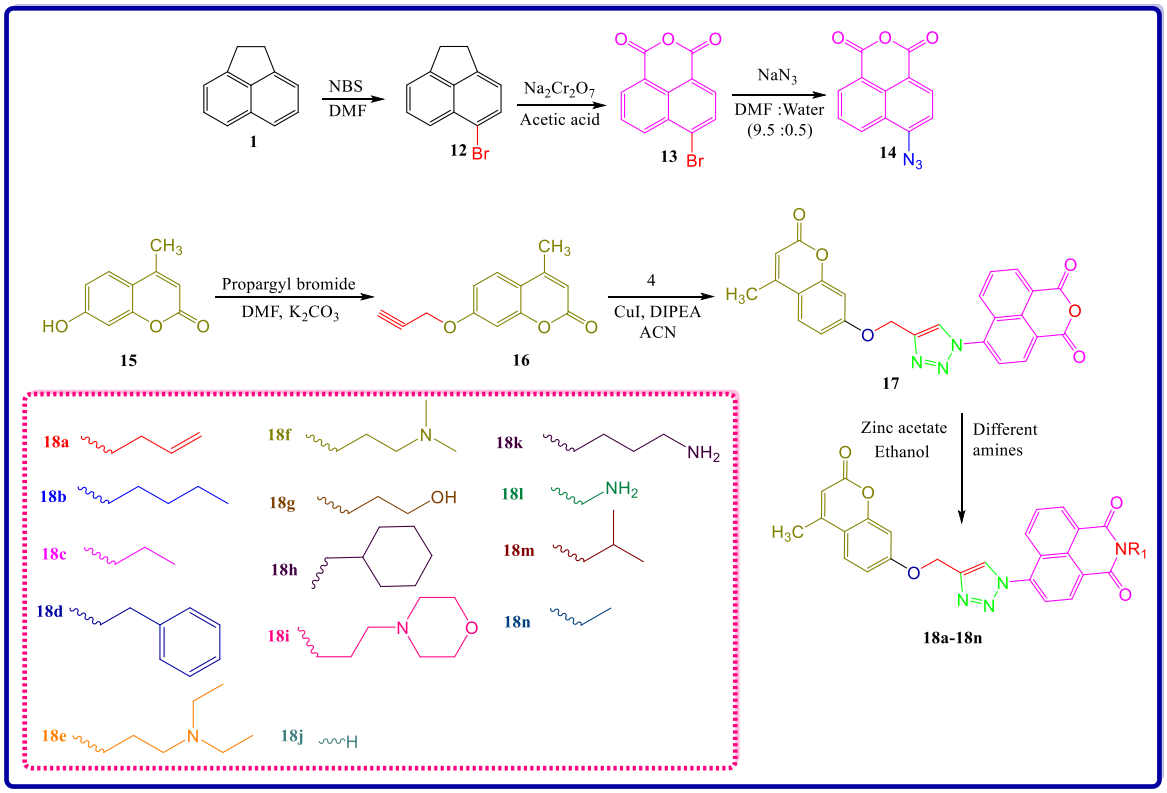

4.1.4 Quantum chemical studies

Quantum chemical studies is an effective tool to recognize the pharmacokinetic properties and interaction with biomacromolecules of drug candidates, that can help in predicting the bioactivity of compounds. It also inspects the interaction and ease of reaction between ligands, receptors and biomolecules.[123] Hence, the Frontline Molecular Orbital (FMO) studies were conducted, and the energy gaps between HOMO and LUMO of all the synthesized compounds were calculated, and the same is represented in **Table 4.1**. Compounds **18a**, **18b**, **18e** and **18f** exhibited the lowest energy gap between HOMO and LUMO and the ΔE was found to be 3.398 eV, 2.835 eV, 2.701 eV and 2.066 eV, respectively. A lower energy gap was exhibited in all four compounds, and the LUMO was located mainly on naphthalimide and triazole rings, inferring that these bind to positively charged biological ions by electrostatic forces. HOMO was localized on coumarin in **18a**, whereas in **18b**, **18e** and **18f**, it is positioned on alkyl chain attached to naphthalimide ring manifesting that it binds to negatively charged biological ions. Thus, of all the synthesized compounds, **18a**, **18b**, **18e** and **18f** exhibited higher bioactivity towards target sites and hence, can have the potential to inhibit the growth of cancer cells.

Table 4.1: Atomic orbital HOMO-LUMO compositions of compounds **18a, 18b**, **18e**, and **18f**

Compound	HOMO (eV)	LUMO (eV)	ΔE (eV)
18a	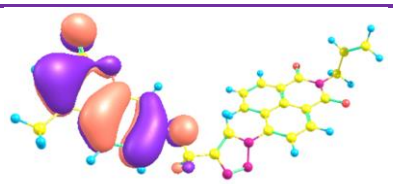	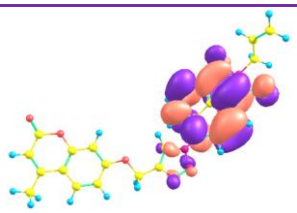	3.398
18b	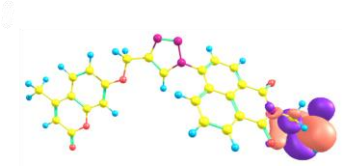	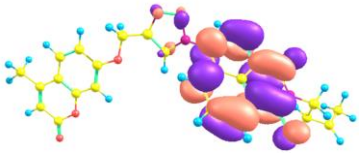	2.835
18c	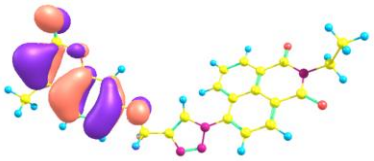	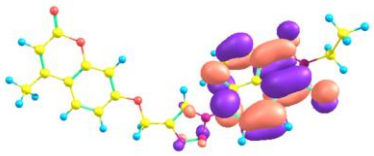	3.465
18d	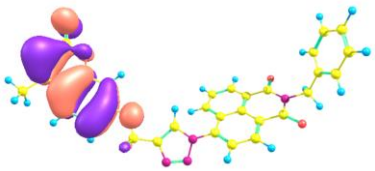	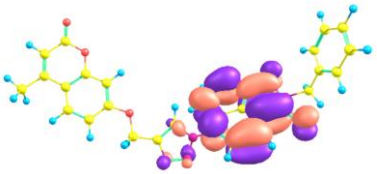	3.434
18e	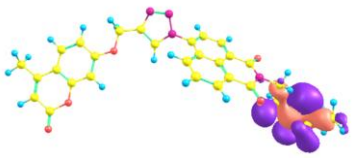	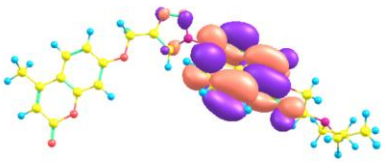	2.701
18f	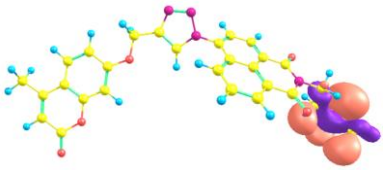	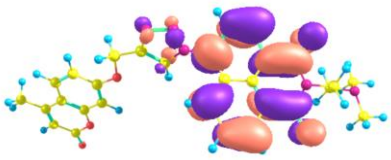	2.066
18g	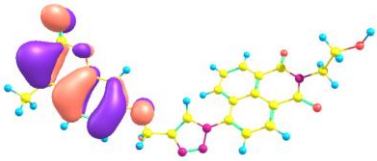	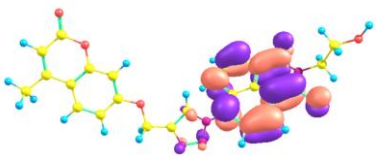	3.726

18h	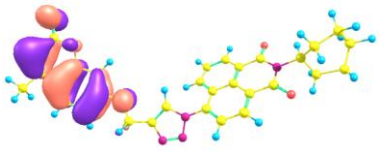	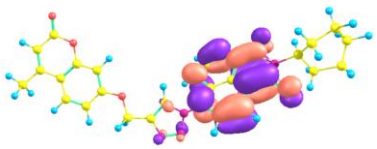	3.417
18i	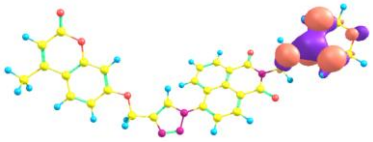	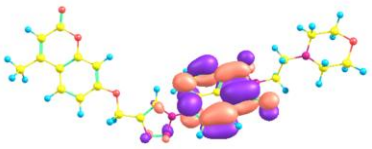	3.877
18j	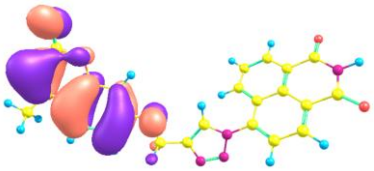	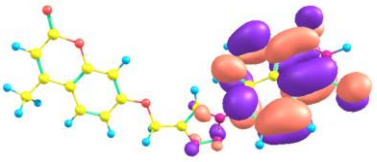	3.885
18k	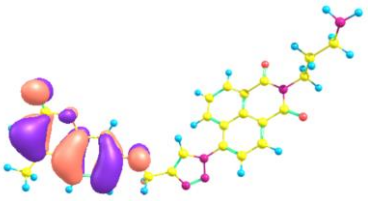	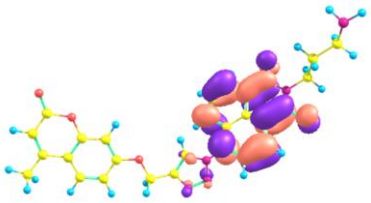	3.486
18l	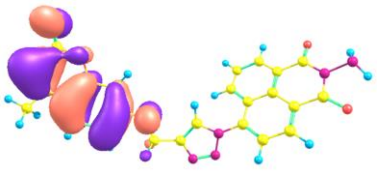	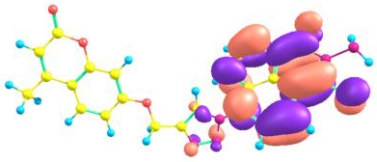	3.555
18m	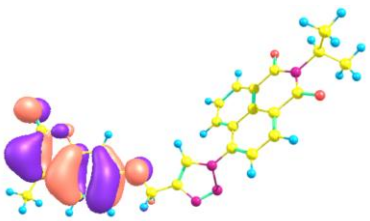	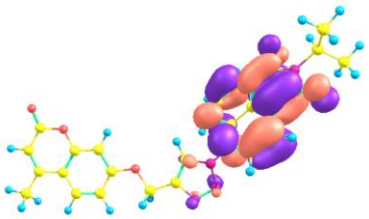	3.455
18n	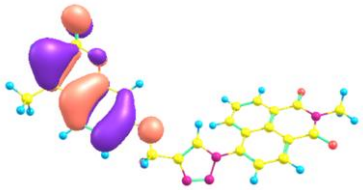	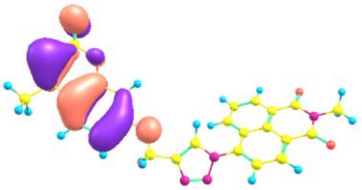	3.886

4.1.5 *In vitro* anticancer activity

FMO studies gave the idea that these newly synthesized derivatives will exhibit good bioactivity. Therefore, these compounds were evaluated *in vitro* for their potential to exist as anticancer agents. The naphthalimide-triazole-coumarin conjugates **18a-n** were selected by National Cancer Institute, USA, to examine their antiproliferative activity on account of computing modelling techniques.[77] Preliminary evaluations were tested against a full panel of 60 human cancer cell lines at one dose concentration of 10 μM, and the results obtained were compared to the known drugs amonafide and 5-fluorouracil. The evaluated compounds showed moderate to excellent results in inhibiting the growth of cancer cells. Most of the compounds displayed fascinating antitumor activity, having negative growth inhibition with greater cytotoxicity against most of the cancer cell lines. A series of 15 compounds were tested, and 5 compounds, mainly **18a**, **18b**, **18e**, **18f**, and **18h,** displayed astonishing results in inhibiting the growth of tumor cells with growth inhibition ranging from -97.21 to 52.28 % at 10 μM (**Tables 4.2** and **4.3**).

Table 4.2: Cytotoxicity of derivatives **18a-g** at 10 μM concentration

Panel	18a	18b	18c	18d	18e	18f	18g
Leukemia							
CCRF-CEM	12.55	11.42	6.22	-	86.82	80.78	-
HL-60(TB)	4.46	21.25	5.61	-	-56.66	-56.83	2.75
K-562	9.14	26.8	6.7	9.03	-28.84	-19.49	5.45
MOLT-4	7.27	13.44	-	2.93	-28.66	-24.9	1.18
RPMI-82226	37.51	38.88	-	-	-7.74	95.22	-
SR	27.92		-	-	NT	NT	NT
Lung Cancer							
A549	31.15	92.4	-	9.67	-52.11	-13.06	-
EKVX	25.95	67.91	-	32.07	13.08	-28.71	2.1
HOP-62	99.36	86.3	-	23.75	32.5	-58.44	-
HOP-92	-7.86	98.04	-	74.59	15.41	-47.61	4.35
NCI-H226	-13.85	79.46	-	38.88	-81.2	-82.86	1.46
NCI-H23	76.97	87.47	-	21.48	-52.43	-13.31	-
NCI-H460	58.92	-10.69	-	-	-36.11	-6.4	-
NCI-H522	-4.71	96.39	9.43	48.3	22.51	-46.09	28.85
Colon Cancer							
COLO 205	-	38.34	-	-	62.42	-60.47	-
HCC-2998	48.57	27.63	-	5.33	37.85	-95.54	-
HCT-116	40.64	83.38	-	18.42	-61.8	99.77	-
HCT-15	25.26	54.26	-	13.45	-82.12	-80.92	-

HT29	8.47	54.68	-	-	-53.47	-28.27	-
KM12	19.05	66.78	-	-	-86.92	-86.18	-
SW-620	30.74	76.32	-	-	-62.42	-26.54	-
CNS Cancer							
SF-268	92.89	84.55	-	27.43	-40.46	-6.46	2.05
SF-295	80.93	-5.98	-	51.23	22.5	-54.9	3.31
SF-539	64.29	-42.66	1.35	56.21	-94.13	-75.04	12.66
SNB-19	-15.18	92.03	4.7	63.01	-80.59	-48.91	9.25
SNB-75	-23.1	-31.07	-	43.34	94.22	73.05	12.99
U251	87.29	-28.53	-	41.23	-71.76	-22.25	-
Melanoma							
LOX IMVI	31.87	-46.24	-	36.4	-91.51	-72.63	3.44
MALME-3M	44.16	30.48	5.75	28.6	-	-63.09	2.12
M14	-	52.28	-	-	-78.67	-67.37	-
MDA-MB-435	2.35	68.11	-	-	-66.31	-51.51	-
SK-MEL-2	36.96	61.9	2.54	28.67	4.27	79.12	-
SK-MEL-28	-	76.62	-	4.99	1.34	-69.58	-
SK-MEL-5	4.23	50.49	-	-	15.23	-69.97	-
UAAC-257	6.58	47.71	-	-	-	-	-
UAAC-62	27.66	37.19	7.3	14.42	2.13	5.8	6.18
Ovarian Cancer							
IGROV1	33.84	10.57	-	11.28	5.4	-45.55	-
OVCAR-3	78.77	76.71	-	-	-75.12	-42.35	-
OVCAR-4	81.7	-5.3	-	-	-56.02	-22.49	-
OVCAR-5	22.67	40.26	-	5.08	96.8	-86.08	-
OVCAR-8	71.66	-8.74	-	31.38	-51.88	-22.57	-
NCI-RES	49.91	78	-	27.64	-71.17	-56.78	-
SK-OV-3	88.14	54.22	-	9.43	-	-25.11	-
Renal Cancer							
786-0	62.87	85.73	-	34.72	-77.6	-31.15	-
A498	14.4	-	-	-	-	-	-
ACHN	86.56	87.57	-	63.45	45.71	-76.09	8.94
CAKI-1	64.65	85.55	-	15.91	-49.55	-62.35	1.85
RXF 393	-6.01	-10.85	-	67.58	-86.81	-54.82	5.76
SN12C	41.07	85.81	3.75	28.6	-91.07	-75.27	6.63
TK-10	87.56	76.96	-	16.11	-85.71	-64.23	-
UO-31	64.54	75.58	7.48	14.67	-75.72	-54.09	7.59
Prostate Cancer							
PC-3	42.23	79.69	-	-	-15.85	-24.25	-
DU-145	39.75	89.72	-	-	-79.49	-79.67	-
Breast Cancer							
MCF7	65	73.66	6.82	21.79	-73.35	-63.65	10.83
MDA-MB-231	68.89	61.5	-	27.61	-88.41	-82.36	4.94
HS 578T	78.62	99.81	-	49.32	3.21	-29.46	-
BT-549	14.05	33.27	17.26	30.27	-	-37.64	-

T-47D	40.59	29.82	-	12.21	-	-29.1	-
MDA-MB-468	92.13	78.16	5.75	55.34	51.99	-81.52	5.66

Table 4.3: Cytotoxicity of derivatives **18h-n** at 10 μM concentration

Panel	18h	18i	18j	18k	18l	18m	18n
Leukemia							
CCRF-CEM	-71.41	-	-	5.12	-	3.86	-
HL-60(TB)	-97.21	-	-	4.04	-	2.49	-
K-562	75.81	6.09	-	36.58	-	9.57	-
MOLT-4	-92.63	-	-	19.94	-	5.48	-
RPMI-82226	-97.87	-	-	7.1	-	5.15	-
SR	-	NT	-	NT	NT	NT	NT
Lung Cancer							
A549	96.82	3.39	-	28.3	-	3.09	-
EKVX	-40.40	14.52	-	22.66	-	-	NT
HOP-62	-69.84	-	-	66.31	2.68	-	9.67
HOP-92	-43.14	59.81	-	-	-	2.46	-
NCI-H226	-33.77	5.66	-	51.09	-	3.84	14.78
NCI-H23	-63.30	7.26		34.43	9.6	-	-
NCI-H460	-52.29	13.68	-	48.71	-	-	-
NCI-H522	-36.07	40.48	-	81.43	21.64	20.69	4.99
Colon Cancer							
COLO 205	96.9	-	-	-	-	1.62	-
HCC-2998	-25.36	5.86	-	24.06	-	-	-
HCT-116	-38.37	10.71	-	22.54	-	-	3.77
HCT-15	-24.67	4.97	-	11.73	-	-	-
HT29	96.22	-	-	16.92	-	6.66	-
KM12	-32.17	-	-	42.85	-	-	-
SW-620	96.56	-	-	11.49	-	-	-
CNS Cancer							
SF-268	-4.55	34.07	-	64.37	-	2.9	-
SF-295	-29.72	36.38	-	53.3	-	1.81	8.07
SF-539	-50.60	36.58	-	69.57	7.96	4.27	8.64
SNB-19	93.01	28.45	-	76.11	-	9.75	9.53
SNB-75	-24.12	40.91	-	-	-	12.37	-
U251	-41.77	5.78	-	26.3	-	17.99	0.88
Melanoma							
LOX IMVI	-61.16	13.77	-	81.95	4.34	-	-
MALME-3M	85.52	6.86	-	48.88	5.26	3.27	-
M14	-12.36	-	-	55.63	-	-	-
MDA-MB-435	-39.92	-	-	22.76	-	1.88	-
SK-MEL-2	-65.22	-	-	-	-	-	-
SK-MEL-28	-2.14	-	-	59.81	-	-	-

SK-MEL-5	-95.01	8.32	-	50.77	-	2.33	-
UAAC-257	-62.86	-	-	17.27	-	-	-
UAAC-62	-33.42	13.8	-	51.98	3.78	11.4	4.04
Ovarian Cancer							
IGROV1	-26.29	-	-	3.36	-	5.61	NT
OVCAR-3	-65.83	2.03	-	-	-	-	-
OVCAR-4	-4.65	35.45	-	19.67	-	7.52	NT
OVCAR-5	NT	-	-	11.37	-	4.77	-
OVCAR-8	97.96	33.16	-	39.85	-	2.91	-
NCI-RES	-4.10	13.18	-	63.21	4.11	19.89	6.21
SK-OV-3	-44.09	7.25	-	9.8	13.84	-	-
Renal Cancer							
786-0	-35.95	4.5	-	15.89	-	1.5	NT
A498	-33.90	-	-	-	-	-	-
ACHN	-10.07	23.83	-	16.57	7.77	3.86	7.15
CAKI-1	-16.43	12.84	-	27.92	9.98	4.84	NT
RXF 393	-10.57	22.65	-	NT	NT	-	-
SN12C	-14.68	15.6	-	27.54	13.09	6.63	10.75
TK-10	91.06	-	-	-	-	5.05	-
UO-31	NT	30.5	-	85.81	30.2	11.37	NT
Prostate cancer							
PC-3	-29.21	5.57	-	29.42	1.24	-	NT
DU-145	90.65	-	-	44.61	-	-	-
Breast Cancer							
MCF7	-10.31	18.32	-	56.78	11.23	7.7	10.48
MDA-MB-231	NT	14.57	-	21.7	16.29	8.76	12.81
HS 578T	-35.41	37.3	-	60.82	6.44	-	2.01
BT-549	-23.72	40.01	-	77.1	-	-	NT
T-47D	-	13.3	-	1.82	-	7.32	-
MDA-MB-468	-74.22	12.49	-	-	-	20.22	11.62

4.1.6 Structure-activity relationships

The results obtained for derivatives having different chemical structures enable some fascinating structure-activity relationships to be uncovered. It is observed that derivatives having substituents such as ethyl amine (**18c**), ethanol amine (**18g**), ammonia (**18j**), hydrazine (**18l**), isopropyl amine (**18m**) and methyl amine (**18n**) were poor performers in suppressing the growth of cancer cells and regarded as to be least effective in the series. An increase in hydrophobicity and chain length in case of benzylamine (**18d**), ethyl-morpholine (**18i**), and propandiamine (**18k**), resulted in enhancement of bioactivity of compounds to some extent. Surprisingly, analogs bearing substitution of allyl amine (**18a**), butyl amine (**18b**), *N*,*N*-diethyl

ethylenediamine (**18e**), *N,N*-dimethyl ethylenediamine (**18f**), and cyclohexyl amine (**18h**) exhibited promising results; these not only inhibited the growth but also killed the cancer cells, hence, outperformed the known drugs amonafide and 5-fluorouracil. The results showed that the substituted amines' chain length played a crucial role in increasing the bioactivity of compounds. Preliminary studies inferred that compound **18d** suppressed the growth of lung cancer (HOP-22), CNS cancer (SF – 295, SF – 539, SNB-19), renal cancer (ACHN, RXF 393) and breast cancer (MDA-MB-468) with growth inhibition ranging from 55.3 to 74.5% whereas compound **18i** inhibited the growth of lung cancer HOP-22 with an inhibition rate of 59.8%. Compound **18k** was able to suppress the growth of most of the cancer lines, such as lung cancer (HOP-62 (66.3%), NCI-H226 (51.0%), NCI-H522 (81.4%)), CNS cancer (SF-268 (64.3%), SF-539 (69.5%), SNB-19 (76.1%)), and melanoma cancer (LOX IMVI- (81.9%), MI4 (55.6%), SK-MEL-28 (59.8%), SK-MEL-5 (50.7%) and UAAC-62 (51.9%). It selectively inhibited ovarian cancer cell line NCI-RES with a growth inhibition of 63.2% and renal cancer cell line UO-31 with an inhibition rate of 85.8%. It can be seen from the results predicted in **Tables 4.2** and **4.3** that compounds **18a**, **18b**, **18e**, **18f,** and **18h** showed excellent performance in suppressing the growth of most of the cancer cell lines, hence exhibiting broad-spectrum anticancer activity. Compounds **18a** and **18b** were mostly cytostatic, whereas **18e, 18f** and **18h** exhibited cytotoxicity against most of the cancer cell lines. Out of these five highly active compounds, four compounds, **18a, 18b, 18e** and **18f,** were selected further to evaluate their anticancer activity at five dose concentrations (10^{-4} to 10^{-8} M), where TGI (Total Growth Inhibition), GI_{50} (Growth Inhibition) and LC_{50} (Lethal concentration) were examined in micromolar range for each cell line. The results manifested that these four compounds displayed broad-spectrum antiproliferative activity against most of the cancer cell lines having MG-MID GI_{50} values of 3.18 μM (**18a**), 13.11 μM (**18b)**, 7.68 μM (**18e**) and 1.75 μM (**18f**). Compounds **18e** and **18f** exhibited greater efficacy against breast cancer and leukemia cancer with GI_{50} of 1.75 μM and 1.29 μM, respectively. Compound **18e** inhibited the growth of cancer cell lines with GI_{50} ranging from 1.75 to 15.1 μM, whereas **18f** exhibited a low value of GI_{50} against all the cancer cell lines ranging from 1.29 to 2.75 μM (**Table 4.4**). Moreover, comparing the compounds with standard drugs amonafide and 5-fluorouracil, these compounds exhibited promising results in inhibiting cancer growth with low values of GI_{50} and can be further taken for clinical trials.

Table 4.4: GI_{50} (μM), TGI (μM), and LC_{50} (μM) of derivatives **18a**, **18b**, **18e** and **18f** for *in vitro* tumour cell lines

	Activity (μM)	I	II	III	IV	V	VI	VII	VIII	IX	MG-MID
18a	GI_{50}	-	1.23	-	5.48	2.03	2.68	6.60	-	1.09	**3.18**
	TGI	-	7.29	-	-	-	-	-	-	9.14	8.21
	LC_{50}	-	-	-	-	-	-	-	-	-	-
18b	GI_{50}	-	2.96	-	9.37	3.90	26.3	18.67	-	17.46	**13.11**
	TGI	-	30.50	-	26.00	27.3	-	35.5	-	7.44	25.30
	LC_{50}	-	-	-	68.0	91.3	-	-	-	-	79.65
18e	GI_{50}	2.11	8.72	3.88	11.30	9.57	5.40	15.1	1.75	11.32	**7.68**
	TGI	5.66	22.4	10.3	24.10	19.72	12.64	15.54	3.34	24.16	15.31
	LC_{50}	9.36	57.3	26.8	47.7	40.19	6.27	43.91	6.26	36.82	30.51
18f	GI_{50}	1.29	1.82	1.61	1.73	1.69	1.58	2.75	1.72	1.57	**1.75**
	TGI	4.17	3.68	6.14	3.44	3.36	3.30	3.00	3.56	3.33	3.76
	LC_{50}	8.28	6.86	6.24	6.86	6.45	7.03	6.17	5.87	5.82	6.62
A	GI_{50}	1.51	-	8.40	72.10	70.60	61.40	45.60	22.70	76.40	**39.85**
B	GI_{50}	2.09	3.35	2.93	4.15	3.43	4.24	2.76	2.57	3.96	**3.32**

Leukemia (I), non-small cell lung (II), colon (III), CNS (IV), melanoma (V), ovarian (VI), renal (VII), prostate (VIII), breast (IX) cancers; MG-MID: the average sensitivity of all cell lines towards the test agent (μM); GI_{50} = concentration for 50% of maximal inhibition of cell proliferation, TGI = concentration of the compound resulting in total growth inhibition, LC_{50} = lethal concentration required to kill 50% of the population; A = 5-Fluorouracil, B = Amonafide

4.1.7 Cytotoxicity towards normal cell lines

Further, to evaluate the biosafety and ability of active compounds **18a**, **18b**, **18e,** and **18f** to selectively kill cancer cells, their cytotoxicity towards normal cell line Hek 293 was examined by MTT assay. The results manifested that all the compounds were less toxic to normal cells and could selectively affect the growth of cancer cells only. Compounds **18a, 18b, 18e** and **18f** showed cytotoxicity towards normal cell lines ranging from 14.52%-10.20%, 13.23%-11.01%, 12.32%-8.43% and 11.45%-6.76%, respectively (**Figure 4.3**), further confirming the biosafety of all compounds towards non-cancerous cell lines.

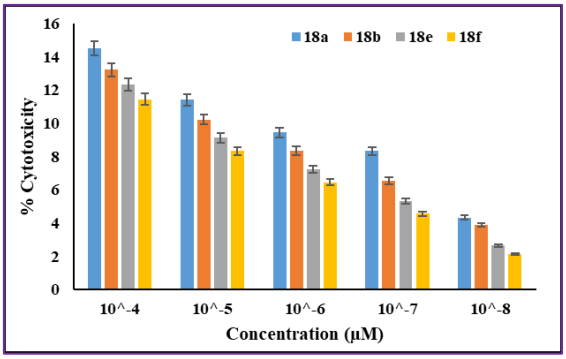

Figure 4.3: Cytotoxic effects of compounds **18a**, **18b**, **18e,** and **18f** against normal cell line HEK 293

4.1.8 *In silico* ADMET studies of active compounds

For drug screening and drug designing, ADMET study of drug candidates is a remarkable approach. Generally, molecules having low toxicity, excellent pharmacokinetic properties and good bioavailability are considered to be clinical candidates.[108] Online Swiss ADME software was used to explore the pharmacokinetic properties of **18a**, **18b**, **18e** and **18f** and allocate the affirmations for drug-likeness of these compounds (**Table 4.5**). Significantly, all the compounds exhibited high intestinal adsorption and good oral bioavailability scores similar to amonafide with a value of 0.55. Moreover, these compounds do not have the ability to penetrate the blood-brain barrier, indicating their biosafety and non-toxic nature. Thus, ADMET studies revealed that compounds **18a, 18b, 18e** and **18f** exhibited applicable pharmacokinetic profiles and accountable drug-likeness properties.

Table 4.5: ADME evaluation data of compounds **18a, 18b, 18e, 18f** and amonafide

	18a	**18b**	**18e**	**18f**	**Amonafide**
M.W	492.4	510.5	551.5	523.5	283.3
M logP	3.57	3.72	2.74	2.67	1.72
H-Bond acceptor	7	8	8	8	3
H-Bond donor	0	1	0	0	1
Rotatable bond	6	7	9	7	3
Bioavailability score	0.55	0.55	0.55	0.55	0.55
TPSA	129.4	112.4	112.4	109.2	68.3
Lipinski rule	Yes	Yes	Yes	Yes	Yes
BBB	No	No	No	No	No
GI absorption	High	High	High	High	High
Log Kp	-6.73	-6.80	-7.00	-7.35	-6.96

4.1.9 G-Quadruplex (G4) binding studies

G-quadruplex is formed by nucleic acid, rich in guanine, that folds into four-stranded secondary structure.[148] The stable structure of G4-DNA affects the different biological processes, such as regulation of genes and replication at the level of transcription.[149] Stabilizing G4-DNA in c-MYC region helps to inhibit the c-MYC gene that gets overexpressed in active cancer cell lines, thus bringing back the normal functioning of cell cycle, leading to cell apoptosis and cancer cell death.[150] Therefore, it's worth exploring the ability of compounds displaying potent anticancer activity to bind with G4-DNA and stabilize G-quadruplex in promoter region. The bindings of compounds with G4-DNA were explored by various spectroscopic techniques.

4.1.9a Absorption studies

To get insight into the interaction between molecules and G4-DNA, absorption spectra of **18a**, **18b**, **18e,** and **18f** were recorded in the absence and presence of G4-DNA. Compounds **18a, 18b, 18e,** and **18f** (5μM) displayed strong absorption band at 330 nm in 50 mM Tris HCl and 100 nM KCl at *p*H 7.4. Upon progressive addition of G4-DNA (0-6 μM) to the solution of these compounds, hypochromic shift in the characteristic absorption band was observed in all the cases (**Figure 4.4**) due to strong interaction with G4-DNA *via* external binding or stacking mode. Further, to evaluate the stability of complexes formed between G4-DNA and compounds, Bensei-Hildebrand equation was employed to calculate the binding affinities. The binding constants of **18a, 18b, 18e** and **18f** with G4-DNA were found to be $6.2 \times 10^6\ M^{-1}$, $7.0 \times 10^6\ M^{-1}$, $8.8 \times 10^6\ M^{-1}$ and $9.4 \times 10^6\ M^{-1}$, respectively which revealed the effective binding of molecules with G4-DNA.

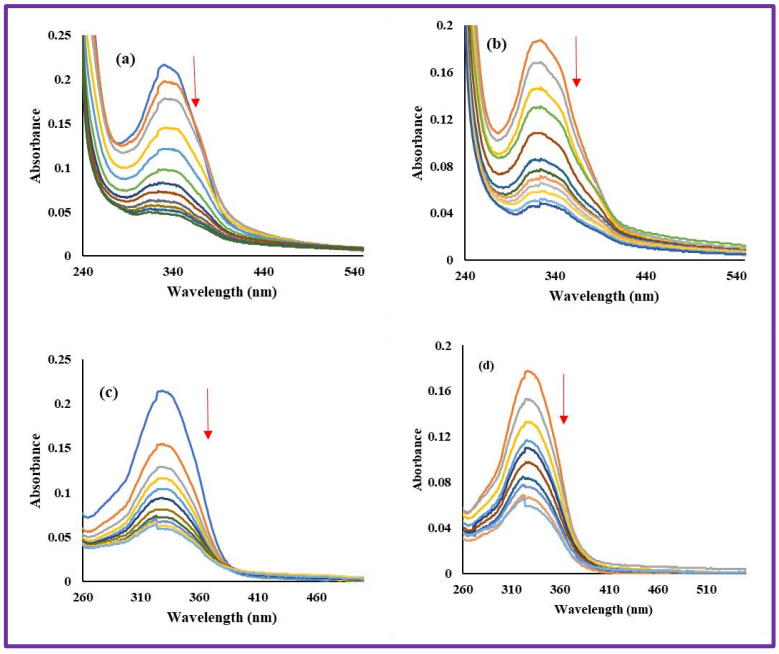

Figure 4: Absorption spectra of (a) **18a**, (b) **18b,** (c) **18e,** and (d) **18f** (5 μM) with increasing concentration of G4-DNA (0–6 μM)

4.1.9b Fluorescence studies

Fluorescence spectroscopy is an effective tool for exploring the interaction of ligands with macromolecules. Upon excitation at 330 nm, compounds **18a**, **18b**, **18e** and **18f** (5 μM) exhibited emission bands at 480 nm, 470 nm, 445 nm and 450 nm, respectively, in 50 mM Tris HCl and 100 mM KCl at *p*H 7.4. Quenching in fluorescence intensity in all cases were noticed upon progressive addition of G4-DNA (0-6 μM). The fluorescence maxima of **18a**, **18e** and **18f** were not shifted significantly, indicating the external interaction, whereas a slight blue shift

from 470 nm to 440 nm, in case of **18b** was observed, revealing the interaction between the base pairs of G4-DNA as well as external stacking (**Figure 4.5**). The considerable changes observed in fluorescence intensity indicated the effective binding of all the molecules with G4-DNA.

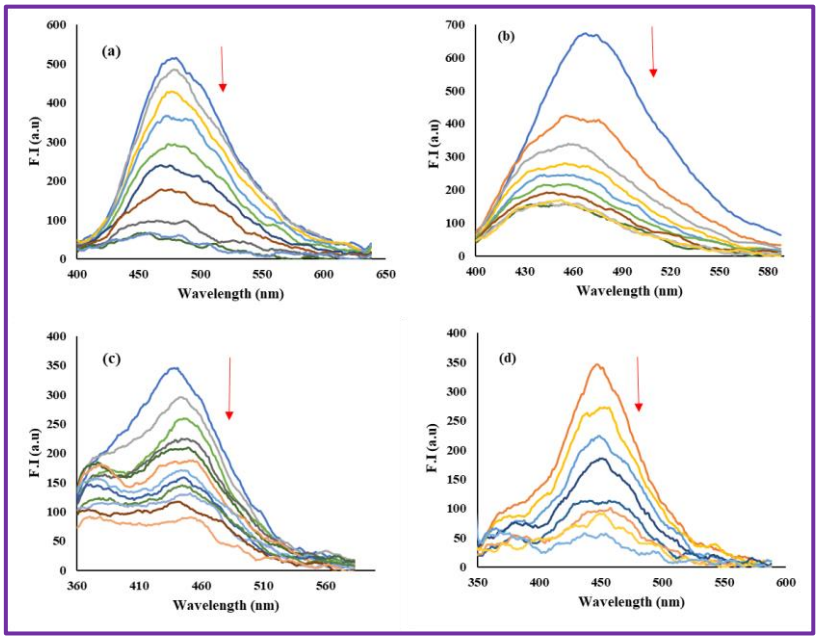

Figure 4.5: Fluorescence spectra of (a) **18a**, (b) **18b,** (c) **18e,** and (d) **18f** (5 μM) with increasing concentration of G4-DNA (0–6 μM)

4.1.9c Analysis of quenching mechanism

Quenching in fluorescence intensities of **18a**, **18b**, **18e** and **18f** were observed in the presence of G4-DNA, so it is necessary to explore the type of mechanism involved in the quenching process, whether static or dynamic. Stern-Volmer plot between F_o/F and G4-DNA at 450 nm (**18a**), 470 nm (**18b**), 445 nm (**18e**), and 450 nm (**18f**) representing the fluorescence quenching with gradual addition of G4-DNA were plotted. A linear regression was recorded in all the cases, and the slope value was employed to deliberate the quenching constant (K_{sv}) and bimolecular quenching rate constant (K_q); the same is represented in **Table 4.6**. The K_{sv} was found to be $5.7 \times 10^6\ M^{-1}$ (**18a**), $6.0 \times 10^6\ M^{-1}$ (**18b**), $6.5 \times 10^6\ M^{-1}$ (**18e**) and $7.3 \times 10^6\ M^{-1}$ (**18f**), and K_q was estimated to be $0.69 \times 10^{15}\ M^{-1}\ s^{-1}$ (**18a**), $1.17 \times 10^{15}\ M^{-1}s^{-1}$ (**18b**), $4.42 \times 10^{15}\ M^{-1}s^{-1}$ (**18e**) and $6.82 \times 10^{15}\ M^{-1}s^{-1}$ (**18f**). Further, it was experimentally approximated that the deliberated K_q values were much higher than the maximal scattering collision quenching constant value ($2 \times 10^{10}\ M^{-1}\ s^{-1}$) of various kinds of biomolecules. Therefore, the quenching mode is postulated to static quenching responsible for interaction of compounds with G4-DNA.

Table 4.6: Quenching constants for compounds **18a, 18b**, **18e** and **18f**

Comps.	K_{sv} (10^6 M^{-1})	K_q (10^{15} M^{-1} s^{-1})	R
18a	5.7	0.69	0.9802
18b	6.0	1.17	0.9882
18e	6.5	4.42	0.9906
18f	7.3	6.82	0.9926

4.1.9d Time resolved fluorescence studies

Time-Correlated Single Photon Counting (TCSPC) studies were conducted to measure the emission decay of **18a**, **18b**, **18e**, and **18f** in the absence and presence of G4-DNA to confirm the quenching mechanism (**Figure 4.6**). Compounds in an unbound state exhibited a lifetime of 8.13 ns (**8a**), 5.11 ns (**8b**), 1.47 ns (**8e**), and 1.09 ns (**8f**) in Tris-HCl buffer. Upon binding with G4-DNA, significant fall in decay time profile of all the molecules were noticed as represented in **Table 4.7,** thus, disclosing the existence of dynamic quenching. Combining the results obtained from steady-state and time-resolved studies, it is concluded that both types of quenching are responsible for the interaction of molecules with G4-DNA.

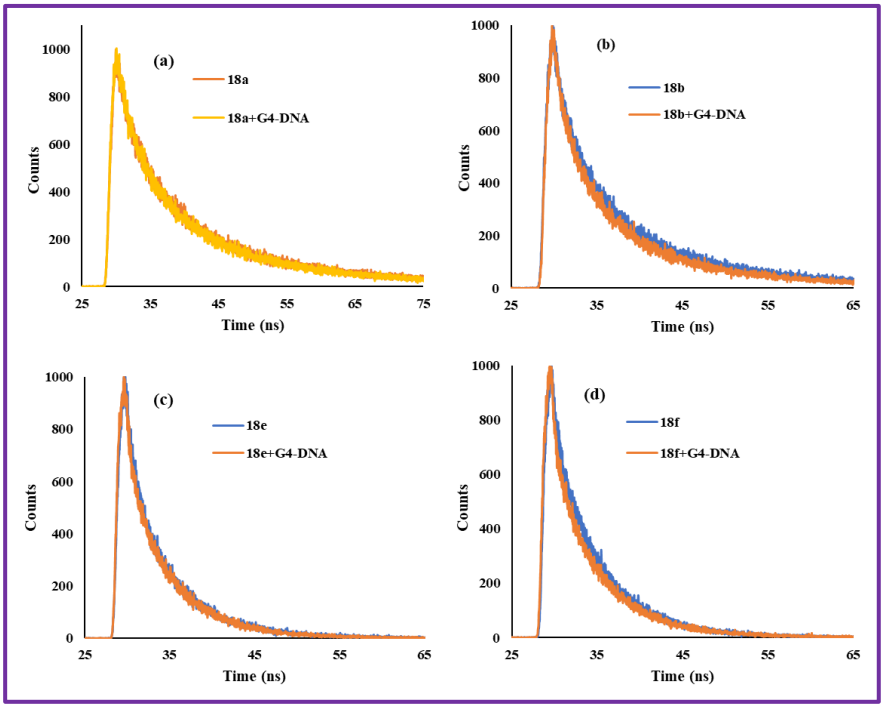

Figure 4.6: Fluorescence decay profile of compounds (a) **18a,** (b) **18b,** (c) **18e** and (d) **18f** on addition of G4-DNA.

Table 4.7: Lifetime fluorescence decay of **18a, 18b, 18e** and **18f** on interaction with G4-DNA

System	Conc.	τ_1 [ns]	τ_2 [ns]	τ_3 [ns]	α_1	α_2	α_3	τ_{av}
18a		5.96	18.08	1.11	0.41	0.29	0.29	8.13
18a: G4-DNA	1:1	6.31	18.49	1.44	0.43	0.26	0.31	7.93
18b		5.06	15.65	0.70	0.39	0.18	0.43	5.11
18b: G4-DNA	1:1	4.60	14.2	0.66	0.38	0.16	0.47	4.28
18e		1.62	5.52	0.19	0.10	0.21	0.69	1.47
18e: G4-DNA	1:1	1.19	5.33	0.10	0.06	0.12	0.82	0.78
18f		1.50	5.47	0.13	0.03	0.17	0.80	1.09
18f: G4-DNA	1:1	1.58	5.63	0.07	0.02	0.07	0.90	0.51

4.1.9e Binding constant and Gibbs free energy

Further, to assess the complex stability formed between molecules and G4-DNA, binding constant (K_b) was obtained, employing double-logarithmic Scatchard's equation. The values of binding constant (K_b) and number of binding sites (n) in each case are depicted in **Table 4.8**. These binding constants indicated the effective binding of all the molecules with G4-DNA. The number of binding sites in each case were found to be approximately 1, delivering that all the molecules bind with G4-DNA at one site only with a stoichiometry of 1:1.

Table 4.8: Binding parameters for compounds **18a, 18b**, **18e** and **18f**

Comp.	K_b (10^6 M^{-1})	n	R
18a	7.00	1.00	0.9855
18b	7.80	1.02	0.9948
18e	8.80	1.00	0.9944
18f	10.30	1.05	0.9871

Further, to analyse the spontaneity of complexes formed between **18a**, **18b**, **18e**, and **18f** and G4-DNA, Gibb's free energy was formulated where ΔG were found to be -9.30 kcal mol^{-1} (**18a**), -9.37 kcal mol^{-1} (**18b**), -9.43 kcal mol^{-1} (**18e**) and -9.52 kcal mol^{-1} (**18f**) (**Table 4.9**). These negative values of ΔG revealed that all the compounds bind efficiently with G4-DNA *via* van der Waals interactions and hydrogen bonding.

Table 4.9: Thermodynamic parameters of G4-DNA binding with compounds **18a, 18b, 18e** and **18f**

T (K)	ΔG, kcal M^{-1} (**18a**)	ΔG, kcal M^{-1} (**18b**)	ΔG, kcal M^{-1} (**18e**)	ΔG, kcal M^{-1} (**18f**)
298	-9.30	-9.37	-9.43	-9.52

4.1.9f Mode of binding

(i) Competitive displacement assay

Further, to recognize the mode of binding of compounds with G4-DNA and to validate the stacking mode of interaction, we performed competitive displacement studies with Ethidium Bromide (EB). In Tris-HCl buffer (*p*H = 7.4), EB didn't exhibit any emission band, but when embedded and stacked in a hydrophobic environment of G4-DNA, its fluorescence was enhanced, and it displayed a strong emission band at 620 nm upon excitation at 520 nm.

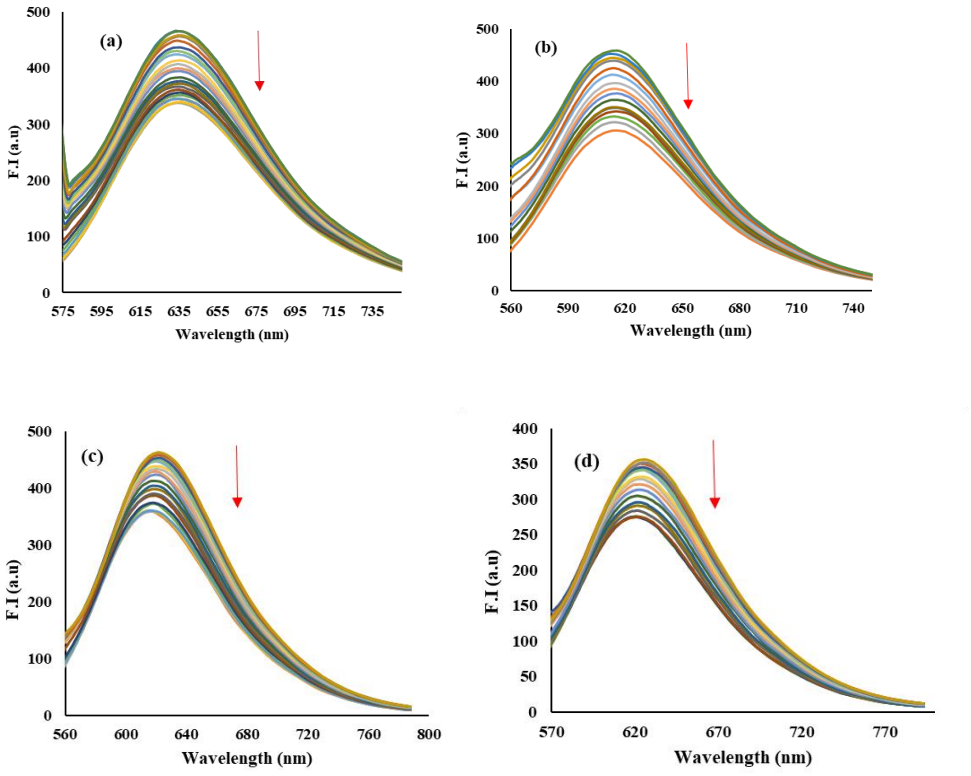

Figure 4.7: Emission spectra of ethidium bromide and G4-DNA complexes upon increasing concentration of compounds (a) **18a** (0-5 μM), (b) **18b** (0-4 μM), (c) **18e** (0-6 μM) and (d) **18f** (0-3 μM).

Incremental additions of compounds **18a**, **18b**, **18e** and **18f** (0-5 μM) to solution of EB-G4-DNA complexe (1:10), a noticeable hypochromicity in fluorescence intensity of EB-G4-DNA complex was observed (**Figure 4.7**), revealing that all the molecules efficiently bind to G4-DNA in a stacking mode of interaction and displaces EB from the complex. Combining the results obtained from various studies, it is put forward that all the compounds are able to interact with G4-DNA *via* stacking outside with the end quarters.

(ii) Molecular docking studies

Further, to acquire more information about the binding and stacking mode of interaction, molecular docking studies of compounds **18a**, **18b, 18e** and **18f** with c-MYC G-quadruplex (PDB:1XAV) were conducted with the help of Autodock 4.2 and best matching pose of ligand bound to G4-DNA was visualized by Discovery Studio. These molecules contain rigid naphthalimide, triazole and coumarin cores having π-surface and alkyl chain between them, making the molecules flexible and thus capable of interacting with G4-DNA. **Figure 4.8** delivers 2D and 3D molecular docked models of **18a, 18b, 18e** and **18f** in the best-suited way. The minimum binding energies of the molecules **18a, 18b, 18e** and **18f** with G4-DNA were formulated to be -7.14, -8.96, -9.24, and -9.53 kcal/mol, respectively.

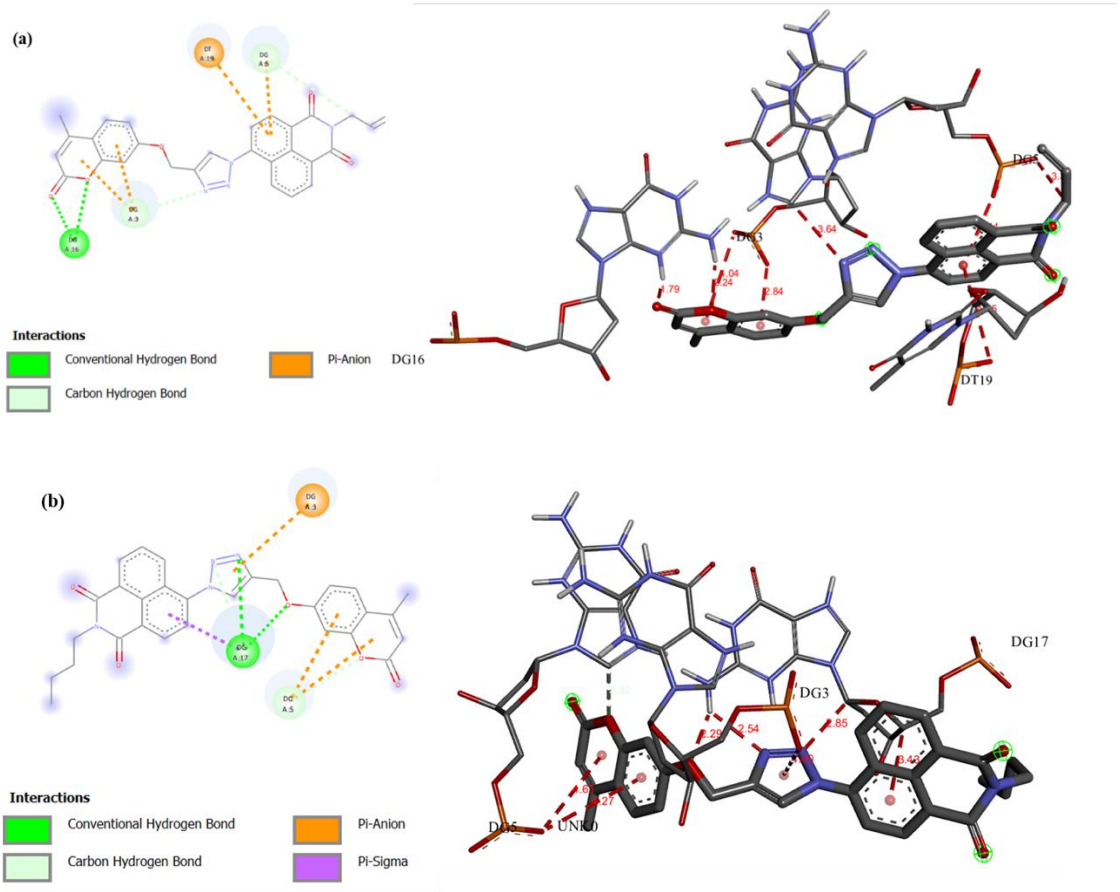

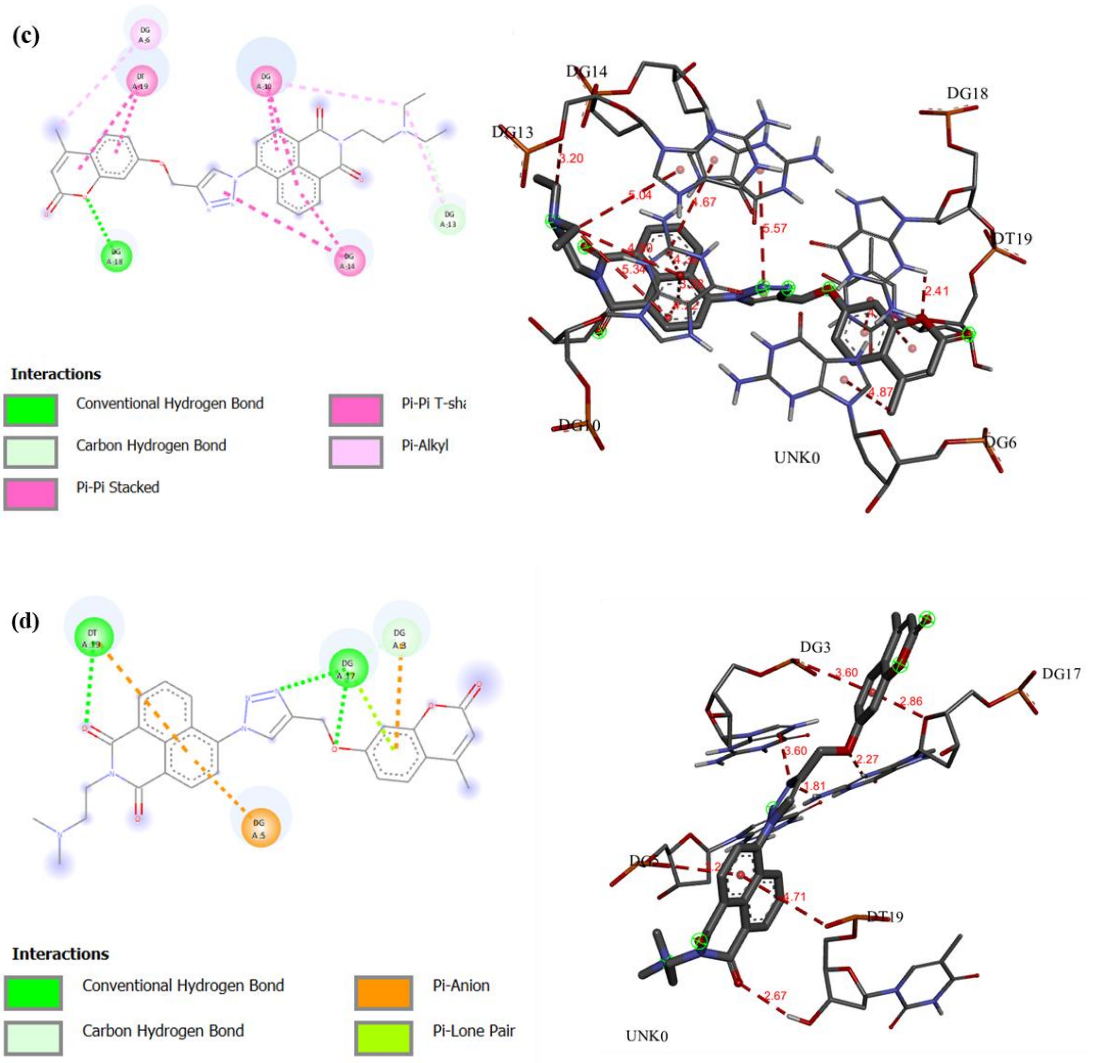

Figure 4.8: Molecular docking of G4-DNA (1XAV) with compounds (a) **18a**, (b) **18b**, (c) **18e** and (d) **18f**

The docking results were further elaborated by 2D dock pose of ligand with G4-DNA having lowest energies, as represented in **Figure 4.8.** The forces responsible for stabilization of G4-DNA were mainly hydrogen bonds, π-σ, π-π stacking and carbon-hydrogen bonds. Hence, the main base pair involved in the interaction process is guanine on the backbone of G4-DNA. The multiple interaction forces existing in the system is favourable for strong binding of **18a, 18b, 18e** and **18f** with G4-DNA and thus stabilizes it.

4.1.9g Dynamic Light Scattering (DLS) studies

DLS experiments were conducted to observe variations in size of G4-DNA upon interacting with **18a, 18b, 18e** and **18f**. The particle size distribution was recorded for free G4-DNA and in bound form, and the same is represented in **Figure 4.9**. The average size of G4-DNA was

recorded to be 531 ± 1.0 nm, whereas in the presence of compounds **18a**, **18b**, **18e** and **18f**, the size was found to be 396 ± 3.0 nm, 342 ± 2.1 nm, 255 ± 3.5 nm and 164 ± 2.0 nm, respectively, (**Figure 4.9**). The emergence of a single sharp peak and decrease in size of G4-DNA upon complex formation manifested the strong binding with G4-DNA.

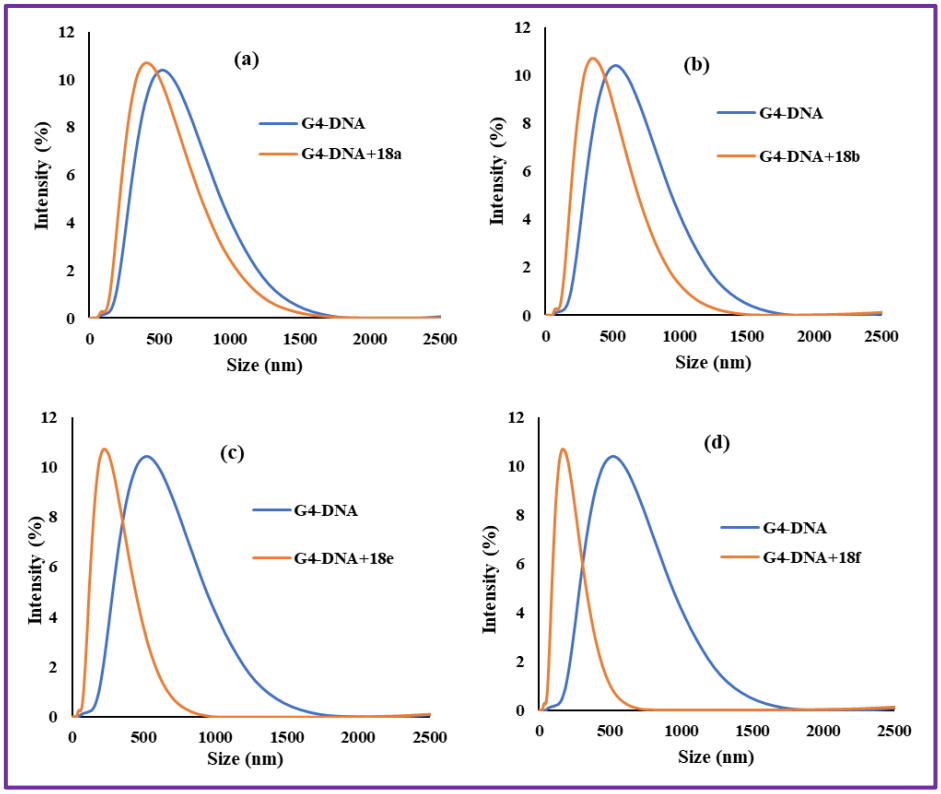

Figure 4.9: DLS studies showing intensity-based particle size distribution for G4-DNA in absence and presence of compounds (a) **18a**, (b) **18b**, (c) **18e**, and (d) **18f**

4.1.9h Zeta potential studies

The net electrical charge on the surface of particle is demonstrated by zeta potential. The value of zeta potential obliquely reveals the net surface charge of the system, thus moulding it as a constructive framework to judge the extent of interaction between molecule and G4-DNA. The binding of G4-DNA with **18a, 18b, 18e** and **18f** *via* zeta potential experiment is formulated, and the net surface charge on free G4-DNA was found to be -4.13 ± 2.32 mV. In the presence of compounds, surface charge decreased to -6.8 ± 1.88 mV (**18a)**, -8.55 ± 1.59 mV (**18b**), -9.04 ± 1.29 mV (**18e**) and -11.3 ± 0.45 mV (**18f**). The change in zeta potential of G4-DNA upon addition of compounds manifested the complex formation.

4.1.10 ct-DNA Binding Studies

In order to check the selectivity of active compounds towards quadruplex DNA, we explored the binding abilities of these compounds **18a**, **18b**, **18e,** and **18f** towards ct-DNA using spectroscopic studies.

4.1.10a UV-visible studies

Compounds **18a, 18b, 18e,** and **18f** (5 μM) exhibited an intense absorption band at 330 nm in phosphate buffer at *p*H = 7.4. Upon incremental addition of ct-DNA (0-30 μM) to the solution of these compounds, no change in absorption band of compounds was recorded in all the cases. **Figure 4.10** indicates that these compounds were unable to bind with ct-DNA in the ground state.

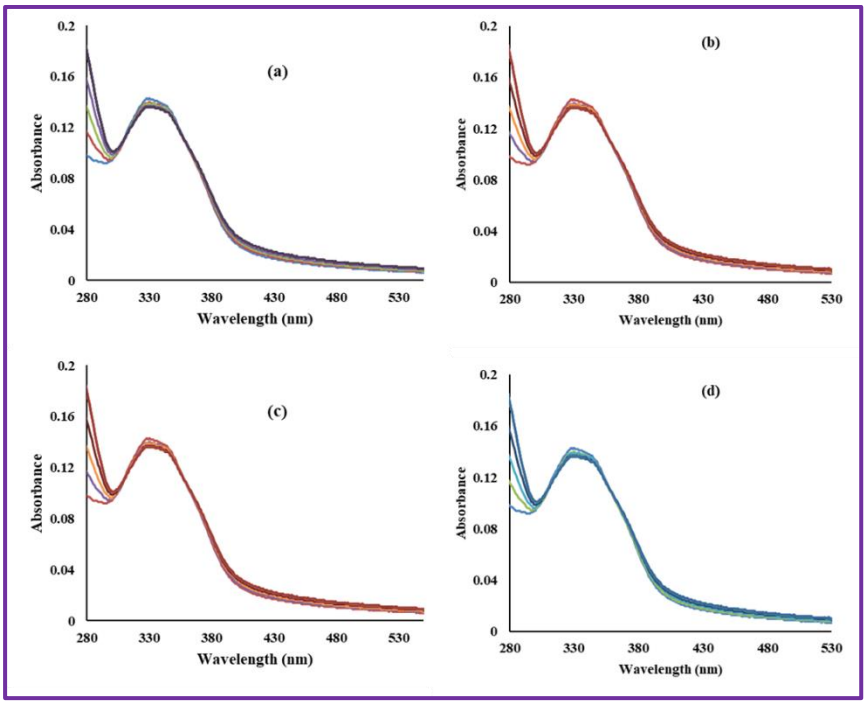

Figure 4.10: Absorption spectra of compounds (a) **8a (b) 8b (c) 8e** and (d) **8f** (5 μM) with increasing concentration of ct-DNA (0–30 μM).

4.1.10b Fluorescence studies

Further, emission studies explored the interaction of these compounds towards ct-DNA. Compounds **18a, 18b, 18e,** and **18f** displayed strong emission bands at 480 nm, 470 nm, 420 nm, and 445 nm, respectively, in phosphate buffer (pH = 7.4) upon excitation at 330 nm. Progressive addition of ct-DNA (0-50 μM) to the solution of compounds **18a** and **18b** resulted

in quenching in fluorescence intensity of compounds, indicating that these compounds interact with ct-DNA in the excited state; hence, the binding constants were calculated from modified Stern-Volmer equation and were found to be $3.2 \times 10^2\ M^{-1}$ (**18a**) and $2.6 \times 10^2\ M^{-1}$ (**18b)**. These low values of binding constant indicate the less affinity of compounds **18a** and **18b** towards ct-DNA. Whereas in the case of compounds **18e** and **18f**, no change in fluorescence intensity of the compound was observed upon incremental addition of ct-DNA, inferring that **18e** and **18f** didn't bind with ct-DNA (**Figure 4.11**).

Comparing the results of ct-DNA and G4-DNA, it is concluded that compounds **18a, 18b, 18e**, and **18f** can selectively bind with G4-DNA over ds-DNA to exert their anticancer mechanism.

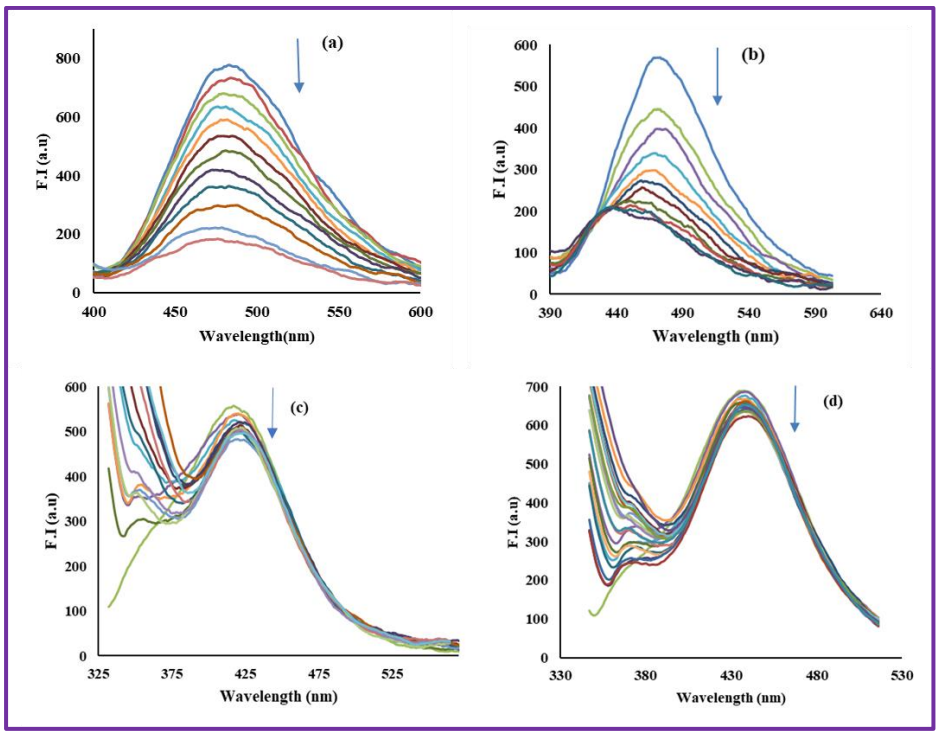

Figure 4.11. Emission spectra of (a) **18a,** (b) **18b,** (c) **18e,** and (d) **18f** in phosphate buffer (*p*H 7.4) upon increasing concentrations of ct-DNA (0–50 μM).

4.1.11 Human Serum Albumin (HSA) binding studies

HSA, a crucial protein in human blood plasma, transports the drugs to the target site, thus improving the solubility of drugs, preventing oxidation in plasma, and lowering toxicity.[87] The binding of drugs with serum albumin regulates the pharmacodynamic, therapeutic value and pharmacokinetic properties through molecular recognition. Due to these excellent properties of HSA, it serves as main target for developing potent anticancer agents.[122] Hence, it is worth

exploring the binding ability of compounds with HSA for transportation of drug to the target site. These interaction studies were performed by various spectroscopic techniques.

4.1.11a UV-visible studies

Due to electronic transition in aromatic rings, HSA exhibited an intense absorption band at 280 nm in phosphate buffer at *p*H 7.4. Incremental addition of compounds **18a**, **18b**, **18e** and **18f** (0-6 μM) led to hyperchromic shift along with the formation of new band at 345 nm in all four cases, inferring the environmental changes around Phe, Trp and Tyr residues in HSA (**Figure 4.12**). No significant change in wavelength maxima of HSA was observed, manifesting the non-covalent interactions between serum albumin and drug candidates. Further, Bensei-Hildebrand equation was employed to calculate the binding constants and check the complexes stability. The binding constants were found to be $2.3 \times 10^4\ M^{-1}$ (**18a**), $2.7 \times 10^4\ M^{-1}$ (**18b**), $3.9 \times 10^4\ M^{-1}$ (**18e**) and $8.7 \times 10^4\ M^{-1}$ (**18f**), displayed that all four molecules bind efficiently with HSA and can be delivered to the target site.

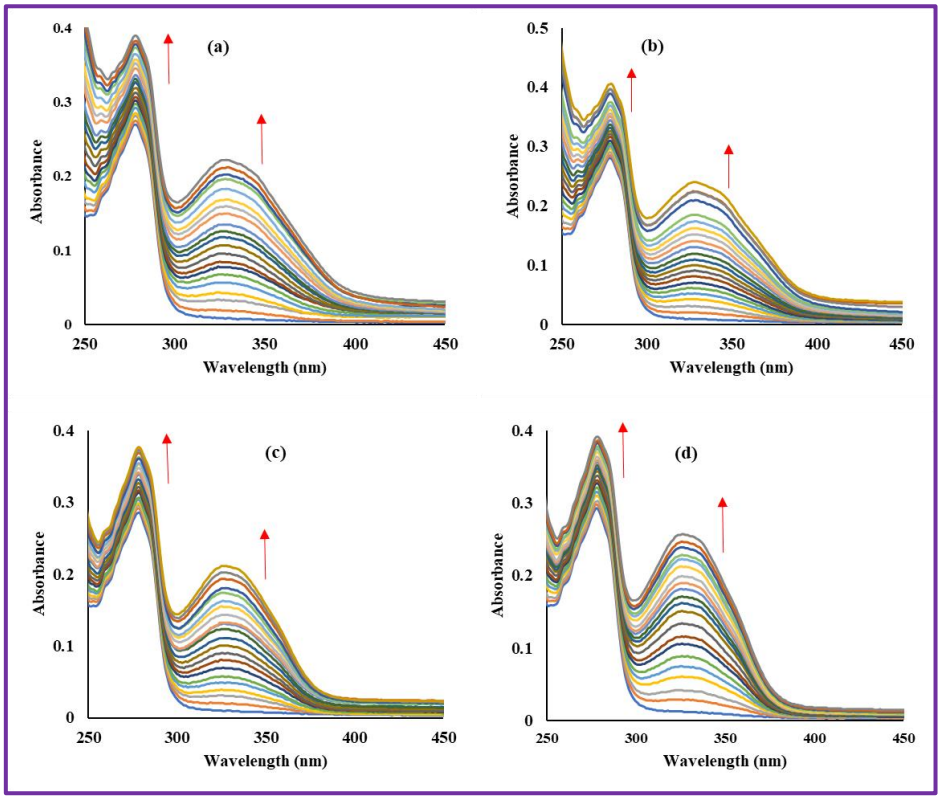

Figure 4.12: Absorption spectra of HSA on increasing concentrations (0-6 μM) of (a) **18a,** (b) **18b,** (c) **18e** and (d) **18f** in phosphate buffer (*p*H 7.4) at 298 K

4.1.11b Fluorescence studies

The absorption studies' results are insufficient to fully understand the binding behaviour of active molecules and HSA. Therefore, steady-state fluorescence studies were carried out to further get insight into the interaction between HSA and compounds **18a**, **18b**, **18e,** and **18f**. Native HSA (10 μM) solution exhibited a strong emission band at 350 nm upon excitation at 280 nm due to Tyr, Phe and Trp residues. The solution of HSA (10 μM) in PBS (*p*H = 7.4) was titrated with incremental additions of all four compounds, i.e. **18a** (0-30 μM), **18b** (0-25 μM), **18e** (0-20 μM) and **18f** (0-18 μM), where progressive decrease in emission intensity of HSA at 350 nm was observed, along with the development and enhancement of a new band at 480 nm in case of compounds **18a** and **18b (Figure 4.13)**. The fluorescence of HSA was fully quenched at higher concentrations of all the compounds, inferring the efficient binding of drug candidates with HSA.

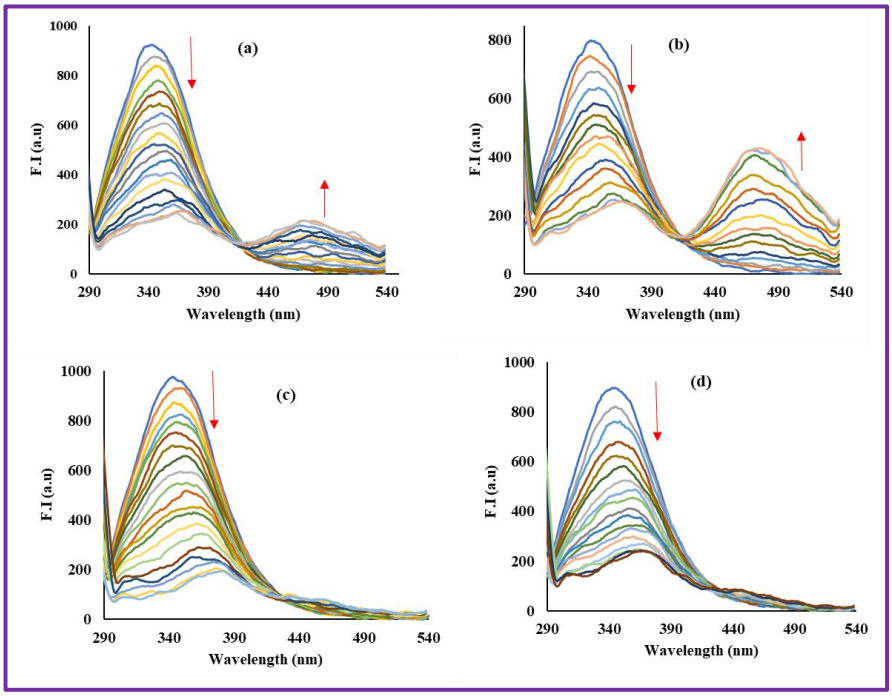

Figure 4.13: Fluorescence spectra of HSA upon progressive additions of (a) **18a**, (b) **18b**, (c) **18e** and (b) **18f** in phosphate buffer (*p*H 7.4) at 298 K

4.1.11c Identification of quenching mechanism

The interaction of foreign ligand with protein changes the microenvironment, resulting in fluorescence quenching of HSA. This quenching can either be static or dynamic, and the Stern Volmer equation was employed to determine the type of quenching mechanism for emission intensity corresponding to 342 nm. The Stern-Volmer plots were plotted between F_o/F and concentration at 342 nm, displaying the quenching in emission intensity of HSA with gradual

addition of compounds. Linear regression was obtained, and the value of slope was used to calculate the quenching constant K_{sv} and bimolecular quenching rate constant K_q (**Table 4.10)**. In all the cases, K_q was found to be in the order of 10^{13} $M^{-1}s^{-1}$, which is higher than the maximum value of dynamic quenching constant (10^{10} $M^{-1}s^{-1}$), inferring that static mechanism occurred during the interaction between compounds and HSA.

Table 4.10: Quenching constants for compounds **18a, 18b**, **18e** and **18f**

Comps.	K_{sv} (10^5 M^{-1})	K_q (10^{13} M^{-1} s^{-1})	R
18a	1.03	1.03	0.9935
18b	1.47	1.47	0.9905
18e	2.31	2.31	0.9821
18f	3.05	3.05	0.9951

4.1.11d Time-resolved fluorescence analysis

Steady-state fluorescence predicted that static quenching is responsible for decrease in fluorescence intensity of HSA. In order to confirm the same with time-resolved, a fluorescence experiment was conducted between HSA and compounds **18a, 18b, 18e**, and **18f**. The time-resolved spectra of free HSA (10 μM) were recorded with gradual additions of **18a**, **18b**, **18e** and **18f** at concentrations of 0-30 μM as shown in **Figure 4.14**.

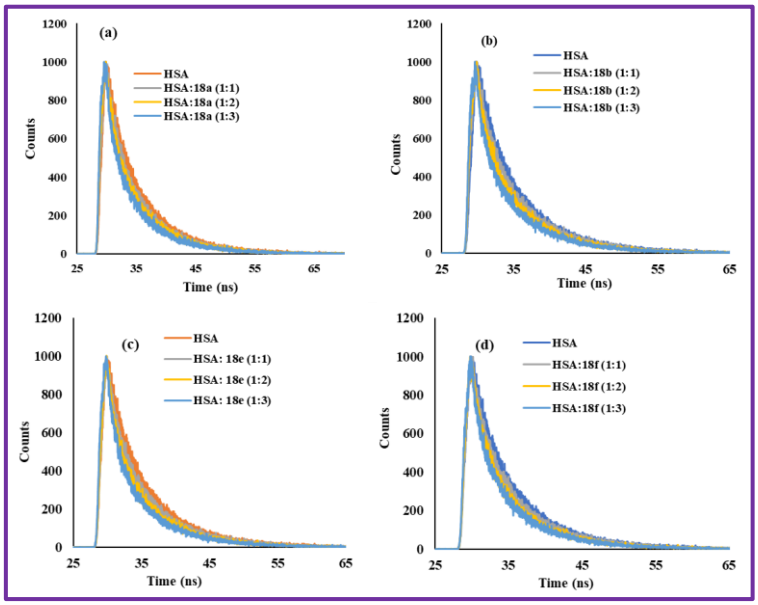

Figure 4.14: Time decay profile of HSA on progressive addition of compounds (a) **18a** (b) **18b** (c) **18e** and (d) **18f** in phosphate buffer (*p*H 7.4).

Progressive addition of compounds to a solution of HSA in phosphate buffer resulted in decrease in decay time of free HSA, disclosing the existence of dynamic quenching (**Table 4.11**). The results obtained from steady-state and time-resolved fluorescence studies observed that both types of quenching, i.e. static as well as dynamic quenching, are responsible for the interaction between HSA and compounds.

Table 4.11: Lifetime fluorescence decay of HSA on interaction with **18a, 18b, 18e** and **18f**

System	Conc.	τ_1 [ns]	τ_2 [ns]	τ_3 [ns]	α_1	α_2	α_3	τ_{av}	$\chi 2$
HSA		4.04	7.76	0.96	0.45	0.34	0.21	4.65	1.02
HSA-18a	01:01	2.89	7.24	0.45	0.35	0.39	0.27	3.95	1.03
	01:02	2.59	6.74	0.37	0.29	0.36	0.35	3.31	1.05
	01:03	2.09	6.16	0.50	0.21	0.33	0.45	2.76	1.09
HSA-18b	01:01	0.99	5.98	1.10	0.32	0.44	0.24	3.21	1.10
	01:02	2.79	6.86	0.25	0.23	0.30	0.47	2.79	1.09
	01:03	1.97	6.38	0.12	0.11	0.16	0.74	1.29	1.13
HSA-18e	01:01	3.31	6.81	0.40	0.40	0.40	0.20	4.14	1.05
	01:02	3.21	7.04	0.80	0.30	0.38	0.31	3.92	1.03
	01:03	3.01	6.70	0.69	0.23	0.31	0.46	3.08	0.98
HSA-18f	01:01	2.57	6.77	0.75	0.29	0.44	0.28	3.95	1.00
	01:02	2.11	6.34	0.47	0.28	0.37	0.35	3.10	1.07
	01:03	2.08	6.16	0.48	0.23	0.33	0.44	2.73	1.11

4.1.11e Binding interactions

The stability of complex formed between HSA and drug candidates was further evaluated with respect to binding constant K_b, which was calculated with the help of modified Stern-Volmer equation. A linear regression curve was plotted between logarithm ratio of difference between the fluorescence intensity of HSA in the absence and presence of compounds **18a, 18b, 18e**, and **18f,** and the logarithm of the concentration of the respective compound; the value of intercept was used to calculate the binding constants (K_b) (**Table 4.12**). The binding constants were found to be $12.0 \times 10^4\ M^{-1}$ (**18a**), $13.0 \times 10^4\ M^{-1}$ (**18b**), $14.2 \times 10^4\ M^{-1}$ (**18e**) and $16.3 \times 10^4\ M^{-1}$ (**18f**) which reflected the efficient binding of all the molecules with HSA. In comparison, **18f** binds more strongly with HSA than others. Further, the number of binding

sites, as calculated from the above equation, was found to be approximately 1 in all the cases, inferring that all the molecules bind to HSA specifically at one site only with binding stoichiometry 1:1.

Table 4.12: Binding constants for compounds **18a, 18b**, **18e** and **18f**

Comps.	K_b (10^4 M^{-1})	n	[a]R
18a	12.0	0.97	0.9931
18b	13.0	0.98	0.9946
18e	14.2	1.1	0.9861
18f	16.3	1.0	0.9967

Further, equation 6 was employed to calculate Gibb's free energy where R is gas constant, and T is the temperature at which the experiment was conducted and found to be -6.89 kcal mol^{-1} (**18a**), -6.94 kcal mol^{-1} (**18b**), -6.99 kcal mol^{-1} (**18e**) and -7.07 kcal mol^{-1} (**18f**) (**Table 4.13**). The negative values of Gibb's free energy manifested that all compounds interact with HSA through hydrogen bonding and van der Waals interactions.

Table 4.13 Thermodynamic parameters of HSA upon binding with compounds

T (K)	ΔG, kcal M^{-1} (18a)	ΔG, kcal M^{-1} (18b)	ΔG, kcal M^{-1} (18e)	ΔG, kcal M^{-1} (18f)
298	-6.89	-6.94	-6.99	-7.07

Thus, the results obtained from different studies for analysing the binding behaviour of HSA with active compounds concluded that all the compounds efficiently bind with HSA and can be transported to the target site easily for treatment of cancer.

4.1.12 Conclusion

In the present subchapter, we have designed a focused library of naphthalimide-triazole-coumarin conjugates by substituting different amines. These compounds were evaluated for their potential to exist as an anticancer agent against 60 human tumour cell lines, and their interactions with c-MYC G4-DNA were explored to understand the mechanism for their anticancer activities. Out of the 14 derivatives, four compounds, mainly **18a**, **18b**, **18e** and **18f**, exhibited promising results and represented broad-spectrum anticancer activity against most of the cancer cell lines with MG-MID GI_{50} values of 3.18 μM, 13.11 μM, 7.68 μM and 1.75 μM, respectively. Underlining the mechanism for their anticancer activity, the ability of these four active molecules to stabilize G4-DNA forming promoters was evaluated by studying their

interaction with c-MYC G4-DNA by various spectroscopic techniques. The results obtained from these studies pointed out that all four molecules readily bind to G4-DNA with high binding constant values. Thus, all four molecules readily stabilized the c-MYC quadruplex forming promoters, leading to the inhibition of cancer cells. The interaction studies of these compounds with HSA manifested that all four molecules readily bind to HSA with binding constants of 12.0×10^4 (**18a**), 13.0×10^4 (**18b**), 14.2×10^4 (**18e**) and 16.3×10^4 (**18f**), thus, can be delivered to the target site easily for the treatment of cancer. This work reveals that compounds **18a**, **18b**, **18e** and **18f**, with promising anticancer results and a class of G4-DNA mediated c-MYC inhibitors with excellent binding ability with HSA, can be taken further to clinical trials for developing potent anticancer agents.

4.1.13 Experimental Section

Synthesis of compound 12[151]

N-Bromosuccinimide (2.75 g, 15.55 mmol) was added portion-wise to a stirred solution of commercially available acenaphthene (2.0 g, 12.98 mmol) in DMF. The reaction mixture was stirred at room temperature for 3h and TLC was used for monitoring the reaction. On completion of the reaction, 50 ml of cold water was added, and the formed precipitates were filtered. The product was air-dried to obtain brown solid of **12** in 2.85 g; 95%; R_f 0.7 (hexane) m.pt: 52-55 °C (Lit. m.pt - 55°C)

Synthesis of compound 13[151]

To a stirred solution of 5-bromo-1,2-dihydroacenaphthylene, (**12**) (2.0 g, 8.6 mmol) in glacial acetic acid (40 ml), sodium dichromate (12.90 g, 43.2 mmol) was added in portion wise on an ice bath, and then the reaction was stirred at room temperature for 30 min followed by refluxed for 3h. On completion of the reaction, 50 ml of cold water was added, and the precipitates were filtered. The product was oven-dried at 90 ºC to obtain white solid **13** in 2.07 g; 90%; R_f 0.4 (40% chloroform in hexane) m.pt: 118-120 °C (Lit. m.pt - 117–119 °C)

Synthesis of compound 14[152]

Sodium azide (0.234 g, 3.6 mmol) was added to a stirred solution of compound **13** (0.5 g, 1.8 mmol) in DMF and water (9.5:0.5), and the reaction was stirred for 30 min at 80 ºC. The reaction was monitored by TLC, and on the completion of the reaction, 100 ml of water was added to the reaction mixture, and the formed precipitates were filtered to obtain a yellow solid **14** in 0.35g; 83%; R_f 0.4 (chloroform) m.pt: 190-192 °C (Lit. m.pt - 185 –186 °C)

Synthesis of compound 16[153]

To a stirred solution of commercially available 7-hydroxy-4-methyl-2*H*-chromen-2-one (1 g, 5.6 mmol) in DMF, propargyl bromide (0.8 g, 6.8 mmol) and potassium carbonate (1.17 g, 8.4 mmol) were added and the reaction was stirred for 6h at room temperature. The reaction was monitored by TLC, and on completion of the reaction, 80 ml water was added to the reaction mixture. The formed precipitates were filtered and oven-dried to obtain a creamish solid of **16** in 1g; 83.3%; R_f 0.5 (50% chloroform in hexane) m.pt: 133-135 °C (Lit. m.pt - 130–132 °C)

Synthesis of compound 17

CuI (0.08 g, 0.4 mmol) and DIPEA (0.12 g, 0.9 mmol) in acetonitrile were refluxed for 5 min. To the stir solution of this, compound **16** (1g, 4.6 mmol) was added, and the reaction was refluxed for 15 min. Then, compound **14** (1.1 g, 4.6 mmol) was added, and reaction was refluxed for another 3h. TLC was employed to monitor the reaction; on completion, acetonitrile evaporated under vacuum. 50 ml water was added to it, and the precipitates formed were filtered to obtain creamish white solid of **17** in 1.7 g; 80.9% R_f 0.4 (20% ethyl acetate in chloroform) m.pt: 251-253 ºC. The compound was used for further reaction without any purification.

General procedure for synthesis of compounds 18a-18n

To a stirred solution of 6-(4-(((4-methyl-2-oxo-2*H*chromen-7yl)oxy)methyl)-1*H*-1,2,3-triazol-1-yl)-1*H*,3*H*-benzo[*de*] Isochromene-1,3-dione (**17**) (150 mg, 0.3 mmol) in ethanol (20 ml) and $Zn(OAc)_2$, various substituted primary amine (1.5 mmol) was added followed by refluxing for 3-4 h. The solid residue formed was filtered and crude product was purified by column chromatography using chloroform and ethyl acetate as eluents.

2-allyl-6-(4-(((4-methyl-2-oxo-2*H*-chromen-7-yl)oxy)methyl)-1*H*-1,2,3-triazol-1-yl)-1*H*-benzo[*de*]isoquinoline-1,3(2*H*)-dione (18a):

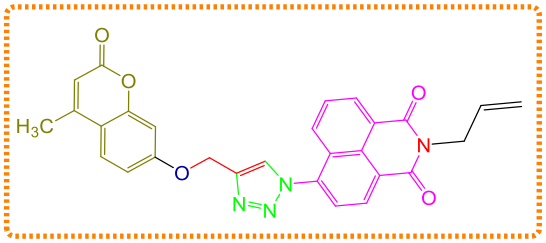

Yield:80%; colour: white; m.pt: 240-242 ºC; ^{1}H NMR ($CDCl_3$, 400 MHz): δ (ppm) 8.76 (d, *J* = 7.68 Hz, 2H, ArH), 8.27 (s, 1H, ArH), 8.22 (d, *J* = 8.48 Hz, 1H, ArH), 7.92 (m, 2H, ArH), 7.64 (d, *J* = 8.84 Hz, 1H, ArH), 7.08 (d, *J* = 8.92 Hz, 1H, ArH), 7.02 (s, 1H, ArH), 6.29 (s, 1H, CH coumarin), 6.03 – 5.93 (m, 1H, CH allyl), 5.50 (s, 2H, -OCH_2), 5.36 (d, *J* = 17.08 Hz, 1H, CH allyl), 5.26 (d, *J* = 10.32 Hz, 1H, CH allyl), 4.84 (d, *J* = 5.84 Hz, 2H, CH_2 allyl), 2.47 (s, 3H, -CH_3 coumarin); ^{13}C NMR ($CDCl_3$, 100 MHz): δ (ppm) 163.5, 163.0, 161.1, 154.8, 154.4, 137.7,

132.8, 131.5, 130.9, 129.3, 129.1, 126.4, 126.2, 124.3, 124.0, 122.8, 118.3, 114.5, 113.2, 111.9, 102.1, 61.7, 42.9, 18.9; HRMS (ESI) Calcd. for $C_{28}H_{20}N_4O_5$ $[M+H]^+$ 493.1512 Found $[M+H]^+$ 493.1510.

2-butyl-6-(4-(((4-methyl-2-oxo-2*H*-chromen-7-yl)oxy)methyl)-1*H*-1,2,3-triazol-1-yl)-1*H*-benzo[de]isoquinoline-1,3(2*H*)-dione (18b)

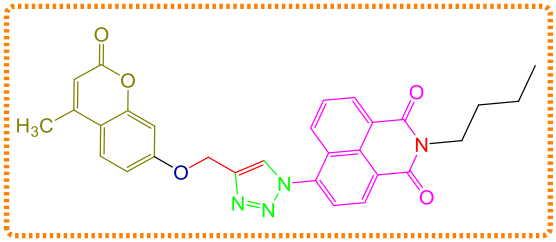

Yield: 83%; colour: cream; m.pt: 245-247 ºC; ^{1}H NMR ($CDCl_3$, 400 MHz): δ (ppm) 8.70 (d, *J* = 7.80 Hz, 2H, ArH), 8.23 (d, *J* = 8.6 Hz, 1H, ArH), 8.17 (s, 1H, ArH), 7.86 – 7.82 (m, 2H, ArH), 7.55 (d, *J* = 8.72 Hz, 1H, ArH), 7.02 – 6.97 (m, 2H, ArH), 6.15 (s, 1H, CH-coumarin), 5.43 (s, 2H, -OCH_2), 4.21 – 4.17 (m, 2H, -NCH_3 butyl), 2.40 (s, 3H, -CH_3 coumarin), 1.76 – 1.68 (m, 2H, CH_2 butyl), 1.49 – 1.40 (m, 2H, CH_2 butyl), 0.99 (t, *J* = 7.36 Hz, 3H, CH_3 butyl), ^{13}C NMR ($CDCl_3$, 100 MHz): δ (ppm) 163.6, 163.1, 161.1, 161.0, 155.2, 152.5, 143.9, 137.9, 132.3, 130.6, 129.2, 129.1, 128.8, 126.5, 125.9, 125.4, 124.3, 123.7, 123.1, 114.3, 112.5, 102.1, 62.2, 40.6, 30.2, 20.4, 18.3, 13.9; HRMS (ESI) Calcd. for $C_{29}H_{24}N_4O_5$ $[M+H]^+$ 509.1825 Found $[M+H]^+$ 509.1825.

2-ethyl-6-(4-(((4-methyl-2-oxo-2*H*-chromen-7-yl)oxy)methyl)-1*H*-1,2,3-triazol-1-yl)-1*H*-benzo[*de*]isoquinoline-1,3(2*H*)-dione (18c)

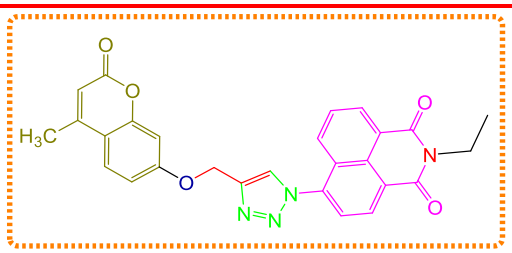

Yield: 78%; colour: yellowish white; m.pt: 250-251 ºC; ^{1}H NMR ($CDCl_3$, 400 MHz): δ (ppm) 8.75 (d, *J* = 7.76 Hz, 2H, ArH), 8.26 (s, 1H, ArH), 8.20 (d, *J* = 8.56 Hz, 1H, ArH), 7.91 – 7.87 (m, 2H, ArH), 7.64 (d, *J* = 8.80 Hz, 1H, ArH), 7.08 (d, *J* = 8.80 Hz, 1H, ArH), 7.02 (s, 1H, ArH), 6.29 (s, 1H, CH-coumarin), 5.50 (s, 2H, -OCH_2), 4.30 (q, *J* = 7.0 Hz, 2H, -NCH_2 ethyl), 2.47 (s, 3H, -CH_3 coumarin), 1.37 (t, *J* = 7.04 Hz, 3H, CH_3 ethyl), ^{13}C NMR ($CDCl_3$, 100 MHz): δ (ppm) 163.6, 163.1, 161.1, 161.0, 155.2, 152.5, 143.9, 137.9, 132.3, 130.6, 129.2, 129.1, 128.8, 126.5, 125.9, 125.4, 124.3, 123.7, 123.1, 114.3, 112.5, 102.1, 62.2, 40.6, 30.2, 20.4, 18.3, 13.9; HRMS (ESI) Calcd. for $C_{27}H_{20}N_4O_5$ $[M+H]^+$ 481.1512 Found $[M+H]^+$ 481.1508.

2-benzyl-6-(4-(((4-methyl-2-oxo-2*H*-chromen-7-yl)oxy)methyl)-1*H*-1,2,3-triazol-1-yl)-1*H*-benzo[*de*]isoquinoline-1,3(2*H*)-dione (18d)

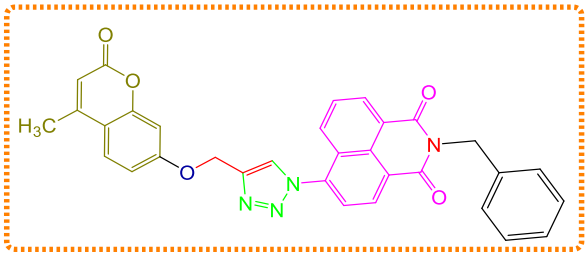

Yield: 72%; colour: creamish white; m.pt: 244-246 ºC; ^{1}H NMR ($CDCl_3$, 400 MHz): δ (ppm) 8.78 (d, *J* = 7.88 Hz, 2H, ArH), 8.29 (s, 1H, ArH), 8.22 (d, *J* = 8.52 Hz, 1H, ArH), 7.94 – 7.90 (m, 2H, ArH), 7.67 (d, *J* = 8.42 Hz, 1H, ArH), 7.52 (d, *J* = 8.48 Hz, 2H, ArH), 7.34 – 7.26 (m, 3H, ArH), 7.11 (dd, ^{1}J = 2.36 Hz, ^{3}J = 8.80 Hz, 1H, ArH), 7.04 (s, 1H, ArH), 6.34 (s, 1H, CH-coumarin), 5.52 (s, 2H, -OCH_2), 5.41 (s, 2H, CH_2 benzyl), 2.50 (s, 3H, -CH_3 coumarin); ^{13}C NMR ($CDCl_3$, 100 MHz): δ (ppm) 164.2, 163.6, 161.2, 156.1, 154.5, 137.5, 136.2, 133.4, 131.3, 129.4, 129.1, 128.3, 128.0, 126.4, 126.3, 126.1, 124.4, 124.3, 122.7, 114.6, 113.7, 113.1, 111.4, 102.1, 61.2, 44.3, 18.9; HRMS (ESI) Calcd. for $C_{32}H_{22}N_4O_5$ $[M+H]^+$ 543.1668 Found $[M+H]^+$ 543.1666.

2-(2-(diethylamino)ethyl)-6-(4-(((4-methyl-2-oxo-2*H*-chromen-7-yl)oxy)methyl)-1*H*-1,2,3-triazol-1-yl)-1*H*-benzo[*de*]isoquinoline-1,3(2*H*)-dione (18e)

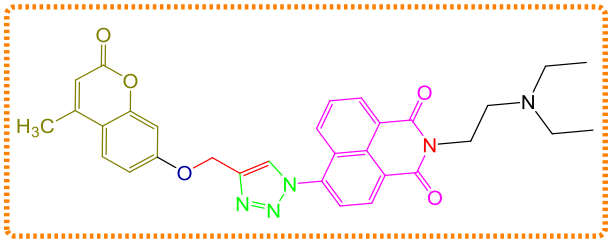

Yield: 84%; colour: yellow; m.pt: 231-233 ºC; ^{1}H NMR ($CDCl_3$, 400 MHz): δ (ppm) 8.67 (d, *J* = 7.72 Hz, 2H, ArH), 8.32 (s, 1H, ArH), 8.19 (d, *J* = 8.48 Hz, 1H, ArH), 7.88 (t, *J* = 7.92 Hz, 2H, ArH), 7.63 (d, *J* = 8.84 Hz, 1H, ArH), 7.08 (dd, ^{2}J = 2.41 Hz, ^{3}J = 8.84 Hz, 1H, ArH), 7.00 (d, *J* = 2.36 Hz, 1H, ArH), 6.25 (s, 1H, CH-coumarin), 5.49 (s, 2H, -OCH_2), 4.61 (t, *J* = 5.92 Hz, 2H, CH_2 diethyl), 3.62 – 3.57 (m, 2H, CH_2 diethyl), 3.52 – 3.37 (m, 4H, 2*CH_2 diethyl), 2.45 (s, 3H, -CH_3 coumarin), 1.40 (t, *J* = 7.24 Hz, 6H, 2*CH_3 diethyl); ^{13}C NMR ($CDCl_3$, 100 MHz): δ (ppm) 164.3, 163.7, 161.2, 155.5, 154.6, 138.0, 133.3, 131.4, 129.9, 129.2, 128.9, 126.4, 126.3, 124.3, 123.5, 122.0, 114.5, 113.6, 111.5, 102.1, 61.3, 50.3, 47.2, 34.9, 18.9, 8.22; HRMS (ESI) Calcd. for $C_{31}H_{29}N_5O_5$ $[M+H]^+$ 552.2247 Found $[M+H]^+$ 552.2275.

2-(2-(dimethylamino)ethyl)-6-(4-(((4-methyl-2-oxo-2*H*-chromen-7-yl)oxy)methyl)-1*H*-1,2,3-triazol-1-yl)-1*H*-benzo[*de*]isoquinoline-1,3(2*H*)-dione (18f)

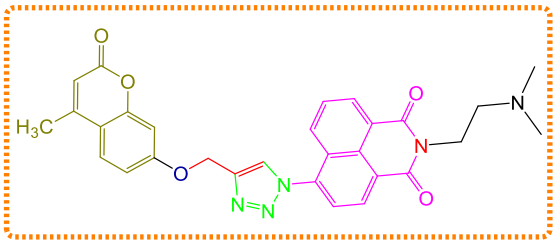

Yield: 86%; colour; light yellow; m.pt: 254-256 ºC; ^{1}H NMR ($CDCl_3$, 400 MHz): δ (ppm) 8.66 (d, *J* = 7.81 Hz, 2H, ArH), 8.31 (s, 1H, ArH), 8.19 (d, *J* = 9.44 Hz, 1H, ArH), 7.89 (t, *J* = 7.76 Hz, 2H, ArH), 7.63 (d, *J* = 8.92 Hz, 1H, ArH), 7.09 (dd, ^{2}J = 2.41 Hz, ^{3}J = 8.84 Hz, 1H, ArH), 7.01 (s, 1H, ArH), 6.26 (s, 1H, CH-coumarin), 5.49 (s, 2H, -OCH_2), 4.63 – 4.60 (m, 2H, CH_2 dimethyl), 3.66 – 3.60 (m, 2H, CH_2 dimethyl), 3.11 (s, 3H, CH_3 dimethyl), 3.10 (s, 3H, CH_3 dimethyl) 2.46 (s, 3H, -CH_3 coumarin); ^{13}C NMR ($CDCl_3$, 100 MHz): δ (ppm) 164.5, 164.4, 164.0, 161.3, 155.6, 154.6, 143.6, 138.0, 133.3, 131.5, 129.9, 129.3, 128.9, 126.3, 124.3, 123.5, 121.9, 116.2, 114.5, 113.6, 113.3, 111.5, 102.1, 61.3, 57.5, 44.4, 35.5, 18.9; HRMS (ESI) Calcd. for $C_{29}H_{25}N_5O_5$ $[M+H]^+$ 524.1934 Found $[M+H]^+$ 524.1936.

2-(2-hydroxyethyl)-6-(4-(((4-methyl-2-oxo-2*H*-chromen-7-yl)oxy)methyl)-1*H*-1,2,3-triazol-1-yl)-1*H*-benzo[*de*]isoquinoline-1,3(2*H*)-dione (18g)

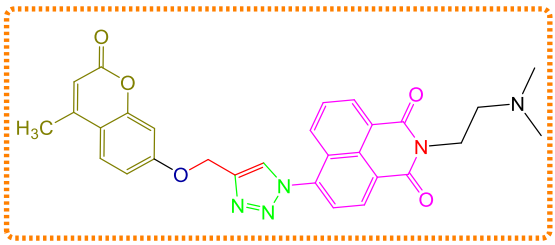

Yield: 76%; colour; whitish yellow; m.pt: 243-245 ºC; ^{1}H NMR ($CDCl_3$, 400 MHz): δ (ppm) 8.78 (t, *J* = 6.68 Hz, 2H, ArH), 8.30 (s, 1H, ArH), 8.24 (d, *J* = 4.16 Hz, 1H, ArH), 7.94 (s, 2H, ArH), 7.68 (d, *J* = 8.76 Hz, 1H, ArH), 7.11 (d, *J* = 8.68 Hz, 1H, ArH), 7.04 (s, 1H, ArH), 6.34 (s, 1H, CH-coumarin), 5.52 (s, 2H, -OCH_2), 4.76 (t, *J* = 4.88 Hz, 1H, CH_2 ethanol), 4.67 (t, *J* = 8.76 Hz, 1H, CH_2 ethanol), 4.55 (br(s), 1H, CH_2 ethanol), 4.16 (br(s), 1H, CH_2 ethanol), 2.50 (s, 3H, -CH_3 coumarin); ^{13}C NMR ($CDCl_3$ + TFA, 100 MHz): δ (ppm) 164.1, 163.6, 161.2, 156.1, 154.5, 137.8, 133.4, 131.4, 129.7, 129.5, 129.2, 126.4, 124.3, 124.0, 122.3, 116.0, 114.7, 113.8, 111.5, 102.1, 65.0, 61.3, 38.9, 18.9; HRMS (ESI) Calcd. for $C_{27}H_{20}N_4O_6$ $[M+H]^+$ 497.1461 Found $[M+H]^+$ 497.1451.

2-cyclohexyl-6-(4-(((4-methyl-2-oxo-2*H*-chromen-7-yl)oxy)methyl)-1*H*-1,2,3-triazol-1-yl)-1*H*-benzo[*de*]isoquinoline-1,3(2*H*)-dione (18h)

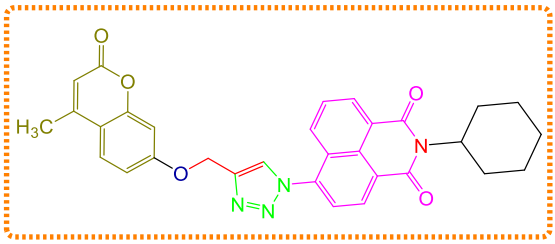

Yield: 70%; colour: brown; m.pt: 258-260 ºC; ^{1}H NMR ($CDCl_3$, 400 MHz): δ (ppm) 8.72 (d, *J* = 7.84 Hz, 2H, ArH), 8.27 (s, 1H, ArH), 8.18 (d, *J* = 8.24 Hz, 1H, ArH), 7.90 – 7.86 (m, 2H, ArH), 7.66 (d, *J* = 8.84 Hz, 1H, ArH), 7.10 (dd, *J* = 2.36 Hz, 8.80 Hz, 1H, ArH), 7.03 (d, *J* = 2.44 Hz, 1H, ArH), 6.32 (s, 1H, CH coumarin), 5.52 (s, 2H, -OCH_2), 5.05 – 4.97 (m, 1H, -N-CH cyclohex), 2.48 (s, 3H, CH_3 coumarin), 1.93 – 1.89 (m, 4H, 2* CH_2 cyclohex), 1.78 – 1.75 (m, 4H, 2* CH_2 cyclohex), 1.46 – 1.43 (m, 2H, CH_2 cyclohex); ^{13}C NMR ($CDCl_3$, 100 MHz): δ (ppm) 164.1, 163.6, 162.7, 161.1, 154.9, 154.0, 143.8, 137.8, 132.4, 130.6, 129.0, 128.7, 126.2, 126.1, 125.7, 125.0, 123.9, 123.6, 114.4, 113.0, 112.0, 102.1, 61.8, 54.4, 29.1, 26.5, 25.4, 24.1, 18.8; HRMS (ESI) Calcd. for $C_{31}H_{26}N_4O_5$ $[M+H]^+$ 535.1923 Found $[M+H]^+$ 535.1968.

6-(4-(((4-methyl-2-oxo-2*H*-chromen-7-yl)oxy)methyl)-1*H*-1,2,3-triazol-1-yl)-2-(2-morpholinoethyl)-1*H*-benzo[*de*]isoquinoline-1,3(2*H*)-dione (18i)

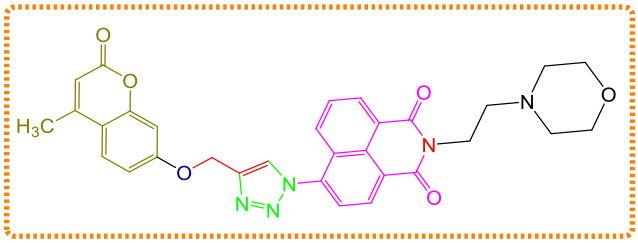

Yield: 80%; colour: white; m.pt: 230-232 ºC; ^{1}H NMR ($CDCl_3$+TFA, (0.7 : 0.05) 400 MHz): δ (ppm) 8.67 (d, *J* = 7.60 Hz, 2H, ArH), 8.28 (s, 1H, ArH), 8.20 (d, *J* = 8.48 Hz, 1H, ArH), 7.89 – 7.85 (m, 2H, ArH), 7.62 (d, *J* = 8.76 Hz, 1H, ArH), 7.08 (dd, ^{2}J = 2.36 Hz, ^{3}J = 8.68 Hz, 1H, ArH), 7.02 (d, *J* = 8.02 Hz, 1H, ArH), 6.25 (s, 1H, CH-coumarin), 5.48 (s, 2H, -OCH_2), 4.64 (br(s), 2H, CH_2 ethyl), 4.09 (t, *J* = 10.36 Hz, 4H, 2*CH_2 morph), 3.91 (t, *J* = 12.32 Hz, 2H, CH_2 ethyl), 3.67 (br(s), 2H, CH_2 morph), 3.50 (br(s), 2H, -CH_2 morph), 2.45 (s, 3H, -CH_3 coumarin); ^{13}C NMR ($CDCl_3$+TFA, 100 MHz); δ (ppm) 170.6, 161.2, 155.3, 154.6, 138.1, 133.4, 131.5, 129.9, 129.3, 126.5, 126.3, 124.3, 123.5, 121.9, 116.1, 114.5, 113.6, 113.3, 111.6, 102.1, 63.7, 61.4, 56.3, 53.2, 34.4, 18.9; HRMS (ESI) Calcd. for $C_{31}H_{27}N_5O_6$ $[M+H]^+$ 566.2040 Found $[M+H]^+$ 566.2043.

6-(4-(((4-methyl-2-oxo-2*H*-chromen-7-yl)oxy)methyl)-1*H*-1,2,3-triazol-1-yl)-1*H*-benzo[*de*]isoquinoline-1,3(2*H*)-dione (18j)

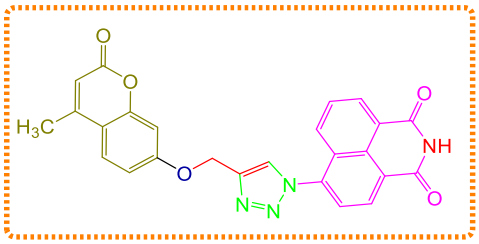

Yield: 65%; colour: brownish yellow; m.pt: 235-237 ºC; ^{1}H NMR ($CDCl_3$+TFA (0.7:0.05 ml), 400 MHz): δ (ppm) 10.4 (s, 1H, NH), 8.82 – 8.79 (m, 2H, ArH), 8.36 – 8.30 (m, 2H, ArH), 8.02 – 7.96 (m, 2H, ArH), 7.69 (d, *J* = 8.84 Hz, 1H, ArH), 7.12 (d, *J* = 8.84 Hz, 1H, ArH), 7.05 (s, 1H, ArH), 6.36 (s, 1H, CH- coumarin), 5.53 (s, 2H, OCH_2), 2.51 (s, 3H, -CH_3 coumarin); ^{13}C NMR ($CDCl_3$, 100 MHz): δ (ppm) 161.2, 160.2, 155.9, 154.5, 143.9, 135.1, 133.1, 130.8, 129.8, 126.4, 125.9, 124.4, 119.1, 118.8, 116.0, 114.6, 113.7, 113.1, 111.5, 110.3, 102.0, 61.3, 18.9; HRMS (ESI) Calcd. for $C_{25}H_{16}N_4O_5$ $[M+H]^+$ 453.1199 Found $[M+H]^+$ 453.1187.

2-(3-aminopropyl)-6-(4-(((4-methyl-2-oxo-2H-chromen-7-yl)oxy)methyl)-1H-1,2,3-triazol-1-yl)-1H-benzo[de]isoquinoline-1,3(2H)-dione (18k)

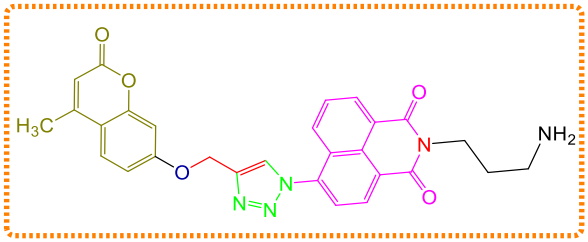

Yield: 68% colour: brown yellow; m.pt: 252-254 ºC; ^{1}H NMR ($CDCl_3$, 400 MHz): δ (ppm) 8.90 – 8.01 (m, 2H, ArH), 8.42 (q, *J* = 8.68 Hz, 2H, ArH), 8.06 – 8.01 (m, 2H, ArH), 7.67 (d, *J* = 9.04 Hz, 1H, ArH), 7.10 (dd, *J* = 2.60 Hz, 8.84 Hz, 1H, ArH), 7.02 (d, *J* = 2.44 Hz, 1H, ArH), 6.33 (s, 1H, -CH coumarin), 5.50 (s, 2H, -OCH_2), 4.37 (br(s), 2H, N-CH_2 propyl), 3.93 (br(s), 2H, N-CH_2 propyly), 2.86 (s, 3H, -CH_3 coumarin), 2.41(br(s), 2H, CH_2 propyl); HRMS (ESI) Calcd. for $C_{25}H_{16}N_4O_5$ $[M-H]^-$ 508.9482 Found $[M-H]^-$ 508.9474.

2-amino-6-(4-(((4-methyl-2-oxo-2H-chromen-7-yl)oxy)methyl)-1H-1,2,3-triazol-1-yl)-1H-benzo[de]isoquinoline-1,3(2H)-dione (18l)

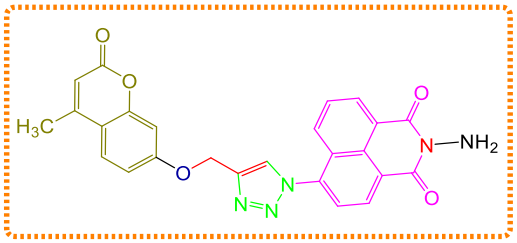

Yield: 70%; colour: Reddish yellow; m.pt: 243-245 ºC; ^{1}H NMR ($CDCl_3$, 400 MHz): δ (ppm) 11.09 (s, 2H, NH_2), 8.82 – 8.79 (m, 2H, ArH), 8.32 – 8.29 (m, 2H, ArH), 7.99 – 7.95 (m, 2H, ArH), 7.69 (d, *J* = 8.84 Hz, 1H, ArH), 7.12 (dd, ^{2}J = 2.52 Hz, ^{3}J = 8.84 Hz, 1H, ArH), 7.05 (s, 1H, ArH), 6.36 (s, 1H, CH-coumarin), 5.53 (s, 2H, OCH_2), 2.51 (s, 3H, -CH_3 coumarin); ^{13}C NMR ($CDCl_3$, 100 MHz),

^{13}C NMR ($CDCl_3$, 100 MHz): δ (ppm) 164.9, 161.2, 156.1, 154.2, 143.8, 134.3, 133.5, 132.4, 131.5, 130.6, 129.6, 126.34, 126.1, 124.4, 118.8, 115.9, 114.7, 113.8, 113.1, 111.4, 110.2, 102.0, 61.3, 18.9; HRMS (ESI) Calcd. for $C_{25}H_{17}N_5O_5$ $[M+H]^+$ 468.1308 Found $[M+H]^+$ 468.1301.

2-isopropyl-6-(4-(((4-methyl-2-oxo-2H-chromen-7-yl)oxy)methyl)-1H-1,2,3-triazol-1-yl)-1H-benzo[de]isoquinoline-1,3(2H)-dione (18m)

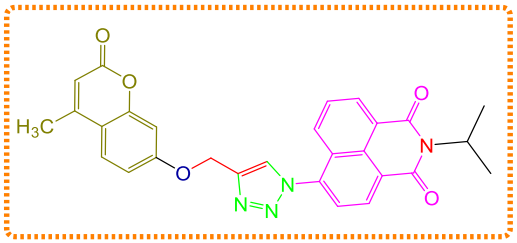

Yield: 75%; colour: white; m.pt: 239-242 ºC; ^{1}H NMR ($CDCl_3$+TFA, 400 MHz): δ (ppm) 8.71 (d, *J* = 7.64 Hz, 2H, ArH), 8.24 (s, 1H, ArH), 8.19 (d, *J* = 8.60 Hz, 1H, ArH), 7.89 – 7.85 (m, 2H, ArH), 7.63 (d, *J* = 8.80 Hz, 1H, ArH), 7.07 (d, *J* = 8.76 Hz, 1H, ArH), 7.02 (d, *J* = 2.48 Hz, 1H, ArH), 6.28 (s, 1H, CH-coumarin), 5.49 (s, 2H, -OCH_2), 5.46 – 5.39 (m, 1H, CH isopropyl), 2.46 (s, 3H, CH_3 coumarin), 1.62 (d, *J* = 6.92 Hz, 2* CH_3 isopropyl); ^{13}C NMR ($CDCl_3$+TFA, 100 MHz); δ (ppm) 164.2, 163.6, 161.6, 154.7, 143.7, 137.2, 132.6, 130.7, 129.2, 129.1, 128.8, 126.2, 125.8, 125.0, 124.0, 123.5, 114.5, 113.5, 111.9, 102.1, 61.6, 46.1, 19.7, 18.9; HRMS (ESI) Calcd. for $C_{28}H_{22}N_4O_5$ $[M+H]^+$ 495.1668 Found $[M+H]^+$ 495.1669.

2-methyl-6-(4-(((4-methyl-2-oxo-2*H*-chromen-7-yl)oxy)methyl)-1*H*-1,2,3-triazol-1-yl)-1*H*-benzo[*de*]isoquinoline-1,3(2*H*)-dione (18n)

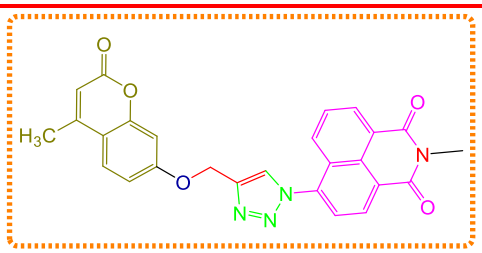

Yield: 85%; colour: creamish; m.pt: 253-255 ºC; ^{1}H NMR ($CDCl_3$+TFA, 400 MHz): δ (ppm) 8.80 (dd, *J* = 4.56, 11.68 Hz, 2H, ArH), 8.34 (s, 1H, ArH), 8.24 (d, *J* = 8.48 Hz, 1H, ArH), 7.96 (t, *J* = 7.80 Hz, 2H, ArH), 7.69 (d, *J* = 8.80 Hz, 1H, ArH), 7.12 (d, *J* = 8.88 Hz, 1H, ArH), 7.04 (s, 1H, ArH), 6.35 (s, 1H, -CH coumarin), 5.53 (s, 2H, ArH), 3.62 (s, 3H, -NCH_3 methyl), 2.51 (s, 3H, CH_3 coumarin); ^{13}C NMR ($CDCl_3$, 100 MHz): δ (ppm) 164.9, 164.3, 161.3, 156.8, 154.4, 143.4, 137.6, 133.6, 131.5, 129.6, 128.9, 126.5, 126.2, 124.4, 124.1, 122.3, 118.7, 115.9, 114.7, 114.0, 113.0, 111.2, 110.2, 102.0, 61.1, 27.8, 18.9; HRMS (ESI) Calcd. for $C_{26}H_{18}N_4O_5$ $[M+H]^+$ 467.1355 Found $[M+H]^+$ 467.1324.

Sub Chapter 4.2

Naphthalimide-Coumarin hybrids with alkyl chain linker as a potent antibacterial agent

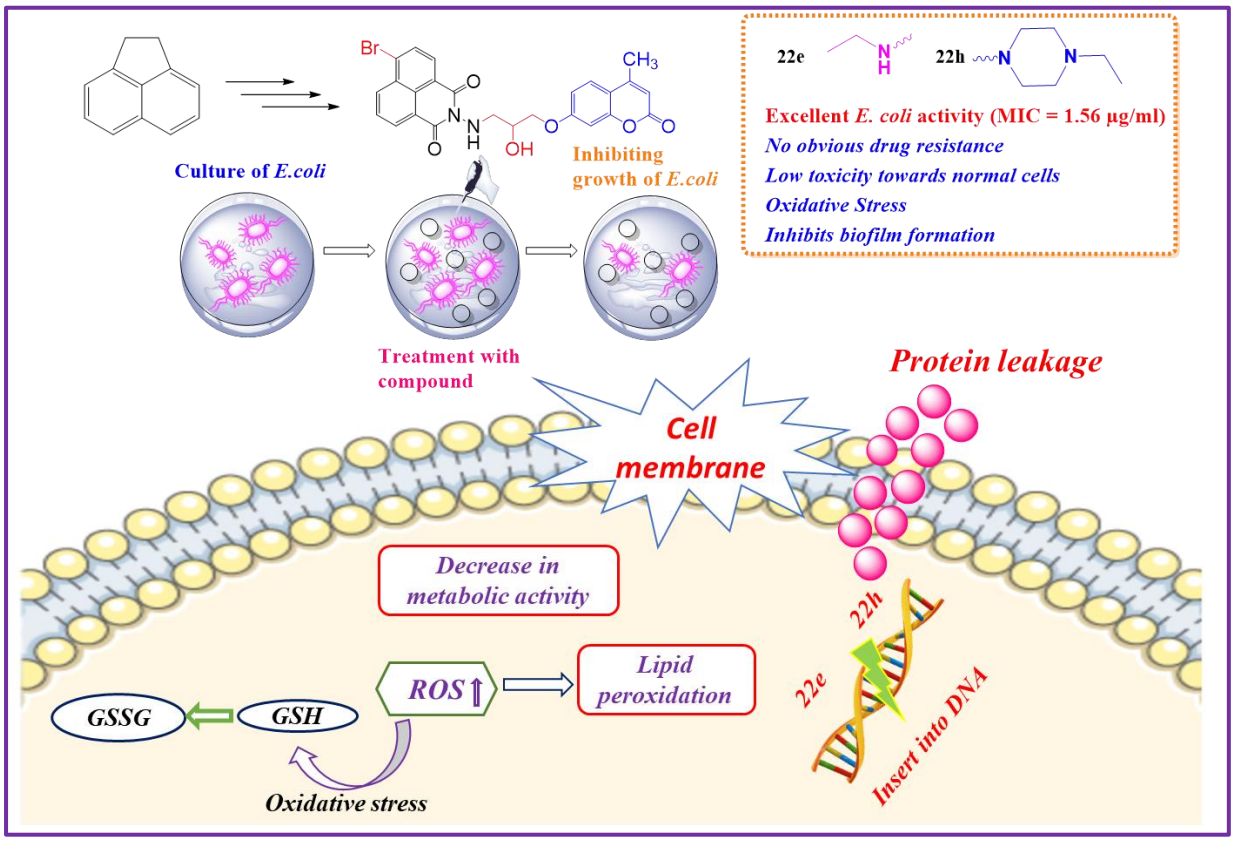

4.2.1 Introduction

After cancer, infections generated by bacterial pathogens serve as the second-leading cause of death and major health challenges across the world, thus posing significant health issues among people.[154] The crucial way to kill bacterial pathogens that cause illness is achieved with the help of antibiotics, but overuse and abuse of antibiotics have limited their therapeutic values for treating deadly infectious diseases, leading to the development of drug resistance to marketed drugs.[155] Hence, the development of drug resistance is a critical medical issue that causes mortality and morbidity.[156] The sensitivity of the drug is lost due to the formation of biofilm by bacteria, which is the main cause of drug resistance, resulting in periodic infections of living organisms.[157] Biofilm is formed in bacteria surrounded by matrix of extracellular polymeric substances that contain extracellular protein (EPs), exopolysaccharides (EPSs), and extracellular DNA (eDNA), which play crucial role in assisting the formation of biofilm and development of drug resistance. EPs strengthen the biofilm formation and stability, EPSs inhibit the host immune responses and converse antibiotic resistance to pathogens.[158] The biofilm network acts as a defensive barrier protecting bacteria from antibiotics, thus making bacteria survive in various environmental stresses. Studies indicated that the dosage of drugs required to kill bacterial cells with biofilm is 10 to 1000 times more than that needed to eliminate plankton-bacteria.[159] Moreover, there are various biofilm-related infections that are difficult to treat and begin as a result of biofilm origination on medical devices as well as in human body.[160] The capability of bacteria to construct biofilm on the surface of abiotic and biotic sources is a major key factor in the development of antibiotic resistance. Mostly, the six superbugs ESKAPE pathogens (*Escherichia coli*, *Staphylococcus aureus*, *Klebsiella pneumonia*, *Acinetobacter baumannii*, *Pseudomonas aeruginosa*, and *Enterobacter species)* are responsible for deadly infectious diseases, posing a serious threat to public health due to their ability to enhance the mortality rate.[161] Out of all pathogens accountable for deadly diseases, treatment of infections caused by E. coli persists a major challenge as it triggers bloodstream infections and hospital-acquired urinary tract, out of which, most of these have become resistant to various marketed drugs such as carbapenems, tigecycline, aminoglycosides, and fluoroquinolones.[162] Moreover, E. coli requires only a few or 10 cells to infect humans and cause serious diseases, which remain untreatable by present antibiotics. The presence of an outer membrane on E. coli serves as a natural hurdle to antibiotics, preventing them from impeding the bacterial cells.[163] E. coli is a contributing agent of surgical site infections, burn injury infections, neonatal omphatasis, necrotizing fasciitis, and cellulitis

localized to lower or upper limbs. Despite various efforts to build new antibacterial agents, no new class of antibiotics has been approved for treating bacterial infections caused by gram-negative bacteria over the past 50 years.[164] Hence, there is a vital need to develop new antibacterial agents with multitargeting potential to combat the awful drug resistance and treatment of bacterial infections by E. coli.

4.2.2 Designing of molecule

In recent years, heterocyclic moieties have gained significant attention in medicinal chemistry in the development of new antibacterial agents with increased therapeutic values due to their ability to bind with various biological targets. Many of the drugs approved by the FDA contain heterocyclic moieties in their core structure.[165] Among different heterocycles moieties, coumarin, and naphthalimide have achieved significant interest in building new antibacterial agents. Numerous reports are available on naphthalimide and coumarin as antibacterial agents with other heterocyclic moieties, but a hybrid of coumarin and naphthalimide with their antibacterial activities is rarely explored and has not received much attention. The design of target molecules (**Figure 4.15**) is based on the following considerations:

- ✓ Coumarin is a naturally occurring heterocyclic moiety found in various plants, foods, and natural species and has been produced by chemists. Coumarin exerts its antibacterial potential by suppressing the key enzyme of the biosynthesis pathway of fatty acids. These remarkable properties make it an important pharmacophore in the field of medicinal chemistry. Many coumarin-based antibiotics such as chlorobiocin, novobiocin, and coumerycin A1 have been used successfully in clinics.[166] Hence, coumarin is considered as a novel scaffold for building new antibacterial agents.
- ✓ Alcohol is widely used for sterilization and disinfection due to its ability to penetrate the membrane and disrupt protein. Specifically, amino alcohols exhibit excellent antibacterial properties and is found in many drug candidates as the presence of OH group increases the water solubility of molecules.[167]
- ✓ Naphthalimide is well-explored for its anticancer potential, but in recent times, it has been widely used in building antibacterial agents as its hydrophobic nature, makes it feasible to impede into phospholipid bilayer of the bacterial membrane, leading to leakage of cytoplasmic contents and bacterial cell death. Naphthalimide is known to bind with DNA and hence helps in building DNA-targeted antibacterial agents. Moreover, naphthalimide serves as the crucial backbone for the development of membrane-targeting antibacterial agents with the potential to combat awful drug resistance.[32-33]

Coumarin appended with a 2-hydroxy amino side chain is reported as an antibacterial agent but having the limitation of low MIC value > 200 µg/ml against tested strains.[168] Considering the above-mentioned factors and prevailing problems, we have modified the coumarin linked with amino alcohol by introducing naphthalimide in its structure and further functionalized the precursor with various amines in order to explore the effect on the antibacterial activity of coumarin. All the synthesized compounds were evaluated for their antibacterial activity against gram-positive and gram-negative bacterial strains. The active drug candidates were further explored for their mode of action against E. coli via biofilm inhibition, auto-aggregation, loss in EPS content, membrane disruption, metabolic inactivation, protein leakage, oxidative damage, and lipid peroxidation assay. Moreover, spectroscopic techniques were employed to examine the interactions of these compounds with DNA and HSA.

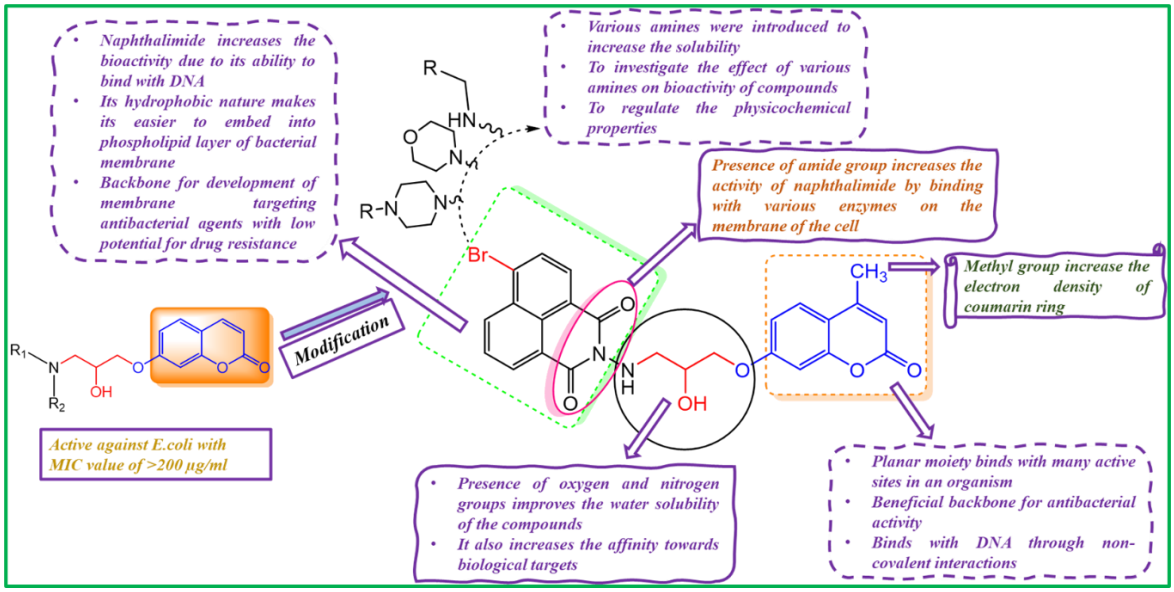

Figure 4.15 Designing of naphthalimide-coumarins as potent antibacterial agents

4.2.3 Chemistry

The pathway followed for the synthesis of designed molecules is represented in **Scheme 4.2**. Acenaphthene (**1**) was brominated at room temperature with *N*-bromosuccinimide in DMF to afford compound **12** in 90% yield, which was oxidized further with sodium dichromate in acetic acid at refluxing temperature to get compound **13** in 93% yield. Compound **13** underwent nucleophilic addition reaction with hydrazine hydrate followed by elimination of water to afford compound **19** in 87% yield. On the other hand, commercially available 7-hydroxy-4-methyl coumarin (**15**) was reacted with excess of epichlorohydrin in the presence of potassium carbonate to afford **20**. Compound **20** was reacted with **19** in ethanol at refluxing temperature

where ring opening of the epoxy ring took place in the presence of free NH_2 group to get compound **21**. The precursor **21** was reacted with various secondary amines in ethanol and primary amines in DMF and potassium carbonate to prepare compounds **22a-22o** in order to evaluate the effect of various substitutions on bioactivity of the compounds. The prepared compounds were characterised by ^{1}H NMR, ^{13}C NMR and HRMS. The molecules were synthesized in good yields ranging from 70% to 90%.

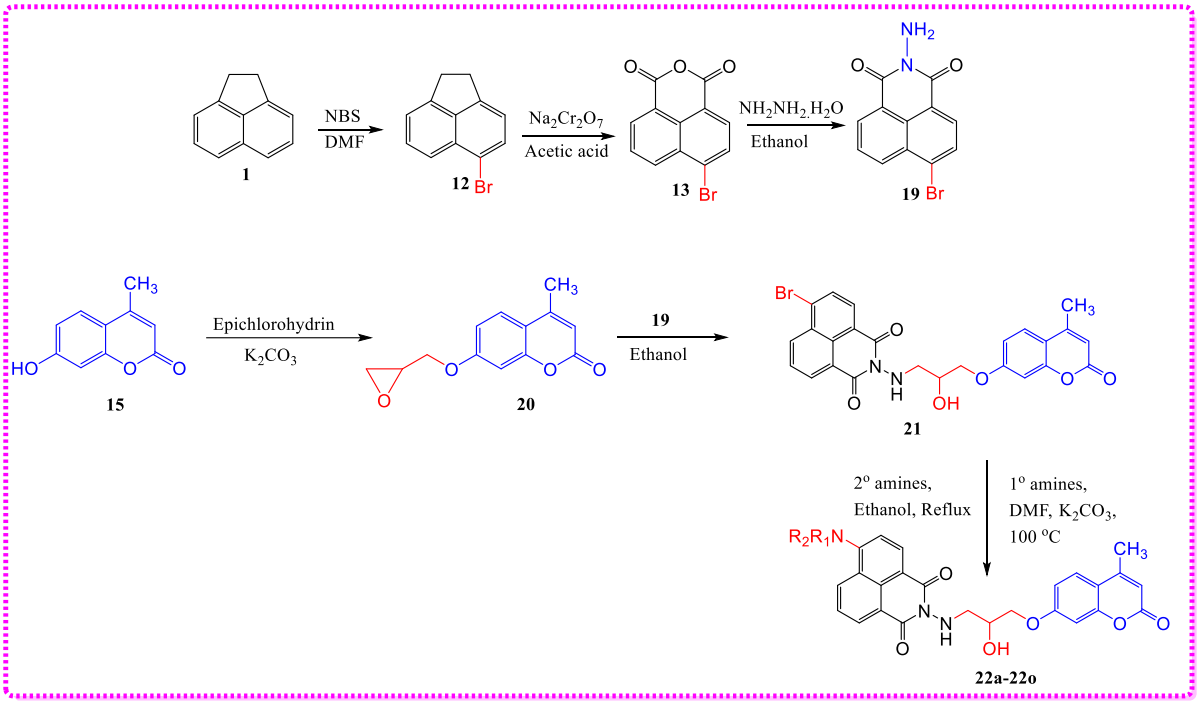

Scheme 4.2: Synthesis of 2-((2-hydroxy-3-((4-methyl-2-oxo-2*H*-chromen-7-yl)oxy)propyl)amino)-6-(substituted)-1*H*-benzo[*de*]isoquinoline-1,3(2*H*)-dione

4.2.4. Quantum chemical studies

The significant pharmacokinetic properties and area feasibly constructing crucial interaction with target molecules are predicted with the help of quantum chemical studies. The interactions between the molecule and the target site are governed by FOMO orbitals, and the energy gap between HOMO and LUMO helps to formulate the bioactivity of the compounds.[123] Most of the compounds exhibited a lower energy gap while compounds **22e** and **22h** possessed lowest energy gap of 3.389 and 3.314 eV, respectively (**Table 4.14)**, manifesting that these compounds could exert the best bioactivity among all the synthesized compounds. The HOMO of **22e** is fastened on the coumarin ring, whereas the LUMO is located on naphthalimide ring, disclosing that coumarin reacts with positively charged biological ions through electrostatic interactions, whereas naphthalimide core interacts with negatively charged residues. In case of **22h,** both HOMO and LUMO are fastened on naphthalimide ring, inferring that only

naphthalimide ring interacts with negative and positively charged ions, indicating the importance of naphthalimide ring for bioactivity. It is well reported that upon illuminating, some drugs transit from ground to excited state, leading to damage to the biont. As for **22e** and **22h,** the energy gaps did not lie in the phototoxic range (ΔE = 7.2 ± 0.4 eV), indicating that both compounds are unable to induce phototoxicity.[34]

Table 4.14: Atomic orbital HOMO-LUMO compositions of compounds **22a-22o**

Compound	HOMO (eV)	LUMO (eV)	ΔE (eV)
22a	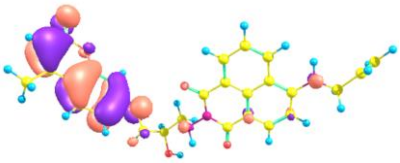	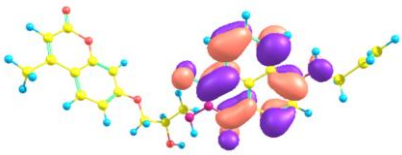	3.492
22b	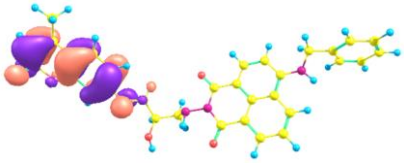	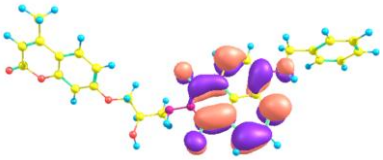	4.430
22c		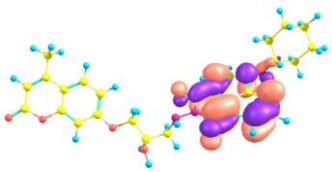	4.398
22d	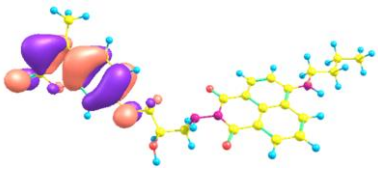	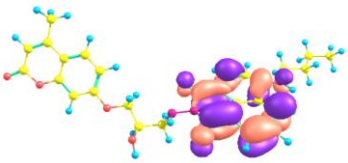	4.369
22e	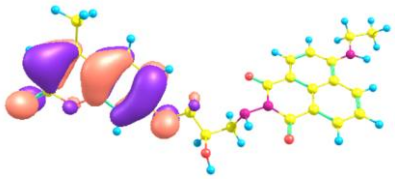	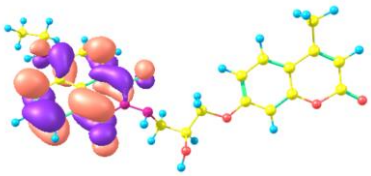	3.389
22f	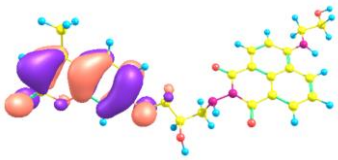	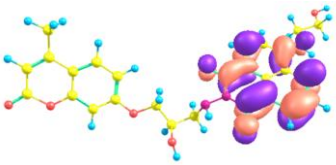	3.472
22g	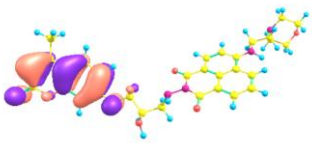	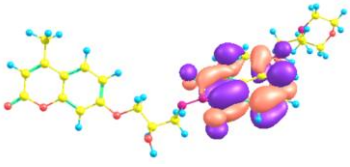	4.363

22h	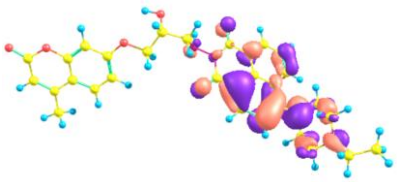	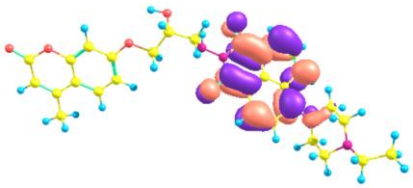	3.314
22i	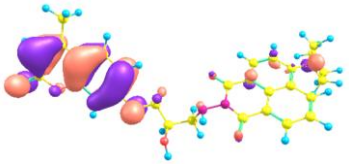	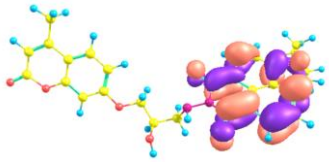	3.965
22j	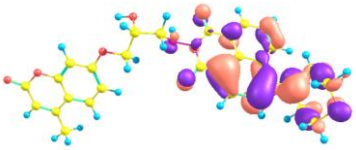	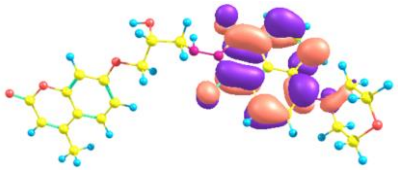	3.885
22k	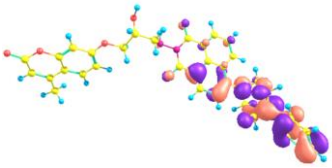	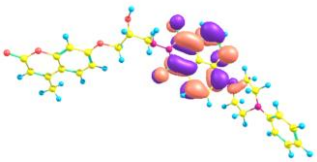	4.3029
22l	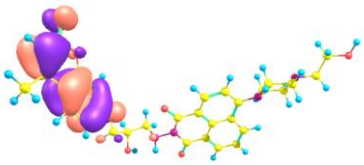	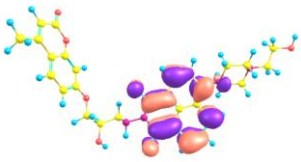	4.4112
22m	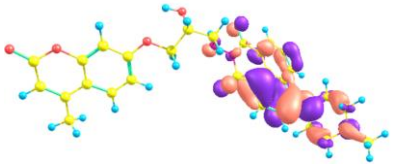	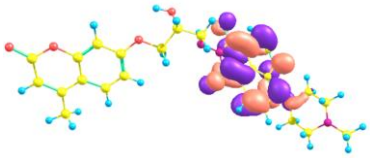	3.563
22n	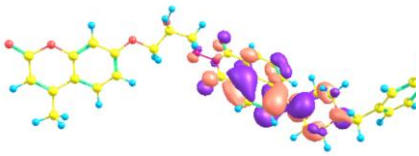	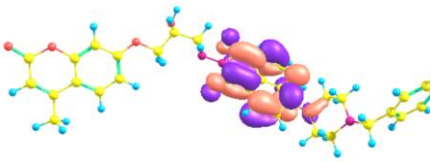	3.968
22o	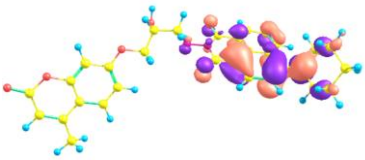	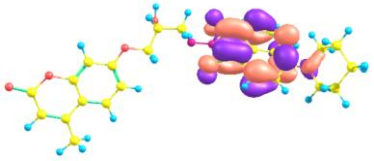	4.352

4.2.5. *In vitro* antibacterial activity

The precursor **21** substituted with various primary and secondary amines was screened for their potential to inhibit bacterial growth by employing a two-fold serial dilution method as

suggested by CLSI.[90,91] The compounds were evaluated towards gram-negative *viz. Escherichia coli, Salmonella enterica, Serratia marcescens, Acinetobacter calcoaceticus* and gram positive *viz. Bacillus subtilis, Enterococcus faecalis, Listeria sp., Staphylococcus aureus* bacterial strains. Interesting results were obtained for conjugates enabling us to develop some fascinating structure-activity relationships. As shown in **Table 4.15**, compound **21** exhibited moderate activity in suppressing the bacterial growth towards tested strains. Replacing Br with allylamine led to increase in bioactivity of the precursor **21**. Compound **22a** effectively suppressed the growth of most of the tested bacterial strains with low MIC values and the results were better than amoxicillin and comparable to tetracycline and chloromycin. Replacement of allylamine with other amines such as benzylamine (**22b**), cyclohexylamine (**22c**), butylamine (**22d**) and ethyl morpholine (**22g**) resulted in complete loss of bioactivity of the compound. This may be due to change in electron density of compounds and increase in chain length of amine led to enhance the hydrophobic character causing poor solubility of compounds in water due to which these were unable to suppress the growth of tested bacterial strains. Introduction of ethylamine (**22e**) and ethanol amine (**22f**) increases the bioactivity of the precursor **21**. Both the compounds inhibited the growth of bacterial strains with higher efficacy and low MIC values ranging from 1.56 – 3.125 μg/ml against all the tested strains. The increase in bioactivity in case of **22e** may be due to shorter chain length of amine and in case of **22f** free OH may bind to biological targets *via* hydrogen bonding. Further structural optimization on precursor **21** and introduction of secondary amines was favourable for enhancing the bioactivity of compounds. Conjugates having a substitution of ethyl piperazine (**22h**), pyrrolidine (**22i**), and morpholine (**22j**) displayed broad-spectrum antibacterial activity against all the tested strains. Compound **22h** effectively suppresses the growth of tested bacterial strains with a low MIC value of 1.56 μg/ml towards all bacterial strains and 6.25 μg/ml against *S. aureus,* manifesting that compound can be built as potent antibacterial agent. Compounds **22i** and **22j** were active towards all the tested strains, but both compounds were unable to suppress the growth of *Listeria sp.* Further introduction of secondary amines such as phenyl piperazine (**22k**), ethanol-piperazine (**22l**), and piperidine (**22o**) in precursor **21** resulted in complete loss of bioactivity. This may be due to an increase in chain length of substituted amine, which elevated the hydrophobic character of compounds, causing a decrease in solubility of compounds. Compound **22m** having methyl piperazine substituent exhibited broad spectrum activity against all the tested bacterial strains with low MIC values ranging from 1.56 – 12.5 μg/ml. Further substitution of benzyl piperazine (**22n**) to compound **21** displayed moderate activity in suppressing the growth of bacterial strains. Thus, in most cases,

compound **21** with secondary amines increased the potency of precursor **21** in suppressing the growth of bacterial strains than primary amines in which only a few amines were able to enhance the bioactivity of compound. The results were also compared to marketed drugs amoxicillin, tetracycline, and chloromycin. Few of the compounds outperformed these marketed drugs, and some exhibited comparable results. Compounds **22e** and **22h** were chosen for further examination of their antibacterial studies and to underline the preliminary mechanism toward *E. coli* based on their potency to inhibit bacterial growth.

Table 4.15 Antibacterial activity data as MIC (μg/ml) for compounds **22a-22o**

	Gram Positive Bacterial Strains				**Gram Negative Bacterial Strains**			
Comp	***E. faecalis***	***B. subtilis***	***L. species***	***S. aureus***	***E. coli***	***S. enterica***	***A. calcoaceticus***	***S. marcescens***
21	25	12.5	50	6.25	25	100	50	25
22a	1.56	6.25	1.56	200	200	3.12	1.56	3.12
22b	-	-	-	-	-	-	-	-
22c	-	-	-	-	-	-	-	-
22d	-	-	-	-	-	-	-	-
22e	1.56	1.56	1.56	3.12	1.56	3.12	1.56	3.12
22f	1.56	3.12	1.56	3.12	3.12	1.56	1.56	3.12
22g	-	-	-	-	-	-	-	-
22h	1.56	1.56	1.56	6.25	1.56	1.56	1.56	1.56
22i	3.12	1.56	-	1.56	6.25	3.12	1.56	6.25
22j	3.12	1.56	-	6.25	1.56	1.56	3.12	6.25
22k	-	-	-	-	-	-	-	-
22l	-	-	-	-	-	-	-	-
22m	6.25	1.56	12.5	1.56	3.12	1.56	1.56	3.12
22n	12.5	1.56	-	1.56	1.56	-	1.56	-
22o	-	-	-	-	-	-	-	-
A	6.25	50	50	25	100	200	50	1.56
B	3.12	1.56	6.25	1.56	1.56	100	1.56	1.56
C	3.12	1.56	1.56	3.12	3.12	50	3.12	1.56

A - amoxicillin; B - tetracycline; C – chloromycin, - > 200

4.2.6 Bactericidal or bacteriostatic action

After carrying out preliminary studies, minimal bacterial concentration (MBC) was examined in order to determine the mode of action exhibited by active compounds **22e** and **22h** and whether bacteriostatic or bactericidal nature towards *E. coli*. The results obtained predicted that

both compounds **22e** and **22h** have MBC/MIC values of 2 and 1, respectively (**Figure 4.16a)**, manifesting that both compounds are bactericidal to *E. coli*.

4.2.7 Bacterial susceptibility evaluation

The treatment of bacterial infections has become a serious challenge due to the abuse of antibiotics, leading to the emergence of bacterial resistance, thus decreasing the efficacy and increasing the dosage of present antibiotics.[169] In the present work, the drug resistance of compounds **22e** and **22h** was examined at MIC values against *E. coli* upto 25 passages using tetracycline and amoxicillin as positive controls. The results designated that both compounds delayed the development of drug resistance with greater efficacy than marketed antibiotics. Compounds **22e** and **22h** did not observe any significant change in MIC value upto 19 and 22 passages, respectively, whereas the MIC values of tetracycline and amoxicillin increased drastically after 8 and 10 passages, respectively **(Figure 4.16b)**. Hence, both compounds have low potential to develop drug resistance against *E. coli* and thus can conquer awful resistance for treating infections.

4.2.8 Cytotoxicity assay

Biosafety of the new drug candidate is a crucial factor for its further development as an antibacterial agent, which is assessed by measuring the cytotoxicity of compounds toward normal cell lines.[107] Therefore, cytotoxicity effect of active drug candidates **22e** and **22h** towards normal cell line (Hek 293) was examined by MTT assay. Compound **22e** showed 3.65 %, 4.32 %. 4.89 %, 5.87 %, and 6.97 % cytotoxicity. In comparison, **22h** showed 2.87 %, 3.12 %, 3.98 %, 4.54 %, and 5.65 % cytotoxicity towards normal cell lines Hek 293 at different concentrations ranging from 0.78 – 12.5 μg/ml (**Figure 4.16c**). The low cytotoxicity values of both compounds inferred that these could selectively kill bacteria cells over normal cells, thus possessing biosafety, and can be taken further for in-depth study for their development as antibacterial agents.

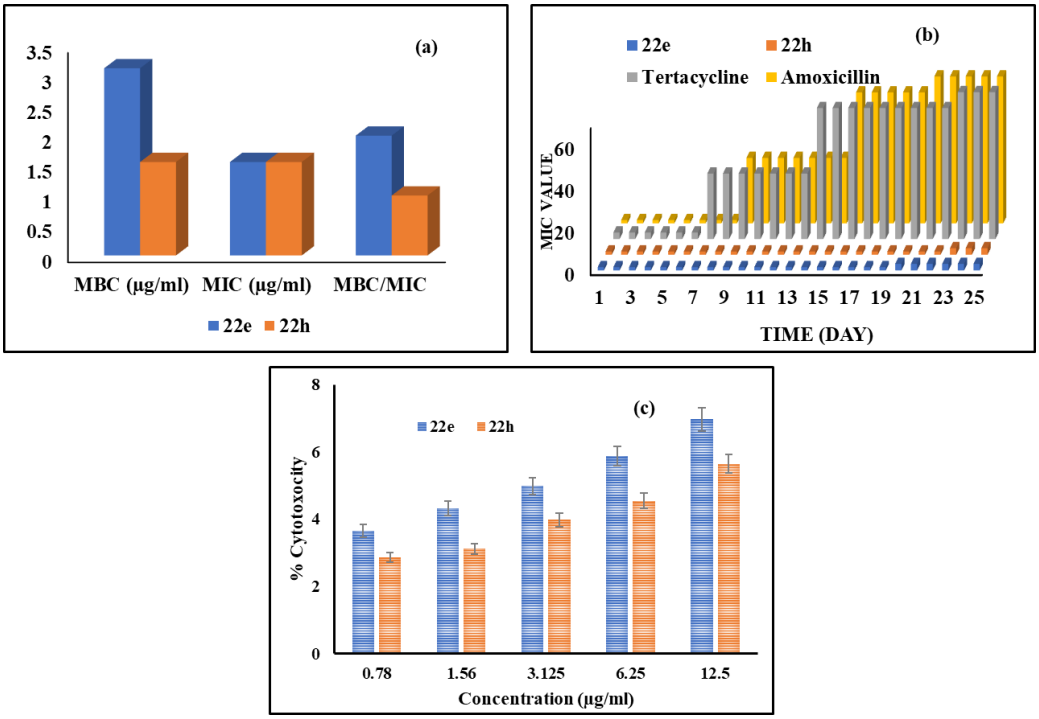

Figure 4.16 (a) Evaluation of MBC and MIC values of compounds **22e** and **22h**, (b) bacterial susceptibility evaluation of **22e, 22h,** tetracycline and amoxicillin towards *E. coli*, (c) cytotoxicity of compounds **22e** and **22h** towards normal cell line Hek293

4.2.9 ADME studies of compounds

Evaluation of pharmacokinetic properties and druggability of active drug candidates is crucial for building new drug candidate with better therapeutic values.[108] Hence, we have conducted ADME calculations by using online Swiss ADME software. As formulated in **Table 4.16**, both compounds **22e** and **22h** followed Lipinski's rule and displayed the same oral bioavailability score as that of control drugs, tetracycline, and amoxicillin. Both compounds are unable to cross blood-brain barrier, indicative of low toxicity to the central nervous system, which were in accordance with cytotoxicity assay. In addition, both compounds have high gastrointestinal absorption. Thus, these results manifested that both compounds displayed drug-likeness and have the potential to be built as antibacterial agents.

Table 4.16: The ADME evaluation data of compounds **22e, 22h,** tetracycline and amoxicillin

	22e	**22h**	**Tetra**	**Amox**
M.W	487	556	444.5	365.4
M logP	3.07	3.08	2.17	0.95
H-Bond acceptor	6	7	7	6
H-Bond donor	3	2	5	4
Rotatable bond	8	8	2	5
Bioavailability score	0.55	0.55	0.55	0.55

TPSA	122.7	117.2	144.3	158.2
Lipinski rule	Yes	Yes	0	0
BBB	No	No	No	No
GI absorption	High	High	Low	Low

4.2.10 Kinetics of bactericidal activity

The occurrence of bacterial resistance is prevented by the antibiotics having significant bactericidal properties.[119] Hence, the time-kill kinetics is a crucial test to measures the bactericidal properties of the drug at different concentrations. As represented in **Figure 4.17** *E. coli* in the control inoculum entered its exponential phase within 3 h, where the growth *of E. coli* was retarded, and cells were killed in the inoculum upon treatment with active compounds **22e** and **22h.** Compounds **22e** and **22h** started displaying their bactericidal action within 4h and 3h at MIC, respectively. When treated with higher concentrations of compounds, i.e. at 2 × MIC, 4 × MIC, and 8 × MIC, the time required for killing bacteria in the inoculum were reduced from 4h to 2h in case of **22e** and 3h to 1.5h in case of **22h**. Thus, both compounds exhibited not only superior antibacterial properties but also possessed magnificent bactericidal effects, thus reducing the time of treatment.

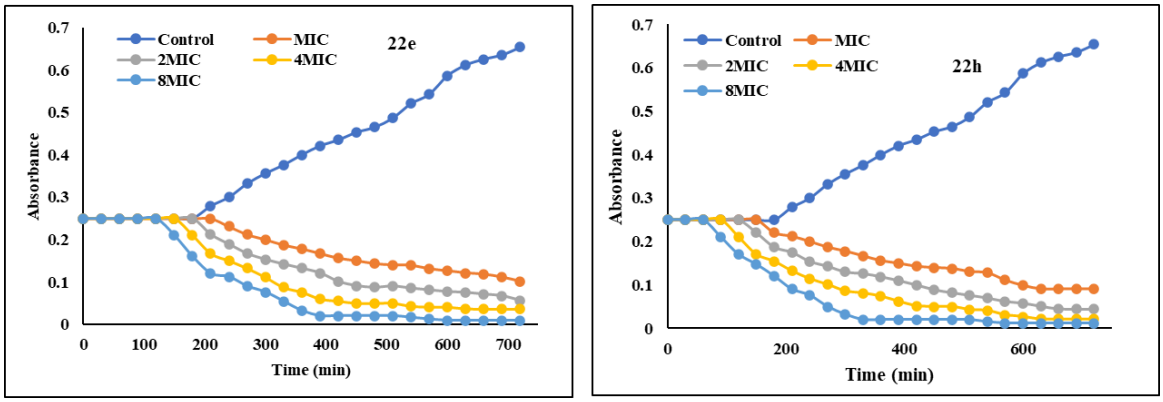

Figure 4.17: Time-killing kinetics of *E. coli* by (a) **22e** and (b) **22h** at various concentrations

4.2.11 Biofilm inhibition assay

Bacteria are prevented by the attack of antibiotics due to formation of biofilm on their surface that enhances the pathogenicity and virulence of bacteria, thus assisting the formation of bacterial resistance, hence decreasing the bactericidal efficacy of antibacterial candidates.[170] These biofilms also assist the reproduction capacity and bacterial absorption on the surface of medical devices that actually hinder their clinical use.[171] In the present study, we have assessed the biofilm inhibition capacity of active compounds **22e** and **22h** by crystal violet assay towards *E. coli*. The biofilm inhibition ability of both compounds **22e** and **22h** were increased with an increase in concentration (**Figure 4.18a**). Compounds **22e** and **22h** were able to inhibit the

formation of biofilm of *E. coli* upto 38.5% and 43.7%, respectively at MIC values while, 83.2% and 92.3% inhibition of biofilm were achieved at 8 × MIC. These results inferred that both compounds have potential to inhibit the biofilm formation of *E. coli,* thus delaying the development of bacterial resistance.

4.2.12 Biofilm virulence factor

4.2.12a Auto-aggregation

Biofilm formed by bacteria is nourished due to bacterial auto-aggregation and adhesion, thus decreasing the treatment efficacy of antibiotics and facilitating drug resistance.[172] Therefore, it is worth exploring whether our drug candidates have the potential to reduce bacterial auto-aggregation or not. As represented in **Figure 4.18b,** the absorbance value at 600 nm of supernatant rises upon incubating *E. coli* cells with compounds **22e** and **22h**, revealing that both compounds have the ability to disrupt the self-auto aggregation of *E. coli* in a concentration-dependent mode, thus delaying the development of drug resistance.

4.2.12b Surface hydrophobicity inhibition assay

The successive colonization and bacterial cell adhesion on the solid surface are strengthened due to hydrophobicity of cell surface, which is a crucial virulence factor leading to formation of a strong biofilm.[173] The potential of compounds **22e** and **22h** to inhibit the hydrophobicity of *E. coli* surface was conducted by microbial adhesion to hydrocarbon assay. The hydrophobicity of *E. coli* was greatly reduced in the presence of compounds **22e** and **22h**. As depicted in **Figure 4.18c**, the inhibition of surface hydrophobicity by both compounds increases in a concentration-dependent mode. Compounds **22e** and **22h** were able to decrease the *E. coli* surface hydrophobicity upto 80.6% and 91.2%, respectively, at 8 × MIC concentration. These results infer that both compounds could successfully reduce the hydrophobicity of *E. coli* surface, thus hindering the biofilm virulence factor responsible for formation of biofilm.

4.2.12c Reduction in exopolysaccharides (EPS)

Biofilm network construction and cell aggregation are facilitated by the presence of EPS, leading to development of drug resistance. Hence, in order to evaluate the ability of drug candidate to inhibit the biofilm formation, a decrease in exopolysaccharide content was examined.[174] Upon incubating *E. coli* with compounds **22e** and **22h**, the loss in EPS content was found to be 36.4% and 40.6% at MIC, respectively. The loss in EPS content was more pronounced with increasing concentration of both compounds **22e** and **22h** and at 8xMIC value upto 85.3% (**22e**) and 93.9% (**22h**) loss in EPS content was noticed. **Figure 4.18d**, indicates

that both the compounds could effectively reduce the exopolysaccharides content of *E. coli*, thus hindering the construction of biofilm and delay the emergence of drug resistance.

Combining the above results, it is concluded that both compounds could effectively hinder the biofilm virulence factor responsible for the formation of strong biofilm. These could also facilitate the disruption of mature biofilm favourable for enhancing the antibacterial activity of the new compounds and decreasing the development of drug resistance.

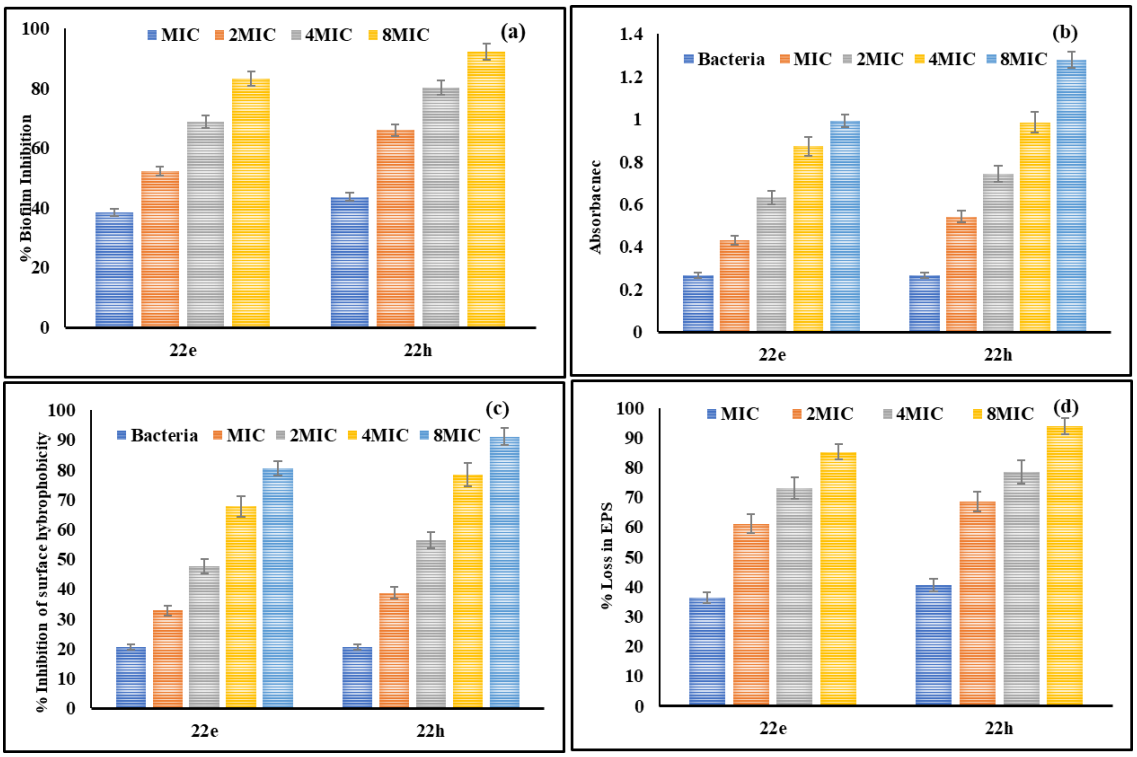

Figure 4.18: (a) Inhibition of biofilm; (b) auto-aggregation; (c) inhibition of surface hydrophobicity; and (d) loss in EPS content of *E. coli* in the presence of **22e** and **22h**

4.2.13 Membrane disruption assay

The membranes of bacteria play a significant role in maintaining the different biochemical reactions that work in proper order by protecting them from extracellular substances. The protective obstacle constructed by bacterial membranes serves as the key factor for reduced permeability of antibiotics, leading to alteration in the concentration of drugs entering the bacteria, which directly affects their efficacy and therapeutic values, leading to the development of drug resistance.[175] Targeting the cell membrane of bacteria has become a hot spot for the development of new antibacterial agents. Impressed by the excellent antibacterial activity, low potential for drug resistance, and rapid bactericidal properties of **22e** and **22h** inspired us to further explore their potential to disrupt the bacterial cell membrane.

4.2.13a Membrane depolarisation

Most of the drugs exhibited their bactericidal effects by disrupting the transmembrane potential of cells, leading to cell death.[176] The ability of active compounds **22e** and **22h** to depolarise the cell membrane of bacterial cells was accessed by 3,5-(dipropylthiadicarbocyanine), a potentiometric dye employed for measuring depolarization. In the presence of **22e** and **22h**, dye is released from the cell, resulting in an increase of fluorescence intensity, which is an indicator of membrane depolarization.[177] As shown in **Figure 4.19**, the fluorescence intensity of dye in *E. coli* upon incubating with **22e** and **22h**, increased progressively in a concentration and time-dependent modes, whereas no change was noticed in case of untreated cells. These results indicated that both compounds **22e** and **22h** could successfully disrupt the membrane potential leading to delay in growth of drug resistance.

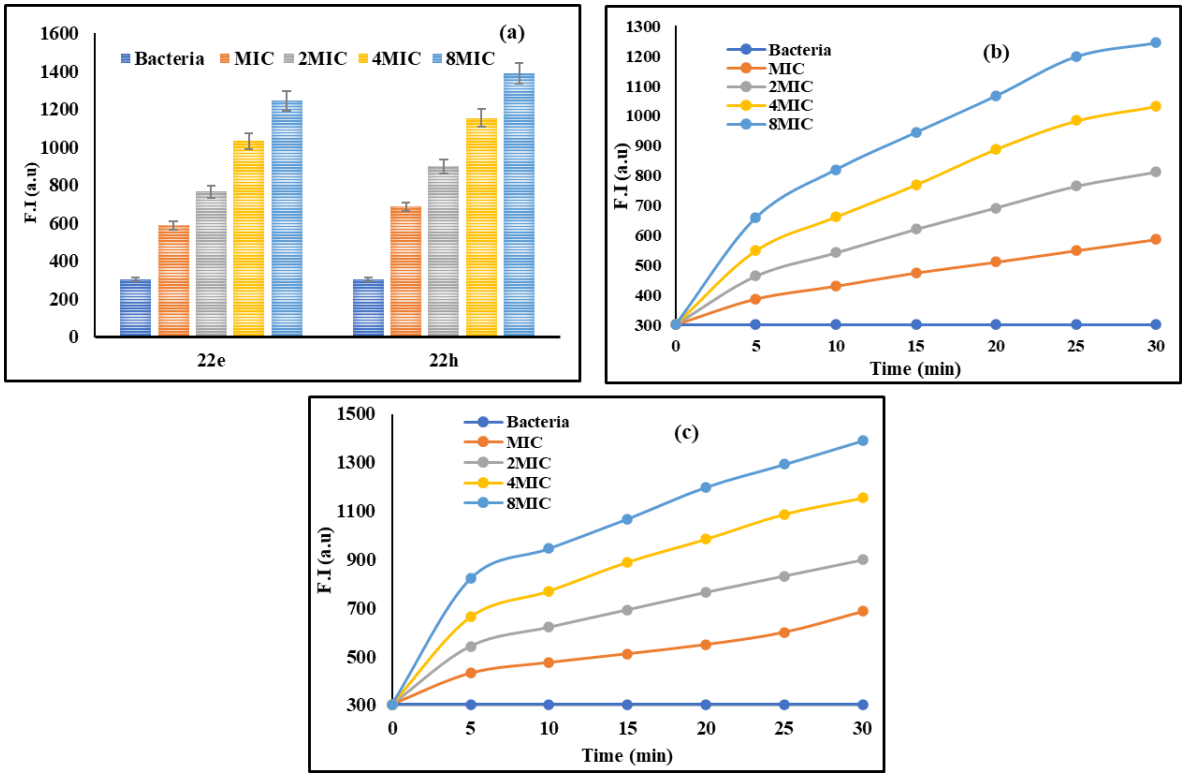

Figure 4.19: Membrane depolarisation of *E. coli* by compounds (a) at different concentrations and in time-dependent modes of (b) **22e** and (c) **22h**

4.2.13b Outer membrane permeability

The outer membrane of *E. coli* acts as a defensive hurdle to antibiotics, preventing them from entering the cell, thus decreasing the therapeutic values.[178] The NPN-a fluorescent dye, was used to assess the outer membrane permeabilization of *E. coli* with compounds **22e** and **22h**. The fluorescence intensity of NPN is increased upon penetrating the damaged outer membrane of bacteria, while only low fluorescence is seen in the intact cell membrane.[179] As shown in **Figure 4.20**, the emission intensity was enhanced progressively upon treating *E. coli* with

compounds **22e** and **22h** in both time and concentration-dependent modes. These results manifested that both compounds could effectively destroy the outer membrane of *E. coli*, thus delaying the development of drug resistance.

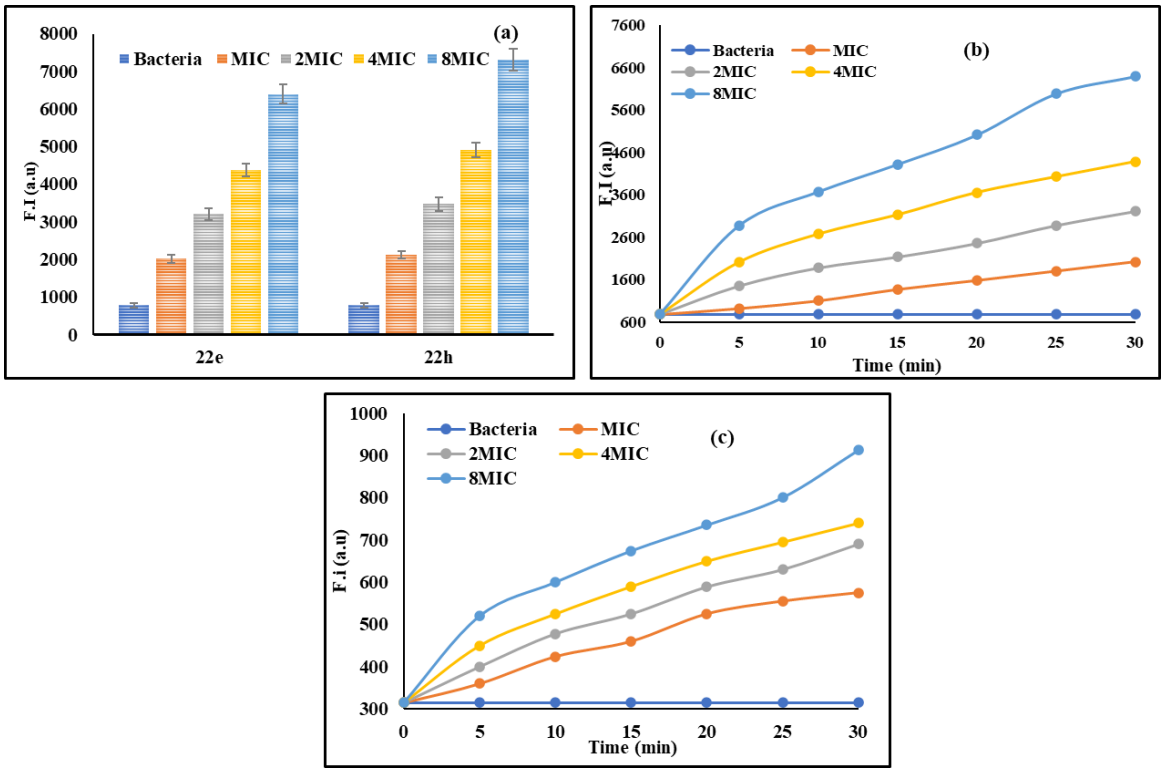

Figure 4.20: Outer membrane permeability of *E. coli* by compounds (a) at different concentrations and in time-dependent modes of (b) **22e** and (c) **22h**

4.2.13c Inner membrane permeability

In order to get insight into the mechanism for antibacterial activity of compounds **22e** and **22h**, inner membrane assay was conducted using ethidium bromide (EtBr). Ethidium bromide penetrates the cell membrane but can impede the bacterial cells having damaged membranes where it binds with DNA to exhibit fluorescence.[180] Upon incubating *E. coli* cells with compounds **22e** and **22h** at a known concentration of EtBr, a progressive elevation in fluorescence intensity was observed, indicating the increase in number of bacterial cells with disrupted membranes in the inoculum. The fluorescence intensity increases in concentration and time-dependent modes (**Figure 4.21**), inferring that both compounds have the potential to disrupt the inner membrane of *E. coli*.

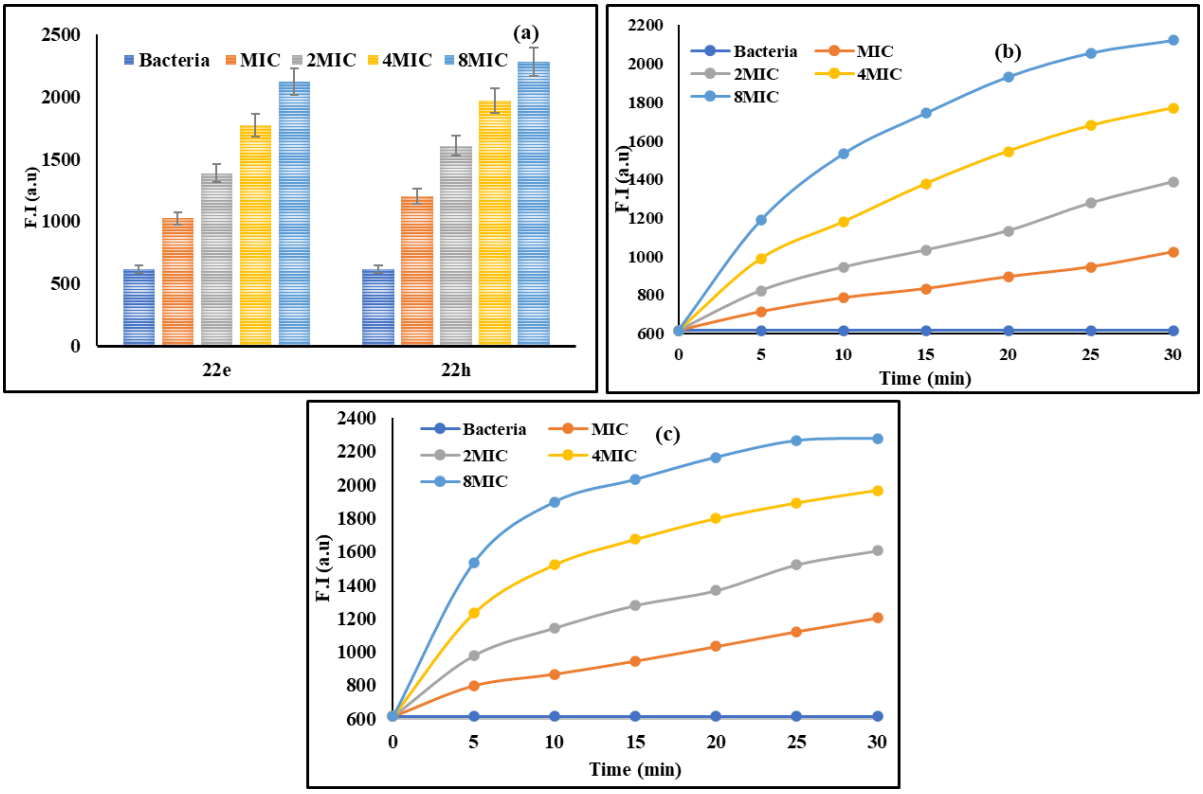

Figure 4.21: Inner membrane permeability of *E. coli* by active compounds (a) at different concentrations and in time-dependent modes of (b) **22e** and (c) **22h**

Combining the above results, it is put forward that both compounds **22e** and **22h** could effectively damage the cell membranes of *E. coli* and can cause membrane depolarisation, leading to cell apoptosis, and ultimately cell death to exert their antibacterial mechanism.

4.2.14 Leakage of cytoplasmic content

The bacterial cell membrane's integrity helps to conserve their stability and biological activity, and any disruption caused to membranes allow the cytoplasmic contents, such as protein and nucleic acids, to leak out, thus causing cell death.[181]

4.2.14a Protein leakage assay

In order to confirm the membrane damage caused by both compounds, the concentration of leaked protein from *E. coli* was determined with the help of Follin's assay. As shown in **Figure 4.22a**, there was a proportional increase in concentration of leaked protein with rise in concentrations of **22e** and **22h**. Thus, the results obtained presented to be positive proof of membrane damage.

4.2.14b Nucleic acid leakage

Further, the damage caused to the membrane integrity by active compounds **22e** and **22h** was illustrated by measuring the concentration of leaked nucleic acids from *E. coli* cells. As represented in **Figure 4.22b**, the concentration of nucleic acid leaked from bacterial cells

increases in a concentration-dependent mode in both cases i.e. **22e** and **22h**. The results obtained was in accordance with the membrane damage.

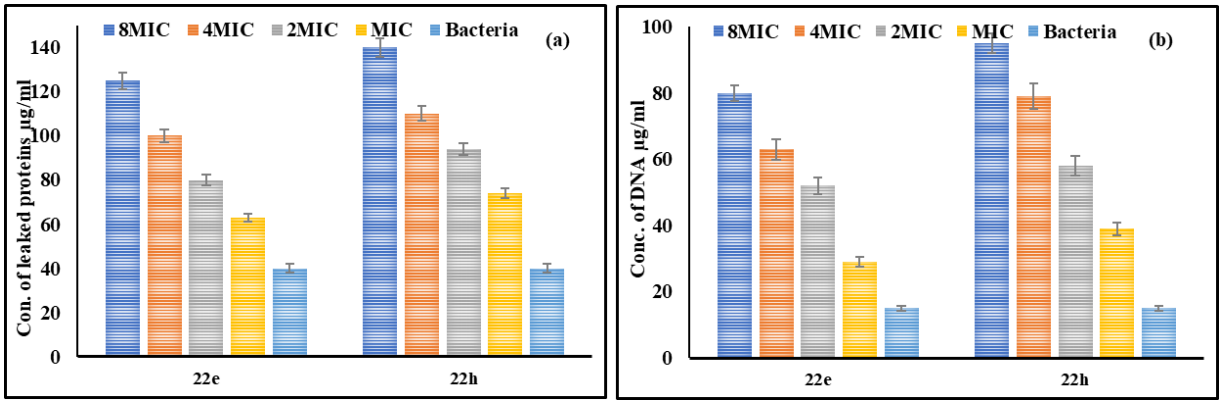

Figure 4.22: (a) Protein leakage and (b) DNA leakage from *E. coli* in the presence of **22e** and **22h** at different concentrations

Combining the results obtained from protein and nucleic acid leakage, it is concluded that both compounds **22e** and **22h** effectively disrupt the integrity of cell membrane, causing the leakage of cellular components, hence leading to cell death.

4.2.15 Metabolic dysfunction assay

The growth of bacteria and its survival is maintained by the metabolic activity of bacteria. Bacteria gain their energy, regulate cellular homeostasis and synthesize essential biomolecules through different metabolic pathways.[182] Disruption of cell membranes causes protein denaturation on their surface, leading to metabolic dysfunction, that leads to cell apoptosis. Almar blue assay was conducted to determine the intracellular metabolic activity of *E. coli* in the presence of compounds **22e** and **22h**. As shown in **Figure 4.23a**, the metabolic activity of *E. coli* upon incubating with **22e** and **22h** was decreased significantly in a concentration-dependent mode. The metabolic activity was decreased to 25% and 19.6% at 8xMIC values in the presence of compounds **22e** and **22h**, respectively. Thus, both compounds upon interacting with bacteria, cause damage to the membrane, leading to significant loss in metabolic activity.

4.2.16 Intracellular oxidative stress

4.2.16a Reactive oxygen species (ROS)

The accumulation of ROS in the bacteria cells is elevated upon obtaining any external stress, causing the disruption of cellular structure, leading to oxidative stress. The production of ROS significantly contributes to the antibacterial properties of many antibiotics.[183] The ability of compounds **22e** and **22h** to induce oxidative stress inside *E. coli* was measured fluorometrically by determining the level of ROS using DCFH-DA fluorescence dye in untreated and treated cells. A progressive increase in emission intensity of *E. coli* treated with **22e** and **22h** was

noticed in a concentration-dependent mode. **Figure 4.23b** indicates that both compounds can increase the level of reactive oxygen species, thus causing oxidative damage to *E. coli* leading to bacterial cell death.

4.2.16b Glutathione activity

Bacterial cells are shielded from the destruction caused by accumulation of oxidative stress by antioxidant glutathione (GSH), which is a tripeptide containing thiol presented in a reduced state in excessive concentration in normal bacterial cells, maintaining the normal functioning of the cells.[184] Accumulation of excessive ROS inside the cells facilitates the transformation of GSH from its reduced state to its oxidized state, thus making GSH incapable to save DNA, proteins, enzymes, etc., from oxidative damage.[185] The loss in GSH activity of bacterial cells is an indicator of production of oxidative stress that can be examined by Elmann's method. The ability of compounds **22e** and **22h** to decrease the level of GSH in *E. coli* cells was determined. A significant loss in GSH level of bacterial cells was noticed in the presence of compounds (**Figure 4.23c**). The decrease in level of GSH was proportional to the concentration of compounds. About 45% and 50% loss in GSH activity of *E. coli* was observed in the presence of **22e** and **22h**, respectively, at 8xMIC. The results obtained further validate the production of ROS by both compounds.

4.2.16c Lipid peroxidation

The lipid peroxidation of the cells is promoted by accumulation of ROS inside the cells. The antioxidant potential and level of oxidative damage to cells are represented by the degree of malondialdehyde (MDA) in cells.[186] The increase in level of MDA inside the cell is used as a parameter to determine the level of lipid peroxidation. As shown in **Figure 4.23d**, the level of MDA produced in *E. coli* enhanced significantly in the presence of compounds **22e** and **22h**. Furthermore, the MDA production increases gradually with increase in concentration of compounds. As the concentration reaches 8×MIC, the increase in MDA production was found to be 56.3% in case of **22e** and 61.3% in case of **22h**. The results obtained infer that both compounds could successfully increase the MDA production and were consistent with ROS production, thus promoting bacterial cell death.

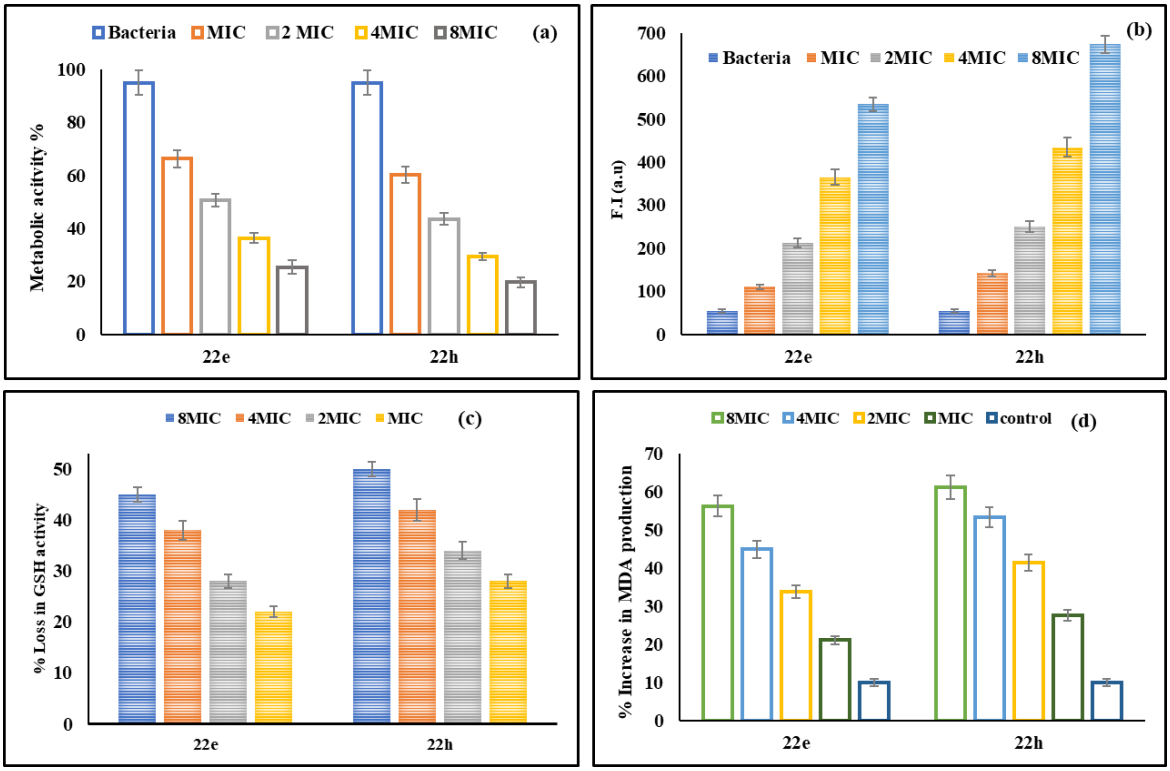

Figure 4.23: (a) Loss in metabolic activity; (b) intracellular ROS production; (c) loss in GSH activity and (d) malondialdehyde production in *E. coli* treated with **22e** and **22h.**

4.2.17 Change in morphology of *E. coli* cells

Damage caused to the membrane of *E. coli* with compounds **22e** and **22h** was further confirmed by the bacterial morphology change via Scanning Electron Microscopic (SEM) images. Figure 10a illustrates the SEM pictures of untreated E. coli cells revealing regular, symmetrical, intact, and rod shapes. Upon treating E. coli with compounds 8e and 8h at 2 MIC, rupturing of cell wall and leakage of cytoplasmic contents from E. coli were observed in both cases (Figures 10b and 10c). Moreover, E. coli cells were found shrunken and broken in the presence of these compounds. These results confirmed the membrane damage of E. coli by both the compounds.

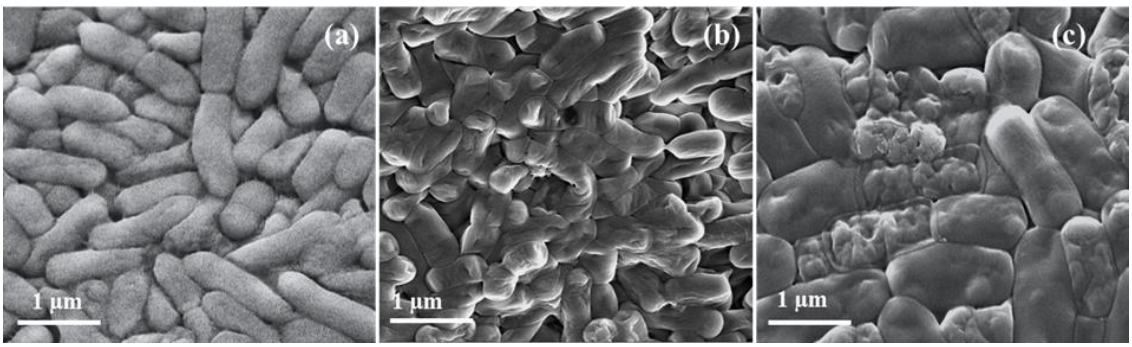

Figure 10: SEM images at 1μm of (a) untreated *E. coli* and treated *E. coli* with compounds (b) **22e** and (c) **22h** at 2 × MIC

4.2.18 Interaction with DNA

DNA is a crucial target in development of effective antibacterial agents as it serves as the transporter of genetic information essential for the reproduction and survival of organisms.[121] Most of the compounds interact with DNA *via* groove binding, intercalation, or electrostatic interaction, causing microbial death.[187] An increase in oxidative stress in cells led to DNA damage since compounds **22e** and **22h** have the ability to produce ROS inside the cells so these can bind with DNA.

In phosphate buffer (*p*H = 7.4) at room temperature, compound **22e** (5 μM) showed two absorption bands at 280 nm and 458 nm, while compound **22h** (5 μM) exhibited absorption bands at 330 nm and 416 nm. Incremental addition of DNA (0-20 μM) led to enhancement in absorption bands of both compounds **22e** and **22h** (**Figure 4.25**). In case of compound **22e**, hyperchromicity was seen only at 280 nm, whereas no change in the absorption band at 460 nm was observed. In case of **22h**, hyperchromicity was observed in both the absorption bands at 330 nm and 416 nm. These hyperchromic effects may be attributed to the interaction of electronic states between the compounds and DNA.

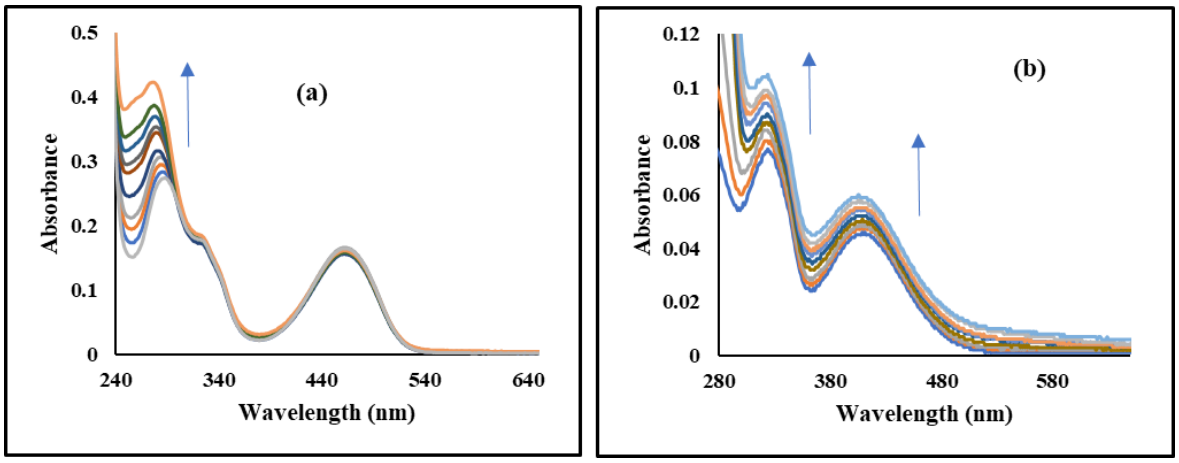

Figure 4.25: Absorption spectra of (a) **22e** (5 μM) and (b) **22h** (5 μM) with increasing concentrations of ct-DNA (0–20 μM).

Further, emission studies were conducted to get details about the interaction of compounds **22e** and **22h** with DNA. Compound **22e** exhibited an intense emission band at 534 nm upon excitation at 280 nm, whereas **22h** displayed its emission band at 550 nm on being excited at 330 nm. Gradual quenching in fluorescence intensity of both compounds **22e** and **22h** were noticed with incremental additions of ct-DNA (0-30 μM) (**Figure 4.26**), indicating the effective binding of both compounds with ct-DNA. The binding constant values for both systems was calculated using equation

$$\frac{E-E_0}{E\,max-E} = K[M] \ldots\ldots (7)$$

Where E_o, E, and E_{max} are the fluorescence intensities of compounds **22e** and **22h** in the absence of ct-DNA, at an intermediate and at saturation, respectively, [M] is the concentration of ct-DNA at an intermediate, and K is the binding constant.

The binding constants for the interaction of ct-DNA with **22e** and **22h** were found to be 6.8×10^4 M^{-1} and 13.0×10^4 M^{-1}, respectively. These binding constants unfolded that both compounds bound effectively with DNA. These results acquired from ct-DNA studies ascertain the inner membrane damage by both compounds **22e** and **22h**.

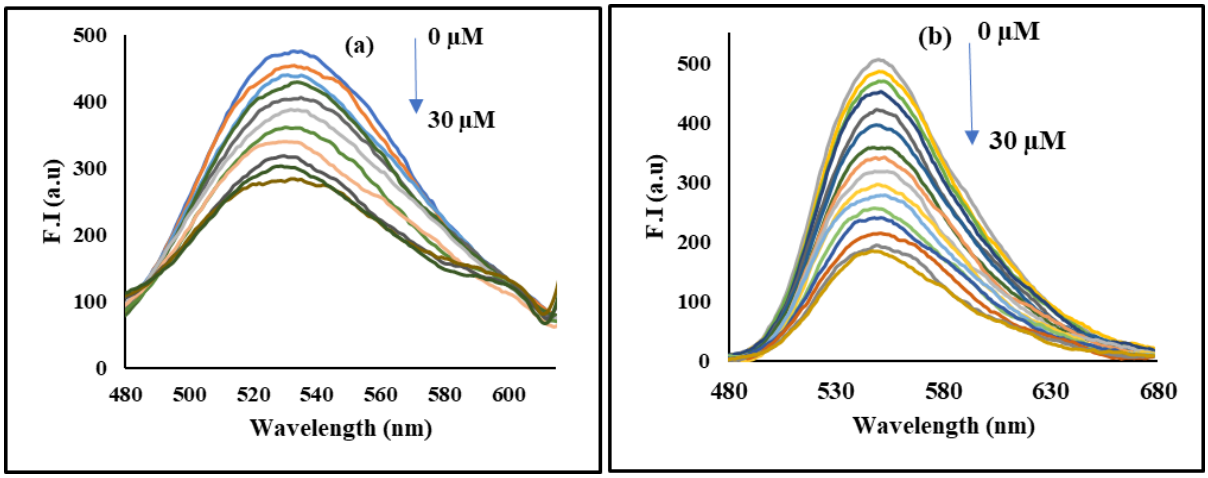

Figure 4.26: Emission spectra of (a) **22e** and (b) **22h** in phosphate buffer (*p*H 7.4) at 298 K upon progressive additions of ct-DNA (0–30 μM).

Furthermore, the bindings of drug candidates **22e** and **22h** with ct-DNA (PDB: 1BNA) were assessed by employing Autodock program, and the discovery studio was used for visualization of interactions. The minimum binding energies of compounds **22e** and **22h** with ct-DNA were found to be -9.84 kcal/mol and -11.15 kcal/mol, respectively. In case of **22e**, the ester oxygen atom of coumarin ring binds with DG14 (*d* = 2.34 Å, chain B), whereas the carbonyl oxygen atom of coumarin binds to DG12 (*d* = 1.84 Å, chain A). The oxygen atom in the alkyl chain binds to DG16 (*d* = 2.76 Å, chain B), the OH in the chain interacts with DC11 (*d* = 1.97 Å, chain A) and the NH in the alkyl chain binds to DA17 (*d* = 2.47 Å, chain B). The oxygen atom of naphthalimide binds with DG10 (*d* = 3.06 Å, chain A) and DG16 (*d* = 2.44 Å, chain B), and the NH of amine group binds with DT19 (*d* = 2.01 Å, chain B). These interactions occurred *via* hydrogen bonding. In comparison to this, oxygen in coumarin ring of **22h** binds with DG22 (*d* = 2.50 Å, chain B). The oxygen atom in alkyl chain interacts with DG4 (*d* = 1.75 Å, chain A) and the OH binds with DA6 (*d* = 2.33 Å, chain A). The NH interacts with DC21 (*d* = 1.87 Å, chain B), and the oxygen of naphthalimide binds with DA5 (*d* = 2.36 Å, chain A) and DA6 (*d* = 2.99 Å, chain A). Conventional hydrogen bonding is responsible for the

interaction of **22h** with ct-DNA (**Figure 4.27**). Comparing the results of both compounds, **22h** binds more firmly with ct-DNA than **22e**, thus assisting the experimental results.

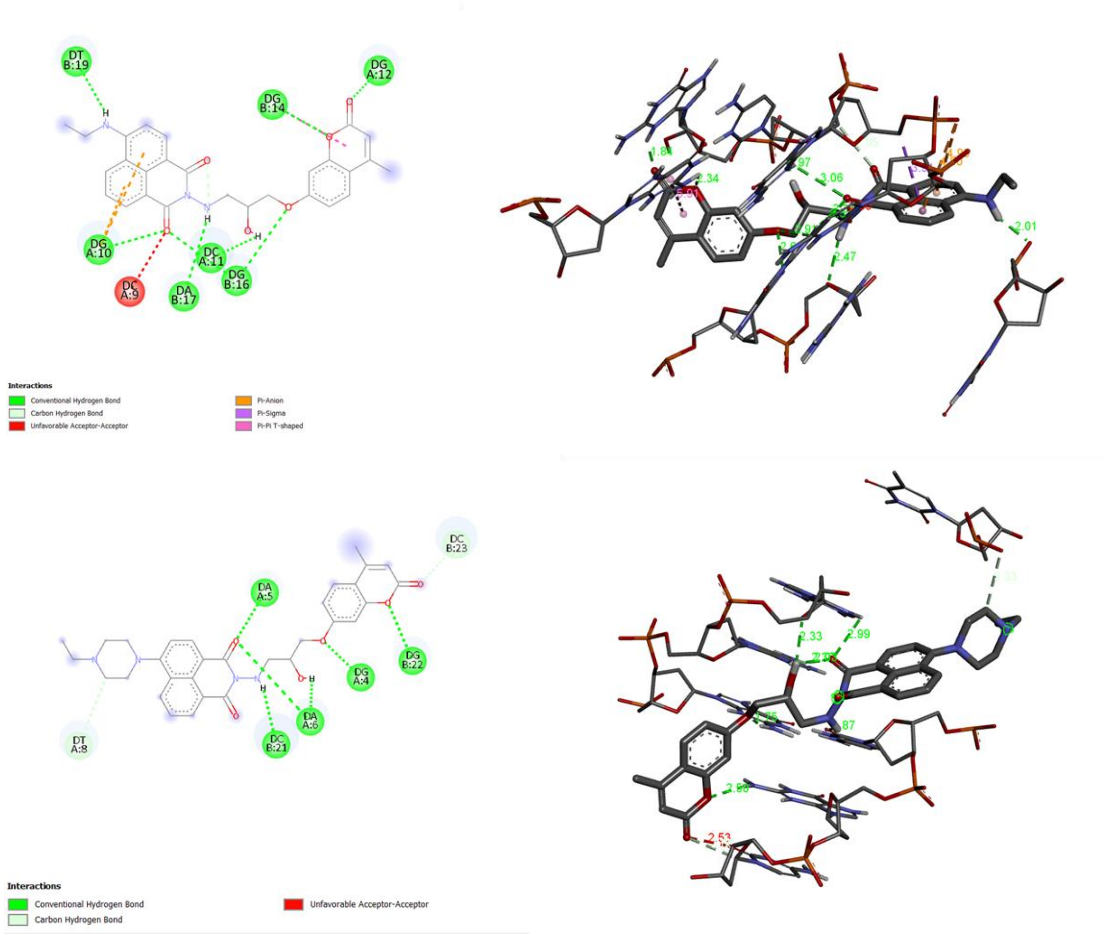

Figure 4.27: Molecular docking of DNA (1BNA) with compounds **(a) 22e and (b) 22h**

4.2.19 HSA binding studies

The pharmacokinetic and pharmacodynamic properties of drugs, such as distribution and metabolism, are modulated upon binding with HSA as it serves as the crucial transporter protein for the transportation and deposition of drugs to the specific target site.[87] Hence, after successfully conducting studies for antibacterial mechanism of compounds **22e** and **22h**, it is essential to investigate the binding of active compounds towards HSA. Therefore, the binding potential of compounds **22e** and **22h** were explored by spectroscopic techniques.[88]

HSA (10 μM) in phosphate buffer displayed an absorption band at 280 nm corresponding to Trp-214, Phe-403, and Tyr-411 amino acid residues. Progressive addition of compounds **22e** (0-6 μM) and **22h** (0-6 μM) to HSA solution in phosphate buffer resulted in enhancement of absorption band at 280 nm along with formation of new band at 460 nm in case of **22e**, and 330 nm and 430 nm in case of **22h (Figure 4.28a** and **4.28b**)**.** The absorption maxima of HSA remain unchanged in the presence of compounds, inferring that both

compounds bind with HSA through non-covalent interactions. Bensei-Hildebrand equation was used to calculate the binding constants for HSA-compounds systems and were found to be $2.2 \times 10^4\ M^{-1}$ (for **22e**) and $4.3 \times 10^4\ M^{-1}$ (for **22h**). These binding constant values revealed the potent binding of **22e** and **22h** with HSA while **22h** binds more strongly with HSA than **22e**.

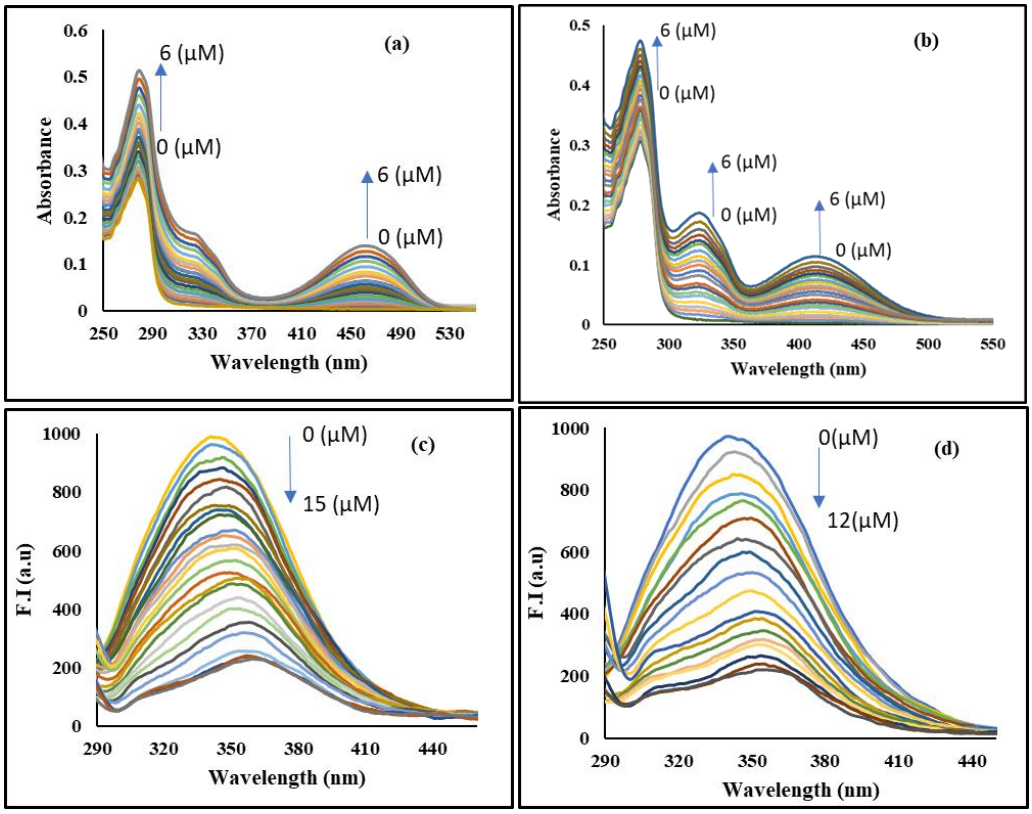

Figure 4.28: Absorption and emission spectra of HSA on increasing concentrations of (a,c) **22e** and (b,d) **22h** in phosphate buffer (*p*H 7.4) at 298 K.

The results obtained from UV-visible studies are incapable of explaining the binding interaction with HSA in detail. Therefore, emission studies were performed to get insight into the interaction between compounds **22e** and **22h** with HSA. The free HSA (10 μM) in phosphate buffer (*p*H = 7.4) upon excitation at 280 nm displayed an intense fluorescence band at 350 nm due to amino acid residues such as Tyr, Trp, and Phe. Upon titrating the solution of HSA (10 μM) in phosphate buffer with gradual addition of compounds **22e** (0-15 μM) and **22h** (0-12 μM), resulted in depletion of fluorescence intensity of HSA at 350 nm (**Figure 4.28c** and **4.28d**). At higher concentrations of compounds **22e** and **22h,** the emission intensity of HSA was quenched fully, disclosing the efficient binding of active drug candidates with HSA.

The quenching in fluorescence intensity of HSA results from a change in the microenvironment upon interacting with foreign ligands. This quenching can be either dynamic or static; therefore, Stern Volmer equation was used to find out the type of quenching mechanism from where quenching constants (K_{sv}) and bimolecular quenching (K_q) were

analysed and found to be 3.5×10^5 M^{-1} (K_{sv}) and 1.02×10^{14} M^{-1} (K_q) for **22e** and 3.8×10^5 M^{-1} (K_{sv}) and 1.11×10^{14} M^{-1} (K_q) for **22h**, inferring the existence of static quenching in both cases (**Table 4.17**).

Table 4.17 Binding parameters for compounds **22e** and **22h** at 298 K

Compound	K_{sv} (10^5 M^{-1})	K_q (10^{14} M^{-1} S^{-1})	[a]R	K_b (10^6 M^{-1})	n	[a]R
22e	3.5	1.02	0.9937	3.9	1.00	0.9974
22h	3.8	1.11	0.9966	6.2	1.02	0.9955

[a]R is the correlation coefficient

Further, time-resolved emission studies were conducted to ascertain the quenching mechanism responsible for compounds binding with HSA. Steady-state emission studies predicted that static quenching is responsible for the binding interactions between HSA and both compounds. To ensure the same, the time-resolved spectra of native HSA (10 μM) alone and with incremental addition of compounds **22e** and **22h** (0-30 μM) were recorded (**Figure 4.29**). A decline in time decay profile of native HSA was observed with the addition of both compounds **22e** and **22h**; indicating the existence of dynamic quenching (**Table 4.18**). Combining the results obtained from steady-state fluorescence and time-resolved studies, it is put forward that both static and dynamic quenching's are responsible for the interaction of compounds **22e** and **22h** with HSA.

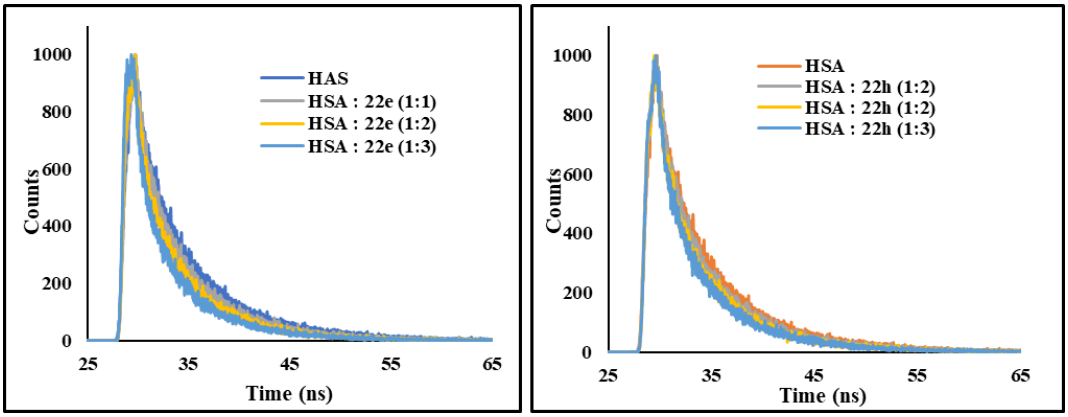

Figure 4.29 Time decay profile of HSA in presence of compounds **22e** and **22h**

Table 4.18 Lifetime fluorescence decay of HSA on interaction with **22e** and **22h**

System	Conc.	τ_1 [ns]	τ_2 [ns]	τ_3 [ns]	α_1	α_2	α_3	τ_{av}	χ^2
HSA		2.48	6.21	0.76	0.29	0.40	0.32	3.43	1.16
HSA-22e	01:01	2.93	6.60	0.43	0.24	0.34	0.42	3.15	1.02

	01:02	2.38	5.93	0.61	0.25	0.29	0.46	2.61	1.10
	01:03	1.92	5.88	0.14	0.11	0.13	0.76	1.90	1.00
HSA-22h	01:01	1.85	5.61	0.31	0.24	0.33	0.43	2.45	1.18
	01:02	1.75	5.42	0.42	0.20	0.22	0.58	1.81	1.20
	01:03	2.27	5.83	0.24	0.16	0.17	0.67	1.51	1.11

Further, the stability of the complexes formed upon interaction of compounds **22e** and **22h** with HSA were assessed by determining the binding constant values. Thus, modified Stern-Volmer equation was employed to calculate the binding stoichiometry (n) and binding constant parameters and were found to be 3.9×10^6 M^{-1} (K_b) for **22e** and 6.2×10^6 M^{-1} (K_b) for **22h** reflecting the efficient binding of both the compounds with HSA (**Table 4.17**). The binding stoichiometry in both cases was found to be 1, manifesting that the compounds **22e** and **22h** bind with HSA specifically at one site, having a stoichiometry of 1:1. In addition Gibb's free energy was deliberated and found to be -9.0 kcal/mol (**22e**) and -9.2 kcal/mol (**22h**) (**Table 4.19**).

Table 4.19: Thermodynamic parameters of HSA binding with compounds **22e** and **22h**

T (K)	ΔG, kcal M^{-1} (**22e**)	ΔG, kcal M^{-1} (**22h**)
298	-9.00	-9.20

These negative values of ΔG predicted the spontaneous binding process between compounds and HSA, predicting that hydrogen bonding and van der Waals interactions are responsible for binding of compounds with HSA.

Combining all the results obtained from various studies to depict the binding behaviour of compounds **22e** and **22h** towards HSA, it was concluded that both the compounds bind effectively with HSA and can be transported to the target site easily for treatment of bacterial infections.

4.2.20 Conclusion

Recent times have demanded the building of new antibacterial drugs to battle multiple resistant bacteria, but forming an ideal drug with a low potential for resistance remains a great challenge. In light of this, we have synthesized a series of naphthalimide-coumarin conjugates as a potent antibacterial agent to overcome dreadful drug resistance. The preliminary bioactivity and structure-activity relationship disclosed that some compounds displayed excellent activity in suppressing bacterial growth. Astoundingly, compounds **22e** and **22h** displayed excellent

antibacterial activity against most of the tested strains with low MIC values ranging from 6.25 μg/ml to 1.56 μg/ml and exceeded the marketed drugs. The biofilm formation is inhibited by both compounds, thus delaying the development of drug resistance. The mechanistic studies manifested that compounds **22e** and **22h** effectively disrupt the membrane of bacteria, reducing metabolic activity and disrupting the biofilm virulence factor responsible for the formation of strong biofilm, thus causing the leakage of intercellular protein and nucleic acid contents. Further, biofunctional evaluation discloses that these compounds have ability to produce ROS inside the cells, thus accumulating oxidative stress and causing the oxidation of GSH to GSSG, leading to a loss in GSH activity, thus causing oxidative damage to the cells. Both compounds have the ability to bind with DNA and HSA to form supramolecular complexes, thus exhibiting excellent antibacterial activity, and can be transported to the target site easily. The experimental results were supported by computational and molecular docking studies. Comparing the bioactivity of both compounds, **22h** exhibited superior activity against bacterial strains, membrane disruption, drug-likeness, biofilm inhibition, oxidative stress damage, and metabolic dysfunction. These compounds successfully overcome the awful drug resistance and have the ability to be taken further for clinical trials for their development as effective antibacterial agents.

4.2.21 Experimental section

Synthesis of compound 19

To a stirred solution of compound **13** (2 g, 7.22 mmol) in ethanol, hydrazine hydrate (361 mg, 7.22 mmol) was added to it, and the reaction mixture was stirred at room temperature for 1.5 h. The resulting residue was filtered and vacuum dried to obtain a dark yellow solid product **19** in 88 % yield; m.pt. 260-263 ºC

Synthesis of compound 20[168]

To a stirred solution of commercially available compound **15** (2 g, 11.36 mmol) in excess of epichlorohydrin (15 ml), potassium carbonate (2.35 g, 17.04 mmol) was added and the reaction was heated at 100 ºC for 8 h. The reaction was monitored with the help of TLC. On completion of reaction, the reaction was filtered, and the filtrate obtained was collected, the excess epichlorohydrin was evaporated to obtain a white precipitate, which was recrystallized from chloroform to give a pure white coloured product in 85 % yield; m.pt. 80-82 ºC (Lit. m.pt. 78-80 ºC).

Synthesis of compound 21

Compound **20** (0.62g, 2.11 mmol) was added to a stirred solution of compound **19** (0.50mg, 2.1 mmol) in ethanol and the reaction was refluxed for 4 h. On completion of the reaction, 50

ml of cold water was added to the reaction mixture, resulting in the formation of a crude solid, which was filtered and oven-dried to obtain off-white crude product. The crude product was purified by column chromatography using ethyl acetate: chloroform (2:8) as a solvent system to obtain a creamish white product **21** in 80% yield; m.pt. 270-272 ºC

General procedure for the synthesis of compound 22a-22o:

To a stirred solution of compound **7** (200 mg, 0.38 mmol) various primary amines (1.9 mmol) was added in presence of DMF (10 ml) and K_2CO_3 (0.079 g, 0.57 mmol), wheres ethanol (20 was used in case of secondary amines (1.9 mmol), and the reaction was refluxed for 3h. After completion of the reaction, cold water was added to the reaction mixture, and the residue obtained was filtered to obtain a pure product.

Spectral data of 6-(allylamino)-2-((2-hydroxy-3-((4-methyl-2-oxo-2*H*-chromen-7-yl)oxy)propyl)amino)-1*H*-benzo[*de*]isoquinoline-1,3(2*H*)-dione (22a):

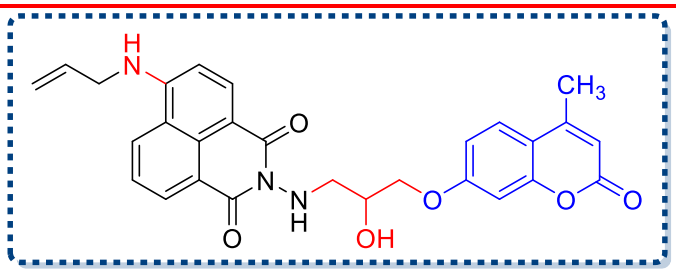

Yield: 78%; colour: yellow; m.pt: 250-253 ºC; ^{1}H NMR ($CDCl_3$, 400 MHz): δ (ppm) 8.62 (d, *J* = 7.28 Hz, 1H), 8.48 (d, *J* = 8.52 Hz, 1H), 8.17 (d, *J* = 8.40 Hz, 1H), 7.66 (t, *J* = 7.88 Hz, 1H), 7.44 (d, *J* = 8.80 Hz, 1H), 6.88 (dd ^2J = 8.80 Hz, ^3J = 11.04 Hz, 1H), 6.76 – 6.72 (m, 2H), 6.09 (s, 1H), 6.05 – 5.97 (m, 1H), 5.63 (t, *J* = 5.24 Hz, 1H), 5.39 (d, *J* = 5.38 Hz, 1H), 5.32 (d, *J* = 10.28 Hz, 1H), 4.10 – 4.04 (m, 4H), 3.42 (d, *J* = 12.24 Hz, 1H), 3.24 (dd, ^2J = 8.52 Hz, ^3J = 13.36 Hz, 1H), 2.35 (s, 3H); ^{13}C NMR ($CDCl_3$, 100 MHz): δ (ppm) 164.0, 163.6, 161.7, 161.3, 155.1, 152.5, 149.9, 135.4, 132.6, 132.0, 129.3, 126.7, 125.5, 125.0, 122.5, 120.3, 118.2, 113.7, 112.5, 112.0, 109.5, 105.1, 101.6, 70.0, 67.1, 54.3, 46.1, 18.7; HRMS (ESI) Calcd. for $C_{28}H_{25}N_3O_6$ $[M+H]^+$ 500.1815 Found 500.1821.

Spectral data of 6-(benzylamino)-2-((2-hydroxy-3-((4-methyl-2-oxo-2*H*-chromen-7-yl)oxy)propyl)amino)-1*H*-benzo[de]isoquinoline-1,3(2*H*)-dione (22b):

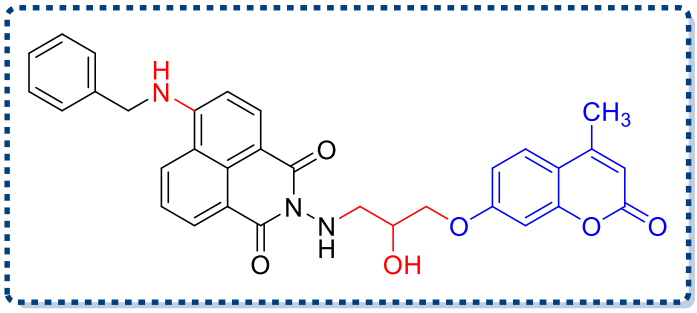

Yield: 80%; colour: bright yellow; m.pt: 255-257 ºC; ^{1}H NMR ($CDCl_3$, 400 MHz): δ (ppm) 8.58 (d, *J* = 7.32 Hz, 1H), 8.42 (d, *J* = 7.88 Hz, 1H), 8.21 (d, *J* = 8.36 Hz, 1H), 7.64 (t, *J* = 7.88 Hz, 1H), 7.47 (d, *J* = 8.92 Hz, 1H), 7.40 - 7.33 (m, 4H), 6.88 (d, ^{2}J = 8.88 Hz, ^{3}J = 11.24 Hz, 1H), 6.76 (d, *J* = 8.64 Hz, 1H), 6.72 (d, *J* = 2.16 Hz, 1H), 6.16 (s, 1H), 4.62 (s, 2H), 4.29 (s, 1H), 4.11 (d, *J* = 4.52 Hz, 2H), 4.29 (s, 1H), 4.11 (d, *J* = 4.52 Hz, 2H), 3.54 (t, *J* = 7.28 Hz, 1H), 3.40 (t, *J* = 9.40 Hz, 1H), 2.37 (s, 3H); ^{13}C NMR ($CDCl_3$, 100 MHz): δ (ppm) 164.0, 163.6, 163.0, 161.6, 154.7, 154.2, 136.5, 132.6, 129.2, 128.3, 127.7, 125.8, 125.2, 113.9, 113.0, 111.6, 105.5, 101.6, 69.7, 67.3, 53.7, 48.1, 18.8; HRMS (ESI) Calcd. for $C_{32}H_{27}N_3O_6$ $[M+H]^+$ 550.1979 Found 550.1975.

Spectral data of 6-(cyclohexylamino)-2-((2-hydroxy-3-((4-methyl-2-oxo-2*H*-chromen-7-yl)oxy)propyl)amino)-1*H*-benzo[*de*]isoquinoline-1,3(2*H*)-dione (22c):

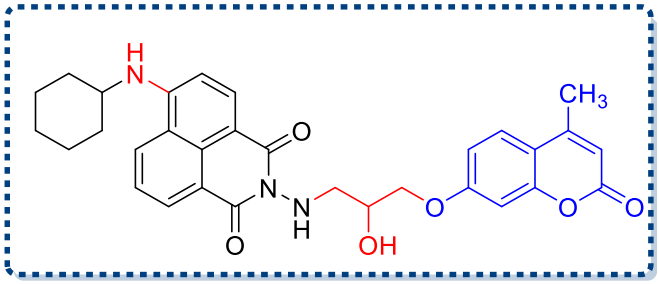

Yield: 75%; colour: pale yellow; m.pt: 245-247 ºC; ^{1}H NMR ($CDCl_3$, 400 MHz): δ (ppm) 8.61 (d, *J* = 7.12 Hz, 1H), 8.46 (d, *J* = 8.60 Hz, 1H), 8.12 (d, *J* = 8.36 Hz, 1H), 7.64 (t, *J* = 7.76 Hz, 1H), 7.44 (d, *J* = 8.84 Hz, 1H), 6.86 (dd, ^{2}J = 8.84 Hz, ^{3}J = 11.36 Hz, 1H), 6.78 – 6.73 (m, 2H), 6.09 (s, 1H), 4.11 – 4.04 (m, 3H), 3.63 (t, *J* = 3.41 Hz, 1H), 3.23 – 3.18 (m, 1H), 2.35 (s, 3H), 2.20 (d, *J* = 9.84 Hz, 2H), 1.88 (m, 2H), 1.75 – 1.72 (m, 1H), 1.62 (br(s), 3H), 1.52 – 1.42 (m, 3H); ^{13}C NMR ($CDCl_3$, 100 MHz): δ (ppm) 164.0, 161.7, 155.1, 152.6, 149.3, 135.6, 132.1, 129.7, 126.7, 125.5, 124.7, 122.5, 120.2, 113.8, 112.5, 112.0, 108.5, 104.9, 101.7, 70.1, 67.1, 54.4, 52.0, 32.8, 25.7, 24.9, 18.8; HRMS (ESI) Calcd. for $C_{31}H_{31}N_3O_6$ $[M+H]^+$542.2280 Found 542.2287.

Spectral data of 6-(butylamino)-2-((2-hydroxy-3-((4-methyl-2-oxo-2*H*-chromen-7-yl)oxy)propyl)amino)-1*H*-benzo[*de*]isoquinoline-1,3(2*H*)-dione (22d):

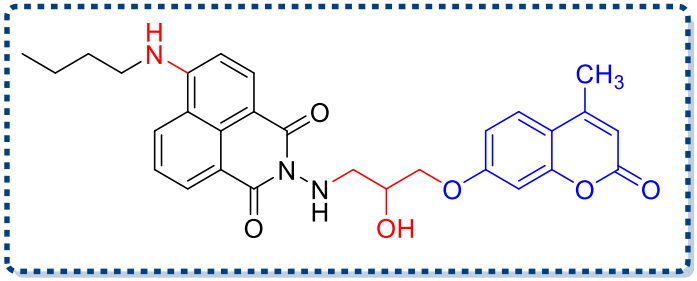

Yield: 79%; colour: yellow; m.pt: 243-245 ºC; ^{1}H NMR ($CDCl_3$, 400 MHz): δ (ppm) 8.60 (d, *J* = 7.28 Hz, 1H), 8.48 (d, *J* = 8.52 Hz, 1H), 8.14 (d, *J* = 8.20 Hz, 1H,), 7.64 (t, *J* = 7.56 Hz, 1H), 7.44 (d, *J* = 8.84 Hz, 1H), *J* = 7.56 Hz, 1H), 7.44 (d, *J* = 8.84 Hz, 1H), 6.86 (dd, ^{2}J = 8.84 Hz, ^{3}J = 11.36 Hz, 1H), 6.75 (d, *J* = 2.4 Hz, 1H), 6.73 (d, *J* = 8.60 Hz, 1H), 6.09 (s, 1H), 4.09 – 4.04 (m, 3H), 3.42 – 3.39 (m, 3H), 3.24 – 3.18 (m, 1H), 2.35 (s, 3H), 1.87 – 1.76 (m, 2H), 1.57 – 1.47 (m, 2H), 1.03 (t, *J* = 7.32 Hz, 3H); ^{13}C NMR ($CDCl_3$, 100 MHz): δ (ppm) 164.1, 161.4, 155.1, 152.6, 150.4, 135.7, 132.0, 129.4, 126.7, 125.7, 124.8, 122.5, 120.2, 113.8, 112.0, 108.9, 104.9, 101.7, 70.1, 67.1, 54.4, 43.6, 31.0, 20.4, 18.8, 13.9; HRMS (ESI) Calcd. for $C_{29}H_{29}N_3O_6$ $[M+H]^+$516.2130 Found 516.2131.

Spectral data of 6-(ethylamino)-2-((2-hydroxy-3-((4-methyl-2-oxo-2*H*-chromen-7-yl)oxy)propyl)amino)-1*H*-benzo[*de*]isoquinoline-1,3(2*H*)-dione (22e):

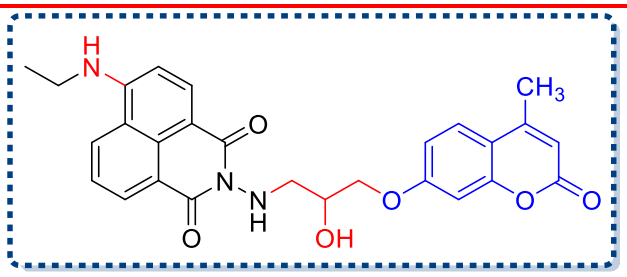

Yield: 89%; colour: reddish yellow; m.pt: 240-243 ºC; ^{1}H NMR ($CDCl_3$, 400 MHz): δ (ppm) 8.52 (d, *J* = 7.24 Hz, 1H), 8.38 (d, *J* = 8.60 Hz, 1H), 8.18 (d, *J* = 8.24 Hz, 1H), 7.60 (t, *J* = 7.72 Hz, 1H), 7.44 (d, *J* = 8.84 Hz, 1H), 6.86 (d, *J* = 7.40 Hz, 1H), 6.67 (d, *J* = 8.60 Hz, 2H), 6.16 (s, 1H), 4.39 (br(s). 1H), 4.12 (br(s), 2H), 3.62 (d, *J* = 12.16 Hz, 1H), 3.50 – 3.43 (m, 3H), 2.36 (s, 3H), 1.46 (t, *J* = 7.16 Hz, 3H); ^{13}C NMR ($CDCl_3$, 100 MHz): δ (ppm) 164.3, 163.5, 161.8, 161.4, 155.7, 153.3, 152.6, 134.5, 132.9, 132.0, 130.9, 125.5, 123.1, 122.4, 121.8, 113.8, 112.5, 112.0, 109.2, 108.7, 101.7, 70.1, 67.1, 54.4, 53.4, 26.2, 18.8; HRMS (ESI) Calcd. for $C_{27}H_{25}N_3O_6$ $[M+H]^+$488.1823 Found 488.1819.

Spectral data of 2-((2-hydroxy-3-((4-methyl-2-oxo-2H-chromen-7-yl)oxy)propyl) amino)-6-((2-hydroxyethyl)amino)-1H-benzo[de]isoquinoline-1,3(2H)-dione (22f):

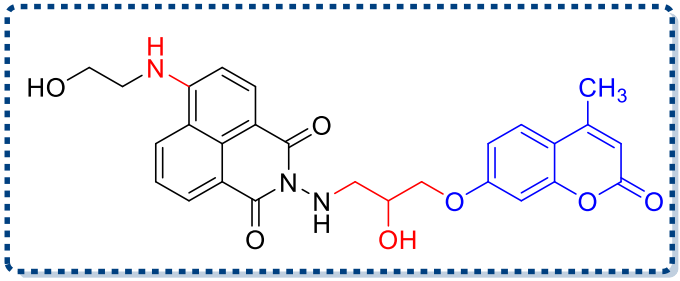

Yield: 72%; colour: bright yellow; m.pt: 270-272 ºC; ^{1}H NMR ($CDCl_3$ + DMSO-d_6, 400 MHz): δ (ppm) 8.63 (d, *J* = 8.36 Hz, 1H), 8.54 (d, *J* = 7.32 Hz, 1H), 8.38 (d, *J* = 8.52 Hz, 1H), 7.63 (t, *J* = 7.68 Hz, 1H), 7.49 (d, *J* = 8.88 Hz, 1H), 6.89 (d, *J* = 8.80 Hz, 1H), 6.80 (s, 1H), 6.75-6.70 (m,1H), 6.09 (s, 1H), 4.13 (br(s), 3H), 3.89 (br(s), 2H), 3.52 (d, *J* = 4.84 Hz, 2H), 3.40 – 3.33 (m, 2H), 2.39 (s, 3H); ^{13}C NMR ($CDCl_3$ + DMSO-d_6, 100 MHz): δ (ppm) 163.6, 163.2, 161.7, 161.2, 154.9, 152.7, 150.4, 135.3, 131.6, 129.1, 128.6, 125.5, 124.7, 121.8, 120.6, 113.5, 112.4, 111.6, 108.2, 103.2, 101.5, 70.1, 68.5, 60.6, 55.9, 44.4, 18.7; HRMS (ESI) Calcd. for $C_{27}H_{25}N_3O_7$ $[M+H]^+$ 504.1763 Found 504.1769.

Spectral data of 2-((2-hydroxy-3-((4-methyl-2-oxo-2*H*-chromen-7-yl)oxy)propyl)ami no)-6-((2-morpholinoethyl)amino)-1*H*-benzo[*de*]isoquinoline-1,3(2*H*)-dione (22g):

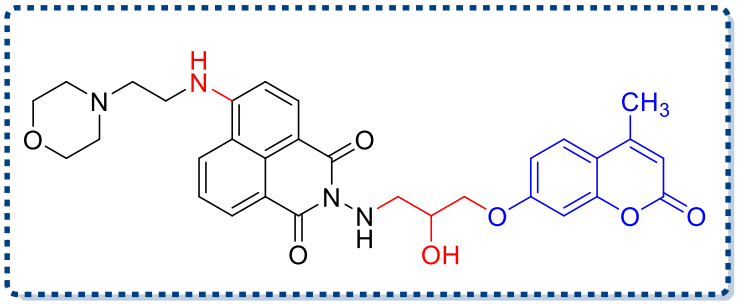

Yield: 76%; colour: bright yellow; m.pt: 253-255 ºC; ^{1}H NMR ($CDCl_3$, 400 MHz): δ (ppm) 8.55 (d, *J* = 7.40 Hz,1H),8.43 (d, *J* = 8.52 Hz, 1H), 8.28 (d, *J* = 8.36 Hz, 1H,), 7.60 (t, *J* = 7.36 Hz, 1H), 7.46 (d, *J* = 8.92 Hz, 1H), 6.89 (dd, ^{2}J = 9.92 Hz, ^{3}J = 12.52 Hz, 1H), 6.79 (d, *J* = 2.32 Hz, 1H), 6.60 (d, *J* = 8.56 Hz, 1H), 6.10 (s, 1H), 4.50 (t, *J* = 11.16 Hz, 2H), 4.13 – 4.08 (m, 3H), 3.90 (d, *J* = 7.16 Hz, 3H), 3.85 – 3.81 (m, 3H), 3.53 (td, ^{2}J = 11.56 Hz, ^{3}J = 22.92 Hz, 2H), 3.41 (t, *J* = 12.52 Hz, 3H), 3.24 – 3.19 (m, 1H), 2.38 (s, 3H); ^{13}C NMR ($CDCl_3$, 100 MHz): δ (ppm) 163.6, 163.2, 161.7, 161.2, 154.9, 152.7, 150.4, 135.3, 131.6, 129.1, 128.6, 125.5, 124.7, 121.8, 120.6, 113.5, 112.4, 111.6, 108.2, 103.2, 101.5, 70.3, 67.0, 66.9, 64.5, 61.2, 53.8, 29.6, 18.6; HRMS (ESI) Calcd. for $C_{31}H_{32}N_4O_7$ $[M+H]^+$ 573.2349 Found 573.2347.

Spectral data of 2-(4-ethylpiperazin-1-yl)-2-((2-hydroxy-3-((4-methyl-2-oxo-2H-chromen-7-yl)oxy)propyl)amino)-1*H*-benzo[*de*]isoquinoline-1,3(2*H*)-dione (22h):

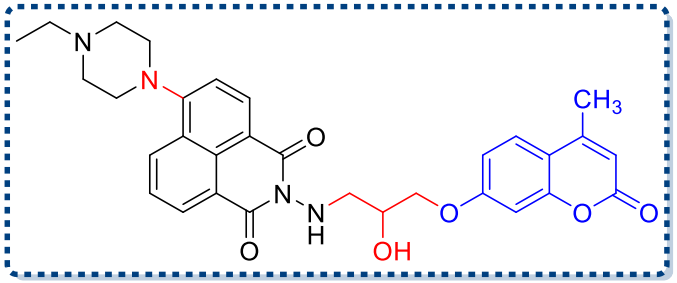

Yield: 88%; colour: yellow; m.pt: 256-259 ºC; ^{1}H NMR ($CDCl_3$, 400 MHz): δ (ppm) 8.65 (d, *J* = 7.16 Hz, 1H), 8.58 (d, *J* = 8.12 Hz, 1H), 8.47 (d, *J* = 8.24 Hz, 1H,), 7.75 (t, *J* = 7.88 Hz, 1H), 7.48 (d, *J* = 8.80 Hz, 1H), 7.25 (d, *J* = 8.16 Hz, 1H), 6.90 (dd, ^{2}J = 2.40 Hz, ^{3}J = 8.80 Hz, 1H), 6.81 (d, *J* = 2.36 Hz, 1H), 6.12 (s, 1H), 4.14 – 4.09 (m, 3H), 3.46 – 3.42 (m, 1H), 3.36 (br (s), 4H), 3.27 (t, *J* = 4.64 Hz, 1H), 2.80 (br(s), 4H), 2.62 (q, *J* = 7.16 Hz, 2H), 2.38 (s, 3H), 1.12(t, *J* = 7.20 Hz, 3H); ^{13}C NMR ($CDCl_3$, 100 MHz): δ (ppm) 163.9, 163.4, 161.6, 161.2, 156.9, 155.1, 152.4, 133.6, 131.9, 131.2, 129.4, 126.1, 125.7, 125.5, 122.6, 115.5, 115.0, 113.7, 112.4, 112.0, 101.6, 70.1, 67.1, 54.3, 53.1, 52.8, 52.4, 18.7, 12.0; HRMS (ESI) Calcd. for $C_{31}H_{32}N_4O_6$ $[M+H]^+$ 557.2416 Found 557.2418.

Spectral data of 2-((2-hydroxy-3-((4-methyl-2-oxo-2*H*-chromen-7-yl)oxy)propyl) amino)-6-(pyrrolidin-1-yl)-1*H*-benzo[*de*]isoquinoline-1,3(2*H*)-dione (22i):

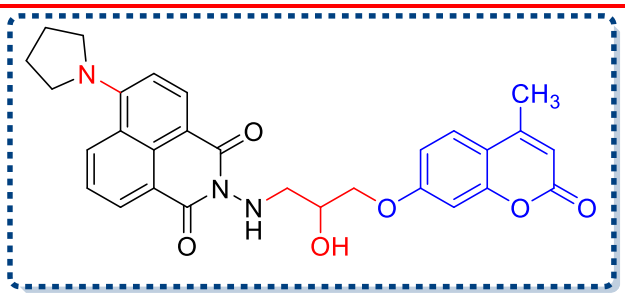

Yield: 81%; colour: bright yellow; m.pt: 240-243 ºC; ^{1}H NMR ($CDCl_3$, 400 MHz): δ (ppm) 8.61 (t, *J* = 8.40 Hz, 2H), 8.42 (d, *J* = 8.72 Hz, 1H), 7.55 (t, *J* = 8.44 Hz, 1H), 7.44 (d, *J* = 8.84 Hz, 1H), 6.86 (dd, ^{2}J = 8.84 Hz, ^{3}J = 11.36 Hz, 1H), 6.79 (d, *J* = 8.83 Hz, 1H), 6.76 (d, *J* = 2.44 Hz, 1H), 6.08 (s, 1H), 4.09 – 4.03 (m, 3H), 3.81 (t, *J* = 6.36 Hz, 4H), 3.43 – 3.39 (m, 1H), 3.24 – 3.18 (m, 1H), 2.34 (s, 3H), 2.12 – 2.08 (m, 4H); ^{13}C NMR ($CDCl_3$, 100 MHz): δ (ppm) 164.3, 163.5, 161.8, 161.4, 155.7, 153.3, 152.6, 134.5, 132.9, 132.0, 130.9, 125.5, 123.1, 122.4, 121.8, 113.8, 112.5, 112.0, 109.2, 108.7, 101.7, 70.1, 67.1, 54.4, 53.4, 26.2, 18.8; HRMS (ESI) Calcd. for $C_{29}H_{27}N_3O_6$ $[M+H]^+$ 514.1971 Found 514.1978.

Spectral data of 2-((2-hydroxy-3-((4-methyl-2-oxo-2*H*-chromen-7-yl)oxy)propyl) amino)-6-morpholino-1*H*-benzo[*de*]isoquinoline-1,3(2*H*)-dione (22j):

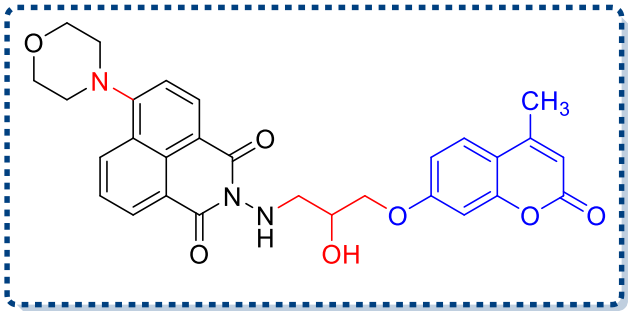

Yield: 83%; colour: light yellow; m.pt: 250-252 ºC; ^{1}H NMR ($CDCl_3$, 400 MHz): δ (ppm) 8.63 (d, *J* = 7.20 Hz, 1H), 8.57 (d, *J* = 8.08 Hz, 1H), 8.45 (d, *J* = 8.36 Hz, 1H), 7.74 (t, *J* = 7.84 Hz, 1H), 7.45 (d, *J* = 8.84 Hz, 1H), 7.24 (s, 1H), 6.86 (dd, ^{2}J = 8.84 Hz, ^{3}J = 11.36 Hz, 1H), 6.77 (d, *J* = 2.44 Hz, 1H), 6.09 (s, 1H), 5.78 (s, 1H), 4.66 (s, 1H), 4.10 – 4.05 (m, 3H), 4.02 (t, *J* = 4.04 Hz, 4H), 3.28 (t, *J* = 4.16 Hz, 4H), 2.35 (s, 3H); ^{13}C NMR ($CDCl_3$, 100 MHz): δ (ppm) 163.8, 163.4, 161.6, 161.2, 156.5, 155.1, 152.4, 133.5, 132.0, 131.0, 129.4, 126.1, 125.5, 122.7, 116.1, 115.1, 113.8, 112.4, 112.1, 101.7, 70.1, 67.2, 66.9, 54.3, 53.5, 18.7; HRMS (ESI) Calcd. for $C_{29}H_{27}N_3O_7$ $[M+H]^+$ 530.1919 Found 530.1924.

Spectral data of 2-((2-hydroxy-3-((4-methyl-2-oxo-2*H*-chromen-7-yl)oxy)propyl) amino)-6-(4-phenylpiperazin-1-yl)-1*H*-benzo[*de*]isoquinoline-1,3(2*H*)-dione (22k):

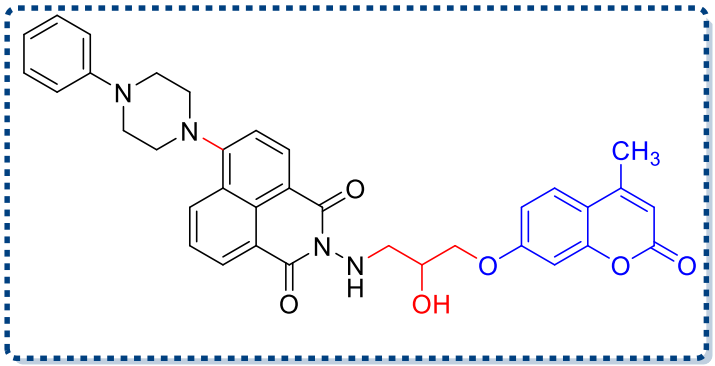

Yield: 85%; colour: reddish yellow; m.pt: 247-249 ºC; ^{1}H NMR ($CDCl_3$, 400 MHz): δ (ppm) 8.65 (dd, ^{2}J = 7.28 Hz, ^{3}J = 8.40 Hz, 1H), 8.59 (d, *J* = 8.12 Hz, 1H), 8.51 (dd, ^{2}J = 8.52 Hz, ^{2}J = 9.48 Hz, 1H), 7.76 (t, *J* = 8.28 Hz, 1H), 7.46 (d, *J* = 8.88 Hz, 1H), 7.34 – 7.28 (m, 3H), 7.04 (d, *J* = 7.96 Hz, 2H), 6.95 (t, *J* = 7.24 Hz, 1H), 6.87 (dd, ^{2}J = 8.92 Hz, ^{3}J = 11.32 Hz, 1H), 6.79 (d, *J* = 2.52 Hz, 1H), 6.11 (s, 1H), 4.11 – 4.04 (m, 3H), 3.50 – 3.40 (m, 9H), 3.25 – 3.20 (m, 1H), 2.36 (s, 3H); ^{13}C NMR ($CDCl_3$, 100 MHz): δ (ppm) 163.6, 161.7, 161.3, 156.7, 155.1, 152.6, 133.7, 132.2, 131.2, 129.4, 126.2, 126.0, 125.6, 122.7, 122.6, 116.5, 115.3, 112.5, 101.7, 70.1, 67.2, 54.4, 53.2, 49.6, 18.7; HRMS (ESI) Calcd. for $C_{35}H_{32}N_4O_6$ $[M+H]^+$ 605.2390 Found 605.2398.

Spectral data of 2-((2-hydroxy-3-((4-methyl-2-oxo-2H-chromen-7-yl)oxy)propyl) amino)-6-(4-(2-hydroxyethyl)piperazin-1-yl)-1H-benzo[de]isoquinoline-1,3(2H)-dione (22l):

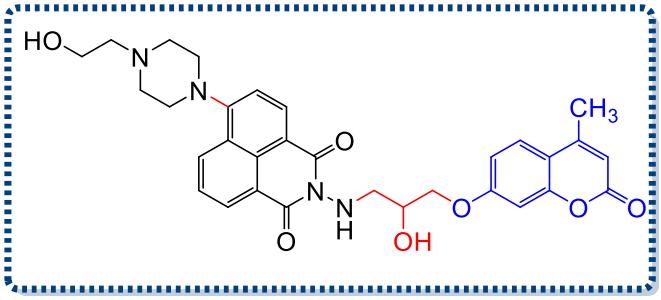

Yield: 70%; colour: dark yellow; m.pt: 260-263 ºC; ^{1}H NMR (DMSO-d_6 + $CDCl_3$, 400 MHz): δ (ppm) 8.50 – 8.45 (m, 2H), 8.41 (d, *J* = 8.12 Hz, 1H), 7.80 (t, *J* = 7.64 Hz, 1H), 7.56 (d, *J* = 8.72 Hz, 1H), 7.45 (d, *J* = 8.16 Hz, 1H), 6.89 – 6.84 (m, 2H), 6.11 (s, 1H), 4.21 (d, *J* = 8.20 Hz, 2H), 4.15 (dd, ^{2}J = 9.44 Hz, ^{3}J = 12.88 Hz, 2H), 4.01 – 3.98 (m, 4H), 3.95 (d, *J* = 4.84 Hz, 3H), 3.57 (br(s), 4H), 3.20 (m, 1H), 3.03 – 2.98 (m, 1H), 2.32 (s, 3H); ^{13}C NMR (DMSO-d_6 + $CDCl_3$, 100 MHz): δ (ppm) 162.5, 161.5, 160.6, 154.6, 152.6, 151.1, 134.9, 133.4, 131.1, 130.0, 129.0, 128.5, 128.1, 125.4, 123.9, 121.7, 120.3, 113.2, 112.1, 111.3, 110.3, 107.6, 103.8, 101.2, 70.4, 66.8, 59.2, 53.1, 45.9, 29.2, 18.4; HRMS (ESI) Calcd. for $C_{31}H_{32}N_4O_7$ $[M+H]^+$ 573.2351 Found 573.2358.

Spectral data of 2-((2-hydroxy-3-((4-methyl-2-oxo-2*H*-chromen-7-yl)oxy)propyl) amino)-6-(4-methylpiperazin-1-yl)-1*H*-benzo[*de*]isoquinoline-1,3(2*H*)-dione (22m):

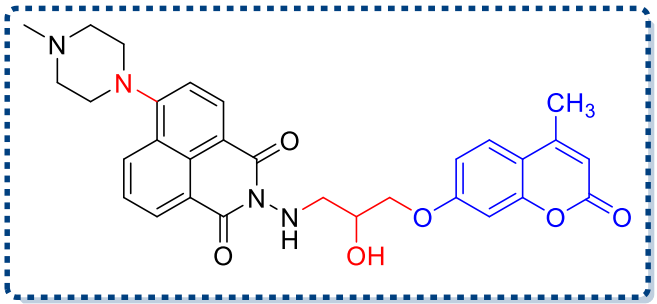

Yield: 90%; colour: brown yellow; m.pt: 242-244 ºC; ^{1}H NMR ($CDCl_3$, 400 MHz): δ (ppm) 8.61 (d, ^{2}J = 7.04 Hz, 1H), 8.54 (d, *J* = 8.08 Hz, 1H), 8.43 (d, *J* = 8.32 Hz, 1H), 7.71 (t, *J* = 7.88 Hz, 1H), 7.44 (d, *J* = 8.80 Hz, 1H), 7.25 – 7.20 (m, 1H), 6.86 (dd, ^{2}J = 8.64 Hz, ^{3}J = 11.00 Hz, 1H), 6.77 (d, *J* = 2.28 Hz, 1H), 6.08 (s, 1H), 4.11 – 4.06 (m, 3H), 3.42 (m, 1H), 3.31 (br(s), 4H), 3.22 – 3.18 (m, 1H), 2.73 (br(s), 4H), 2.42 (s, 3H), 2.39 (s, 3H); ^{13}C NMR ($CDCl_3$, 100 MHz): δ (ppm) 163.9, 163.5, 161.6, 161.2, 156.9, 155.1, 152.4, 133.6, 132.0, 131.2, 129.4, 126.1, 125.7, 125.5,

122.6, 115.6, 115.1, 113.8, 112.4, 112.0, 101.7, 70.1, 67.1, 55.0, 54.3, 53.0, 46.1, 18.7; HRMS (ESI) Calcd. for $C_{30}H_{30}N_4O_6$ $[M+H]^+$ 543.2276 Found 543.2278.

Spectral data of 2-((2-hydroxy-3-((4-methyl-2-oxo-2*H*-chromen-7-yl)oxy)propyl) amino)-6-(piperidin-1-yl)-1*H*-benzo[*de*]isoquinoline-1,3(2*H*)-dione (22o):

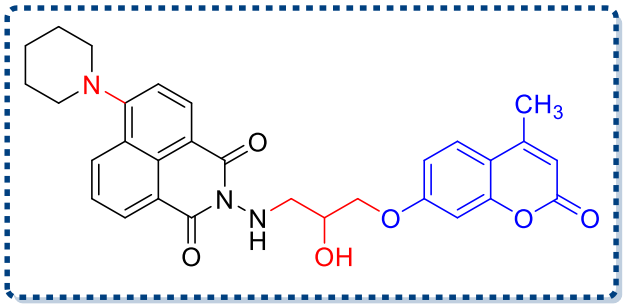

Yield: 73%; colour: yellow; m.pt: 241-244 ºC; ^{1}H NMR ($CDCl_3$, 400 MHz): δ (ppm) 8.61 (d, *J* = 6.72 Hz, 1H), 8.53 (d, *J* = 8.16 Hz, 1H), 8.41 (d, *J* = 8.40 Hz, 1H), 7.70 (t, *J* = 7.68 Hz, 1H), 7.45 (d, *J* = 8.80 Hz, 1H), 7.18 (d, *J* = 8.20 Hz, 1H), 6.87 (dd, ^2J = 8.84 Hz, ^3J = 11.20 Hz, 1H), 6.78 (d, *J* = 2.40 Hz, 1H), 6.10 (s, 1H), 4.72 (s, 1H), 4.10 – 4.05 (m, 3H), 3.43 – 3.39 (m, 1H), 3.26 (m, 4H), 2.39 (s, 3H), 1.90 – 1.82 (m, 4H), 1.73 (d, *J* = 5.00 Hz, 2H); ^{13}C NMR ($CDCl_3$, 100 MHz): δ (ppm) 164.1, 161.7, 158.3, 155.1, 152.6, 133.8, 132.0, 131.6, 129.6, 126.2, 125.6, 122.5, 114.9, 113.8, 112.5, 112.1, 101.7, 70.1, 67.1, 54.4, 54.4, 26.2, 24.4, 18.8; HRMS (ESI) Calcd. for $C_{30}H_{29}N_3O_6$ $[M+H]^+$ 528.2130 Found 528.2134.

Summary of chapter 4

Cancer and bacterial diseases are spreading around the globe at an alarming rate, and the development of resistance by cancer and bacterial cells to present marketed drugs poses a serious health issue among people and thus leads to difficulty in the treatment of diseases. So, in view of the above condition, we have purposely designed and synthesized two different series of naphthalimides and coumarins with triazole (**18a-18n**) and alkyl chain (**22a-22o**) as linker and evaluated them for their biological activities towards human cancer cell lines and bacterial strains.

Naphthalimide and coumarin with triazole linker exhibited its most promising results in suppressing the growth of cancer cells. Significantly, compounds **18a, 18b, 18e**, and **18f** displayed the most potent results at one dose concentration of 10 μM and were further evaluated at five dose concentrations (0.01 to 100 µM). These four compounds exhibited cytostatic and cytotoxic effects against cancer cells with low GI_{50} values of 3.18 μM (**18a**), 13.11 μM (**18b**), 7.68 μM (**18e**), and 1.75 μM (**18f**). Further, mechanistic exploration revealed that these compounds selectively bind with G4-DNA over ds-DNA to exert their anticancer activity. This compound stabilizes the G4-DNA in the promoter region, causing the inhibition of cancer cells.

In comparison, naphthalimide linked to coumarin *via the* alkyl chain exhibited its most promising results in inhibiting the growth of bacterial strains. Significantly, compounds **22e** and **22h** displayed excellent antibacterial activity in most of the tested bacterial strains and outperformed marketed drugs. These drug candidates efficiently suppressed the biofilm formation and disrupted the biofilm virulence factor responsible for the formation of strong biofilm. Both the compounds exhibited rapid bactericidal properties, delaying the development of drug resistance upto 20 passages. Further, bio-functional evaluation indicated that both compounds **22e** and **22h** efficiently disrupted the membrane integrity of the cell, leading to accumulation of excessive ROS inside cells and causing oxidative damage of the cells. Further, both compounds bound readily with DNA to obstruct the DNA replication process, leading to bacterial death. The active compounds **18a, 18b, 18e, 18f, 22e** and **22h** have ability to bind with serum albumin and can be transported to target site easily.

Thus, concluding our finding, the results obtained inferred that these newly synthesized naphthalimide-coumarin derivatives exhibited excellent result in inhibiting the cancer and bacterial growth and have the potential to be taken to clinical trials for their development as anticancer and antibacterial agents.

Chapter 5

Naphthalimide-triazine conjugates as an effective antibacterial agent

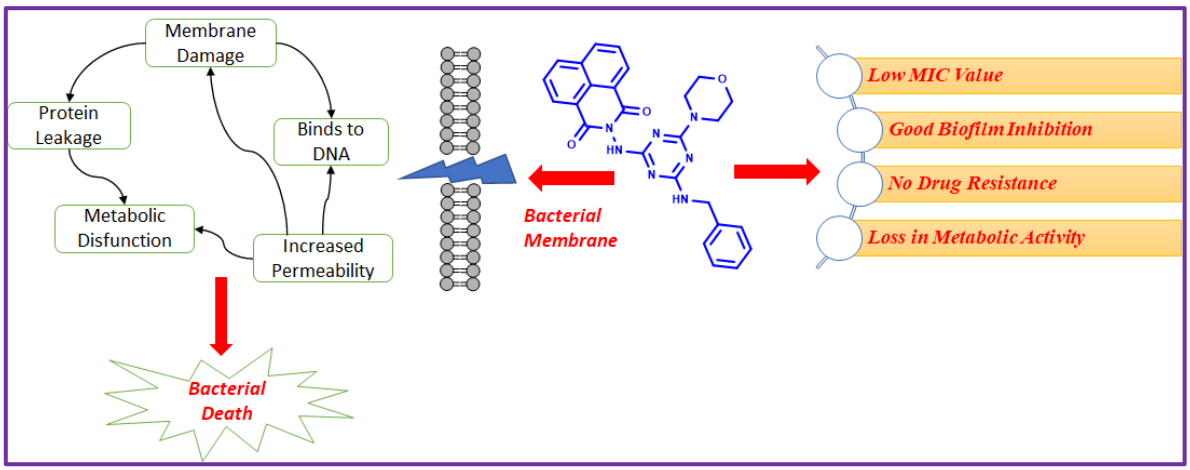

5.1 Introduction

Currently, people are significantly affected by communicable infectious diseases caused by various bacterial pathogens, leading to higher death rates worldwide.[188] The efficiency of drugs exhibiting antibacterial activity is limited due to the fast occurrence of resistance to target bacteria.[189] The wide range of development of drug resistance to diseases caused by bacteria has become a severe public health issues.[190] The ESKAPE pathogens (*Enterococcus facelis*, *Staphylococcus aureus*, *Klebsiella pneumonia*, *Acinetobacter baumannii*, *Pseudomonas aeruginosa*, and *Enterobacter species*) are responsible for infections worldwide.[191] Various factors led to changes in microbial genomes that cause acute resistance to already present antibiotics. Excessive use of antibiotics can sharply increase the occurrence of genotype resistance.[192] Many clinical reports showed that multi-drug-resistant microorganisms are increasing day by day, leading to search for new antibacterial agents. Efforts have been made by medical science in past decades to develop a class of analogues that is more effective against resistant bacterial infections.

However, many pharmaceutical companies are leaving this area due to economic reasons. A new class of antibacterial agents is needed as many bacterial strains are resistant to existing antibiotics.[193] Therefore, there is an urgent need to build new therapeutics to show more efficiency toward microbial targets. In search of new analogues as antibacterial agents, heterocyclic moieties have gained significant importance in pharmaceutical chemistry.[14]

5.2 Designing of the target molecules

In recent years, 1,3,5 triazine moiety has become an important scaffold due to excellent biological properties.[194] Thus, this scaffold is widely used for designing new biologically important structures with well-known medicinal properties such as antibacterial, analgesic, antifungal, antiprotozoal anti-malignant antiviral, herbicidal, anti-inflammatory and many more.[195] Various research groups have reported 1,3,5-triazine analogues as effective antibacterial agents with potent inhibitory activity against many pathogenic organisms.[196]

Naphthalimide is an another pharmacophore that exhibits antibacterial properties, and it is considered as the main backbone for the development of membrane targeting antibacterial agents having low potential for drug resistance. The alterations in N- and 4-positions of the naphthalimide moiety helps in building new antibacterial agents with improved bioactivity.[197] Naphthalimide is also reported as a well-known DNA intercalator, so we thought of combining naphthalimide with a triazine core to investigate the synergetic antibacterial

effects. Considering the above-mentioned factors, we have designed new antibacterial agents using the scaffolds of triazine, naphthalimide, and morpholine, and further derivatization was furnished *via* nucleophilic substitution on the triazine ring using various substituted primary and secondary amines. Herein, we have developed a hybrid of two active biological moieties, *i.e.*, triazine and naphthalimide. Various primary and secondary amines were substituted on the triazine ring as these may enhance the water solubility and modulates the pharmacokinetics properties of the structure. These may also use in study the effect of various amines on the biological activity of the designed molecules and to develop the structure-activity relationship (**Figure 5.1**). All the synthesized derivatives were tested for their antibacterial properties towards eight bacterial strains; four gram-positive and four gram-negative strains.

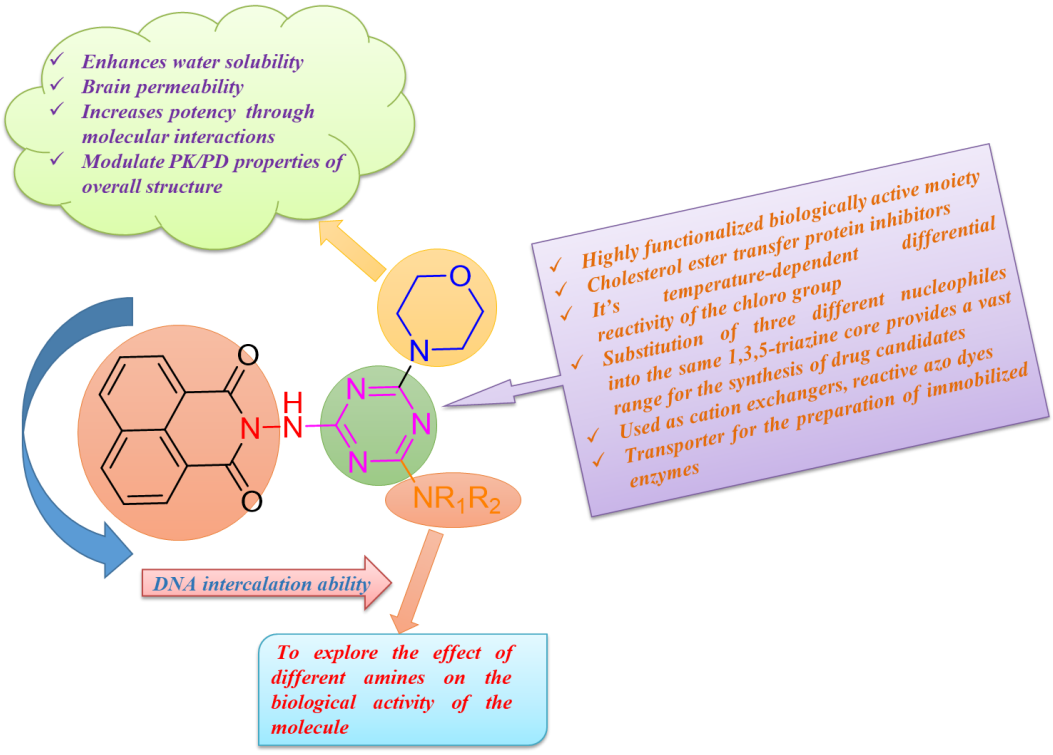

Figure 5.1: Designing of the desired molecules

5.3 Chemistry

The synthetic route for building conjugates of naphthalimide and 1,3,5-triazine is depicted in **Scheme 5.1**. Initially, the benzo[*de*]isochromene-1,3-dione (**2**) was prepared by reacting commercially available acenaphthene (**1**) with sodium dichromate in the presence of acetic acid under reflux condition. Compound **10** was prepared by reacting benzo[*de*]isochromene-1,3-dione (**2**) with hydrazine hydrate in ethanol at room temperature. Further, 2-((4,6-

dichloro-1,3,5-triazin-2-yl)amino)-1*H*-benzo[*de*]isoquinoline-1,3(2*H*)-dione (**24**) was achieved by nucleophilic substitution of commercially available 1,3,5-triazine (**23**) with 2-amino-1*H*-benzo[*de*]isoquinoline-1,3(2*H*)-dione (**10**) in the presence of isopropyl alcohol at room temperature. The reaction of cyanuric chloride is proved to be temperature and time-dependent. Due to the bulky group of naphthalimide, the reaction did not proceed at 0 ºC, but only monosubstituted product was formed at room temperature in the absence of any base, and on heating, traces of disubstituted product was also obtained. The product was purified by column chromatography using chloroform and ethyl acetate as eluents. The synthesis of compound **25** was achieved by reacting **24** with morpholine using isopropyl alcohol. The reaction was carried out at room temperature for 3 h, where monosubstituted and disubstituted products were formed in the ratio of 95:5, but when the reaction proceeded for more than 3 h at room temperature, both monosubstituted and disubstituted products were formed in equal ratio (50:50). The appearance of two multiplets of 2H each at δ 3.87 – 3.83 and 3.73 – 3.69 corresponding to CH_2 morpholine and a multiplet at δ 3.54 – 3.43 of 4H corresponding to CH_2 morpholine and six protons in the aromatic region corresponding to naphthalimide in ^{1}H NMR spectrum confirmed the formation of compound **24**. Finally, derivatives **26a-s** were prepared by reacting 2-((4-chloro-6-morpholino-1,3,5-triazin-2-yl)amino)-1*H*-benzo[*de*]isoquinoline-1,3(2*H*)-dione (**25**) with various primary and secondary amines in the presence of isopropyl alcohol at reflux temperature. ^{1}H NMR of compound **26a** showed an increase in signals due to the allyl group present at triazine. Multiplet at δ 5.89 – 5.76 of one proton of CH allyl, doublet of doublets at δ 5.14 due to two protons of CH_2 allyl and a broad singlet of 2H at δ 3.91 due to CH_2 allyl confirmed the formation of compound **26a**. The appearance of a new signal at δ 43.3 ppm in ^{13}C NMR spectrum and the increase of molecular weight to m/z 432.18 also confirmed the formation of compound **26a**. Similarly, all the products (**26b-s**) were characterized by ^{1}H NMR, ^{13}C NMR, and mass spectrometry. All the derivatives were synthesized in good yields ranging from 65% to 76%.

Scheme 5.1. Synthesis of 2-((4-amino(substituted)-6-morpholino-1,3,5-triazin-2-yl)amino)-1*H*-benzo[*de*]isoquinoline-1,3(2*H*)-dione

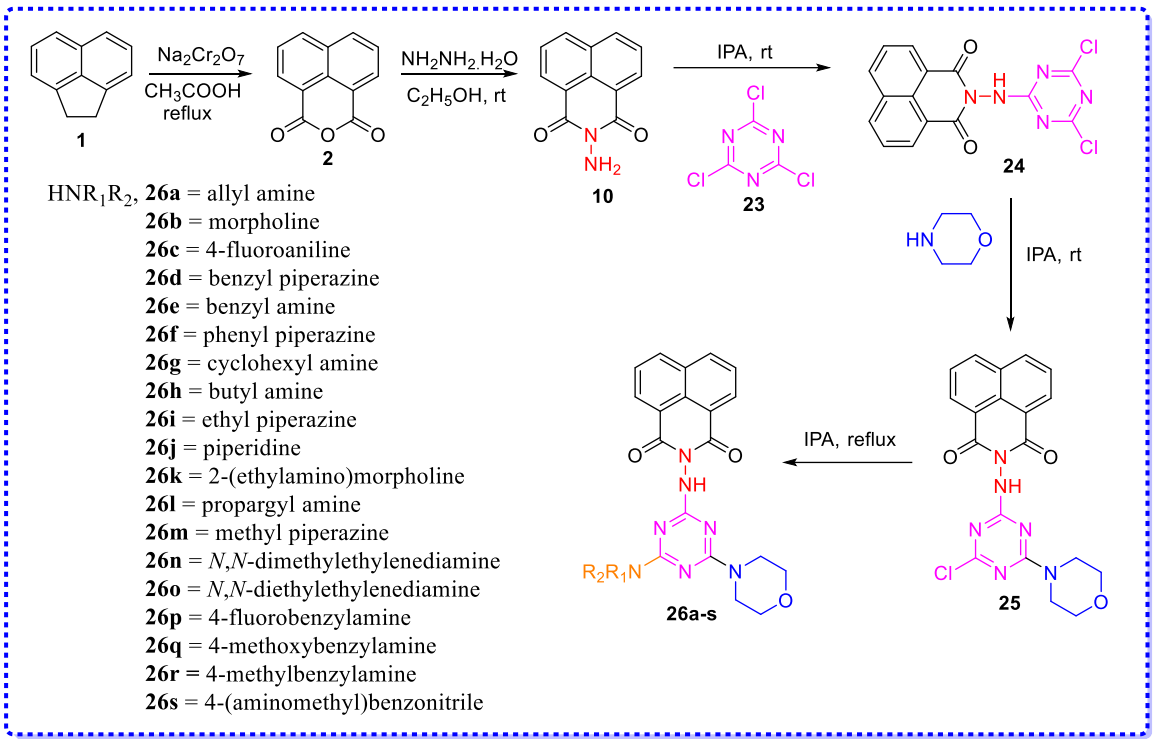

5.4. *In vitro* antibacterial activity

All synthesized derivatives were evaluated for their antibacterial activity against four gram-positive bacterial strains *viz. Staphylococcus aureus*, *Enterococcus faecalis*, *Bacillus subtilis*, *Listeria sp.*, and four gram-negative strains such as *Escherichia coli*, *Salmonella enterica*, *Acinetobacter calcoaceticus*, *Serratia marcescens*. Some compounds displayed higher activity than reference drugs (chloromycin and amoxicillin) in inhibiting bacterial growth, indicating that these new compounds can overcome infectious bacteria efficiently (**Table 1**). A two-fold serial broth dilution method in 96-well micro-test plates, as recommended by the National Committee for Clinical Laboratory Standards (NCCLS), was adopted to test the antibacterial activities of the prepared compounds.[90,91] Of all the derivatives, compounds **26a–d** displayed no significant antibacterial properties against most tested bacterial strains (MIC > 25 μg/ml), although **26b** and **26d** inhibited the growth of *Staphylococcus aureus* and *Listeria sp* with low MIC values of 1.56 and 6.25 μg/ml, respectively. Surprisingly, the benzylamine-substituted triazine (**26e)** significantly affected the growth of bacterial strains. Compound **26e** was chosen with the most promising results against all the tested gram-positive bacteria, with MIC values ranging from 0.003 - 1.56 μg/ml. Compound **26e** also showed better activity than the marketed drugs amoxicillin and chloromycin with most bacterial strains. Compounds **26f** and **26g** limited the bacterial growth of *Listeria sp.* and *Enterococcus faecalis* at low concentrations of 0.39 μg/ml and 3.12 μg/ml, respectively. Compound **26h** showed potent activity against the tested bacterial strain *Enterococcus*

faecalis with MIC value of 0.09 μg/ml and was 17 and 34-folds more active than amoxicillin and chloromycin. Compound **26i** with ethyl piperazine selectively inhibits the growth of *Listeria sp.* with MIC value of 3.12 μg/ml. Derivatives **26j, 26k,** and **26l** displayed good to moderate activities against the tested bacterial strains. These compounds showed promising results against *S. aureus, Listeria sp.*, and *E. faecalis* with MIC values of 1.56, 0.048, and 0.048 μg/ml, respectively. Compounds **26m** and **26o** displayed the most promising results towards *Listeria sp.* with low MIC values of 0.006 and 0.19 μg/ml, respectively. Compound **26e** was chosen as a representative molecule for detailed examination in light of its potent antibacterial effect. Further, any substitution on the benzene ring of benzylamine resulted in decrease in bioactivity, compared to parent compound **26e**. Compound **26p** having 4-fluoro benzylamine showed low potency against most of the tested bacterial strains. It could suppress the bacterial growth of *E. faecalis* with a low concentration of MIC value of 6.25 μg/ml. Compound **26q,** having 4-methoxy benzylamine, showed better activity than compound **26p** but less activity than lead compound **26e** due to the presence of electron donating group. Compound **26q** inhibited the bacterial growth of gram-positive bacterial strains with MIC values of 3.125 μg/ml and 6.25 μg/ml against *E. faecalis* and *S. aureus*, respectively. Replacement of methoxy group in the benzylamine with methyl group resulted in loss of bioactivity of the compound. Further, introducing electron-withdrawing group (**26s**) on benzylamine also revealed loss of bioactivity of compound. Thus, any substitution on the benzene ring of benzylamine resulted in loss of bioactivity compared to parent compound **26e**.

Table 1. Antibacterial activity data as MIC (μg/ml) for compounds **8a-p**

Comp	Gram Positive Bacterial Strains				Gram Negative Bacterial Strains			
	E. faecalis	***B. subtilis***	***L. species***	***S. aureus***	***E. coli***	***S. enterica***	***A. calcoaceticus***	***S. marcescens***
26a	100	**50**	100	**25**	200	200	100	200
26b	200	100	200	**1.56**	200	100	200	200
26c	200	200	NA	**50**	400	200	200	200
26d	200	200	**6.25**	100	200	200	200	**50**
26e	**0.003**	**3.125**	**6.25**	**1.56**	100	200	200	100
26f	200	**50**	**0.39**	100	NA	200	200	**50**
26g	**3.12**	**50**	**25**	100	200	200	200	200
26h	**0.09**	**25**	200	**12.5**	400	100	200	200
26i	200	200	**3.12**	**50**	100	200	200	100
26j	NA	**6.25**	**50**	**1.56**	400	200	200	200
26k	200	200	**0.048**	**3.12**	100	200	200	**50**
26l	**0.048**	**25**	200	**50**	100	100	200	200

26m	200	200	**0.006**	**1.56**	100	200	200	**12.50**
26n	200	200	**50**	100	200	100	100	**25**
26o	200	**50**	**0.19**	100	200	200	200	**12.50**
26p	**6.25**	100	200	25	100	200	100	200
26q	**3.125**	**12.5**	**50**	**6.25**	200	100	100	200
26r	50	**12.5**	**25**	**12.5**	200	200	100	100
26s	100	**400**	**200**	100	200	400	100	**200**
A	**1.56**	**50**	**50**	**25**	100	200	**50**	**1.56**
B	**3.125**	**1.56**	**1.56**	**3.125**	**3.125**	**50**	**3.25**	**1.56**

A - amoxicillin; B - chloromycin; NA. - not active

5.5. Bactericidal or bacteriostatic action

Once the Minimum Inhibitory Concentration (MIC) was calculated for the synthesized compounds, we were also interested to know the mode of action of most active compound **26e** toward bactericidal or bacteriostatic activity. We have calculated the Minimal Bactericidal Concentration (MBC) of **26e** against *Enterococcus faecalis* and *Staphylococcus aureus* (**Table 2**). The results depicted that compound **26e** has shown MBC/MIC values greater than 32 with *E. faecalis,* indicating bacteriostatic action, whereas bactericidal activity was demonstrated with *S. aureus.* Thus, the tested compound **26e** exhibited both bactericidal and bacteriostatic actions against resistant and sensitive bacterial strains.

Table 2. Comparison of MIC and MBC values of active compound **26e**

Bacterial Strains	**MBC (μg/ml)**	**MIC (μg/ml)**	**MBC/MIC**
Enterococcus faecalis	0.19	0.003	≥32
Staphylococcus aureus	3.25	1.56	2

5.6. Time-killing kinetics of *Staphylococcus aureus*

For a compound to exist as a potent antibacterial agent, it must possess rapid bactericidal performance. A bacterial reduction assay for *S. aureus* was carried out to examine the efficacy of compound **26e** in killing the cell as a function of time.[106] The time-kill assay of *S. aureus* was performed for 6 h with variable concentrations of compound **26e** (MIC, ½ MIC, ¼ MIC). The absorbance of untreated bacteria increases with time, indicating the bacterial growth of *S. aureus,* whereas the absorbance value of treated cells decreases with time, displaying the bactericidal action. The difference in number of bacteria cells in the inoculum can explain the decrease in absorbance value of control upon incubating with compound. **Figure 5.2a** showed that the absorbance value of treated bacterial cells with compound **26e** at MIC concentration started decreasing within 1 h, indicating the fast-bactericidal nature of compound. Even at sub-

MIC, the compound could kill the bacteria at a concentration of ½ MIC; the absorbance started decreasing within 2 h, indicating its bactericidal nature. At ¼ MIC, the compound could inhibit bacterial growth for first 3 h, after which bacteria start growing. Thus, these results depicted that derivative **26e** effectively kills the bacterial cells in the inoculum in a dose-depended mode, leading to reduced time for treatment of bacterial infections and, thus, hampering the development of bacterial resistance.

5.7. Multipassage drug resistance assay

The development of resistance to the present antibiotics decreases their effectiveness and service life, imposing severe health issues on the public. The low ability to develop resistance is a crucial property of drug candidates.[169] The multi-passage assay was employed to determine the potential of compound **26e** to resist induction of resistance against *S. aureus* taking chloromycin as a positive control. **Figure 5.2b** showed that the MIC value of naphthalimide-triazine (**26e**) did not observe any significant change even after 11 passages, indicated that *S. aureus* has low ability to develop resistance against the tested compound. In contrast, the MIC value of chloromycin was increased 32-fold after 11 passages. Thus, compound **26e** exhibited better results than the standard chloromycin, which implies a promising therapeutic potential.

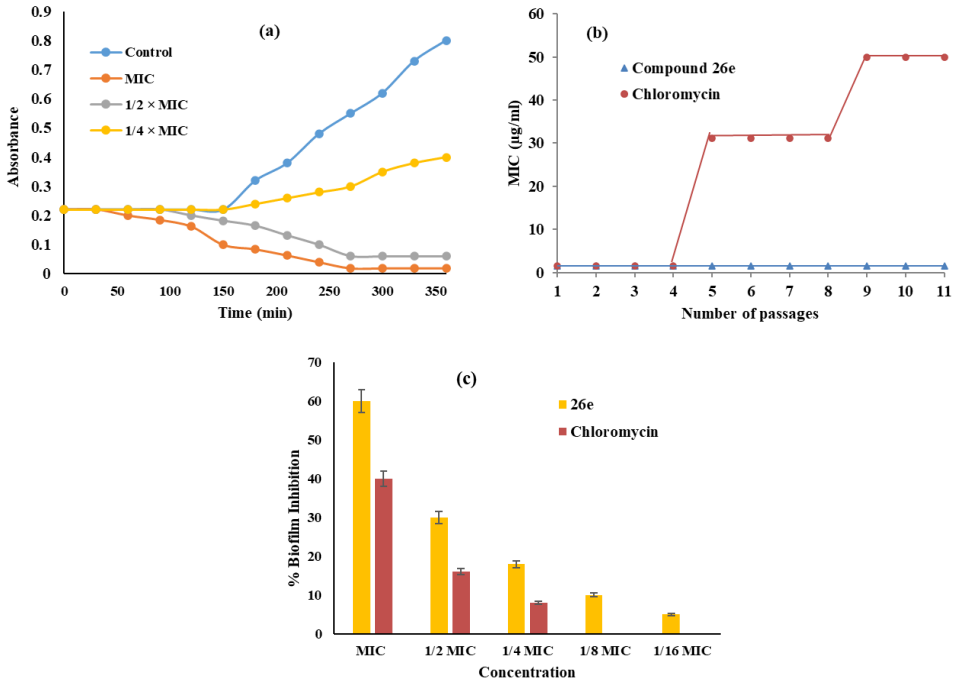

Figure 5.2. (a) Time killing kinetics of *S. aureus* with compound **26e** at different concentrations, (b) multi-passage drug resistance assay for compound **26e** and standard drug chloromycin against *S.aureus*, and (c) Inhibition of biofilm of *S. aureus* in the presence of compound **26e** at different concentrations (MIC – 1/16 MIC).

5.8. Anti-biofilm assay

After carrying out the time kill and multi-passage assay for compound **26e,** we were keen to know the potential of a new active candidate to inhibit biofilm formation. Bacterial resistance is facilitated by forming biofilm, affecting the bactericidal property of the antibacterial agents.[170] These biofilms create a challenging issue to eradicate the infectious biofilm population with antibiotics, thus weakening the therapeutic properties of drugs.[171] *S. aureus* is a biofilm-growing bacteria that is difficult to remove; therefore, there is an utmost requirement for new drugs that can inhibit biofilm formation. Crystal violet assay was implemented to examine the ability of compound **26e** to inhibit biofilm formation. We exposed variable concentrations of compounds ranging from MIC to 1/16 MIC to three days old grown biofilm of *S. aureus,* as represented in **Figure 5.2c**. The results demonstrated that compound **26e** could inhibit biofilm formation up to 60% at MIC value. Furthermore, the compound inhibited biofilm formation up to 30% at 1/2 MIC value. Good biofilm inhibition potential was observed at very low MIC values, i.e., 1/8 MIC and 1/16 MIC (10% and 5%, respectively), indicated that the compound interferes with the growth process of *S. aureus* even at very low concentrations. Thus, compound **26e** showed the most promising inhibitory effect on *S. aureus* biofilm and helped in delay bacterial resistance. The chloromycin was able to inhibit the biofilm formation up to 1/4 MIC, but at a concentration lower than 1/4 MIC value, it was unable to inhibit the biofilm growth. On the other hand, compound **26e** inhibited the biofilm formation even at very low concentrations, i.e., up to 1/16 MIC value.

5.9 Membrane disruption

Destruction of the membrane's integrity is an efficient way to cause cell death, as the cell membrane plays a vital role in maintaining the metabolic balance by preventing the entrance of extracellular substances into the cell.[175] Further, any damage caused to the cell membrane with compound **26e** was examined to explore its antibacterial mechanism.

5.9.1 Outer membrane disruption

S. aureus doesn't have an outer membrane; instead, it contains a thick cell wall of peptidoglycan, which is hard to penetrate and facilitates drug resistance. The permeabilization of this cell wall is vital to building a potent antibacterial agent. The ability of compound **26e** to penetrate the bacteria cell wall was evaluated using 1-*N*-phenylnaphthylamine (NPN). Upon interacting with peptidoglycan of *S. aureus,* NPN gave fluorescence which gradually decreased upon incubating with compound **26e** in a concentration and time-dependent manners. **Figures 5.3a** and **5.3b** revealed that compound **26e** effectively penetrates the thick bacterial cell wall, reducing bacterial resistance. The fluorescent intensity decreased more when treated with

compound **26e** than chloromycin. Thus, compound **26e** has greater potential to penetrate the thick cell wall than chloromycin.

5.9.2 Inner membrane disruption

In the case where antimicrobial agents kill bacteria by damaging the integrity of cell membrane, there is a low propensity for developing drug resistance.[180] An inner membrane assay was employed to examine the ability of compound **26e** to penetrate and damage the inner membrane of *S. aureus*. Ethidium bromide (EtBr) is a dye that enters the damaged cell membrane and produces fluorescence upon binding with DNA. *S. aureus* cells were incubated with increasing concentrations of compound **26e** and a known concentration of EtBr dye. **Figures 5.3c** and **5.3d** show that the fluorescence intensity increases in a concentration and time-dependent manners, suggesting the elevation in the percentage of cells with damaged membranes. The results demonstrated that compound **26e** can effectively damage the inner membrane, leading to bacterial death. The increase in fluorescent intensity was even more when treated with compound **26e** than chloromycin. Thus, compound **26e** has a more significant potential to damage the inner membrane than chloromycin leading to cell death.

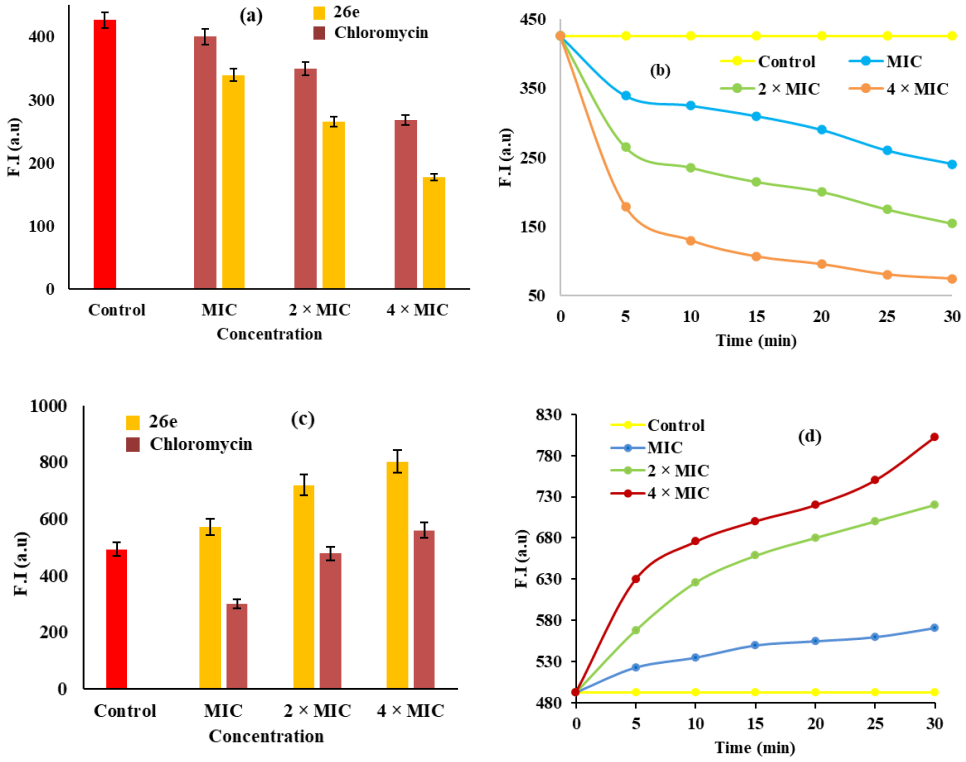

Figure 5.3. Outer membrane permeabilization of *S. aureus* with compound **26e** (a) at different concentrations, and (b) in a time-dependent mode, and inner membrane permeabilization of *S. aureus* with compound **26e,** (c) at different concentrations, and (d) in a time-dependent mode

5.10 Leakage of intercellular protein

Bacterial cytoplasmic contents are released from the cells upon disrupting the cell membrane.[181] Leakage of protein from the cell incubated with naphthalimide-triazine analogue **26e** was determined to verify the cell membrane damage. **Figure 5.4a** shows an elevation in the concentration of leaked protein with increasing concentrations of compound **26e**. The concentration of leaked protein was much higher when treated with **26e** than the reference drug chloromycin. The results obtained from the protein leakage assay followed the membrane permeability, thus confirming the damage of *S. aureus* membrane by compound **26e**.

5.11 Metabolic activity

The normal metabolic activity is related to the protein on the cell membrane.[182] Protein denaturation in the cells occurs due to cell membrane damage, leading to metabolic dysfunction. Resazurin, a purple non-fluorescent dye in an oxidized state, is reduced to pink fluorescence with functionally active enzymes in the viable cells. Alamar blue dye assay was employed to examine the effect of compound **26e** on bacterial metabolism. **Figure 5.4b** shows that the metabolic activity of *S. aureus* cells decreases with increasing concentrations of compound **26e**; thus, membrane destruction leads to loss in metabolic activity. The loss in metabolic activity of *S. aureus* when treated **26e**, was much higher than the reference drug chloromycin.

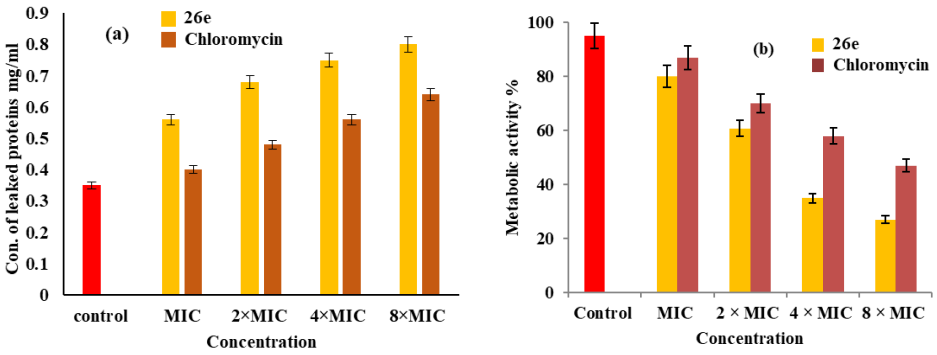

Figure 5.4. (a) Protein leakage from *S. aureus* and (b) metabolic activity of *S. aureus* in the presence of compound **26e**

5.12 Change in morphology of *S. aureus* cells

To confirm the damage caused to the cell membrane, a Scanning Electron Microscope (SEM) was employed to see the changes in the morphology of *S. aureus* incubated with compound **26e**. **Figure 5.5a** represents the SEM images of untreated *S. aureus* cells, indicating the regular and circular surfaces. The cell membrane was broken in the presence of compound **26e (**2 × MIC) (**Figures 5.5b** and **5.5c**). Disruption of the cell membrane caused the leakage of cellular

contents from the cells, leading to corrugation, which confirmed the cleavage of cell and membrane permeability on treatment with compound **26e**. When cells were treated with the reference drug chloromycin, corrugation was seen around the *S. aureus*, and leakage of cellular contents was also observed (**Figure 5.5d)**, but the results were better, and disruption of cell wall clearly seen when the *S. aureus* were treated were compound **26e.**

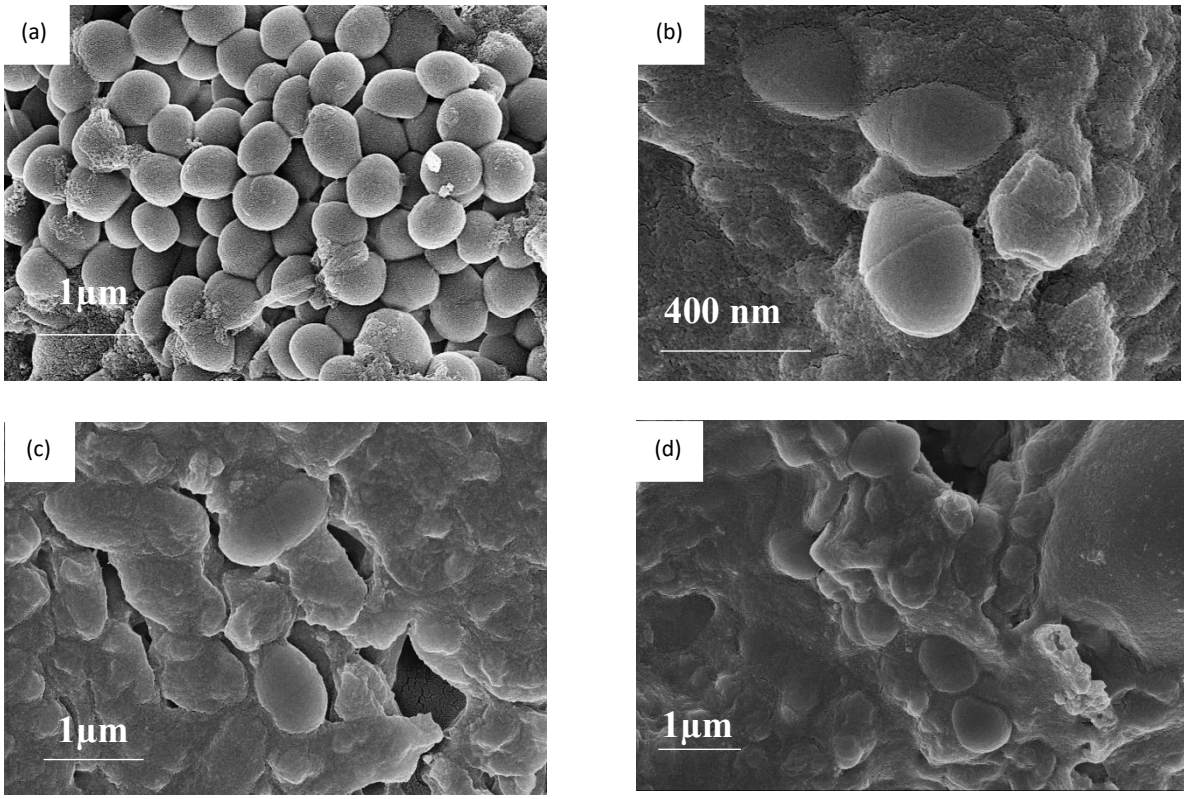

Figure 5.5. SEM micrographs of (a) untreated *S. aureus*, (b) and (c) treated *S. aureus* with compound **26e** at 2 ×MIC, and (d) chloromycin at 2 ×MIC

5.13 Cytotoxicity toward normal cell lines

To determine the cytotoxicity of the most active compounds **26e** against Hek293 non-cancerous human cell lines, an MTT assay was employed. It has been revealed that compound **26e** showed only 13.4%, 12.2%, 11.8%, 10.5%, and 9.01% cytotoxicity to normal cell lines (**Figure 5.6**). The low cytotoxicity value of compound **26e** against normal cell lines indicated that these compounds could selectively kill cancer cells.

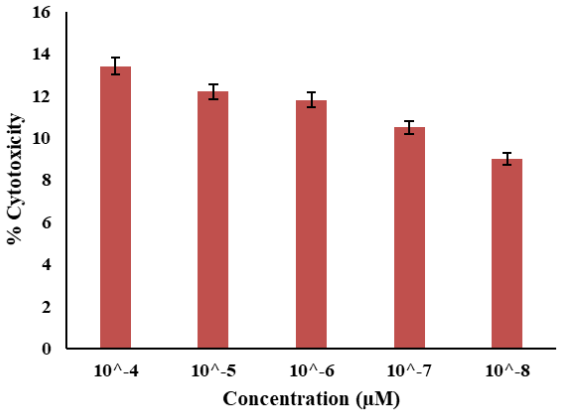

Figure 5.6. Cytotoxic effect of compound **26e** against normal cell line Hek293

5.14. HSA binding studies

HSA is the main protein in human blood plasma that binds to drugs readily, thus decreasing the toxicity, protecting the oxidation in plasma, and improving the solubility of drug substance. The building of potent antibacterial and anticancer agents is based upon their binding with serum albumin and drug transportation to the target site. The most active compound, **26e,** towards bacterial strains was chosen for interaction with Human Serum Albumin (HSA) using various spectroscopic techniques.[87-88]

5.14.1. UV-visible studies

The UV-visible spectrum of HSA (7 μM) revealed an absorption band at 280 nm in phosphate buffer (*p*H 7.4) at 298 K. The incremental additions of compound **26e** (0-18 μM) showed a hyperchromic shift at 280 nm along with the development and enhancement of a new band at 344 nm, corresponding to compound **26e** (**Figure 5.7a**). The binding constant (K_b) was determined using the Benesi-Hildebrand equation and calculated as 1.32×10^5 M^{-1}. The binding constant demonstrated excellent binding interaction between HSA and compound **26e**.

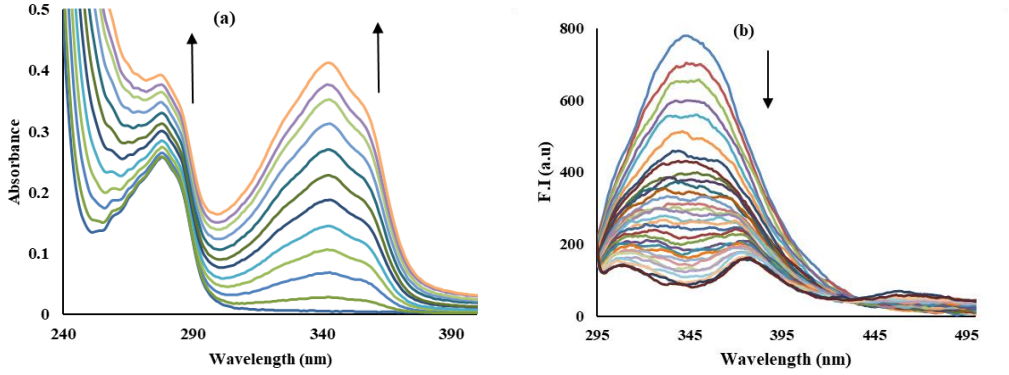

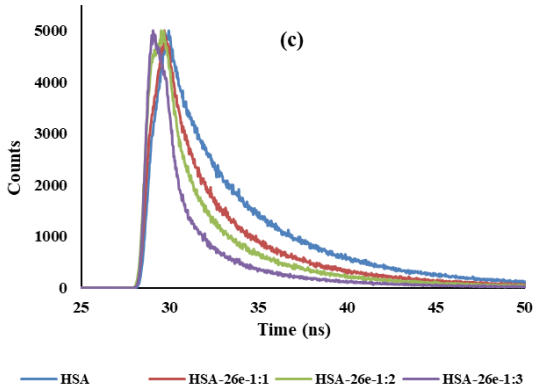

Figure 5.7. (a) Absorption spectra and (b) emission spectra of HSA upon incremental additions of compound **26e**, (c) Fluorescence decay profile of HSA on addition of various concentrations of compound **26e** in phosphate buffer (*p*H 7.4).

5.14.2. Fluorescence studies

Further, HSA (7 μM) interaction was investigated with an increasing concentration of compound **26e** (0-35 μM) in phosphate buffer (*p*H 7.4) at temperatures of 298 K, 308 K, and 318 K. Free HSA showed an emission band at 350 nm upon excitation at 280 nm. The addition of compound **26e** caused quenching in emission band at 350 nm at all temperatures (**Figures 5.7b**). The effective quenching displayed interaction between HSA and compound **26e**. The binding parameters were determined by the Stern-Volmer equation and calculated as 1.63×10^5 M^{-1} (K_{sv}) and 1.63×10^{13} M^{-1} (K_q) at 298 K. Binding constants (K_b) and the number of binding sites (n) were calculated using the modified Stern-Volmer equation where K_b value was found to be 11.01×10^4 M^{-1} at 298 K, indicating the strong binding of compound **26e** with HSA.

5.14.3 Time-resolved fluorescence analysis

Time-resolved fluorescence studies were carried out to confirm the mechanism of quenching of HSA with compound **26e**. The static quenching was predicted with the help of steady-state fluorescence spectroscopic studies. To further ensure the same, time-resolved fluorescence spectra of HSA (7 μM) were recorded with incremental additions of **26e** (0-21 μM), as shown in **Figure 5.7c**. The decrease in decay time indicates dynamic quenching, while no change shows static quenching. Upon incremental additions of compound **26e** in HSA solution of 7 μM, a decreasing trend in the decay time of HSA was observed, revealing the existence of dynamic quenching (**Table 3**). These steady-state and time-resolved fluorescence studies confirmed that static and dynamic quenchings are responsible for the interaction between the compound and HSA.

Table 3. Lifetime fluorescence decay of HSA on interaction with **26e**

System	Conc.	τ_1 [ns]	τ_2 [ns]	τ_3 [ns]	α_1	α_2	α_3	τ_{av}	χ^2
HSA		2.97	6.58	0.66	0.17	0.11	0.13	3.40	1.14
HSA-26e	1:1	2.28	6.25	0.48	0.29	0.12	0.07	2.02	1.11
	1:2	2.18	5.97	0.54	0.30	0.16	0.03	1.56	1.20
	1:3	1.61	5.35	0.33	0.20	0.18	0.02	0.79	1.16

5.15. DNA Binding studies

For the normal functioning and development of an organism, DNA is a vital macromolecule; therefore, targeting DNA is one of the essential tools in building potent drugs. Compound **26e** has naphthalimide in its structure, and this moiety is a well-known DNA intercalator. Thus, exploring the binding ability of synthesized compounds with DNA can help us to build a potent drug.[121]

5.15.1. UV-visible studies

The binding studies of compound **26e** with ct-DNA were evaluated using absorption spectroscopy. The absorption spectrum of compound **26e** showed an intense band at 344 nm in phosphate buffer (*p*H 7.4) at 298 K. Compound **26e** (5 μM) was further titrated with incremental addition of ct-DNA (0-68 μM) that produced a hypochromic shift in the absorption band at 344 nm, characteristic of interaction of compound into DNA base pairs (**Figure 5.8a**). The binding constant (K_b) for DNA interaction was calculated to be 5.99×10^4 M^{-1} using the Benesi-Hildebrand equation that reveals strong binding interaction between compound **26e** and DNA.

5.15.2 Thermal denaturation studies

Conformational changes in DNA upon adding compound **26e** with increasing temperature were studied to get information about the binding strength and mode of interaction of compound with DNA.[198] A denaturation study has been carried out for free ct-DNA, indicating that DNA's melting temperature (T_m) was 76 °C. The melting temperature of DNA was increased to 88.8 °C with the addition of compound **26e**. The increase in temperature value (ΔT_m) of 12.8 °C of DNA suggests the stabilization of double helix DNA upon binding with compound **26e**, thus, indicating the intercalative mode.

5.15.3. Fluorescence studies

Fluorescence studies further explored the binding interaction of compound **26e** with ct-DNA. The fluorescence spectrum of compound **26e** showed an emission band at 475 nm upon excitation at 345 nm in phosphate buffer (*p*H 7.4) at 298 K. The emission of compound **26e** (5 μM) at 475 nm showed quenching upon incremental additions of ct-DNA (0-20 μM) (**Figure 5.8b**), confirming the binding interaction of compound **26e** with DNA. The Stern-Volmer quenching constant (K_{sv}) was calculated from the plot of the compound; concentration versus F_o/F and found to be 1.22×10^4 M^{-1}. The bimolecular quenching rate constant (K_q) has been calculated to check whether the quenching phenomena is static or dynamic. It was found to be 1.22×10^{12} $M^{-1}s^{-1}$, representing the static quenching mechanism in the binding interaction of compound **26e** and ct-DNA. The modified Stern-Volmer equation was used to calculate the binding constant (K_b) and the number of binding sites (n), which were determined from the plot of log[DNA] and log[(F_o-F)/F] and found to be 8.26×10^4 M^{-1} and 1.16, respectively.

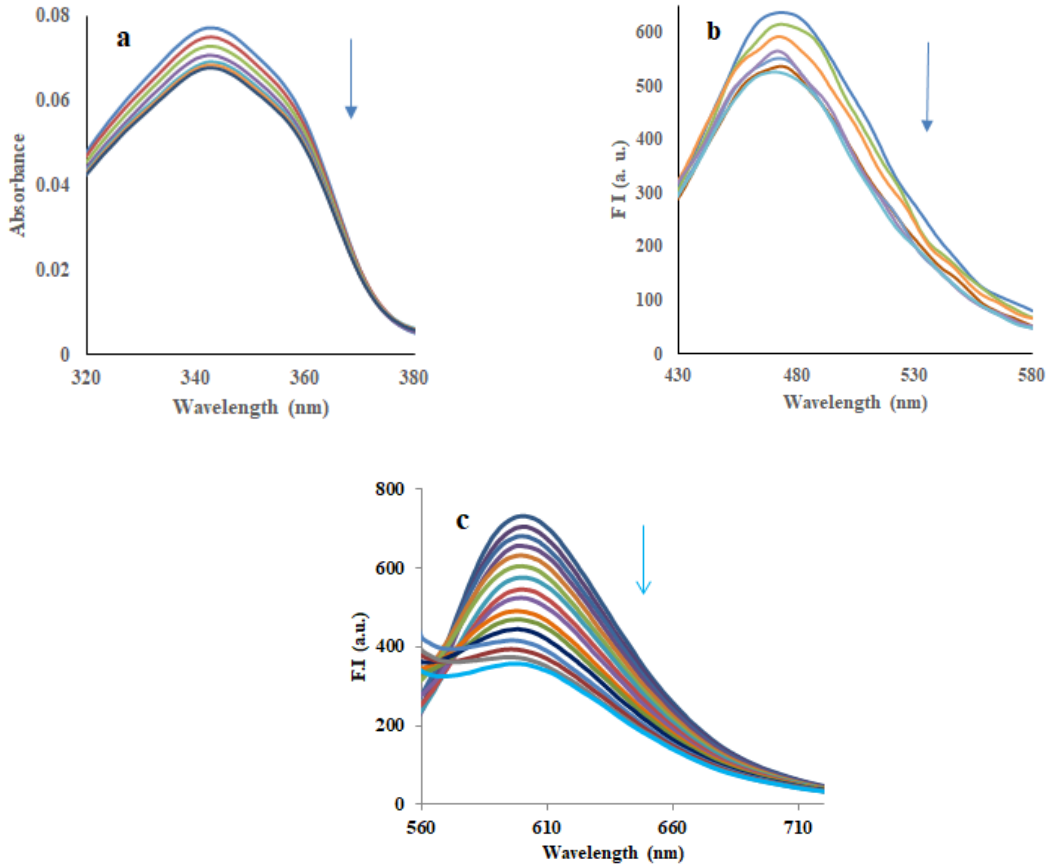

Figure 5.8. (a) Absorption spectra, (b) emission spectra of compound **26e** upon incremental additions of ct-DNA, and (c) emission spectra of ethidium bromide and ct-DNA complex upon incremental addition of compound **26e**

5.15.4. Competitive displacement assay

The ethidium bromide competitive displacement assay was executed to further confirm the intercalation binding mode of compound **26e** with ct-DNA. The complex of ethidium bromide (3 μM) and ct-DNA (30 μM) showed an intense emission band at 601 nm with excitation at 520 nm in phosphate buffer (*p*H 7.4). Adding compound **26e** (0-90 μM) to this complex caused quenching in the emission band at 601 nm because of ethidium bromide displacement from the complex (**Figure 5.8c**). The ethidium bromide displacement by compound **26e** from the ethidium bromide-ct-DNA complex further confirmed the intercalation binding mode.[60]

5.15.5. Molecular Docking

The elevated clusters were rated using their energy levels, and compound **26e** showed the minimum binding energy of -13.86 kcal mol^{-1} with DNA (PDB:1BNA). The nitrogen of the triazine ring and oxygen of the naphthalimide ring of compound **26e** showed hydrogen bonding with the guanine base (DG-4, A chain) of DNA, having bond lengths of 2.37 Å and 2.56 Å, respectively. The oxygen of naphthalimide ring formed two hydrogen bonds with guanine base (DG-10, chain A and DG-16 chain B) having bond lengths of 2.31 Å and 2.73 Å. Cytosine base (DC-9, chain A) of DNA formed a hydrogen bond with amino linker (-NH-) between triazine and naphthalimide ring having a bond length of 3.15 Å (**Figures 5.9a** and 5.**9b**).

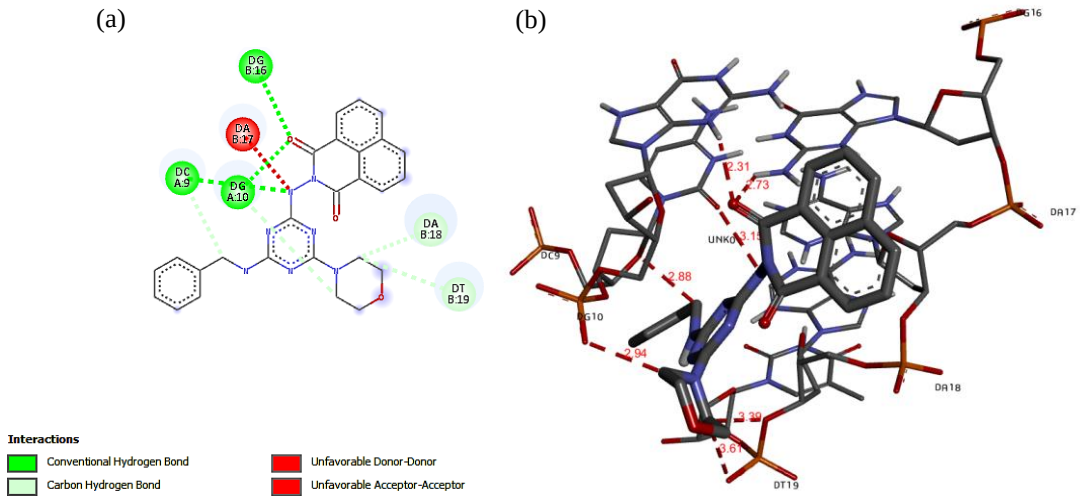

Figure 5.9. (a) 2D-representation and (b) docked pose of compound **26e** into 3D crystal structure of DNA

5.16 Quantum chemical study

The low energy gap in HOMO and LUMO of the target molecules brings greater stabilizing interaction with receptors to exhibit better bioactivity. The atomic orbitals HOMO-LUMO compositions of compound **26e** is represented in **Table 4**; it has been observed that HOMOs

of the target molecule were mainly localized on the triazine and morpholine rings, whereas the LUMOs were located on the naphthalimide ring. The results depicted that the triazine and morpholine rings bind to positively charged biological ions through electrostatic interaction, whereas the naphthalimide ring binds with negatively charged ions or residues. Among the synthesized derivatives, compound **26e** exhibited the lowest energy gap of 3.416 eV between HOMO and LUMO orbitals. The low energy gap suggested high reactivity towards the microbes to enhance inhibition potency.

Table 4: Atomic orbitals HOMO-LUMO compositions of compounds **26a-s**

Compound	HOMO (eV)	LUMO (eV)	ΔE (eV)
26a	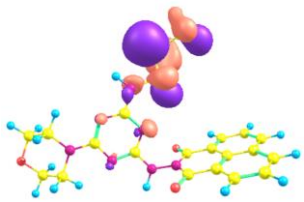	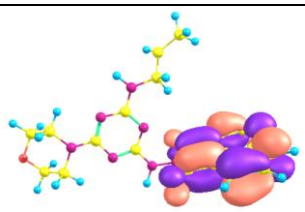	3.642
26b	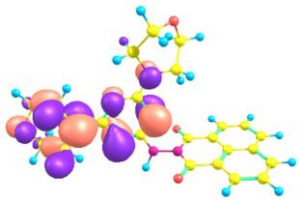	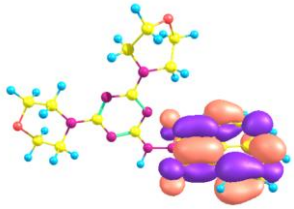	3.442
26c	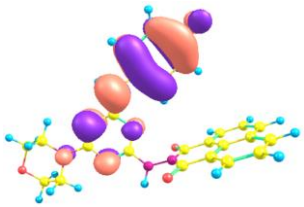	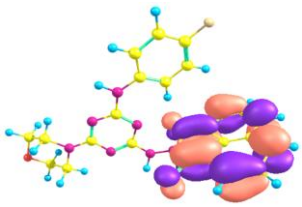	3.473
26d	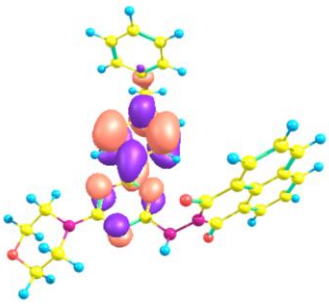	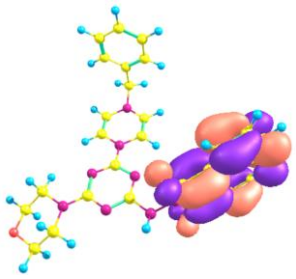	4.029

26e	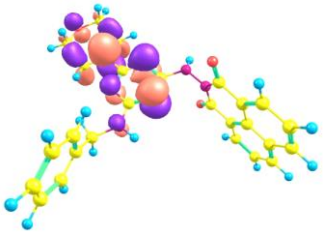	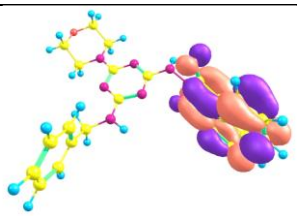	3.416
26f	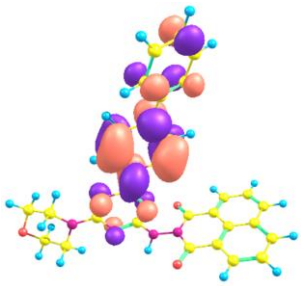	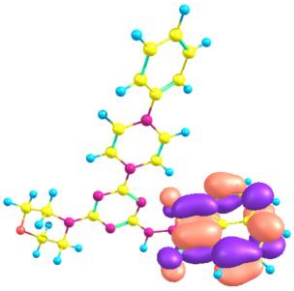	3.384
26g	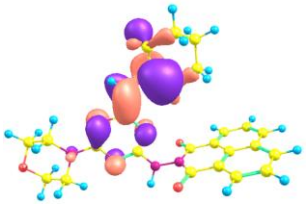	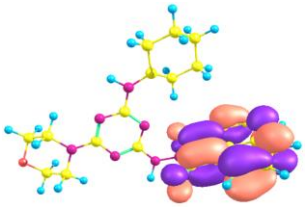	3.489
26h	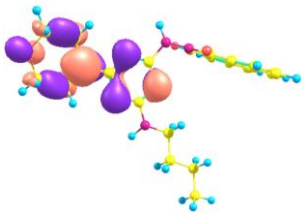	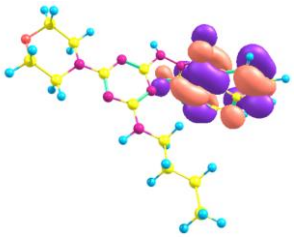	3.567
26i	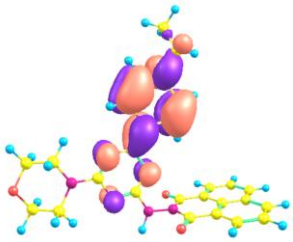	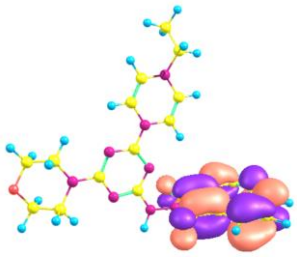	4.021
26j	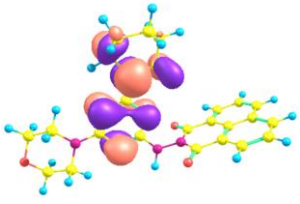	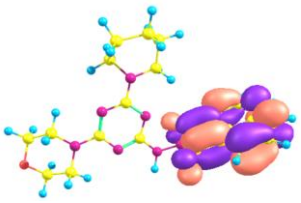	4.020

26k	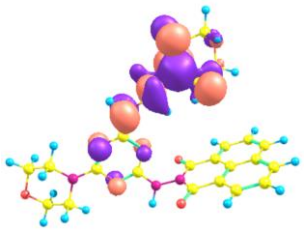	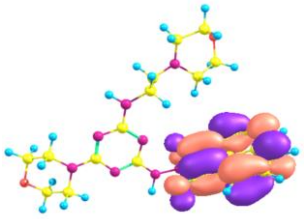	3.758
26l	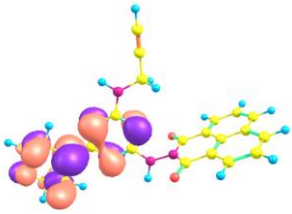	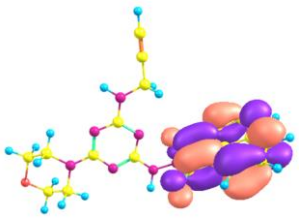	3.708
26m	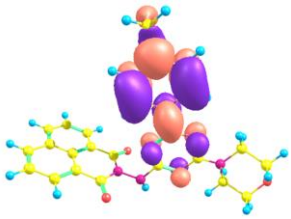	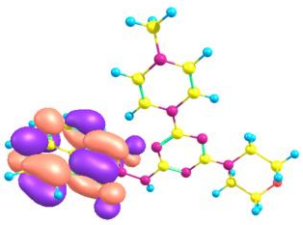	4.104
26n	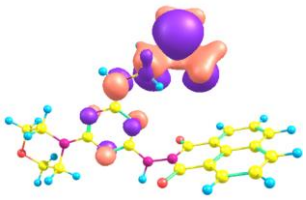	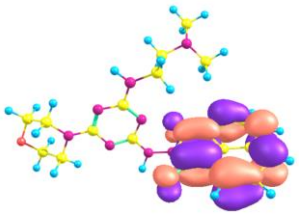	3.610
26o	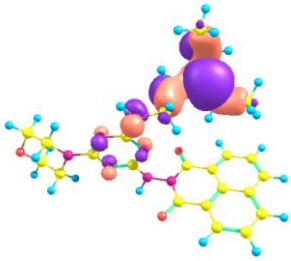	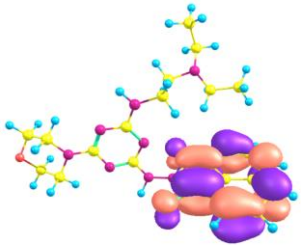	3.599
26p	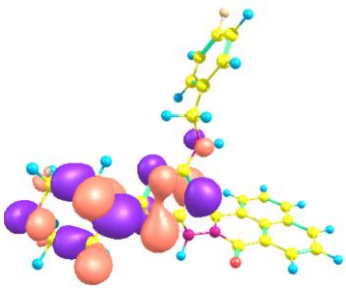	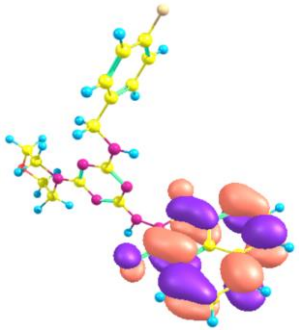	3.712

26q	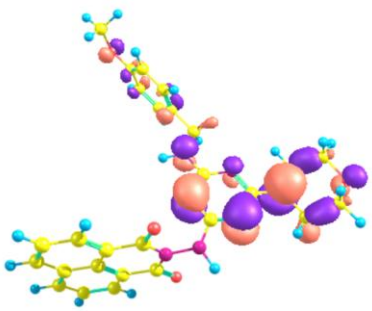	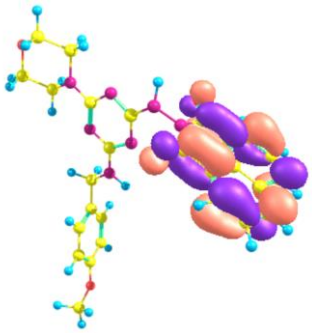	3.447
26r	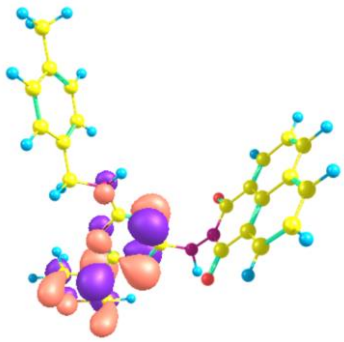	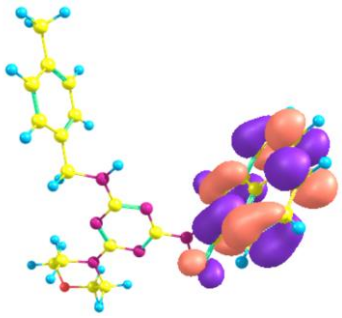	3.634
26s	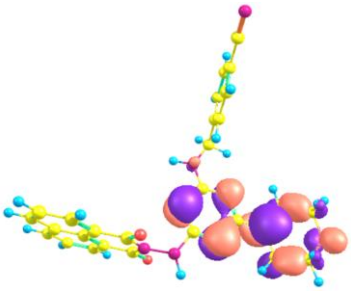	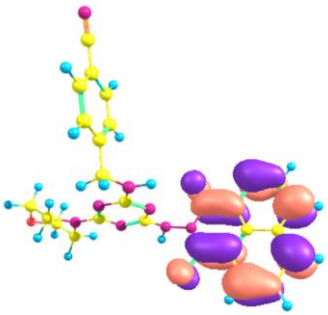	3.867

5.17. Conclusion

In summary, we have developed a series of naphthalimide-triazine conjugates to overcome drug-resistance bacterial infections. Most of the targeted compounds were active toward both gram-positive and gram-negative bacteria. SARs indicated that the presence of the benzyl group facilitates better inhibitory activity. Remarkably, naphthalimide-triazine **26e** displayed promising results against *S. aureus* (MIC = 1.56 μg/ml) than the marketed drugs chloromycin and amoxicillin. The mechanistic studies of compound **26e** revealed its membrane damage ability leading to leakage of intercellular proteins. Moreover, compound **26e** inhibited the biofilm formation of *S. aureus*, thus precluding bacterial resistance within 11 days. Compound **26e** effectively binds to HSA, indicating that the compound could quickly deliver to the targeted site. Further, the DNA binding ability of compound **26e** hindered the reproduction of

bacteria. Thus, due to the excellent results displayed with compound **26e**, pre-clinical evaluation is under consideration for its further development as an antibacterial agent.

5.18 Experimental section

Synthesis of compound 24:

To a stirred solution of 2-amino-1*H*-benzo[*de*]isoquinoline-1,3(2*H*)-dione (**10**) (1 g, 4.71 mmol) in isopropyl alcohol (20 ml), cyanuric chloride (**23**) (1.04 g, 5.45 mmol) was added to it, and the reaction was stirred at room temperature for 6 h. On completion of the reaction, 100 ml water was added to it, and the formed product was filtered and purified by column chromatography using chloroform and ethyl acetate (10:1) as eluent. The product was obtained in an off-white color, 0.76 g, 76%, R_f 0.5 (chloroform), m.pt. 165-168 ^oC.

Synthesis of compound 25:

To a stirred morpholine (120 mg, 13.80 mol) in isopropyl alcohol (10 ml), 2-((4,6-dichloro-1,3,5-triazine-2-yl)amino)-5*H*-benzo[*de*]isoquinoline-1,3(2*H*)-dione (**24**) (500 mg, 13.80 mmol) was added, and the reaction was allowed to stir at room temperature for 3 h. The water was added to the reaction mixture, and the precipitate formed was filtered and washed with water. The crude was purified by column chromatography using chloroform and ethyl acetate (10:0.6) as eluents.

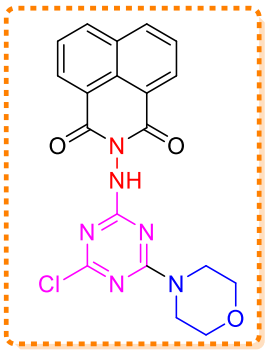

Yield: 71%; colour: off white; m.pt. 211-213 ^oC. ^1H NMR ($CDCl_3$, 400 MHz): δ (ppm) 8.68 (dd, J = 7.3, 0.8 Hz, 2H), 8.35 (d, J = 8.0 Hz, 2H), 7.85 (t, J = 7.8 Hz, 2H), 3.87 – 3.83 (m, 2H, CH_2 morph), 3.73 – 3.69 (m, 2H, CH_2 morph), 3.54 – 3.43 (m, 4H, 2 × CH_2 morph). ^{13}C NMR ($CDCl_3$, 100 MHz) δ (ppm) 167.1, 165.2, 163.0, 131.9, 128.1, 127.1, 122.5, 66.8, 43.6; MS ESI (m/z) $[M+H]^+$: 411.18; Anal Calcd for $C_{19}H_{15}ClN_6O_3$: C, 55.55; H, 3.68; N, 20.46; found C, 55.52; H, 3.65; N, 20.45.

General procedure for synthesis of compounds 26a-s:

To a stirred solution of 2-((4-chloro-6-morpholino-1,3,5-triazine-2-yl)amino)-5*H*-benzo[*de*]isoquinoline1,3(2*H*)-dione (**25**) (100 mg, 24.39 mmol) in isopropyl alcohol (10 ml), various substituted primary or secondary amine (36.58 mmol) was added, and the reaction was allowed to reflux for 10-15 h. Water was added to the reaction mixture, and the solid residue was filtered. Crude was purified by column chromatography using chloroform and ethyl acetate as eluents.

2-((4-(allylamino)-6-morpholino-1,3,5-triazin-2-yl)amino)-1*H*-benzo[*de*]isoquinoline-1,3(*2H*)-dione (26a):

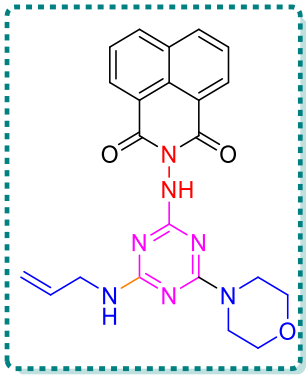

White solid; 71% yield; m.pt.: 240-246 ºC; ^{1}H NMR ($CDCl_3$, 400 MHz): δ (ppm) 8.64 (d, J = 7.24 Hz, 2H, ArH), 8.27 (d, J = 8.16 Hz, 2H, ArH), 7.79 (t, J = 7.68 Hz, 2H, ArH), 5.89-5.76 (m, 1H, CH allyl), 5.14 (dd, 2H, CH_2 allyl), 3.91 (br(s), 2H, CH_2 allyl), 3.63 (br(s), 8H, 4×CH_2 morph); ^{13}C NMR ($CDCl_3$, 100 MHz): δ (ppm) 165.7, 165.4, 163.1, 134.8, 134.6, 132.0, 131.9, 128.2, 127.1, 122.5, 116.0, 66.8, 43.5, 43.3; MS ESI (m/z) $[M+H]^+$: 432.1; Anal Calcd for $C_{22}H_{21}N_7O_3$: C, 61.24; H, 4.91; N, 22.73; found C, 61.14; H, 4.81; N, 22.71.

2-((4,6-dimorpholino-1,3,5-triazin-2-yl)amino)-*1H*-benzo[*de*]isoquinoline-1,3(*2H*)-dione (26b):

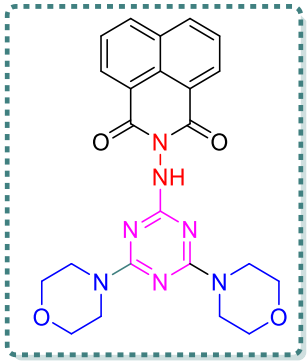

White solid; 74% yield; m.pt: 233-247 ºC; ^{1}H NMR ($CDCl_3$, 400 MHz): δ (ppm) 8.67 (d, J = 5.80 Hz, 2H, ArH), 8.29 (d, J = 6.48 Hz, 2H, ArH), 7.82 (t, J = 6.08 Hz, 2H, ArH), 3.64 (br(s), 16H, 8×CH_2 morph); ^{13}C NMR ($CDCl_3$, 100 MHz): δ (ppm) 167.0, 165.2, 163.0, 134.7, 132.1, 131.9, 128.1, 127.1, 122.5, 66.8, 43.59; MS ESI (m/z) $[M+H]^+$: 462.1; Anal Calcd for $C_{23}H_{23}N_7O_4$: C, 59.86; H, 5.02; N, 21.25; found C, 59.84; H, 5.00; N, 21.21.

2-((4-((4-fluorophenyl)amino)-6-morpholino-1,3,5-triazin-2-yl)amino)-1*H*-benzo[*de*] isoquinoline-1,3(*2H*)-dione (26c):

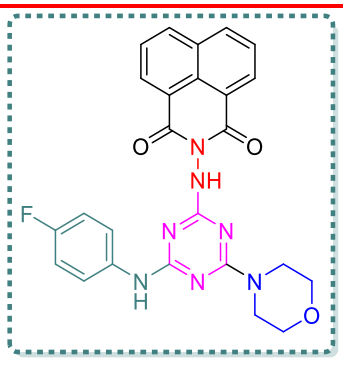

White solid; 72% yield; m.pt.: 250-255 ºC; ^{1}H NMR ($CDCl_3$, 400 MHz): δ (ppm) 8.69 (d, J = 6.96 Hz, 2H, ArH), 8.36 (d, J = 8.04 Hz, 2H, ArH), 7.85 (t, J = 7.40 Hz, 2H, ArH), 7.41 (s, 2H, ArH), 7.06 (s, 2H, ArH), 3.73 (br(d), J = 18.08 Hz, 4H, 2×CH_2 morph), 3.50 (br(s), 4H, 2×CH_2 morph); ^{13}C NMR ($CDCl_3$, 100 MHz): δ (ppm) 171.6, 169.7, 169.2, 167.4, 141.6, 139.7, 132.6, 132.2, 127.5, 127.2, 126.2, 120.0, 118.5,

71.3, 48.6; MS ESI (m/z) $[M+H]^+$: 486.1; Anal Calcd for $C_{25}H_{20}FN_7O_3$: C, 61.85; H, 4.15; N, 20.20; found C, 61.83; H, 4.13; N, 20.18

2-((4-(4-benzylpiperazin-1-yl)-6-morpholino-1,3,5-triazin-2-yl)amino)-1*H*-benzo[*de*] isoquinoline-1,3(2*H*)-dione (26d):

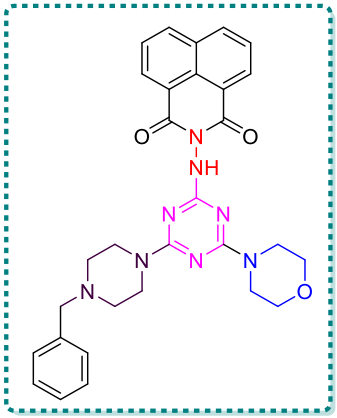

White solid; 70% yield; m.pt: 220-224 ^oC; ^1H NMR ($CDCl_3$, 400 MHz): δ (ppm) 8.65 (d, J = 7.24 Hz, 2H, ArH), 8.26 (d, J = 8.2 Hz, 2H, ArH), 7.79 (t, J = 7.88 Hz, 2H, ArH), 7.27 (br (s), 5H, ArH), 3.71 (br(s), 8H, 4×CH_2 morph), 3.54 (br(s), 2H, CH_2 pip), 3.48 (q, J = 7.12 Hz, 2H, CH_2 pip), 2.39 (s, 2H, CH_2), 1.66 (br(s), 4H, 2×CH_2 pip); ^{13}C NMR ($CDCl_3$, 100 MHz): δ (ppm) 167.1, 165.3, 164.9, 163.0, 134.5, 132.0, 131.9, 129.3, 128.3, 128.1, 127.2, 127.1, 122.5, 66.6, 62.9, 52.7, 43.5, 43.0 ; MS ESI (m/z) $[M+H]^+$: 551.2; Anal Calcd for $C_{30}H_{30}N_8O_3$: C, 65.44; H, 5.49; N, 20.35; found C, 65.38; H, 5.48; N, 20.31.

2-((4-(benzylamino)-6-morpholino-1,3,5-triazin-2-yl)amino)-*1H*-benzo[*de*]isoquinol ine-1,3(*2H*)-dione (26e):

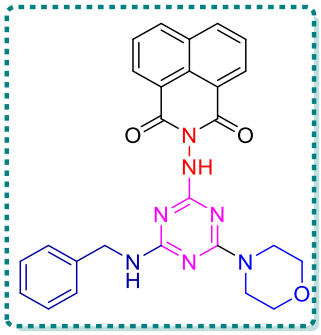

White solid; 68% yield; m.pt: 240-245 ^oC; ^1H NMR ($CDCl_3$, 400 MHz): δ (ppm) 8.61 (d, J = 6.6 Hz, 2H, ArH), 8.25 (d, J = 8.28 Hz, 2H, ArH), 7.78 (t, J = 7.68 Hz, 3H, ArH), 7.22 (br(s), 4H, ArH), 4.48 (s, 2H, CH_2), 3.67 (br(s), 8H, 4×CH_2 morph); ^{13}C NMR ($CDCl_3$, 100 MHz): δ (ppm) 165.4, 163.1, 139.0, 136.1, 134.6, 132.0, 131.8, 128.5, 128.1, 127.7, 127.1, 122.5, 66.7, 44.8, 29.7; MS ESI (m/z) $[M+H]^+$: 482.2;

Anal Calcd for $C_{26}H_{23}N_7O_3$: C, 64.85; H, 4.81; N, 20.36; found C, 64.81; H, 4.79; N, 20.31.

2-((4-morpholino-6-(4-phenylpiperazin-1-yl)-1,3,5-triazin-2-yl)amino)-*1H*-benzo[*de*] isoquinoline-1,3(*2H*)-dione (26f):

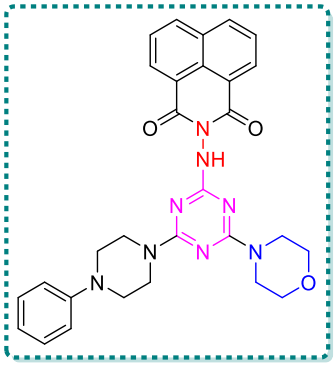

Creamish solid; 70% yield; m.pt: 230-233 ^{o}C; ^{1}H NMR ($CDCl_3$, 400 MHz): δ (ppm) 8.66 (d, J = 7.28 Hz, 2H, ArH), 8.28 (d, J = 8.28 Hz, 2H, ArH), 7.81 (t, J = 7.76 Hz, 2H, ArH), 7.22-6.83 (m, 5H, ArH), 3.69 (br(s), 12H, 4×CH_2 morph, 2×CH_2 pip), 3.11 (br(s), 4H, 2×CH_2 pip); ^{13}C NMR ($CDCl_3$, 100 MHz): δ (ppm) 167.1, 165.3, 165.1, 163.0, 151.3, 134.6, 132.0, 129.2, 128.1, 127.1, 122.5, 120.1, 116.6, 66.7, 49.3, 43.5, 43.0; MS ESI (m/z) $[M+H]^+$: 537.2; Anal Calcd for $C_{29}H_{28}N_8O_3$: C, 64.91; H, 5.26; N, 20.88; found C, 64.85; H, 5.21, N, 20.82.

2-((4-(cyclohexylamino)-6-morpholino-1,3,5-triazin-2-yl)amino)-*1H*-benzo[*de*]isoquinoline-1,3(*2H*)-dione (26g)

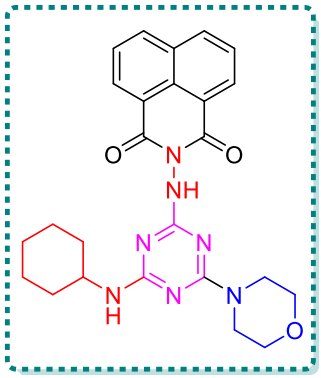

White solid; 65% yield; m.pt: 220-225 ^{o}C; ^{1}H NMR ($CDCl_3$, 400 MHz): δ (ppm) 8.66 (d, J = 7.16 Hz, 2H, ArH), 8.26 (d, J = 8 Hz, 2H, ArH), 7.78 (t, J = 7.16 Hz, 2H, ArH), 3.67 (br(s), 8H, 4 × CH_2 morph), 1.90 (br(s), 1H, CH cyclohex), 1.68 (br(s), 1H, CH cyclohex), 1.56 (br(s), 1H, CH cyclohex), 1.37-1.15 (m, 8H, 8 × CH cyclohex); ^{13}C NMR ($CDCl_3$, 100 MHz): δ (ppm) 165.6, 165.3, 163.1, 134.6, 132.0, 131.8, 128.2, 127.1, 122.6, 66.8, 49.2, 43.5, 32.9, 29.7, 24.9; MS ESI (m/z) $[M+H]^+$: 474.2; Anal Calcd for $C_{25}H_{27}N_7O_3$: C, 63.41; H, 5.75; N, 20.71; found C, 63.38; H, 5.71; N, 20.65.

2-((4-(butylamino)-6-morpholino-1,3,5-triazin-2-yl)amino)-*1H*-benzo[*de*]isoquinoline-1,3(*2H*)-dione (26h)

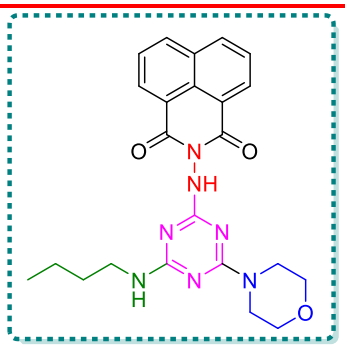

White solid; 69% yield; m.pt: 250-253 ^{o}C; ^{1}H NMR ($CDCl_3$, 400 MHz): δ (ppm) 8.65 (d, J = 7.24 Hz, 2H, ArH), 8.27 (d, J = 8.16 Hz, 2H, ArH), 7.80 (t, J = 7.76 Hz, 2H, ArH), 3.65 (br(s), 8H, 4×CH_2 morph), 3.26 (br(s), 2H, CH_2 butyl), 1.69 (br(s), 4H, 2×CH_2 butyl), 0.85 (br(s), 3H, CH_3 butyl); ^{13}C NMR ($CDCl_3$, 100 MHz): δ (ppm) 165.7, 163.1, 134.6, 132.0, 131.8, 128.2, 127.1, 122.6, 66.8, 43.5, 40.6, 29.8, 20.0,

13.6; MS ESI (m/z) $[M+H]^+$: 448.2; Anal Calcd for $C_{23}H_{25}N_7O_3$: C, 61.73; H, 5.63; N, 21.91; found C, 61.71; H, 5.61; N, 21.86.

2-((4-(4-ethylpiperazin-1-yl)-6-morpholino-1,3,5-triazin-2-yl)amino)-1*H*-benzo[*de*] isoquinoline-1,3(*2H*)-dione (26i)

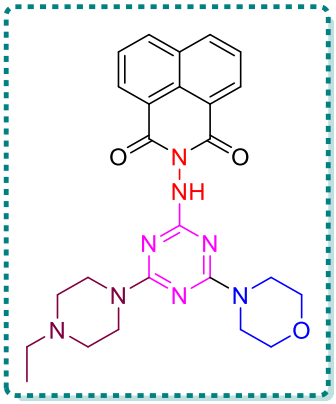

White solid; 69% yield; m.pt: 260-265 °C; ^{1}H NMR ($CDCl_3$, 400 MHz): δ (ppm) 8.68 (d, J = 7.20 Hz, 2H, ArH), 8.30 (d, J = 8.16 Hz, 2H, ArH), 7.83 (t, J = 8.12 Hz, 2H, ArH), 3.68 (br(s), 16H, 4×CH_2 morph, 4×CH_2 pip), 2.27-2.25 (m, 2H, CH_2 pip), 1.37 (br(s), 3H, CH_3 pip); ^{13}C NMR ($CDCl_3$, 100 MHz): δ (ppm) 165.1, 163.0, 134.7, 132.1, 132.0, 128.9, 127.3, 123.3, 122.6, 66.6, 57.4, 56.4, 53.1, 43.5, 13.3; MS ESI (m/z) $[M+H]^+$: 489.2; Anal Calcd for $C_{25}H_{28}N_8O_3$: C, 61.46; H, 5.78; N, 22.94; found C, 61.42; H, 5.74; N, 22.95.

2-((4-morpholino-6-(piperidin-1-yl)-1,3,5-triazin-2-yl)amino)-*1H*-benzo[*de*]isoquinoli ne-1,3(*2H*)-dione (26j):

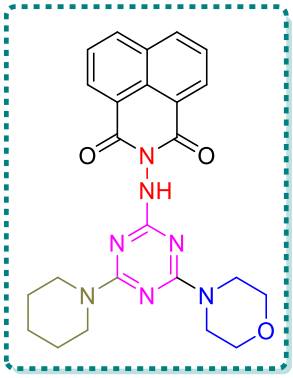

White solid; 71% yield; m.pt: 230-233 °C; ^{1}H NMR ($CDCl_3$, 400 MHz): δ (ppm) 8.65 (d, J = 7.16 Hz, 2H, ArH), 8.27 (d, J = 8.28 Hz, 2H, ArH), 7.80 (t, J = 7.88 Hz, 2H, ArH), 3.63 (br(s), 12H, 4×CH_2 morph, 2×CH_2 pip), 1.66 (br(s), 6H, 3×CH_2 pip); ^{13}C NMR ($CDCl_3$, 100 MHz): δ (ppm) 167.1, 165.4, 164.8, 163.1, 134.5, 132.0, 131.9, 128.1, 127.1, 122.6, 66.8, 44.2, 43.8, 25.7, 24.8; MS ESI (m/z) $[M+H]^+$: 460.2;

Anal Calcd for $C_{24}H_{25}N_7O_3$: C, 62.73; H, 5.48; N, 21.34; found C, 62.71; H, 5.41; N, 21.31.

2-((4-morpholino-6-((2-morpholinoethyl)amino)-1,3,5-triazin-2-yl)amino)-1*H*-benzo [*de*]isoquinoline-1,3(2*H*)-dione (26k):

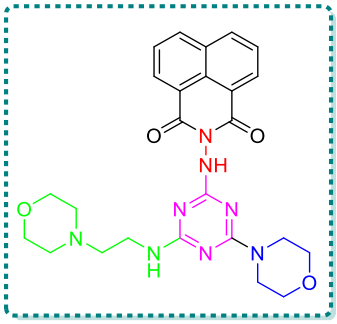

Off white solid; 76% yield; m.pt: 240-243 ^{o}C; ^{1}H NMR ($CDCl_3$, 400 MHz): δ (ppm) 8.66 (d, J = 7.24 Hz, 2H, ArH), 8.28 (d, J = 8.16 Hz, 2H, ArH), 7.80 (t, J = 7.72 Hz, 2H, ArH), 3.65 (br(s), 14H, 7×CH_2 morph), 2.47-2.40 (m, 6H, 2 × CH_2 morph); ^{13}C NMR ($CDCl_3$, 100 MHz): δ (ppm) 169.5, 168.4, 166.6, 134.4, 133.0, 132.0, 131.9, 126.9, 122.3, 68.9, 60.1, 59.2, 55.8, 53.3, 48.0; MS ESI (m/z) $[M+H]^+$: 505.2;

Anal Calcd for $C_{25}H_{28}N_8O_4$: C, 59.51; H, 5.59; N, 22.21; found C, 59.49; H, 5.52; N, 22.19.

2-((4-morpholino-6-(prop-2-yn-1-ylamino)-1,3,5-triazin-2-yl)amino)-1*H*-benzo[*de*]isoquinoline-1,3(2*H*)-dione (26l):

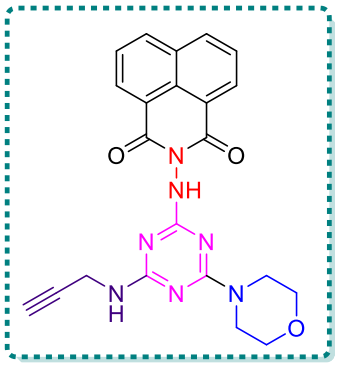

White solid; 75% yield; m.pt: 245-248 ^{o}C; ^{1}H NMR ($CDCl_3$, 400 MHz): δ (ppm) 8.65 (d, J = 7.32 Hz, 2H, ArH), 8.27 (d, J = 8.28 Hz, 2H, ArH), 7.80-7.76 (m, 2H, ArH), 4.11-3.93 (m, 2H, CH_2 propargyl), 3.66 (br(s), 8H, 4×CH_2 morph), 2.07 (br(s), 1H, CH propargyl); ^{13}C NMR ($CDCl_3$, 100 MHz): δ (ppm) 168.3, 167.4, 165.3, 134.7, 138.1, 132.1, 131.3, 127.7, 127.2, 122.5, 74.5, 71.0, 66.8, 43.6, 30.5; MS ESI (m/z)

$[M+H]^+$: 430.1; Anal Calcd for $C_{22}H_{19}N_7O_3$: C, 61.53; H, 4.46; N, 22.83; found C, 61.49; H, 4.41; N, 22.81.

2-((4-(4-methylpiperazin-1-yl)-6-morpholino-1,3,5-triazin-2-yl)amino)-*1H*-benzo[*de*]isoquinoline-1,3(*2H*)-dione (26m):

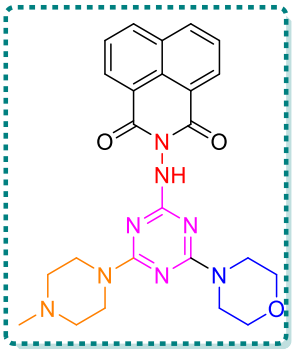

Off white solid; 71% yield; m.pt: 230-234 ^{o}C; ^{1}H NMR ($CDCl_3$, 400 MHz): δ (ppm) 8.53-8.49 (m, 4H, ArH), 7.90-7.86 (m, 2H, ArH), 3.69-3.49 (m, 12H, 4×CH_2 morph, 2×CH_2 pip), 2.77 (s, 3H, CH_3 pip), 2.62-2.46 (m, 4H, 2×CH_2 pip); ^{13}C NMR ($CDCl_3$, 100 MHz): δ (ppm): 168.5, 166.8, 165.1, 163.0, 135.4, 132.0, 128.0, 127.1, 123.2, 122.2, 66.6, 54.7, 53.8, 44.0, 44.3; MS ESI (m/z) $[M+H]^+$: 475.22; Anal

Calcd for $C_{24}H_{26}N_8O_3$: C, 60.75; H, 5.52; N, 23.61; found C, 60.72; H, 5.50; N, 23.58.

2-((4-((2-(dimethylamino)ethyl)amino)-6-morpholino-1,3,5-triazin-2-yl)amino)-1*H*-benzo[*de*]isoquinoline-1,3(2*H*)-dione (26n):

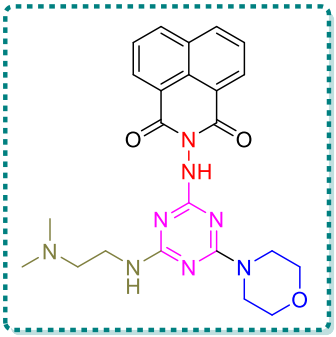

White solid; 75% Yield; m.pt: 242-246 ^{o}C; ^{1}H NMR ($CDCl_3$, 400 MHz): δ (ppm) 8.66 (d, J = 7.28 Hz, 2H, ArH), 8.27 (d, J = 8.16 Hz, 2H, ArH), 7.80 (d, J = 7.6 Hz, 2H, ArH), 3.62 (br(s), 8H, 4×CH_2 morph), 2.48 (br (s), 4H, 2×CH_2 dimethyl), 1.65 (s, 6H, 2×CH_3 dimethyl); ^{13}C NMR ($CDCl_3$, 100 MHz): δ (ppm): 167.4, 166.4, 165.1, 163.1, 134.3, 134.0, 132.0, 131.3, 127.1, 122.6, 66.6, 57.4, 56.1, 45.7, 45.0, 43.3;

MS ESI (m/z) $[M+H]^+$: 463.1; Anal Calcd for $C_{23}H_{25}N_8O_3$: C, 59.86; H, 5.46; N, 24.28; found C, 59.80; H, 5.42; N, 24.25.

2-((4-((2-(diethylamino)ethyl)amino)-6-morpholino-1,3,5-triazin-2-yl)amino)-1*H*-benzo[*de*]isoquinoline-1,3(2*H*)-dione (26o):

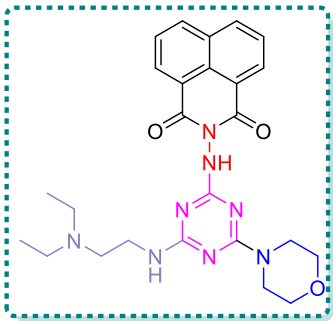

off white; 70% Yield; m.pt: 220-223 ^{o}C; ^{1}H NMR ($CDCl_3$, 400 MHz): δ (ppm) 8.66 (d, J = 7.28 Hz, 2H, ArH), 8.27 (d, J = 8.16 Hz, 2H, ArH), 7.80 (d, J = 7.60 Hz, 2H, ArH), 3.62 (br(s), 8H, 4 × CH_2 morph), 3.33 (br(s), 4H, CH_2 ethyl), 2.47 (br(s), 2H, CH_2 ethyl), 1.75 (br(s), 4H, 2 × CH_2 diethyl), 0.92 (br(s), 6H, 2 × CH_3 diethyl); ^{13}C NMR ($CDCl_3$, 100 MHz): δ (ppm): 168.9, 167.8, 164.0, 163.0, 134.7, 132.1, 132.0,

131.6, 126.6, 122.6, 66.6, 57.8, 46.6, 42.0, 11.5; MS ESI (m/z) $[M+H]^+$: 491.1; Anal Calcd for $C_{25}H_{29}N_8O_3$: C, 61.34; H, 5.97; N, 22.89. found C,61.30; H, 5.90; N, 22.84.

2-((4-((4-fluorobenzyl)amino)-6-morpholino-1,3,5-triazin-2-yl)amino)-1*H*-benzo[*de*] isoquinoline-1,3(2*H*)-dione (26p):

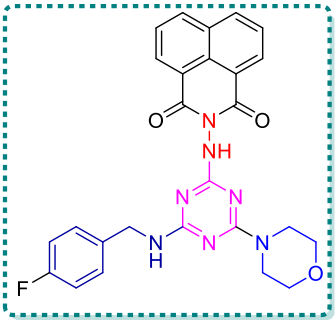

White solid; 67% Yield; m.pt: 230-232 ^{o}C; ^{1}H NMR ($CDCl_3$, 400 MHz): δ (ppm) 8.64 (d, J = 7.0 Hz, 2H, ArH), 8.33 (d, J = 8.1 Hz, 2H, ArH), 7.82 (t, J = 7.6 Hz, 2H, ArH), 7.26 (d, J = 6.5 Hz, 2H, ArH), 7.01 (t, J = 7.5 Hz, 2H, ArH), 4.58 (s, 2H, CH_2), 3.73 (d, J = 45.7 Hz, 4H, 2×CH_2 morph), 3.47 (d,

J = 11.3 Hz, 4H, 2×CH_2 morph); ^{13}C NMR ($CDCl_3$, 100 MHz): δ (ppm): 162.2, 160.9, 160.5, 135.6, 132.7, 132.5, 132.0, 129.5, 129.4, 127.3, 121.5, 115.7, 115.5, 113.6, 66.20, 44.5, 44.3; HRMS (ESI) Calcd. for $C_{26}H_{22}N_7O_3F$ $[M+H]^+$ 500.0095 Found 500.0085.

2-((4-((4-methoxybenzyl)amino)-6-morpholino-1,3,5-triazin-2-yl)amino)-1*H*-benzo[*de*]isoquinoline-1,3(2*H*)-dione (26q)

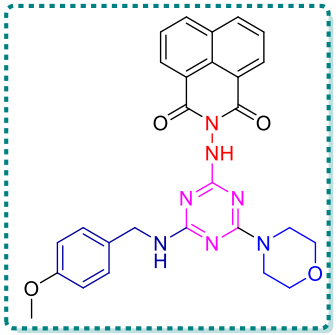

Off white solid; 63% Yield; m.pt: 235-238 ^oC; ^1H NMR ($CDCl_3$, 400 MHz): δ (ppm) 8.65 (d, J = 7.2 Hz, 2H, ArH), 8.33 (d, J = 8.2 Hz, 2H, ArH), 7.82 (t, J = 7.5 Hz, 2H, ArH), 7.22 (d, J = 7.2 Hz, 2H, ArH), 6.86 (d, J = 7.7 Hz, 2H, ArH), 4.55 (s, 2H, CH_2), 3.83 (s, 2H, CH_2 morph), 3.80 (s, 4H, 1H - CH_2 morph, 3H - CH_3), 3.71 (s, 2H, CH_2 morph), 3.48 (d, J = 17.4 Hz, 3H, CH_2 morph); ^{13}C NMR ($CDCl_3$, 100 MHz): δ (ppm):160.4, 160.0, 135.7, 132.8, 132.0, 129.1, 128.7, 127.3, 121.5, 116.3, 114.2, 113.5, 66.2, 55.4, 44.5, 44.4; HRMS (ESI) Calcd. for $C_{27}H_{25}N_7O_4$ $[M+H]^+$ 512.2046 Found 512.2048.

2-((4-((4-methylbenzyl)amino)-6-morpholino-1,3,5-triazin-2-yl)amino)-1*H*-benzo[*de*]isoquinoline-1,3(2*H*)-dione (26r):

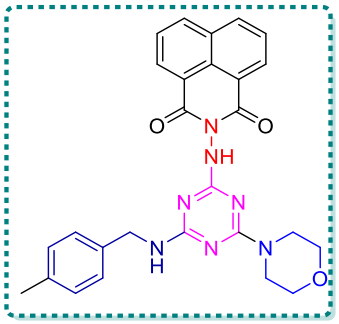

Off white solid; 72% Yield; m.pt: 240-243 ^oC; ^1H NMR ($CDCl_3$, 400 MHz): δ (ppm) 8.63 (d, J = 6.7 Hz, 2H, ArH), 8.31 (d, J = 8.0 Hz, 2H, ArH), 7.81 (t, J = 7.3 Hz, 2H, ArH), 7.15 (d, J = 11.7 Hz, 4H, ArH), 4.57 (s, 2H, CH_2), 3.72 (d, J = 54.6 Hz, 4H, 2×CH_2 morph), 3.45 (d, J = 5.3 Hz, 4H, 2×CH_2 morph), 2.32 (s, 3H, O-CH_3); ^{13}C NMR ($CDCl_3$, 100 MHz): δ (ppm): 156.7, 154.9, 137.7, 135.5, 133.6, 132.6, 132.0, 129.4, 127.7, 121.6, 116.5, 113.7, 66.2, 44.7, 44.5, 21.1; HRMS (ESI) Calcd. for $C_{27}H_{25}N_7O_3$ $[M+H]^+$ 496.0358 Found 496.0357.

4-(((4-((1,3-dioxo-1*H*-benzo[*de*]isoquinolin-2(3*H*)-yl)amino)-6-morpholino-1,3,5-triazin-2-yl)amino)methyl)benzonitrile (26s):

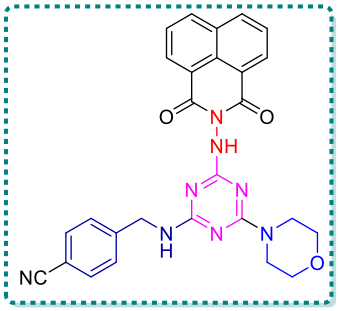

Light yellow solid; 60% Yield; m.pt: 238-240 ^{o}C; ^{1}H NMR (DMSO-d_6, 400 MHz): δ (ppm) 8.49 (d, J = 7.3 Hz, 3H, ArH), 8.41 (d, J = 6.7 Hz, 1H, ArH), 7.90 – 7.87 (m, 2H, ArH), 7.67 (d, J = 8.2 Hz, 1H, ArH), 7.47 (d, J = 6.4 Hz, 1H, NH), 7.34 (d, J = 8.1 Hz, 1H, ArH), 6.99 (d, J = 8.2 Hz, 1H, ArH), 6.59 (d, J = 8.1 Hz, 1H, ArH), 4.29 (d, J = 6.1 Hz, 1H, CH_2), 3.84 (d, J = 6.0 Hz, 1H, CH_2), 3.59 (dd, J = 23.6, 19.4 Hz, 8H, 4×CH_2 morph); ^{13}C NMR (DMSO-d_6, 100 MHz): δ (ppm): 162.2, 159.4, 159.0, 135.2, 132.3, 131.8, 128.4, 127.3, 122.2, 116.7, 113.8, 66.3, 44.0, 43.8, 43.6; HRMS (ESI) Calcd. for $C_{27}H_{22}N_8O_3$ $[M+H]^+$ 507.0094 Found; 507.0096.

References

1. D.R.S. Middleton, V.A. McCormack, M.J. Watts, J. Schüz, *Environ. Geochem. Health*. **2020,** *42,* 1047–1056.
2. Cancer Research UK; https://www.cancerresearchuk.org/health-professional/cancer-statistics/worldwide-cancer#heading-Two [Accessed on July/2019].
3. Kerru,N.; Singh, P.; Koorbanally, N.; Raj, R.; Kumar. V. *Eur. J. Med. Chem.* **2017,** *142*, 179–212.
4. Lolak, N.; Akocak, S.; Bua, S.; Supuran, C.T. *Bioorg. Chem.* **2019**, *82*, 117–122.
5. Singh, M.; Modi, A.; Narayan, G.; Singh, S.K. *Anticancer. Drugs.* **2016,** *27*, 519–532.
6. Hurley, L.H. *Nat. Rev. Cancer.* **2002**, *2*,188–200.
7. Helleday, T.; Petermann, E.; Lundin, C.; Hodgson, B.; Sharma, R.A. *Nat. Rev. Cancer.* **2008**, *8*,193–204.
8. Bradshaw, T.; Stevens, M.F.; Westwell, A. *Curr. Med. Chem.* **2012**, *8*, 203-210.
9. Laxminarayan, R.; Matsoso, P.; Pant, S.; Brower, C.; Røttingen, J.A.; Klugman, K.; Davies, S. *Lancet.***2016**, *387*,168–175.
10. Liu, H.; Long, S.; Rakesh, K.P. *Eur. J. Med. Chem.***2020**, *185*,111804.
11. Palumbi, S.R. *Science*, **2001**, *293*,1786–1790.
12. Zhang, Y.; Yu, K.; Jin, J.; Li, Y.; Sun, P.; Zheng, J.; Piao, R.; *Bioorganic Med. Chem. Lett.* **2018**, *28*,1657–1662.
13. Ravindar, L.; Bukhari, A.; Rakesh, P.; Manukumar, H.; Vivek, K.; Mallesha, N.; Xie, Z.; Qin, L. *Bioorg. Chem.* **2018**, *81*, 107–118.
14. Bhat, H.; Masih, A.; Shakya, A.; Ghosh, S.; Singh, U.; *J. Heterocycl. Chem.* **2020**, *57* 390–399.
15. Petri, Li.; Holl, G.; Spano, R.; Barreca, V.; Sardo, M.; Raimondi, M. V. *Front. Chem.*, **2023**, *11*, 1202192.
16. Kalaria, P. N.; Karad, S. C.; Raval, D. K. *Eur. J. Med. Chem.* **2018**, *158*, 917-936.
17. Kerru, N.; Gummidi, L.; Maddila, Gangu, K.K.; Jonnalagadda, S.B. *Molecules* **2020**, *25*(8), 1909-1951.
18. Zhang, B.; Studer, A. *Chem. Soc. Rev.***2015**, *44*, 3505–3521.
19. Kabir, E.; Uzzaman, M. *Results Chem.* **2022**, *4* , 100606.
20. Li, C.; Sridhara, M. B.; Rakesh, K. P.; Vivek, H. K.; Manukumar, H. M.; Shantharam, C. S.; Qin, H. L. *Bioorg. Chem.* **2018**, *81*, 389–395.

21. Helleday, T.; Petermann, E.; Lundin, C.; Hodgson, B.; Sharma, R. A. *Nat. Rev. Cancer* **2008**, *8*, 193–204.
22. Liang, S. M.; Liang, G. Bin; Wang, H. L.; Jiang, H.; Ma, X. L.; Wei, J. H.; Huang, R. Z.; Zhang, Y. *Eur. J. Med. Chem.* **2024**, *263*, 115937.
23. Zeki, N. M.; Mustafa, Y. F. *J. Mol. Struct.* **2024**, *1309*, 138192.
24. Sharma, O.; Srivastava, S.; Sharma, M.; Malik, R. *J. Mol. Struct.* **2024**, *1308*, 138078.
25. Gadali, K. El; Rafya, M.; El Mansouri, A. eddine; Maatallah, M.; Vanderlee, A.; Mehdi, A.; Neyts, J.; Jochmans, D.; De Jonghe, S.; Benkhalti, F.; Sanghvi, Y. S.; Taourirte, M.; Lazrek, H. B. *Eur. J. Med. Chem.* **2024**, *268*, 116235.
26. Dai, F.; Li, Q.; Wang, Y.; Ge, C.; Feng, C.; Xie, S.; He, H.; Xu, X.; Wang. C.; *J. Med. Chem.* **2017**, *60*, 2071–2083.
27. Ge, C.; Liu, L.; Wang, Y.; Di, X.; Luo, X.; Liu, H.; Qian, Y. *ACS Med. Chem. Lett.* **2023**, *14*, 1551–1557.
28. Liang, S. M.; Liang, G. Bin; Wang, H. L.; Jiang, H.; Ma, X. L.; Wei, J. H.; Huang, R. Z.; Zhang, Y. *Eur. J. Med. Chem.* **2024**, *263*, 115937.
29. Chen, X. M.; Zhou, J. Y.; Liu, S. Q.; Song, L. H.; Wang, H. L.; Wang, Q.; Liang, S. M.; Lu, L.; Wei, J. H.; Huang, R.; Zhang, Y. *Bioorganic Med. Chem. Lett.* **2023**, *85*, 129218.
30. Singh, I.; Luxami, V.; Choudhury, D.; Paul, K. *RSC Adv.* **2021**, *12*, 483–497.
31. JawalePatil, P. D.; Bhamidipati, K.; Damale, M. G.; Sangshetti, J. N.; Puvvada, N.; Bhosale, R. S.; Ingle, R. D.; Pawar, R. P.; Bhosale, S. V.; Bhosale, S. V. *J. Mol. Struct.* **2022**, *1263*, 133173.
32. Zhang, P. L.; Laiche, M. H.; Li, Y. L.; Gao, W. W.; Lin, J. M.; Zhou, C. H. *Eur. J. Med. Chem.* **2022**, *241*, 114657.
33. Zhang, P. L.; Gopala, L.; Zhang, S. L.; Cai, G. X.; Zhou, C. H. *Eur. J. Med. Chem.* **2022**, *229*, 114050.
34. Chen, Y. Y.; Gopala, L.; Bheemanaboina, R. R. Y.; Liu, H. B.; Cheng, Y.; Geng, R. X.; Zhou, C. H. *ACS Med. Chem. Lett.* **2017**, *8*, 1331–1335.
35. Kang, J.; Gopala, L.; Reddy Tangadanchu, V. K.; Gao, W. W.; Zhou, C. H. *Future Med. Chem.* **2018**, *10*, 711–724.
36. Jin, Y.; He, S.; Wu, F.; Luo, C.; Ma, J.; Hu, Y. *Eur. J. Pharm. Sci.* **2023**, *188*, 106520.
37. Zengin Kurt, B.; Celebi, G.; Ozturk Civelek, D.; Angeli, A.; Akdemir, A.; Sonmez, F.; Supuran, C. T. *ACS Omega* **2023**, *8*, 5787–5807.

38. El-Sayed, W. A.; Alminderej, F. M.; Mounier, M. M.; Nossier, E. S.; Saleh, S. M.; Kassem, A. F. *Molecules* **2022**, *27*, 2047.
39. Di Filippo; L. D.; S. G.; Duarte, J.; L. Luiz; M. T.; Dutra, J.; A. P.; Conde, J. *Materials Today Bio*, **2023,** *20*, 100671.
40. Sayed, M. T.; Elsharabasy, S. A.; Abdel-Aziem, A. *Sci. Rep.* **2023**, *13*, 9912.
41. Yang, X. C.; Zeng, C. M.; Avula, S. R.; Peng, X. M.; Geng, R. X.; Zhou, C. H. *Eur. J. Med. Chem.* **2023**, *245*, 114891.
42. Yang, X. C.; Zhang, P. L.; Kumar, K. V.; Li, S.; Geng, R. X.; Zhou, C. H. *Eur. J. Med. Chem.* **2022**, *232*, 114192.
43. Abo-Salem, H. M.; AboBaker Ali, E.; El-Mowafi, S. A.; Abdel-Aziz, M. S.; El-Sawy, E. R.; Abd El Salam, H. A. *J. Mol. Struct.* **2024**, *1296*, 136860.
44. Wu, B. W.; Huang, W. J.; Liu, Y. H.; Liu, Q. G.; Song, J.; Hu, T.; Chen, P.; Zhang, S. Y. *Eur. J. Med. Chem.* **2024**, *265*, 116118.
45. Tiwari, G.; Mishra, V. K.; Kumari, P.; Khanna, A.; Sharma, S.; Sagar, R. *RSC Adv.* **2024**, *14*, 1304–1315.
46. Guo, Y.; Hou, J.; Wu, H.; Chen, Y.; Liu, G.; Wang, D.; Wang, H.; Mao, L.; Li, S.; Wang, T. *J. Mol. Struct.* **2024**, *1298* , 137042.
47. Natália Machado, N. M. P.; Cardoso, G. de A.; Silva, H.; de Freitas, R. P.; Alves, R. B. *Med. Chem. Res.* **2023**, *32* (8), 1816–1831.
48. Miao, Z. Y.; Zhang, X. Y.; Yang, M. H.; Huang, Y. J.; Lin, J.; Chen, W. M. *J. Med. Chem.* **2023**, *66* (23), 15823–15846.
49. Bitla, S.; Gayatri, A. A.; Puchakayala, M. R.; Kumar Bhukya, V.; Vannada, J.; Dhanavath, R.; Kuthati, B.; Kothula, D.; Sagurthi, S. R.; Atcha, K. R. *Bioorganic Med. Chem. Lett.* **2021**, *41*, 128004.
50. Saeed, S.; Zahoor, A. F.; Kamal, S.; Raza, Z.; Bhat, M. A. *Molecules* **2023**, *28*, 6007.
51. Gadali, K. El; Rafya, M.; Mansouri, A. eddine El; Maatallah, M.; Van-der lee, A.; Mehdi, A.; Ouahrouch, A.; Benkhalti, F.; Sanghvi, Y. S.; Taourirte, M.; Lazrek, H. B. *J. Mol. Struct.* **2023**, *1282*, 135179.
52. Zou, J. P.; Zhang, Z.; Lv, J. Y.; Zhang, X. Q.; Zhang, Z. Y.; Han, S. T.; Liu, Y. W.; Liu, W. W.; Ji, J.; Shi, D. H. *Tetrahedron* **2023**, *134*, 133293.
53. Santra, S.; Sharapov, A. D.; Fatykhov, R. F.; Potapova, A. P.; Khalymbadzha, I. A.; Valieva, M. I.; Kopchuk, D. S.; Zyryanov, G. V; Bunev, A. S.; Melekhin, V. V; Gaviko, V. S.; Zonov, A. A. *Pharmaceuticals*, **2023**, *16*, 403.

54. Zain-Alabdeen, A. I.; El-Moselhy, T. F.; Sharafeldin, N.; Angeli, A.; Supuran, C. T.; El-Hamamsy, M. H. *Sci. Rep.* **2022**, *12*, 16756.
55. Haiba, N. S.; Khalil, H. H.; Bergas, A.; Abu-Serie, M. M.; Khattab, S. N.; Teleb, M. *ACS Omega* **2022**, *7*, 21131–21144.
56. Younis, M. H.; Mohammed, E. R.; Mohamed, A. R.; Abdel-Aziz, M. M.; Georgey, H. H.; Abdel Gawad, N. M. *Bioorg. Chem.* **2022**, *124*, 105807.
57. Green, K. D.; Pang, A. H.; Thamban Chandrika, N.; Garzan, A.; Baughn, A. D.; Tsodikov, O. V.; Garneau-Tsodikova, S. *ACS Infect. Dis.* **2022**, *8*, 757–767.
58. Xia, Q.; Li, J.; Yang, Z.; Zhang, D.; Tian, J.; Gu, B. *Chem. Biol. Drug Des.* **2023**, *101*, 271–277.
59. Maliszewski, D.; Demirel, R.; Wróbel, A.; Baradyn, M.; Ratkiewicz, A.; Drozdowska, D. *Pharmaceuticals* **2023**, *16*, 1248.
60. Fan, Y. R.; Wang, B. J.; Jia, D. G.; Yang, X. Bin; Huang, Y. *J. Inorg. Biochem.* **2021**, *219*, 111425.
61. Rong, R. X.; Sun, Q.; Ma, C. L.; Chen, B.; Wang, W. Y.; Wang, Z. A.; Wang, K. R.; Cao, Z. R.; Li, X. L. *Medchemcomm* **2016**, *7*, 679–685.
62. Chen, X. M.; Zhou, J. Y.; Liu, S. Q.; Song, L. H.; Wang, H. L.; Wang, Q.; Liang, S. M.; Lu, L.; Wei, J. H.; Huang, R.; Zhang, Y. *Bioorganic Med. Chem. Lett.* **2023**, *85*, 129218.
63. Rong, R. X.; Wang, S. S.; Liu, X.; Li, R. F.; Wang, K. R.; Cao, Z. R.; Li, X. L. *Bioorganic Med. Chem. Lett.* **2018**, *28*, 742–747.
64. Malik, M. S.; Farooq Adil, S.; Moussa, Z.; Altass, H. M.; Althagafi, I. I.; Morad, M.; Ansari, M. A.; Sajid Jamal, Q. M.; Obaid, R. J.; Al-Warthan, A. A.; Shaik, T. B.; Ahmed, S. A. *Front. Chem.* **2021**, *9*, 781291.
65. Huang, Y.; Wu, C. X.; Song, Y.; Huang, M.; Tian, D. N.; Yang, X. Bin; Fan, Y. R. *Molecules* **2018**, *23*, 266.
66. Middleton, D. R. S.; McCormack, V. A.; Watts, M. J.; Schüz, J. *Environ. Geochem. Health* **2020**, *42*, 1047–1056.
67. Lolak, N.; Akocak, S.; Bua, S.; Supuran, C. T. *Bioorg. Chem.* **2019**, *82*, 117–122.
68. Singh, M.; Modi, A.; Narayan, G.; Singh, S. K.; *Anticancer Drugs* 2016, **27**, 519–532.
69. Singh, I.; Luxami, V.; Paul, K. *Org. Biomol. Chem.* **2019**, *17*, 5349–5366
70. Li, X.; Wu, Z.; Xu, L.; Chi, C. L.; Chen, B. Q. *Med. Chem. Res.* **2020**, *29*, 180–188.
71. Singh, I.; Luxami, V.; Paul, K. *Bioorg. Chem.* **2020**, *96*, 103631.

72. Dai, F.; Li, Q.; Wang, Y.; Ge, C.; Feng, C.; Xie, S.; He, H.; Xu, X.; Wang, C. *J. Med. Chem.* **2017**, *60* (5), 2071–2083.
73. Vitaku, E.; Smith, D. T.; Njardarson, J. T. *J. Med. Chem.* **2014**, *57* (24), 10257–10274.
74. Singh, M.; Modi, A.; Narayan, G.; Singh, S. K. *Anticancer. Drugs* **2016**, *27* (6), 519–532.
75. Seliga, R.; Pilatova, M.; Sarissky, M.; Viglasky, V.; Walko, M.; Mojzis, J. *Mol. Biol. Rep.* **2013**, *40* (6), 4129–4137.
76. Rong, R. X.; Wang, S. S.; Liu, X.; Li, R. F.; Wang, K. R.; Cao, Z. R.; Li, X. L. *Bioorganic Med. Chem. Lett.* **2018**, *28* (4), 742–747.
77. A. Monks, D. Scudiero, P. Skehan, R. Shoemaker, K. Paull, D. Vistica, C. Hose, J. Langley, P. Cronise, A. *J. Natl. Cancer Inst.* 1991, **83**, 757–766.
78. N. Joksimović, J. Petronijević, N. Janković, D. Baskić, S. Popović, D. Todorović, S. Matić, G. A. Bogdanović, M. Vraneš, A. Tot and Z. Bugarčić, *Bioorg. Chem.* 2019, **88**, 102954.
79. K. Mihajlović, N. Joksimović, S. Radisavljević, J. Petronijević, I. Filipović, N. Janković, E. Milović, S. Popović, S. Matić and D. Baskić, *J. Mol. Struct.* 2022, **1270**, 133943.
80. A. Garofalo, L. Goossens, B. Baldeyrou, A. Lemoine, S. Ravez, P. Six, M. H. David-Cordonnier, J. P. Bonte, P. Depreux, A. Lansiaux, J. F. Goossens, *J. Med. Chem.* 2010, **53**, 8089–8103.
81. J. R. Lakowicz, G. Weber, *Biochemistry* 1973, **12**, 4171–4179
82. J. R. Lakowicz, G. Weber, *Biochemistry* 1973, **12**, 4161–4170.
83. P. Srivastava, K. Singh, M. Verma, S. Sivakumar, A. K. Patra, *Eur. J. Med. Chem.* 2018, **144**, 243–254.
84. L. Wang, Y. Wen, J. Liu, J. Zhou, C. Li, C. Wei, *Org. Biomol. Chem.* 2011, **9**, 2648–2653.
85. M. Czaja, K. Skirlińska-Nosek, O. Adamczyk, K. Sofińska, N. Wilkosz, Z. Rajfur, M. Szymoński, E. Lipiec, *Int. J. Mol. Sci.* 2022, **23**, 3524.
86. J. Kim, J. Kwon, M. Kim, J. Do, D. Lee, H. Han, *Polym. J.* 2016, **48**, 829–834.
87. D. Wu, J. Yan, J. Wang, Q. Wang, H. Li, *Food Chem.* 2015, **170**, 423–429.
88. H. Yang, J. Liu, Y. Huang, R. Gao, B. Tang, S. Li, J. He, H. Li, *Sci. rep.* 2017, **7**, 45514.
89. S. Rani, V. Luxami, K. Paul, *ChemMedChem* 2021, **16**, 1821–1831.

90. V. Patil, A. Noonikara-Poyil, S. D. Joshi, S. A. Patil, S. A. Patil, A. M. Lewis, A. Bugarin, *J. Mol. Struct.* 2020, **1220**, 128687.
91. J. Klenc, E. Raux, S. Barnes, S. Sullivan, B. Duszynska, A. J. Bojarski, L. Strekowski, *J. Heterocycl. Chem.* 2009, **46**, 1259–1265.
92. M. Verma, V. Luxami, K. Paul, *Eur. J. Med. Chem.* 2013, **68**, 352–360.
93. M. Verma, V. Luxami, K. Paul, *RSC Adv*. 2015**, 5**, 41803–41813.
94. I. E. Głowacka, R. Gulej, P. Grzonkowski, G. Andrei, D. Schols, R. Snoeck, D. G.Piotrowska, *Molecules* 2016, **21**, 1420.
95. Privalsky, T. M.; Soohoo, A. M.; Wang, J.; Walsh, C. T.; Wright, G. D.; Gordon, E. M.; Gray, N. S.; Khosla, C. *J. Am. Chem. Soc.* **2021**, *143*, 21127.
96. Rohr, J. R.; Barrett, C. B.; Civitello, D. J.; Craft, M. E.; Delius, B.; DeLeo, G. A.; Hudson, P. J.; Jouanard, N.; Nguyen, K. H.; Ostfeld, R. S.; Remais, J. V.; Riveau, G.; Sokolow, S. H.; Tilman, D. *Nat. Sustain.* **2019**, *2*, 445.
97. Lin, S.; Wade, J. D.; Liu, S. *Acc. Chem. Res.* **2021**, *54*, 104.
98. Ghosh, C.; Sarkar, P.; Issa, R.; Haldar, J. *Trends Microbiol.* **2019**, *27*, 323
99. Biondo, C. *Pathogens* **2023**, *12*, 116.
100. Chen, Z.; Song, K.; Shang, Y.; Xiong, Y.; Lyu, Z.; Chen, J.; Zheng, J.; Li, P.; Wu, Y.; Gu, C.; Xie, Y.; Deng, Q.; Yu, Z.; Zhang, J.; Qu, D. *J. Med. Chem.* **2021**, *64*, 15037.
101. Zhang, Y.; Tangadanchu, V. K. R.; Cheng, Y.; Yang, R. G.; Lin, J. M.; Zhou, *ACS Med. Chem. Lett.* **2018**, *9*, 244.
102. Erskine, E.; MacPhee, C. E.; Stanley-Wall, N. R. *J. Mol. Biol.* **2018**, *430*, 3642.
103. Mohammad, H.; Younis, W.; Chen, L.; Peters, C. E.; Pogliano, J.; Pogliano, K.; Cooper, B.; Zhang, J.; Mayhoub, A.; Oldfield, E.; Cushman, M.; Seleem, M. N. *J. Med. Chem.* **2017**, *60*, 242
104. Spencer, D. C.; Paton, T. F.; Mulroney, K. T.; Inglis, T. J. J.; Sutton, J. M.; Morgan, H. *Nat. Commun.* **2020**, *11*, 532
105. Lin, S.; Liu, J.; Li, H.; Liu, Y.; Chen, Y.; Luo, J.; Liu, S. *J. Med. Chem.* **2020**, *63*, 9284.
106. Ding, R.; Wang, X.; Fu, J.; Chang, Y.; Li, Y.; Liu, Y.; Liu, Y.; Ma, J.; Hu, J. *Eur. J. Med. Chem.* **2022**, *237*, 114398
107. Qian, Q.; Nath, K. A.; Wu, Y.; Daoud, T. M.; Sethi, S. *Am. J. Kidney Dis.* **2010**, *56*, 780.
108. Ghannay, S.; Snoussi, M.; Messaoudi, S.; Kadri, A.; Aouadi, K. *Bioorg. Chem.* **2020**, *104*, 104270.

109. Wang, J.; Zhang, P. L.; Ansari, M. F.; Li, S.; Zhou, C. H. *Bioorg. Chem.* **2021**, *113*, 105039.

110. Liang, W.X.; Yu, Q.; Zheng, Z.X.; Liu, J.Y.; Cai, Q.M.; Liu, S.P.; Lin, S.M. *J. Med. Chem.* **2022**, *65*, 14221.

111. Dai, J.; Battini, N.; Zang, Z.; Luo, Y.; Zhou, C. *Molecules*. **2023,** *28*, 4240

112. Wang, L. L.; Battini, N.; Bheemanaboina, R. R. Y.; Ansari, M. F.; Chen, J. P.; Xie, Y. P.; Cai, G. X.; Zhang, S. L.; Zhou, C. H. *Eur. J. Med. Chem.* **2019**, *179*, 166.

113. Sun, H.; Ansari, M. F.; Fang, B.; Zhou, C. H. *J. Agric. Food Chem.* **2021**, *69*, 7831

114. Ansari, M. F.; Tan, Y. M.; Sun, H.; Li, S.; Zhou, C. H. *Bioorg. Med. Chem. Lett.* **2022**, *76*, 129012

115. Zhang, P.; Tangadanchu, V. K. R.; Zhou, C. *Molecules* **2022**, *27*, 8453.

116. Shimazaki, Y.; Tanaka, J.; Kohara, Y.; Kamahori, M.; Sakamoto, T. *Anal. Chem.* **2017**, *89*, 6305.

117. Wang, J.; Zhang, P. L.; Ansari, M. F.; Li, S.; Zhou, C. H. *Bioorg. Chem.* **2021**, *113*, 105039.

118. Zhang, J.; Battini, N.; Ou, J.M.; Zhang, S.L.; Zhang, L.; Zhou, C.H. *J. Agric. Food Chem.* **2023**, *71*, 2322.

119.Deng, Z.; Bheemanaboina, R. R. Y.; Luo, Y.; Zhou, C. H. *Bioorg. Chem.* **2022**, *127*, 106035.

120. Zang, Z. L.; Wang, Y. X.; Battini, N.; Gao, W. W.; Zhou, C. H. *Eur. J. Med. Chem.* **2024**, *275*, 116626.

121.Tan, Y.M.; Wang, Y.; Li, S.; Zhang, S.L.; Zhou, C.H. *J. Med. Chem.* **2023**, *66*, 4910.

122.Yang, X. C.; Hu, C. F.; Zhang, P. L.; Li, S.; Hu, C. S.; Geng, R. X.; Zhou, C. H. *Biorg. Chem.* **2022**, *124*, 105855.

123.Majumdar, D.; Philip, J. E.; Tüzün, B.; Frontera, A.; Gomila, R. M.; Roy, S.; Bankura, K. *J. Inorg. Organomet. Polym. Mater.* **2022**, *32*, 4320.

124.Cao, D.; Liu, Z.; Verwilst, P.; Koo, S.; Jangjili, P.; Kim, J. S.; Lin, W. *Chem. Rev.* **2019**, *119*, 10403–10519.

125. Kang, J.; Tangadanchu, V. K. R.; Gopala, L.; Gao, W. W.; Cheng, Y.; Liu, H. B.; Geng, R. X.; Li, S.; Zhou, C. H. II. *Chinese Chem. Lett.* **2017**, *28*, 1369–1374.

126. Vanden Broeck, A.; McEwen, A. G.; Chebaro, Y.; Potier, N.; Lamour, V. *J. Med. Chem.* **2019**, *62*, 4225–4231.

127.Yang, X. C.; Zeng, C. M.; Avula, S. R.; Peng, X. M.; Geng, R. X.; Zhou, C. H. *Eur. J. Med. Chem.* **2023**, *245*, 114891

128. J. Ferlay, M. Ervik, F. Lam, M. Colombet, L. Mery, M. Piñeros, Global cancer observatory: cancer today, Lyon: International Agency for Research on Cancer, **2020** https://gco.iarc.fr/today , accessed February 2021

129. Bhat-Ambure, J.; Ambure, P.; Serrano-Candelas, E.; Galiana-Roselló, C.; Gil-Martínez, A.; Guerrero, M.; Martin, M.; González-García, J.; García-España, E.; Gozalbes, R. *Cancers (Basel).* **2023**, *15*, 3817

130. Zugazagoitia, J.; Guedes, C.; Ponce, S.; Ferrer, I.; Molina-Pinelo, S.; Paz-Ares, L. *Clin. Ther.* **2016**, *38*, 1551–1566.

131. Sawyers, C. Targeted Cancer Therapy. *Nature* **2004**, *432*, 294–297.

132. Wu, W.; Hu, X.; Zeng, Z.; Wu, D.; Li, H.; Li, H. *J. Phys. Chem. B* **2023**, *127*, 874–883.

133. Belmonte-reche, E.; Pirota, V.; Jong, A. De; Morales, J. C.; Freccero, M.; Doria, F.; Kuipers, O. P. *J. Med. Chem,* **2022**, *65*, 4752-4766.

134. Catalano, R.; Moraca, F.; Amato, J.; Cristofari, C.; Rigo, R.; Via, L. D.; Rocca, R.; Lupia, A.; Maruca, A.; Costa, G.; Catalanotti, B.; Artese, A.; Pagano, B.; Randazzo, A.; Sissi, C.; Novellino, E.; Alcaro, S. *Eur. J. Med. Chem.* **2019**, *182*, 111627.

135. Long, W.; Zeng, Y.; Zheng, B.; Li, Y.; Wang, Y.; Chan, K.; She, M.; Lu, Y.; Cao, C.; Wong, W. *J. Med. Chem.* **2024,** *67*, 13363-13382.

136. Ahmed, A. A.; Chen, S.; Escorza, M. R.; Angell, R.; Oxenford, S.; Mcconville, M.; Barton, N.; Sunose, M.; Neidle, D.; Haider, S.; Arshad, T.; Neidle, S. *Sci. Rep.* **2024**, *14*, 3447.

137. Benassi, A.; Peñalver, P.; Pérez-Soto, M.; Pirota, V.; Freccero, M.; Morales, J. C.; Doria, F. *J. Med. Chem.* **2024**, *67*, 10643-10654.

138. Mendes, E.; Bahls, B.; Aljnadi, I. M.; Paulo, A. *Bioorganic Med. Chem. Lett.* **2022**, *72*, 128862.

139. Jana, S.; Panda, D.; Saha, P.; Pantos, G. D.; Dash, J. *J. Med. Chem.* **2019**, *62*, 762–773.

140. Liu, H. Y.; Chen, A. C.; Yin, Q. K.; Li, Z.; Huang, S. M.; Du, G.; He, J. H.; Zan, L. P.; Wang, S. K.; Xu, Y. H.; Tan, J. H.; Ou, T. M.; Li, D.; Gu, L. Q.; Huang, Z. S. *J. Med. Chem.* **2017**, *60*, 5438–5454.

141. Chaudhuri, R.; Bhattacharya, S.; Dash, J.; Bhattacharya, S. *J. Med. Chem.* **2021**, *64*, 42–70

142. Roy, S.; Maiti, B.; Banerjee, N.; Kaulage, M. H.; Muniyappa, K.; Chatterjee, S.; Bhattacharya, S. *ACS Pharmacol. Transl. Sci.* **2023**, *6*, 546–566.

143. Wang, Y. H.; Yang, Q. F.; Lin, X.; Chen, D.; Wang, Z. Y.; Chen, B.; Han, H. Y.; Chen, H. Di; Cai, K. C.; Li, Q.; Yang, S.; Tang, Y. L.; Li, F. G4LDB 2.2: *Nucleic Acids Res.* **2022**, *50*, 150–160.
144. Wang, X.; Zhang, M.; Xiong, X; Q, Yang; H, Wang; P., Zhang, K; Zhang, W. *Life Sciences*, **2022**, *302*, 120651
145. Li, M. L.; Dai, L. T.; Gao, Z. Y.; Yan, J. T.; Xu, S. M.; Tan, J. H.; Huang, Z. S.; Chen, S. Bin; Chen, X. C. *J. Med. Chem.* **2024**, *67*, 1961–1981.
146. Ou, Z.; Li, Z.; Gao, Y.; Xing, W.; Jia, H.; Zhang, H.; Yi, N *J. Mol. Struct.* **2019**, *1185*, 27–37.
147. Das, T.; Panda, D.; Saha, P.; Dash, J. *Bioconjug. Chem.* **2018**, *29*, 2636–2645.
148. Roy, S.; Ali, A.; Kamra, M.; Muniyappa, K.; Bhattacharya, S. *Eur. J. Med. Chem.* **2020**, *195*, 112202.
149. Tassinari, M.; Richter, S. N.; Gandellini, P. *Nucleic Acids Res.* **2021**, *49*, 3617–3633.
150. Patidar, R. K.; Tiwari, K.; Tiwari, R.; Ranjan, N. *ACS Appl. Bio Mater.* **2023**, *6*, 2196–2210.
151. Rani, S.; Gupta, S.; Luxami, V.; Paul, K. *New J. Chem.* **2022**, *46*, 12082–12092.
152. Li, X.; Lin, Y.; Wang, Q.; Yuan, Y.; Zhang, H.; Qian, X. *Eur. J. Med. Chem.* **2011**, *46*, 1274–1279.
153. Zeydi, M. M.; Kalantarian, S. J.; Kazeminejad, Z. Overview on Developed Synthesis Procedures of Coumarin Heterocycles. *J. Iran Chem. Soc.* **2020**, *17*, 3031–3094.
154. Fayed, E. A.; Ebrahim, M. A.; Fathy, U.; Elawady, A. M.; Khalaf, W. S.; Ramsis, T. M. *J. Mol. Struct.* **2024**, *1295*, 136663.
155. Li, S. R.; Tan, Y. M.; Zhang, L.; Zhou, C. H. *Pharmaceutics* **2023**, *15*, 1348.
156. Majumder, A.; Sarkar, C.; Das, I.; Sk, S.; Bandyopadhyay, S.; Mandal, S.; Bera, M. *ACS Appl. Mater. Interfaces* **2023**, *15*, 22781–22804.
157. Deusenbery, C.; Carneiro, O.; Oberkfell, C.; Shukla, A. *ACS Infect. Dis.* **2023**, *9* , 1949–1963.
158. Wang, Z.; Yang, Q.; Wang, X.; Li, R.; Qiao, H.; Ma, P.; Sun, Q.; Zhang, H. *Int. J. Biol. Macromol.* **2020**, *153*, 539–544.
159. Xin, L.; Zhang, C.; Chen, J.; Jiang, Y.; Liu, Y.; Jin, P.; Wang, X.; Wang, G.; Huang, P. *ACS Appl. Mater. Interfaces* **2022**, *14*, 47420–47431.
160. Jayasankari, S.; Vishnuvarthan, P.; Rubini, D.; Subramaniyan, S. B.; Vadivel, V.; Anbazhagan, V.; Nithyanand, P. *ACS Food Sci. Technol.* **2021**, *1*, 1030–1040.
161. Wang, J.; Ansari, M. F.; Zhou, C. H. *J. Med. Chem.* **2021**, *64*, 7630–7645.

162. Sun, H.; Huang, S. Y.; Jeyakkumar, P.; Cai, G. X.; Fang, B.; Zhou, C. H. *J. Med. Chem.* **2022**, *65*, 436–459.
163. Gao, F.; Wang, P.; Yang, H.; Miao, Q.; Ma, L.; Lu, G. *Eur. J. Med. Chem.* **2018**, *157*, 1223–1248.
164. Fang, S.; Kang, W. T.; Li, H.; Cai, Q.; Liang, W.; Zeng, M.; Yu, Q.; Zhong, R.; Tao, Y.; Liu, S.; Lin, S. *Eur. J. Med. Chem.* **2024**, *266*, 116149.
165. Stephany-Brassesco, I.; Bereswill, S.; Heimesaat, M. M.; Melzig, M. F. *Eur. J. Microbiol. Immunol.* **2019**, *9*, 100–104.
166. Hu, C. F.; Zhang, P. L.; Sui, Y. F.; Lv, J. S.; Ansari, M. F.; Battini, N.; Li, S.; Zhou, C. H.; Geng, R. X. *Bioorg. Chem.* **2020**, *94*, 103434.
167. Lin, S.; Liu, J.; Li, H.; Liu, Y.; Chen, Y.; Luo, J.; Liu, S. *J. Med. Chem.* **2020**, *63*, 9284–9299.
168. Priyanka; Singh, V.; Ekta; Katiyar, D. *Bioorg. Chem.* **2017**, *71*, 120–127.
169. Zhang, J.; Tan, Y. M.; Li, S. R.; Battini, N.; Zhang, S. L.; Lin, J. M.; Zhou, C. H. *Eur. J. Med. Chem.* **2024**, *265*, 116107.
170. Guo, W.; Yang, Z.; Wang, K.; Li, W.; Zhao, Y.; Yang, Y.; Chang, W.; Gong, Z.; Liu, Z.; Chen, Y.; Li, Q. *J. Med. Chem.* **2024**, *67*, 2129–2151.
171. Guo, S.; Huang, Q.; Chen, Y.; Wei, J.; Zheng, J.; Wang, L.; Wang, Y.; Wang, R. *Angew. Chemie - Int. Ed.* **2021**, *60*, 618–623.
172. Lin, Q. W.; Lu, J. Q.; Huang, Y. S.; Liu, J. J.; Chen, W. M.; Lin, J. *J. Med. Chem.* **2023**, *66*, 11927–11939.
173. Ciofu, O., Moser, C., Jensen, P. Ø., Høiby, N. *Nature Rev. Microbiol.* **2022,** *20*, 621-635.
174. Zhang, J.; Chen, C.; Chen, J.; Zhou, S.; Zhao, Y.; Xu, M.; Xu, H. *ACS Appl. Mater. Interfaces* **2020**, *12*, 27866–27875.
175. Guo, Y.; Bao, C.; Li, F.; Hou, E.; Qin, S.; Zhang, Q.; Liu, J. *ACS Infect. Dis.* **2020**, *6*, 2478–2489.
176. Zhou, X. M.; Hu, Y. Y.; Fang, B.; Zhou, C. H. *Eur. J. Med. Chem.* **2023**, *248*, 115088.
177. Chen, J. P.; Battini, N.; Ansari, M. F.; Zhou, C. H. *Eur. J. Med. Chem.* **2021**, *217*, 113340.
178. Zhao, J. S.; Ahmad, N.; Li, S.; Zhou, C. H. *Bioorg. Med. Chem. Lett.* **2024**, *103*, 129709
179. Liu, J.; Li, H.; He, Q.; Chen, K.; Chen, Y.; Zhong, R.; Li, H.; Fang, S.; Liu, S.; Lin, S. *Eur. J. Med. Chem.* **2022**, *243*, 114734.

180. Li, F. F.; Zhao, W. H.; Tangadanchu, V. K. R.; Meng, J. P.; Zhou, C. H. *Eur. J. Med. Chem.* **2022**, *239*, 114521.
181. Zhang, J.; Battini, N.; Ou, J. M.; Zhang, S. L.; Zhang, L.; Zhou, C. H. *J. Agric. Food Chem.* **2023**, *71*, 2322–2332.
182. Zeng, C.; Avula, S. R.; Meng, J.; Zhou, C. *Molecules* **2023**, *28*, 2511.
183. Yang, R.; Cheng, W.; Huang, M.; Xu, T.; Zhang, M.; Liu, J.; Qin, S.; Guo, Y. *Eur. J. Med. Chem.* **2024**, *268*, 116274.
184. Sui, Y. F.; Ansari, M. F.; Fang, B.; Zhang, S. L.; Zhou, C. H. *Eur. J. Med. Chem.* **2021**, *221*, 113557.
185. Roy, S.; Mondal, A.; Yadav, V.; Sarkar, A.; Banerjee, R.; Sanpui, P.; Jaiswal, A. *ACS Appl. Bio Mater.* **2019**, *2*, 2738–2755.
186. Kobryń, J.; Dałek, J.; Musiał, W. *Pharmaceutics* **2021**, *13*, 992.
187. Liang, X. Y.; Battini, N.; Sui, Y. F.; Ansari, M. F.; Gan, L. L.; Zhou, C. H. *RSC Med. Chem.* **2021**, *12*, 602–608.
188. Xu, M.; Wu, P.; Shen, F.; Ji, J.; *Bioorg. Chem.* **2019**, *91*, 103133.
189. Gheng, G.; Dai, M.; Ahmed, S.; Hao, H.; Wang, X.; Yuan, Z. *Front. Microbiol.* **2016**, *7*, 470.
190. Soliman, S.; El-Faham, A.; El Silk, S. *Appl. Organomet. Chem.* **2020**, *34*, 5941.
191. Pendleton, J.; Gorman, S,; Gilmore, B. *Anti. Infect. Ther.* **2013,** *11*, 297–308.
192. Ramadan, D.; Elbardan, A.; Bekhit, A.; El-Faham, A.; Khattab, S. *New J. Chem.* **2018**, *42*, 10676–10688.
193. Li, C.; Sridhara,M.; Rakesh, K.; Vivek, H.; Manukumar, H.; Shantharam, C.; Qin, H. *Bioorg. Chem.* **2018**, *81*, 389–395.
194. Zhou, X.; Lin, K.; Ma, X.; Chui, W.; Zhou, W. *Eur. J. Med. Chem.* **2017**, *125*, 1279–1288.
195. Shah, D.; Modh, R.; Chikhalia, K. *Future Med. Chem.* **2014**, *6*, 463–477.
196. Masih, A.; K.Shrivastava, J.; R. Bhat, H.; Singh, P. *Chem. Biol. Drug Des.* **2020**, *96*, 861–869.
197. Kang, J.; Gopala, L.; Reddy Tangadanchu, V.K.; Gao, W.; Zhou, C.H. *Future Med. Chem.* **2018**, *10*, 711–724.
198. Lepecq, J.; Paoletti, C.; *J. Mol. Biol.***1967**, *27*, 87–106.

Publication from thesis work

1. **Gupta, S**.; Paul, K. DNA Damage and Intercalation by Elinafide Modified Bis-Naphthalimides for Their Anticancer Activity. *J. Mol. Liq.* **2023**, *382*, 121980. (***I.F = 5.3)***

2. **Gupta, S.**; Paul, K. Membrane-Active Substituted Triazines as Antibacterial Agents against *Staphylococcus Aureus* with Potential for Low Drug Resistance and Broad Activity. *Eur. J. Med. Chem.* **2023**, *258*, 115551. (***I.F = 6.0)***

3. **Gupta, S.**; Luxami, V.; Paul, K.; Bacterial Cell Death to Overcome Drug Resistance with Multitargeting Bis-Naphthalimides as Potent Antibacterial Agents Against *Enterococcus faecalis*. *J. Mater. Chem. B* **2024*, (I.F = 6.1)***

4. **Gupta, S.**; Luxami, V.; Paul, K.; Deciphering Binding Potential of Naphthalimide-Coumarin Conjugate with c-MYC G-quadruplex for Developing New Anticancer Agents: A Spectroscopic and Molecular Modelling Approach (Communicated)

5. **Gupta, S.**; Paul, K.; Unlocking the Antibacterial Potential of Naphthalimide-Coumarins to Overcome Drug Resistance with Antibiofilm and Membrane Disruption Ability Against *Escherichia coli* (communicated)

6. **Gupta, S**.; Paul, K.; Structural Modification of Bisnafide for Developing Bis-Napthalimide with Alkyl Spacer as Potent Antibacterial Agents Towards *Listeria sp* and *Acinetobacter calcoacetius* for Combating Awful Drug Resistance (Manuscript prepared)

7. **Gupta, S**.; Rana, R; Paul, K.; In-Sight into Antibacterial Mechanism of Napthalimide-Coumarin-Triazole Derivatives Against Gram-Positive Bacteria *Bacillus subtilis* to Conquer Dreadful Drug Resistance (Manuscript under preparation)

8. **Gupta, S**.; Rana, R; Paul, K.; Synthesis of Triazine-Benzimidazole Conjugates with Membrane Disruption Ability for Developing Potent Antibacterial Agents against *Salmonella enterica* (Manuscript Under Preparation)

Publications Other than this work

1. Sarkar, P.; **Gupta, S**.; Udaya Kumar, A. H.; Das, D.; Sutradhar, S.; Paul, K.; Lokanath, N. K.; Nath Ghosh, B. Protein Interactions and Drug Displacement Studies of Novel Copper(II) and Zinc(II) Complexes of a Dipyrazinylpyridine Ligand. *J. Mol. Liq.* **2023**, *387*, 122561 (***I.F = 5.3)***

2. Rani, S.; **Gupta, S**.; Luxami, V.; Paul, K. A Novel Target and Biomarker Benzothiazolyl-Naphthalimide Probes for Precise and Selective Detection of Serum Albumin and Anticancer Activity. *New J. Chem.* **2022**, *46* (25), 12082–12092. (***I.F = 2.7)***

3. Kaundal, A.; **Gupta, S**.; Kumar, G.; Paul, K.; Luxami, V. A Turn "ON" Bis-Napthalimide Based Chemosensor for Detection of Al^{3+} Ions and Nerve Agent. (Manuscript Prepared)

4. **Gupta, S**.; Kaundal, A.; Kumar, G.; Paul, K.; Luxami, V. A Colormetric and Ratiometric differential detection of Cu^{2+}, CN^{-} and S^{2-} ions in 60% Aqueous medium by fluorescent Napthalimide probe and its real time applications. (Manuscript under preparation)

5. **Gupta, S**.; Luxami, V.; Paul, K. A Ratiometric and Turn "ON" Naphthalimide Probe for Selective Detection of Sulphide Ions In 60% Aqueous Medium and Its Real-Time Application (Under Preparation)

6. **Gupta, S**.; Verma, K; Sharma, S.; Choudhary, D.; Paul, K. Insight into Binding Behavior of Azide Based Naphthalimide Probe Towards Serum Albumin and Cell Imaging (Under Preparation)

7. **Gupta, S**.; Sutradhar, S.; Paul, K.; Nath Ghosh, B. Discovery of Zn Metal complexes as an Effective Antibacterial Agent with Antibiofilm Activity to Overcome Drug Resistance Against *Bacillus subtilis* and *Salmonella enterica* (Manuscript Prepared)

Conferences

1. National Conference (2024) on "**Chemistry for The Sustainable Future"** at Punjabi University, Patiala
2. Prof. Ram Chand Paul National Symposium (2023) on "**Sustainable Development in Chemical Science**" at Punjab University, Chandigarh
3. International Symposium (2022) on "**Recent advances in Self assembled Materials and Supramolecular Chemistry**" at GNDU, Amritsar
4. National Conference on "**Chemical and Environmental Sciences: Advanced Innovations- 2020"** at Punjabi University, Patiala.